UCLA
UCLA Electronic Theses and Dissertations

Title
Outsmarting and Outmuscling Cancer Cells for Next-Generation CAR-T Cell Therapies

Permalink
https://escholarship.org/uc/item/27c8h885

Author
Chen, Laurence Chaoyuen

Publication Date
2022

Supplemental Material
https://escholarship.org/uc/item/27c8h885#supplemental

Peer reviewed|Thesis/dissertation

eScholarship.org Powered by the California Digital Library
University of California

UNIVERSITY OF CALIFORNIA

Los Angeles

Outsmarting and Outmuscling Cancer Cells for Next-Generation CAR-T Cell Therapies

A dissertation submitted in partial satisfaction of the requirements for the degree Doctor of Philosophy in Chemical Engineering

by

Laurence Chen

2022

© Copyright by

Laurence Chen

2022

ABSTRACT OF THE DISSERTATION

Outsmarting and Outmuscling Cancer Cells for

Next-Generation CAR-T Cell Therapies

by

Laurence Chen

Doctor of Philosophy in Chemical Engineering

University of California, Los Angeles, 2022

Professor Yvonne Y. Chen, Chair

CAR-T cell therapy has emerged as a promising cancer treatment modality with curative potential. In this therapeutic regime, T cells are isolated from patient blood, genetically engineered to express tumor-targeting chimeric antigen receptors (CARs), and re-infused back into the patient as a living drug. As living drugs, CAR-T cells have the unique capacity of being able to sense-and-respond to a variety of pathologic stimuli in order to safely and effectively eliminate cancer cells. Furthermore, CAR-T cells can be genetically engineered to execute researcher-defined genetic programs – be it Boolean logic processing in the presence of multiple antigen targets, or straightforward execution of robust T-cell effector responses. Despite clinical success in treating hematological malignancies, CAR-T cells have had limited efficacy in treating vast the majority of cancers, comprising of solid tumors. Two major barriers include CAR target antigen

choice and suboptimal persistence of CAR-T cells. First, because cancer cells are derived from “self”, tumor-exclusive surface antigens that are absent on all other cells are scarce. In practice, tumor-associated antigens are commonly selected as CAR targets, but clinical experience has shown that “on-target, off-tumor” CAR-T cell killing can lead to fatal outcomes. In order to overcome this, we attempt to reprogram the CAR-T cell killing machinery by engineering CAR-T cells to sense-and-respond to intracellular proteins, thereby expanding the repertoire of targetable antigens. Second, suboptimal receptor design and T-cell manufacturing methodologies can limit the anti-tumor efficacy of adoptively transferred CAR-T cells. In order to address this, we dissect the transcriptomes of high- and low-performing CAR-T cells to understand the molecular pathways undermining robust CAR-T cell function, where we identify histone deacetylation as a contributor in driving CAR-T cell dysfunction. We further identify CAR tonic signaling as a guide for rational CAR design and as a druggable signaling pathway that, when minimized, enhances anti-tumor efficacy. Collectively, the work presented in this dissertation provides steps towards outsmarting and outmuscling cancer cells by laying the foundation for reprogramming CAR-T to recognize intracellular antigens and by modulating antigen-independent CAR-T cell signaling pathways for enhanced tumor-killing efficacy.

Pending approval of doctoral thesis committee

Steven J. Bensinger

Junyoung O. Park

Matteo Pellegrini

Yvonne Y. Chen, Committee Chair

University of California, Los Angeles

2022

TABLE OF CONTENTS

LIST OF FIGURES

LIST OF TABLES

LIST OF SUPPLEMENTARY FIGURES

LIST OF SUPPLEMENTARY TABLES

LIST OF SUPPLEMENTARY DATA

Acknowledgements

It is without a doubt that the work shown in the following pages could not have been completed without the mentorship, collaboration, and support from the Chen Lab community, UCLA collaborators, and my friends and family.

First and foremost, I am extremely grateful to my advisor, Prof. Yvonne Y. Chen, for her unfaltering mentorship and support in science and in life. Throughout the past several years, she has been both my biggest critic as well as my most supportive champion. She has embraced this duality of a role with the goal of developing me into a better scientist, thinker, and person – something that I dearly appreciate.

I am also grateful to my doctoral committee advisors, Prof. Steven J. Bensinger, Prof. Junyoung O. Park, and Prof. Matteo Pellegrini for their support, discussions, and collaborations relating to my research. I am thankful for Prof. Bensinger's expert input on lipid metabolism in immune cells. I am thankful for Prof. Park for including me in part of his Metabolism group meetings (learning about metabolism while metabolizing), insightful conversations regarding T-cell metabolism, and collaboration on T-cell metabolomic studies. I am thankful to Prof. Pellegrini for his insight on sequencing analysis-related discussions and for directing the UCLA Collaboratory, a very useful bioinformatics resource that has helped me tremendously.

The collaborative research community at UCLA has enabled me to significantly expand the types of experiments I could perform in my research. I would like to thank Dr. Xinmin Li and the Technology Center for Genomics & Bioinformatics (TCBG) for assistance with RNAseq library preparation and next-generation sequencing (NGS) projects. I would also like to thank Dr. Suhua Feng and Dr. Marco Morselli at the Broad Stem Cell Research Center (BSCRC) High Throughput Screening core for extensive discussions on various NGS library preparation formats, NGS of custom amplicon libraries, and execution of NGS sequencing projects. I am grateful to Dr. Nicolas Rochette at the UCLA Collaboratory for his immense help in setting up a custom NGS analysis pipeline on the UCLA Hoffman2 Cluster. I am also grateful to Katherine Sheu, a former MSTP

student working in Prof. Alex Hoffmann's Lab, for her assistance with VIPER analysis on the CD20 CAR-T cell RNAseq dataset. I would also like to thank Iris Williams and Min Zhou at the UCLA Flow Cytometry Core for their assistance in sorting various cell lines used throughout my projects. I would like to thank Dr. Johanna ten Hoeve-Scott at the UCLA Metabolomics Center for metabolomics assistance. I would also like to thank the veterinary staff at the Division of Laboratory Animal Medicine (DLAM) for taking care of our mice.

The Chen Lab has had the fortune of having wonderful lab neighbors, providing comraderies and last-minute lab reagents in times of need. Shout out to all the graduate students in the Tang, Liao, Segura, and Park Lab in Boelter Hall; I would be remiss to thank the Ribas and Boutros Lab graduate students for welcoming us into CHS. Special thanks to Aliya Lakhani in the Park Lab for extensive discussions on T-cell metabolism and interpretation of metabolomics data.

I am grateful to everyone in the Chen Lab – past and present – for fostering a considerate and collaborative lab environment. I would like to thank Dr. ZeNan Chang, Dr. Eugenia Zah, Dr. Meng-Yin Lin, Dr. Patrick Ho, and Dr. Ximin Chen for serving as role models for success in the Chen Lab. I am especially grateful to Dr. Patrick Ho for spearheading the COVERT project, for always being available for scientific discussions, and for being a great mentor. I am also extremely thankful for Dr. Ximin Chen, who has worn many hats including, but not limited to, mentor, friend, food/snack supplier, and co-author. I'm grateful to Amy Hong for helping me cross the finish line with RNAseq data processing while I was writing my dissertation. I am also thankful for the next generation of PhD students – Amy Hong, Justin Clubb, Tora Gao, and Ryan Shih – for the helpful discussions and for carrying on the torch of advancing CAR-T cell therapies in the Chen Lab. I am also thankful for the comraderies shared with Brenda Ji, our honorary grad student. I am especially thankful for Andrew Hou for having been part of my PhD journey every step of the way (ok, maybe slightly offset by two weeks).

The work shown in this dissertation would not have been doable without a team of strong and willing undergraduate researchers (plus high school student) that I had the fortune of

mentoring. Specifically, I would like to thank Vinya Bhuvan for her passion and dedication towards advancing the COVERT project. I would also like to thank Neha Iyer for her eagerness and readiness to continuously contribute wherever help was needed. I am extremely grateful for Vinya and Neha's help, and their curiosity and passion for research helped provide me with inspiration to persist onwards with research.

I must also thank my village that has provided me with the warmth and support I needed during my PhD journey here at UCLA. I would like to thank George Song, Jason Chen, Elsie Cheng, John Wang, Christina Liu, Thaomi Phuong, and Brice Tanner for making my time in LA more enjoyable with food, sports, and much needed laughter. I would like to thank everyone at the Prunelle House – Kateline Lin, Evan Chang, James Grindell, and George Chang – for always being welcoming, lending an ear whenever asked, while giving me space when needed. You guys are my shi tous. I am extremely grateful to Thaomi Phuong and George Chang, who patiently and gently helped me through rough patches throughout my PhD experience.

Finally, I would like to give my heartfelt thanks to my family. I am grateful to my aunt JJ and uncle Rob for always providing home-cooked food, inviting me over for holidays, and for always making me feel welcome. A home away from home has made the PhD experience much less isolating. I would like to thank my cousin Tiffany for always lending an ear and for providing much-needed life advice. Finally, I would like to express my extreme gratitude for my parents for everything they have done for me. It's hard to coherently put into words how thankful I am to have them. Everything I have accomplished, and hopefully will continue to accomplish, is a would not have been possible if not for their continued support, advice, and love.

Chapter 1 includes excerpts taken from two review paper in press: (1) L.C. Chen and Y.Y. Chen "Outsmarting and outmuscling cancer cells with synthetic and systems immunology", *Current Opinion in Biotechnology* 60:111–118, (2019) and (2) A.J. Hou, L.C. Chen, Y.Y "Navigating CAR-

T cells through the solid-tumor microenvironment", *Nature Reviews Drug Discovery* 20:531–550, (2021).

Chapter 4 contains data and excerpts from a manuscript submission that is undergoing manuscript revision in response to review at the time of this writing: X. Chen & L.C. Chen et al. "Rational protein design boosts CAR-T cell efficacy and reveals non-linear relationship between tonic signaling and CAR-T cell function" (2022).

VITA

EDUCATION

University of California, Los Angeles — Aug. 2016 – Present
Ph.D. Candidate, Chemical & Biomolecular Engineering

University of California, San Diego — Sep. 2012 – June 2016
B.S. Bioengineering, Biotechnology

LICENCES & CERTIFICATIONS

United States Patent and Trademark Office — Feb. 2019 – Present
Patent Agent (Registration #: 77,867)

DOCTORAL RESEARCH PROJECTS

Chen Lab, *UCLA Chemical and Biomolecular Engineering* – Advisor: Yvonne Chen

1. Re-programming T cells to target intracellular antigens
2. Rational engineering of cancer-fighting CAR-T cells to enhance therapeutic potency and durability

Key words: Synthetic biology, cancer immunology, cell-based therapy, systems biology

TECHNICAL SKILLS

- Flow cytometry
- CRISPR gene editing
- Mouse tumor models
- Next-generation sequencing
- Molecular biology
- Python/Bash/R

PUBLICATIONS & PRESENTATIONS

1. X. Chen*, **L.C. Chen***, M. Khericha, A. Lakhhani, X. Meng, E. Salvestrini, N. Iyer, A. Shafer, A. Alag, Y. Ding, D. Nicolaou, J.O. Park, Y.Y. Chen (*denotes equal contribution). Rational protein design boosts CAR-T cell efficacy and reveals non-linear relationship between tonic signaling and CAR-T cell function; *Manuscript under review* (2022).
2. **L.C. Chen** and Y.Y. Chen. Bacteria recycle tumour waste to fuel immune cells. *Nature*, (2021).
3. **L.C. Chen***, A.J. Hou*, Y.Y. Chen (*denotes equal contribution). Getting better mileage with logically primed CARs. *Med*, (2021).
4. A.J. Hou*, **L.C. Chen***, Y.Y. Chen* (*denotes equal contribution). Navigating CAR-T cells through the solid-tumour microenvironment. *Nature Reviews Drug Discovery*, (2021).
5. **L.C. Chen**, A.J. Hou, P. Hou, Y.Y. Chen. Evaluating Cytotoxic Potency of Synthetic Granzyme B Variants via Retroviral Cytotoxicity Assay. **Abstract** and **poster** at the Engineered Immunity & Parker Institute for Cancer Immunotherapy 2019 Retreat, Lake Arrowhead, CA.
6. **L.C. Chen**, A.J. Hou, P. Hou, Y.Y. Chen. Evaluating Cytotoxic Potency of Synthetic Granzyme B Variants via Retroviral Cytotoxicity Assay. **Abstract** and **poster** at the Immunology LA 2019 Conference, Los Angeles, CA.
7. **L.C. Chen**, A.J. Hou, P. Hou, Y.Y. Chen. Evaluating Cytotoxic Potency of Synthetic Granzyme B Variants via Retroviral Cytotoxicity Assay. **Abstract** and **poster** at the Engineering Biology Research Consortium Spring 2019 Retreat, Boston, MA.
8. **L.C. Chen** and Y.Y. Chen. Outsmarting and outmuscling cancer cells with synthetic and systems immunology. *Current Opinion in Biotechnology*, (2019). *Front cover journal feature.

9. **L.C. Chen**, F.H. Hsu, A.Y. Hui, B.L. Schumacher, R.L. Sah. Primary Human Articular Chondrocytes Exhibit Age-Dependent PRG4 Secretion and TGF-β1 Responsiveness. **Abstract** and **poster** at the Orthopaedic Research Society 2016 Annual Meeting, Orlando, FL.

PRIOR RESEARCH EXPERIENCE

Bioengineering Senior Design Team Member **Aug. '15 – June '16**

Systems Biology Research Group, *University of California, San Diego*

- Formulated an *in silico* workflow to identify novel therapeutic targets for cancer metabolism
- Analyzed onco-metabolic mutations using constraint-based analysis on multiple cancer models

Undergraduate Researcher **Mar. '15 – June '16**

Genomics and Systems Biotechnology Lab, *University of California, San Diego*

- Designed and created a semi-rational DNA library for a class of nanobody binders
- Developed a one-step, PCR- and ligation-free method of assembling oligonucleotides

Undergraduate Researcher **Jan. '14 – Sep.'15**

Cartilage Tissue Engineering Lab, *University of California, San Diego*

- Ascertained the effects of TGF–β1 growth factor on PRG4 secretion in primary chondrocytes
- Assisted in the design of a bioreactor for mechanical stimuli on human cartilage tissue

---

TEACHING EXPERIENCE

Teaching Assistant – Molecular Biotechnology for Engineers **Fall 2018, Fall 2019**

Chemical and Biomolecular Engineering Department @ UCLA (CM145/245)

Teaching Assistant – Molecular Biotechnology Laboratory: From Gene to Product **Winter 2019**

Chemical and Biomolecular Engineering Department @ UCLA (CM104D)

MENTORSHIP EXPERIENCE

Graduate Students

- Paul Ayoub (UCLA Pharmacology, PhD student rotation) **Fall 2018**
- Joey Li (UCLA-Caltech MSTP, MD/PhD student rotation) **Summer 2020**
- Ryan Shih (UCLA-Caltech MSTP + MBIDP, MD/PhD student rotation) **Summer 2021**

Undergraduate and High School Students

- Robin Reyes (UCLA Chemical & Biomolecular Engineering) **Spring 2018 – Spring 2019**
- Vinya Bhuvan (UCLA Chemical & Biomolecular Engineering) **Fall 2018 – Spring 2021**
- Neha Iyer (UCLA Bioengineering) **Spring 2019 – Spring 2022**
- Yujung Park (High school student) **Summer 2017, Summer 2018**

LEADERSHIP

Vice Regent **May '14 – May '15**

Theta Tau Professional Engineering Fraternity – Epsilon Delta Chapter, *University of California San Diego*

President **May '13 – May '14**

Learn To Be (non-profit online tutoring organization) – UCSD Chapter, *University of California San Diego*

LANGUAGES

English (native), Chinese (professional working proficiency), Spanish (limited working proficiency), Japanese (elementary proficiency), Taiwanese (native)

Chapter 1. Introduction

Partially adapted, with permissions from (1) L.C. Chen and Y.Y. Chen "Outsmarting and outmuscling cancer cells with synthetic and systems immunology", *Current Opinion in Biotechnology* 60:111–118*,* (2019) and (2) A.J. Hou, L.C. Chen, Y.Y "Navigating CAR-T cells through the solid-tumor microenvironment", *Nature Reviews Drug Discovery* 20:531–550*,* (2021).

Adoptive T cell therapy, or the infusion of disease-targeting T cells as the therapeutic agent, has demonstrated remarkable potential to treat advanced-stage cancers. In this novel treatment paradigm, primary human T cells are genetically modified to express tumor-specific receptors — typically either a chimeric antigen receptor (CAR) or T cell receptor (TCR) — which enable the engineered T cells to mount a tumor-specific immune response when infused into the patient.

In the case of CAR-T cells that target the CD19 antigen expressed in B cells — which became the first gene-therapy product to be approved by the FDA — patients with relapsed or refractory B cell malignancies achieved complete remission rates of up to 90%[1]. However, despite promising outcomes against hematological tumors, adoptive T cell therapy has been much less effective against solid tumors, which comprise the vast majority of cancers. Compared with liquid tumors, solid tumors pose unique challenges to treatment with CAR-T cells. First, high antigen heterogeneity in solid tumors provides them with an effective mechanism of escape from CAR-T cells, which typically encode specificity towards a single antigen target and are thus unable to recognize all cancer cells in the tumor. However, broadening T cell specificity towards multiple antigens increases the risk of on-target, off-tumor toxicity. Second, T cells must also confront highly immunosuppressive tumor microenvironments (TMEs) with cellular, molecular and metabolic profiles that ultimately lead to T cell exhaustion and dysfunction. Furthermore, T cells must also overcome intrinsic pathways of T-cell exhaustion and dysfunction that arise due to non-

productive or excessive stimulation. So far, CAR-T cells have been inadequately equipped to surmount these additional obstacles posed by solid tumors. Throughout this chapter, I highlight and discuss factors that blunt the therapeutic efficacy of CAR-T cells in solid-tumor settings, along with current methods that seek to overcome these hurdles.

Reprogramming T-cell specificity to target cancer

Engineered T cells are programmed to deliver cytotoxic and immunostimulatory outputs upon sensing tumor-associated surface antigens. This is commonly achieved by introducing synthetic receptors that either reroute endogenous signaling pathways or activate orthogonal transgenic programs[2–6]. Here, I introduce several receptor designs that enable major histocompatibility complex (MHC)-independent antigen recognition and logical signal computation in human immune cells.

Interfacing with T cells via endogenous pathways

CARs are synthetic receptors comprised of an extracellular ligand-binding domain fused to an extracellular spacer, transmembrane domain, and the intracellular portion of CD3ζ, which is the dominant signaling domain of the natural T-cell receptor (TCR) complex[2] (**Figure 1-1A, Figure 1-2A**). The highly modular nature of this fusion protein enables user specification of target antigen through the choice of ligand-binding domain, while signaling through the CD3ζ chain couples ligand-binding to an endogenous pathway that results in T-cell activation and polyfunctional outputs, including cytokine production, T-cell proliferation, and target-cell lysis. Second- and third-generation CARs also incorporate co-stimulatory signaling domains in their cytoplasmic tails, resulting in increased T-cell activation upon CAR stimulation[2].

Generalized extracellular molecular sensors (GEMS) are another class of synthetic receptor molecules that interface with endogenous signaling pathways. GEMS consist of extracellular ligand-binding domains fused to the extracellular and transmembrane domains of

erythropoietin receptor (EpoR), followed by endogenous signal-transduction domains on the cytoplasmic end (**Figure 1-1B**)[3]. The EpoR core of GEMS leads to constitutive receptor dimerization, but these pre-formed dimers are spatiotemporally locked, inhibiting downstream signaling[7]. Ligand binding results in the rotation of each receptor chain around its own axis, thereby relieving conformational strain and triggering signaling cascades (**Figure 1-1B**)[3]. GEMS activate distinct signaling pathways depending on the choice of signal-transduction domain. GEMS-responsive promoters, such as JAK/STAT signaling-inducible STAT3 minimal promoters, facilitate inducible transgene expression downstream of ligand binding (**Figure 1-1B**)[3]. GEMS has been used to engineer human embryonic kidney cells (HEK-293T) to sense prostate-specific antigen (PSA) and WEN1.3 immune cells to conditionally secrete IL-10 in response to a RR120, a dye molecule with no endogenous signaling activity[3].

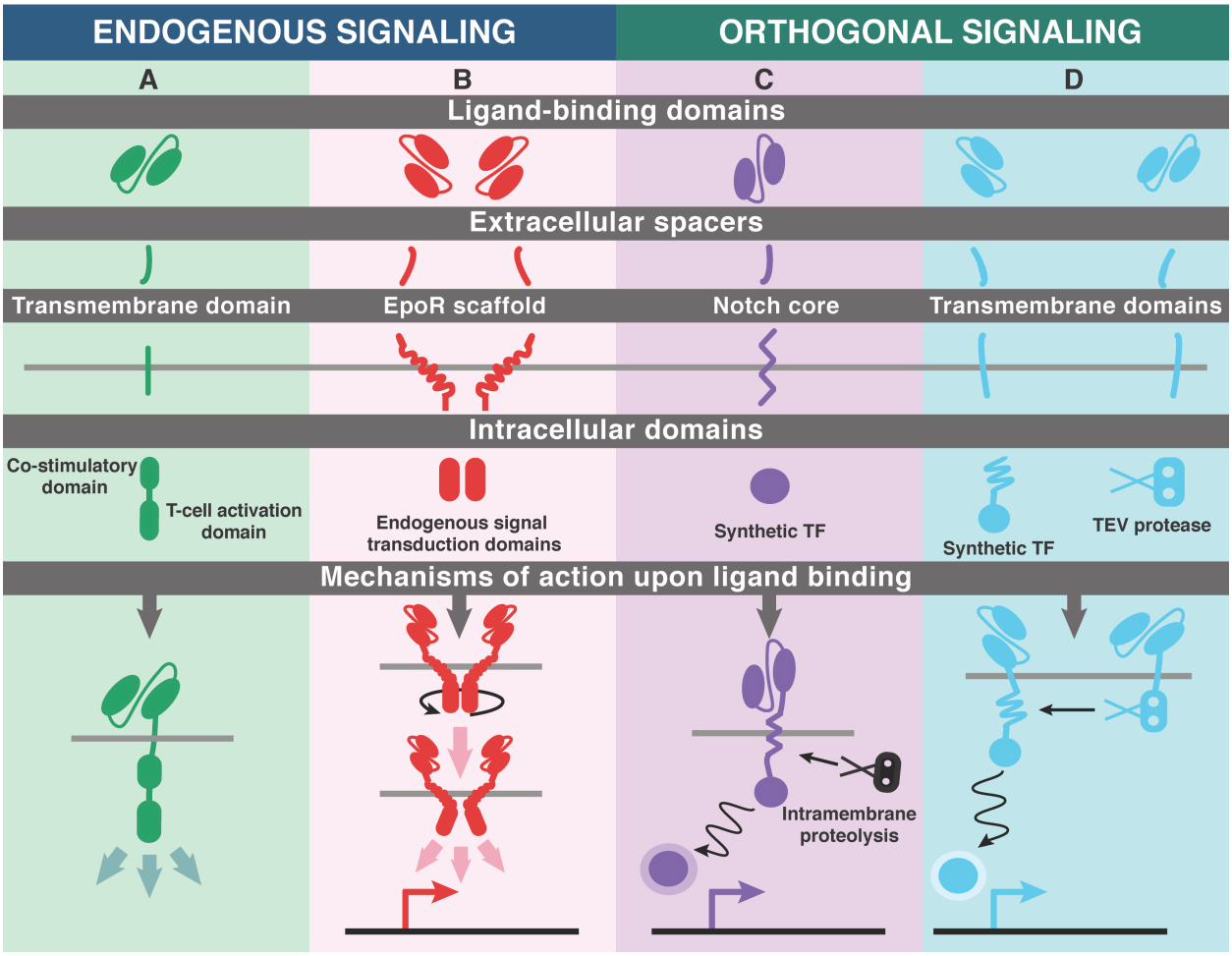

Figure 1-1: Interfacing with T cells using synthetic receptors that rely on endogenous or orthogonal signaling. Core components of a **(A)** second-generation CAR, **(B)** GEMS, **(C)** synNotch, and **(D)** MESA are shown. **(A)** Ligand-binding triggers signaling of a CAR's endogenous intracellular domains, resulting in polyfunctional outputs. **(B)** The EpoR core of GEMS leads to constitutive receptor dimerization in a conformation that inhibits intracellular signaling. Ligand binding results in the rotation of each receptor chain around its own axis, enabling signaling of the intracellular domains and downstream transgene expression from GEMS-responsive promoters. **(C)** Ligand-binding results in intramembrane proteolysis within the Notch core, mediated by sequential proteolysis by a disintegrin and metalloproteinase (ADAM) metalloprotease and the gamma-secretase complex, freeing the synthetic transcription factor for subsequent transgene expression. **(D)** Ligand-binding leads to dimerization of MESA receptors, triggering intracellular *trans*-cleavage, mediated by TEV protease recognition of its cognate cleavage sequence upstream of the synthetic transcription factor. Release of the synthetic transcription factor leads to downstream transgene expression.

Interfacing with T cells via orthogonal signaling

While the use of endogenous pathways requires fewer transgenic components and capitalizes on native signaling, such systems can be affected by crosstalk with other endogenous functions. Receptors that make use of synthetic gene-expression regulation could avoid such confounding factors and enable orthogonal signaling programs. As an example, synthetic Notch (synNotch) receptors—which are comprised of an extracellular ligand-binding domain, a notch core, and an intracellular synthetic transcription factor that is released upon ligand binding—can translate the detection of a user-defined membrane-bound input into the upregulation of a user-defined gene-expression output[4] (**Figure 1-1C**). This system has been used to program primary human T cells to conditionally execute synthetic therapeutic responses (e.g., secrete cytokines or antibodies) upon cancer-cell recognition[8].

An alternative design, termed modular extracellular sensing architecture (MESA), is comprised of two receptor chains, each with an antigen-binding ectodomain fused to an endodomain containing either a tobacco etch virus (TEV) protease or a TEV protease cleavage sequence followed by a synthetic transcription factor[5] (**Figure 1-1D**). Ligand-binding induces dimerization of receptor chains and promotes intracellular *trans*-cleavage, freeing the synthetic transcription factor for transgene expression. Unlike synNotch receptors, the MESA platform could be used to detect soluble ligands.

Collectively, the growing selection of synthetic receptors provides an expanding tool box for the engineering of immune cells to convert an external input into genetically programmed functional outputs. Importantly, the successful application of synthetic receptor systems is contingent upon identification of a suitable target antigen to execute antigen-induced therapeutic programs.

Target antigen choice

Target antigen choice is a major determinant of safety and efficacy for any cell-based therapeutic that relies on receptor-mediated targeting of cancer cells. Synthetic receptors – be it a CAR, TCR, or other synthetic receptor systems – redirects T cell cytotoxicity towards its cognate antigen, irrespective of the identity of the cell that presents the cognate antigen. Consequently, healthy cells that share target-antigen expression are at risk of on-target, off-tumor bystander killing, whereas cancer cells that dynamically regulate target-antigen expression can escape T cell surveillance.

Ensuring tumor specificity

In principle, the ideal tumor antigen should be highly and uniformly expressed on tumor cells but absent on healthy tissue. However, the identification of suitable tumor antigens has been a longstanding challenge, and the vast majority of tumor antigen targets to date, for both hematological and solid malignancies, have shared antigen expression in subsets of healthy cells[9–11] (**Table 1-1**). Consequently, targeting of tumor-associated antigens (TAAs) but not tumor-specific antigens with adoptively transferred T cells carries the risk of on-target, off-tumor toxic effects.

Clinical reports over the years have shown the severities of on-target, off-tumor toxic effects, which range from predictable and clinically manageable to unanticipated and fatal (**Table 1-2**). CAR-T cell therapies targeting the pan-B cell marker CD19 have demonstrated

impressive clinical responses for the treatment of hematological malignancies[12,13], but successful treatment by CD19 CAR-T cells also invariably results in B cell aplasia, which is a predictable consequence of targeting CD19 that can be clinically managed by immunoglobulin transfusion[14].

T cell targeting of other TAAs has similarly led to undesired but clinically tractable adverse events. Melanoma antigen recognized by T cells 1 (MART1) and glycoprotein 100 (gp100) are TAAs expressed not only in melanomas but also in healthy melanocytes in the skin, eyes and ears[15]. Patients with metastatic melanoma who received T cells engineered to express TCRs specific for MART1 or gp100 experienced transient melanocyte toxicity, resulting in damage to skin, eyes or ears that can be treated with steroid applications[15]. Notably, a subset of patients experienced melanocyte toxic effects without appreciable tumor clearance[15], indicating that on-target, off-tumor toxicities can happen even in the absence of robust antitumor response. Patients with metastatic colorectal cancer who received T cells expressing carcinoembryonic antigen (CEA)-targeted TCRs experienced severe transient colitis due to CEA expression on healthy epithelial cells in the gastrointestinal tract, with limited antitumor responses[16]. Similarly, treatment with carboxy-anhydrase IX (CAIX, also known as carbonic anhydrase 9) CAR-T cells in patients with metastatic renal carcinoma resulted in dose-limiting toxicity to the liver and bile duct epithelial cells despite being a first-generation CAR, which is expected to provide limited tumor-killing efficacy[17]. These cases highlight the delicate balance between eliciting potent antitumor activities and preventing severe off-target toxic effects.

In certain clinical studies, unanticipated off-target toxic effects have resulted in life-threatening complications. Melanoma-associated antigens (MAGEs) are cancer testes antigens (CTAs) that are absent from healthy adult tissue but overexpressed in various cancers[18]. However, three of nine patients treated with MAGE-A3-targeted TCR T cells experienced severe neurotoxicity, resulting in two fatalities[18]. This was attributed to cross-reactivity of the MAGE-A3 TCR with unanticipated MAGE-A12 expression in the brain[18]. In a separate MAGE-A3 TCR study, two patients experienced lethal cardiac toxicity due to myocardial damage induced by TCR cross-

reactivity with the protein titin, which is found in myocardium[19,20]. It should be noted that the tested MAGE-A3 TCRs were enhanced for avidity and affinity with the intention of boosting antitumor efficacy, which came at the unfortunate cost of lethal cross-reactivity. Similar unanticipated reactivity to healthy tissue has also been reported in the context of CAR-T cell therapy. A patient receiving human epidermal growth factor receptor 2 (HER2)-targeted CAR-T cells experienced fatal pulmonary toxicity. Histological analysis attributed the toxicity to low HER2 expression in lung cells, which triggered HER2 CAR-T cell activation and led to pulmonary oedema and rapid elevation of serum cytokine levels that triggered cytokine release syndrome (CRS, also known as cytokine storm), ultimately leading to multiorgan failure[21].

Mesothelin has emerged as a promising TAA for solid tumors given its overexpression in various solid tumors and its limited expression in healthy mesothelial cells[22,23]. Clinical trials conducted at multiple institutions have demonstrated minimal on-target, off-tumor toxic effects[24–28]. Despite a favorable safety profile, mesothelin-targeted CAR-T cells have shown limited efficacy in clinical trials as a monotherapy[24–26,28]. Recent clinical data from a phase I trial combining monoclonal antibodies (mAbs) targeting programmed cell death protein 1 (PD1) with intrapleural delivery of mesothelin-targeted CAR-T cells presents encouraging efficacy data with 2 of 14 patients demonstrating complete metabolic response and 5 of 14 patients demonstrating partial response[27].

Given the risk of targeting antigens that are associated with, but not exclusive to, tumor cells, several engineering strategies have been developed to improve the tumor-targeting specificity of CAR-T cells. One strategy is to fine-tune the affinity of CARs to their cognate antigens, such that only tumor cells overexpressing the target antigen are killed while healthy tissue with normal expression levels is spared[29–31]. However, such tuning strategies require a large differential in antigen expression levels between healthy and diseased cell types, or risk a compromise in antitumor efficacy. Furthermore, low-affinity single-chain variable fragment (scFv) sequences may not be readily available for a TAA of interest. Another strategy is to engineer

CARs that target tumor-associated glycopeptide epitopes that stem from mutations that cause aberrant glycosylation[32–35]. Notably, CARs targeting antigens modified with tumor-associated glycan Tn (GalNAcα1-*O*-Ser/Thr) have an innate capacity to recognize other Tn-modified antigens[34]. ScFv protein engineering can further broaden CAR reactivity to various tumor-associated, Tn-modified epitopes[35]. Ultimately, extensive testing of the tolerability of off-tumor toxicity is still necessary to ensure that low TAA or glycopeptide epitope expression by cells essential for survival does not trigger T cell responses to the detriment of healthy tissue.

Multi-input receptors that activate T cells only in the presence of a specific combination of antigens have been developed to increase the tumor-targeting specificity of CAR molecules. Because effective CAR-T cell activation requires both a T cell activation signal and a co-stimulatory signal, splitting the two signals into two receptors that each target a different antigen could enable a higher level of specification, requiring both antigens to be present before triggering a robust T cell response. To do so, second-generation CARs can be split into a first-generation CAR (without co-stimulatory domains) paired with a second, chimeric co-stimulatory receptor (CCR) that comprises an scFv fused to one or more co-stimulatory domains but no CD3ζ chain (**Figure 1-2B**). The first-generation CAR provides only the T cell activation signal, and the CCR provides only the co-stimulatory signal. The antigens for each receptor (such as CD19 and prostate-specific membrane antigen (PSMA)) must both be present to trigger robust CAR-T cell response, thus yielding Boolean AND-gate logic[36].

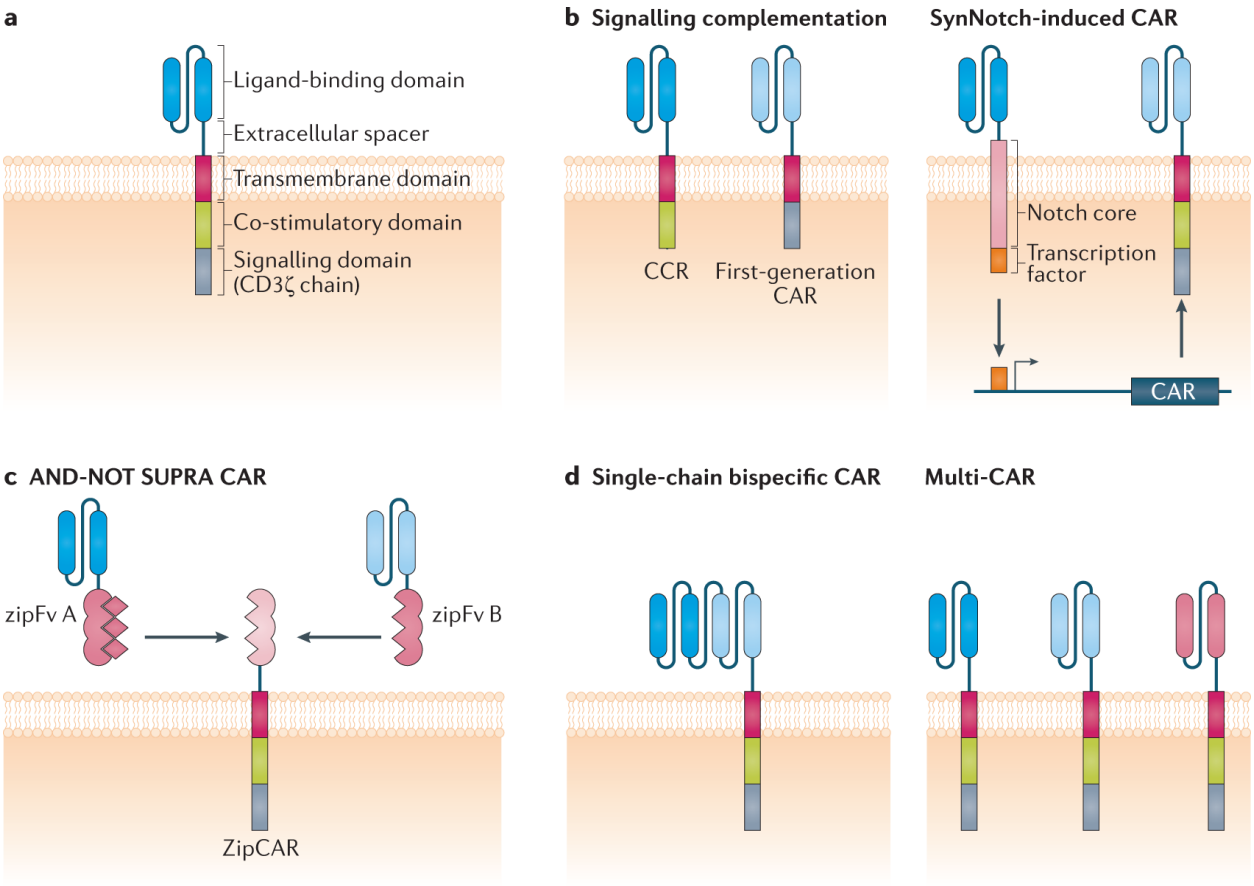

Figure 2-1: CARs are synthetic modular receptors with programmable antigen recognition. (**A**) Chimeric antigen receptors (CARs) — from N terminus to C terminus — include a ligand-binding domain (typically an scFv), extracellular spacer, transmembrane domain and intracellular signalling domains consisting of one or two co-stimulatory domains (typically CD28 or 4-1BB) for second- and third-generation CARs, respectively, and an activation domain (typically CD3ζ). Target specificity can be programmed by incorporating different ligand-binding domains. (**B**) AND-gated antigen recognition can be programmed by signal complementation, or alternatively, by ligand-induced CAR expression, to confer greater specificity. In signal complementation, each of two receptors must engage its own cognate antigen for a full T cell signalling response to occur. Given that T cells require both CD3ζ signalling and co-stimulation to be fully activated, signal complementation can be achieved by pairing a CCR, which lacks ζ-chain signalling, with a first-generation CAR, which lacks co-stimulatory signalling. In synNotch-induced CAR expression, a constitutively expressed synthetic Notch (synNotch) receptor triggers CAR expression upon cognate antigen binding. The target antigen of the CAR must also be present to activate the engineered T cells. For example, EpCAM and B7-H3-targeting synNotch receptors have both been engineered to trigger downstream expression of inactive tyrosine kinase transmembrane receptor (ROR1)-targeting CARs. (**C**)Enhanced specificity through AND-NOT-gated antigen recognition can be achieved through the split, universal and programmable (SUPRA) CAR platform, which consists of zipFvs (scFv sequences fused to leucine zippers) and T cells expressing zipCARs (CARs with extracellular domains consisting of a leucine zipper). AND-NOT-gated computation is achieved with a zipCAR and two zipFv sequences, whereby a HER2-targeting zipFv can pair either with the zipCAR to trigger downstream T cell activation, or with an AXL-targeting zipFv, which acts as a competitive inhibitor for zipCAR binding. When target cells express only HER2 and not AXL, the HER2 zipFv can bind to the zipCAR and trigger downstream

T cell signalling. However, when target cells express both HER2 and AXL, the AXL zipFv outcompetes the zipCAR for binding to the HER2 zipFv, and T cells remain unstimulated. (**D**) To combat antigen heterogeneity, CAR-T cells can be programmed to target multiple tumour antigens. This can be achieved either by engineering a single-chain bispecific CAR that encodes two ligand-binding domains in a single receptor, or by co-expressing multiple receptor chains in a single T cell.

Another AND-gate strategy can be implemented by the use of the synthetic Notch (synNotch) receptor system, which requires lentiviral integration of two transgenes — a synNotch receptor expressed from a constitutive promoter and a CAR expressed from an inducible promoter. The synNotch receptor consists of an extracellular ligand-binding domain (such as a CD19-binding scFv), a transmembrane domain derived from the Notch receptor and an orthogonal transcription factor (such as the transcriptional activator fusion protein Gal4–VP64), which is released via proteolytic cleavage upon ligand binding[8] (**Figure 1-2B**). When bound to its cognate ligand (such as CD19), the synNotch receptor releases its transcription factor to induce transcription of the CAR. The CAR protein can subsequently trigger T cell activation upon binding to its own, separate cognate antigen (such as inactive tyrosine kinase transmembrane receptor 1 (ROR1)[8,37]. Unlike the CAR–CCR combination, which requires simultaneous recognition of antigens A and B, the synNotch system is a sequential AND-gate in which the synNotch receptor recognizes antigen A prior to CAR expression and recognition of antigen B. The synNotch system has been shown to reduce toxicity when the off-tumor target is spatially segregated from the intended tumor cells, but remains vulnerable to off-tumor toxicity when healthy cells expressing antigen B are co-localized with target cells expressing antigen A[37]. A recent variation of the synNotch platform takes advantage of this collateral-damage effect to enable a 'priming' mechanism that overcomes antigen heterogeneity in glioblastoma (GBM)[38]. T cells are engineered to express an anti-epidermal growth factor variant III (EGFRvIII) synNotch receptor, which drives the expression of a bispecific CAR targeting ephrin-A2 (EphA2) and interleukin-13 receptor subunit alpha-2 (IL13Rα2). EGFRvIII is GBM-specific but not uniformly expressed on GBM cells, therefore susceptible to antigen escape. EphA2 and IL13Rα2 are expressed on the

vast majority of GBM cells but are also found on healthy tissue, therefore susceptible to off-tumor toxicity. In this system, presence of EGFRvIII in a subset of GBM cells can prime the expression of the EphA2/IL13Rα2 CAR, and the CAR-T cells can then direct kill of all GBM cells (both EGFRvIII+ and EGFRvIII–) that are colocalized with the T cells. These synNotch/CAR-T cells were shown to eliminate GBM patient-derived xenografts (PDXs) that are heterogeneous in EGFRvIII expression, while restricting the activity of the EphA2/IL13Rα2 CAR to the brain to minimize potential off-tumor toxicity[38].

In addition to AND-gate logic, CARs can increase targeting specificity by triggering T cell activation only in the presence of a TAA and not in the presence of an antigen expressed by healthy cells (Boolean AND-NOT logic)[39]. One method to achieve AND-NOT logic is through the split, universal and programmable (SUPRA) CAR system[40], in which T cells are engineered to express a 'zipCAR' comprising a leucine zipper ectodomain fused to transmembrane and intracellular signaling domains. The zipCARs, which lack ligand-binding domains, must be reconstituted with exogenous zipFv proteins — scFvs fused to a matching leucine zipper — to enable T cell activation in the presence of a TAA. One could simultaneously administer a second class of zipFv molecules designed to compete against the zipCAR for binding to the first zipFv, to prevent the reconstitution of functional CARs in the presence of self-antigens, thus achieving AND-NOT Boolean logic[40] (**Figure 1-2C**).

The AND or AND-NOT gate designs described above require that both input signals be present on the target cell surface, which limits the repertoire of targetable antigens. Cytoplasmic oncoprotein verifier and response trigger (COVERT) molecules are engineered granzyme B molecules fused to an N-terminal inhibitory peptide sequence that is proteolytically removed by tumor-associated intracellular proteases. CAR-T cells equipped with COVERT molecules recognize a surface antigen and initiate the delivery of COVERT proteins into the target cell. Once inside the target cell, COVERT proteins are converted into active granzyme B if, and only if, the cognate tumor-associated protease is present. Active granzyme B triggers target-cell apoptosis

through the proteolytic activation of caspases or through the cleavage of substrates that activate mitochondrial and DNA damage pathways[41]. Therefore, only target cells that express both a surface antigen recognizable to the CAR and an intracellular protease recognizable to the COVERT would be subject to killing[42]. Importantly, T cells equipped with COVERT molecules are able to target intracellular proteases without the need for antigen presentation by the major histocompatibility complex (MHC).

Although AND or AND-NOT-based Boolean logic strategies can increase targeting specificity, they must also contend with a number of limitations. These limitations include an increased risk of tumor escape as the elimination of just one of the two or more inputs required for T cell recognition would be sufficient to protect tumor cells from detection, as well as the necessity for multi-component expression, which reduces transduction efficiency and genetic stability. Emerging strategies have enabled incorporation of Boolean AND-gate logic into single CAR molecules. For example, Boolean AND-gate logic can be achieved with a CAR that targets the Tn glycoform of mucin 1 (Tn-MUC1)[33]. Tumor cells need to both express TAA MUC1 and harbor mutations that lead to aberrant Tn glycosylation in order to be recognized by Tn-MUC1 CAR-T cells. Another strategy incorporates Boolean AND-gate logic by expressing CARs under hypoxia, a prevalent characteristic of the TME[43]. Hypoxia-induced CAR expression can be accomplished through CAR transcription from a hypoxia-inducible promoter[44] or through the C-terminal fusion of the oxygen-dependent degradation domain to the CAR[45].

Intracellular targets and neoantigens

Intracellular antigens presented by MHC molecules can expand the repertoire of targetable antigens beyond the surface proteome. Wilms' tumor antigen 1 (WT1) is an intracellular oncoprotein overexpressed in acute myeloid leukemia (AML), and it has been successfully targeted by T cells expressing WT1-specific TCRs[46,47]. Endogenous T cells undergo thymic self-selection, a process that selects against autoimmunity by depleting T cells bearing TCRs that bind

strongly to self-antigens derived from endogenous proteins. As WT1 is an endogenous protein, most of the WT1-specific TCRs isolated from patients had low binding affinity to MHC-presented WT1[46]. Screening of multiple donors enabled the identification of a high-affinity WT1-specific TCR, which specifically recognizes WT1 peptide fragments presented by the human leukocyte antigen A*201$^+$ (HLA-A2) MHC subtype. In one clinical trial, patients with AML who had undergone allogeneic hematopoietic cell transplantation received prophylactic treatment with donor-derived CD8$^+$ T cells expressing the WT1-specific TCR, with the aim of increasing graft-versus-leukemia effect through WT1 recognition. The treatment resulted in relapse-free survival of all patients during the evaluation period of the trial[47]. MAGE family members are another example of intracellular proteins presented by MHC molecules. T cells expressing a MAGE-A4-specific TCR, isolated from a cytotoxic lymphocyte clone, were well tolerated by patients, although seven of the ten patients who received adoptively transferred T cells developed progressive disease during the study period, suggesting limited efficacy[48]. Although increasing TCR-binding affinity can potentially increase the antitumor response, it can come at the cost of unanticipated cross-reactivity against healthy cells that share low expression of the peptide–MHC (pMHC) target[18–20].

pMHC complexes presenting intracellular antigens can also be targeted by antibody-derived moieties, bypassing the need to isolate TCR sequences from endogenous pMHC-reactive T cells. For example, pMHC-targeting antibodies or scFvs can be obtained by screening phage display libraries, and the identified ligand-binding sequence can be incorporated into a CAR[49,50], with the caveat that this grafting process can sometimes alter the ligand-binding property of the scFv. For example, a high-affinity antibody isolated for the New York esophageal squamous cell carcinoma 1 (NY-ESO-1) antigen through phage display was found to lose its specificity in a CAR format, a result attributed to excessive CAR binding to HLA-A2[49]. Rational engineering of the antigen-binding fragment (Fab) resulted in minimized interactions with HLA-A2, which improved CAR specificity but reduced its binding affinity to NY-ESO-1. Ultimately, the modified CAR-T cells did not effectively eradicate the tumors owing to insufficient signal strength provided by the low-

affinity CAR[49]. Such experiences underscore the need to closely couple screening methods with the final implementation format to ensure translatability of the screening results to the application of interest.

Neoantigens, which are novel epitopes generated through patient-specific tumor mutations, can be a source of tumor-specific targets for T cell therapy. Neoantigens can be computationally predicted following whole-exome sequencing of tumor biopsies[51]. Although bioinformatics algorithms can robustly identify somatic mutations, predictions for processing and display of neoantigen epitopes by MHC molecules remains an active area of research[51]. For instance, putative neoantigens are often ranked by the predicted binding affinity between the neoantigenic peptide and the MHC molecule[52,53], but neoantigen-reactive T cell profiling from patients responding to anti-PD1 therapy showed that neoantigen reactivity only loosely correlates with the predicted binding affinity between the neoantigenic peptide and the MHC molecule[54]. Despite challenges associated with neoantigen prediction, personalized neoantigen vaccines have been successful at expanding diverse neoantigen-reactive T cells from patients with melanoma[55,56]. Administration of synthetic peptide-based neoantigen vaccines resulted in tumor regression without severe autoimmune toxicity in patients with melanoma, highlighting the appeal of targeting neoantigens in the form of vaccines[56].

Neoantigen-specific T cells can be isolated from tumor-infiltrating lymphocytes (TILs) or generated through transgenic expression of neoantigen-reactive TCRs. Because TILs are often found to possess differentiated and exhausted phenotypes[57], they may be less effective at exerting antitumor control in light of emerging evidence that shows that less-differentiated T cells have a higher capacity for mediating tumor control[58]. However, neoantigen-reactive TCRs can be transgenically expressed in less-differentiated T cell subsets to potentiate stronger antitumor responses, but the isolation and characterization of neoantigen-reactive TCRs is challenging, given the rarity of naturally occurring tumor-reactive T cells. As such, the identification of neoantigen-reactive TCRs is an active area of research, and has been reviewed by Yamamoto

and colleagues[59]. Recent work by Peng et al.[54] addressed this challenge by establishing a sensitive and streamlined approach for capturing, characterizing and sequencing the TCR of neoantigen-specific patient T cells. Neoantigen-based therapies are a promising approach for cancers with high tumor mutational burden[60], but remain challenging for cancers with low mutational burden given that only a small subset of somatic mutations generate T cell-reactive neoepitopes[61,62].

Overcoming T-cell exhaustion and dysfunction

Although significant advances have been made in the design of synthetic receptors and therapeutic outputs, a robust T-cell chassis remains an indispensable prerequisite for the success of engineered T cells in eliminating cancer. In the context of adoptive T-cell therapy, T cells are typically isolated from patients, genetically modified, expanded *ex vivo*, and re-infused back into the patient. However, T cells harvested from patients are heterogeneous with respect to important properties that contribute to anti-tumor efficacy[58]. This heterogeneity in T-cell quality likely plays a major role in the disparity of clinical outcomes observed across patients and across CAR-T cell therapy trials[13,63–65].

Broadly speaking, two categories of approaches may be taken to generate more uniform, high-performing T-cell products. First, one could attempt to identify and generate therapeutic products from specific T-cell subtypes with higher anti-tumor potential. Second, if the mechanism of T-cell dysfunction is well understood, one could attempt to introduce genetic or pharmaceutical interventions to prevent dysfunction. Multi-omics data comprised of transcriptomics, proteomics, epigenomics, and metabolomics have been integrated on a systems-level for deep immune profiling of functional anti-tumor T-cell phenotypes, leading to testable hypotheses and clinically translatable findings for obtaining robust therapeutic T-cell chassis (**Figure 1-3**)[65–68].

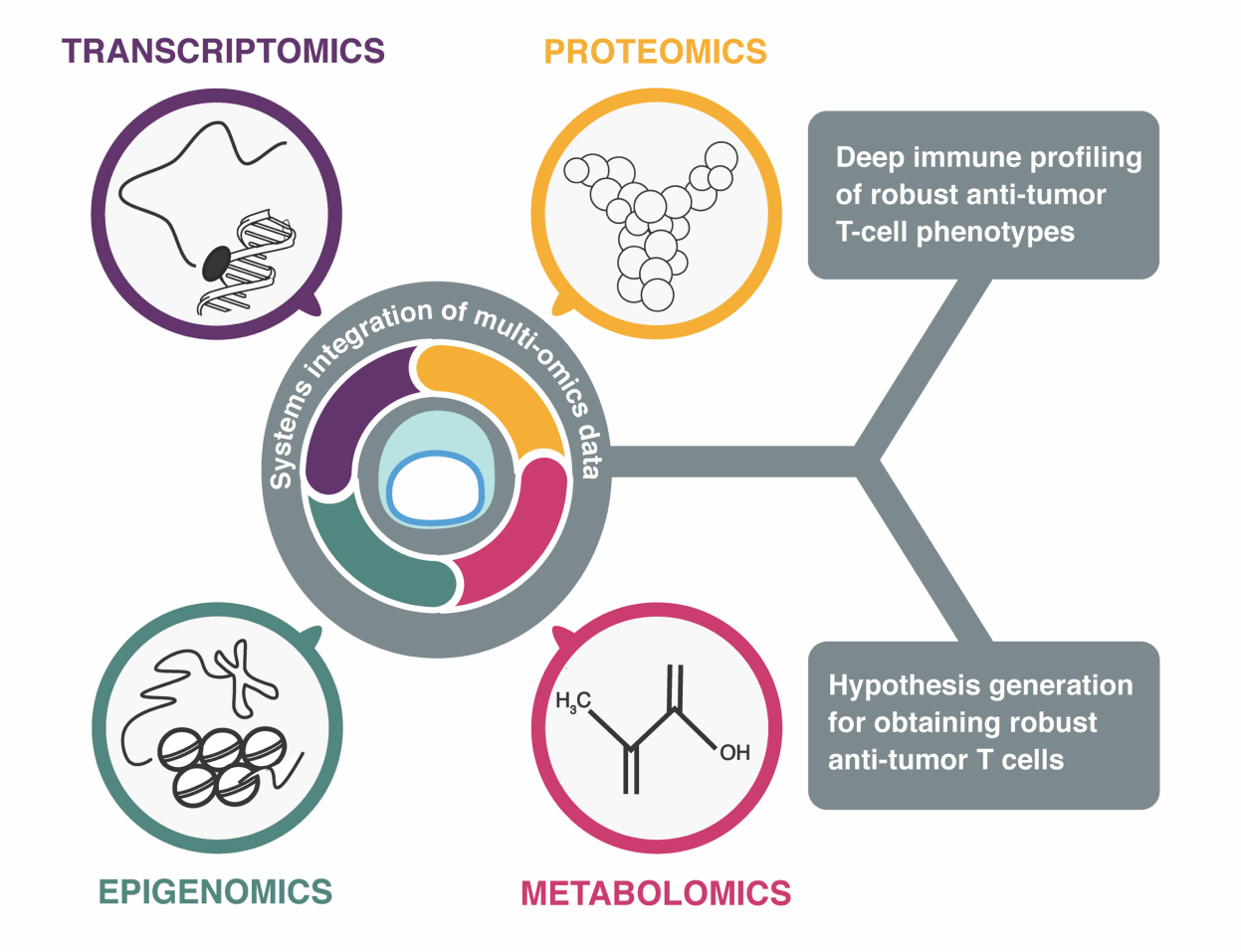

Figure 1-3: Systems-level integration of multi-omics data enables deep immune profiling of functional anti-tumor T cell phenotypes.

T cell exhaustion can be broadly characterized by dysfunction of effector responses, sustained co-inhibitory receptor expression, and reprogrammed transcriptional and epigenetic states[69]. In particular, T cell exhaustion has more recently been defined by the remodeling and plasticity of the epigenetic landscape[70,71]. The development of an assay for transposase-accessible chromatin (ATAC)-seq has enabled tracking of the epigenomic remodeling trajectory of the progression from naive to exhausted T cells at single-cell resolution. For instance, ATAC-seq analysis revealed that early progression towards exhaustion is associated with increased accessibility of nuclear receptor subfamily 4 group A member 1 (NR4A1) motifs, and further progression towards terminal exhaustion is associated with increased accessibility of cis-

elements proximal to the TOX gene[71]. Several transcription factors have also been identified as drivers of T cell exhaustion, such as TOX, which is now recognized as a crucial transcription factor driving the epigenetic remodeling associated with exhausted T cells[72–75]. The NR4A transcription factor family as well as protein tyrosine phosphatase non-receptor type 2 (PTPN2) have also been identified as transcriptional drivers of CD8+ T cell exhaustion[76–78]. Transcription factor T cell factor 1 (TCF1) has also emerged as a marker of stemness among 'progenitor exhausted' CD8+ T cells that dictate the fate of T cells into terminal effectors or exhausted T cells[79–81].

In light of the increasing understanding of T cell exhaustion biology, genetic engineering strategies have been developed to reinvigorate and potentiate CAR-T cell responses. For instance, recent studies reported that CAR-T cells with triple knockout of *Nr4a1*, *Nr4a2* and *Nr4a3* show improved tumor control and reduced exhaustion in mice bearing melanoma tumors[76]; genetic ablation of *Ptpn2* improves antitumor immunity in murine colon adenocarcinoma, mammary carcinoma and melanoma tumor models[77,78]; and overexpression of transcription factor AP-1 (encoded by *JUN*) enhances CAR-T cell resistance to exhaustion, thereby improving antitumor function[82]. Tempering CAR signaling strength through the rational modulation of CD3ζ immunoreceptor tyrosine-based activation motifs (ITAMs) has also been shown to enhance CAR-T cell potency by reducing T cell exhaustion[83]. Finally, therapies combining CAR-T cells with immune checkpoint inhibitors have also been successful at counteracting T cell exhaustion in mouse models of pleural mesothelioma, leukemia, melanoma and ovarian cancer[84,85]. CAR-T cell combination therapies have been comprehensively reviewed elsewhere[86].

Predictive biomarkers of therapeutically robust T cells

While the previous studies dissected gene modules associated with T-cell dysfunction, Fraietta et al. reported the identification of biomarkers of functionally superior T-cell subpopulations for CD19 CAR-T cell therapy[65]. The research team correlated transcriptomic data

on clinically manufactured CD19 CAR-T cells with the clinical outcome of chronic lymphocytic leukemia (CLL) patients treated with those T cells. Results identified $CD8^+CD27^+CD45RO^-$ T cells prior to *ex vivo* expansion and $CD8^+CD27^+PD1^-$ T cells in the post-expansion, pre-infusion product as strong predictors of positive clinical response[65]. Notably, two independent computational algorithms for analyzing high-dimensional flow-cytometry data[87,88] as well as *in vivo* experiments validated the proteomic and transcriptomic analyses[65].

Maintaining T cell metabolic fueling

Aside from cellular mediators of immune suppression, the metabolic profile of the TME is highly unconducive to antitumor immunity. Effective CAR-T cell responses involve the proliferation of CAR-T cells, secretion of cytokines and killing of tumor cells — all of which are metabolically demanding tasks. Therefore, the metabolic fueling of CAR-T cells in the TME is imperative to sustaining the energetic requirements for an effective antitumor response. Both intrinsic and extrinsic factors affect CAR-T cell metabolism in the TME and consequently the therapeutic capacity of CAR-T cells (**Figure 1-4**).

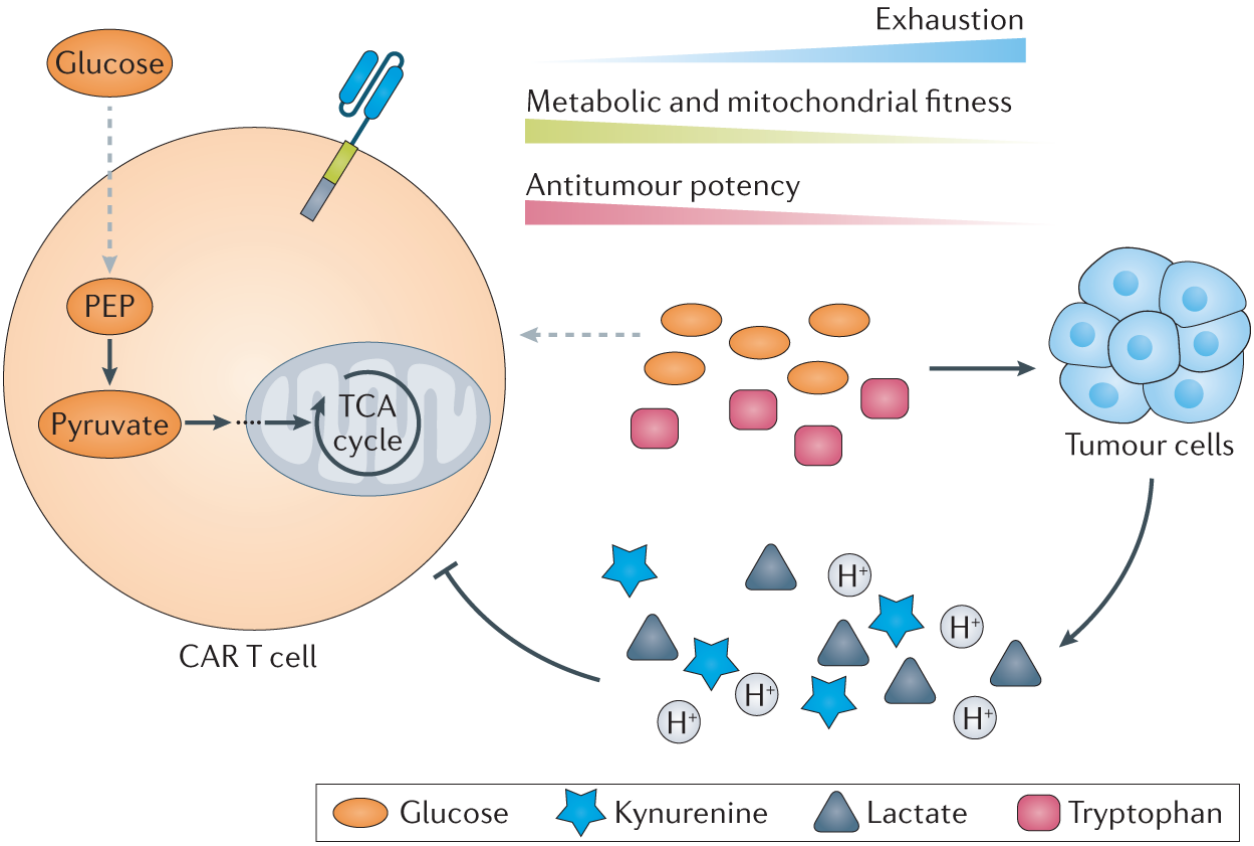

Figure 1-4. CAR-T cells face intrinsic and extrinsic metabolic challenges in the tumour microenvironment. The potency of CAR-T cells can be limited by both intrinsic and extrinsic metabolic factors in the tumour microenvironment (TME). Exhausted T cells in the TME, which have poor antitumour function, are found to be impaired in glycolytic and mitochondrial metabolism and mitochondrial function necessary to mount effective antitumour CAR-T cell responses. Tumour cells can out-compete CAR-T cells for nutrients that are essential for effective CAR-T cell activation, such as glucose and tryptophan, in the TME. Furthermore, metabolites secreted by tumour cells, such as lactic acid and kynurenine, can directly suppress CAR-T cell function by inhibiting lactic acid export by effector T cells and exerting anti-proliferative and cytotoxic effects against effector T cells, respectively. PEP, phosphoenolpyruvate; TCA, tricarboxylic acid.

Competition for metabolic resources in an already nutrient-poor niche is a challenge for CAR-T cells in the TME. Cancer cells often have dysregulated cellular metabolism to support oncogenic growth[89]. One well-characterized feature is the 'Warburg effect', in which cancer cells primarily rely on aerobic glycolysis over the more energetically efficient mitochondrial oxidative phosphorylation to sustain biomass production[90]. As such, tumor cells are able to outcompete T cells for glucose in the TME[91]. Because T cell activation involves rapid induction of aerobic

glycolysis[92], and a glycolytic T cell metabolic signature is linked to increased effector T cell function[93,94], glucose-limited CAR-T cells are unable to function as effectively in the TME. Glucose deficiency in T cells leads to phosphoenolpyruvate (PEP) insufficiency, resulting in a dampening of TCR signaling and effector responses, which can be remedied by PEP supplementation[94]. Acetate supplementation can also reinvigorate IFNγ expression in glucose-restricted T cells[95]. Small-molecule glycolytic inhibitors have also been able to improve responses to checkpoint inhibitor immunotherapy[96,97].

Exhausted T cells have metabolic profiles characterized by suppressed mitochondrial respiration, decreased glucose uptake and glycolytic flux, and impaired mitochondrial function[92,98,99]. Overexpression of peroxisome proliferator-activated receptor-γ coactivator 1α (PGC1α) can improve the metabolic fitness of T cells, thereby resisting T cell exhaustion[92,98,100]. Treatment with mitochondria-targeted antioxidants can restore $CD8^+$ effector T cell function by counteracting the disruption of mitochondrial activity[99,101,102]. Another T cell-intrinsic metabolic constraint is the post-translational impairment of enolase 1 through mechanisms that have yet to be ascertained, which results in the inability to generate PEP and the downstream glycolytic metabolite pyruvate, and subsequent inhibition of effector T cell functions[103]. Glycolytic activity required for effector T cell function can be rescued through the overexpression of phosphoenolpyruvate carboxykinase 1 (PCK1)[94], which converts oxaloacetate into PEP, or through exogenous supplementation of PEP or pyruvate[103]. Another metabolic feature that represses T cell antitumor capacity is the upregulation of sphingosine kinase 1 (SPHK1) in TILs, which polarizes T cells towards the immunosuppressive T_{reg} cell phenotype by acting through the SPHK1–sphingosine 1-phosphate (S1P)–peroxisome proliferator-activated receptor-γ (PPARγ) axis[104]. Furthermore, lipolysis is important for memory T cell development[105] but is suppressed by PPARγ-mediated transcriptional activity, which is activated by SPHK1-generated S1P in TILs[104]. Suppression of the SPHK1–S1P–PPARγ axis through the genetic ablation of *Sphk1* or *Pparg* improved in vivo antitumor control in pre-clinical melanoma mouse models[104].

Extrinsic metabolic factors that limit CAR-T cell efficacy include the presence of immunosuppressive metabolites in the TME. One example is the indoleamine 2,3-dioxygenase (IDO)–tryptophan–kynurenine axis, which suppresses T cell effector function through multiple mechanisms[106]. On the one hand, tryptophan depletion in the TME due to nutrient competition prevents effective mechanistic target of rapamycin (mTOR) function and consequently T cell activation; at the same time, tryptophan conversion into kynurenine by IDO directly suppresses effector T and NK cells while recruiting and activating MDSCs[106]. On the other hand, increased kynurenine to tryptophan ratio in patients receiving anti-PD1 therapy correlated with poor patient survival[107]. However, combination therapy using an IDO1 inhibitor (epacadostat) and a PD1 inhibitor (pembrolizumab) did not improve upon pembrolizumab monotherapy in a phase III clinical trial[108]. As an alternative approach, infusion of PEGylated kynureninase, which can directly degrade kynurenine, synergized with checkpoint inhibitor therapy in a syngeneic mouse model[109]. Direct modulation of the IDO–tryptophan–kynurenine axis by engineered T cells remains an intriguing possibility to be explored.

Adenosine is another immunosuppressive metabolite present in the TME that can be generated through the catalysis of extracellular ATP by ectoenzymes CD39 and CD73, which are expressed by tumor cells, immunosuppressive immune cells and various stromal cell types[110–112]. Genetic ablation of adenosine receptors A_1 and A_{2A} in HER2 CAR-T cells and systemic administration of pharmacological A_{2A} receptor antagonists enhanced antitumor responses in fibrosarcoma and breast cancer syngeneic mouse models[113]. Moreover, systemic administration of pharmacological antagonists targeting adenosine receptors A_1 and A_{2A} synergized with anti-PD1 therapy, leading to striking improvements in antitumor efficacy of CAR T cells compared with CAR-T cells paired with adenosine receptor inhibition alone[113].

Lactate, a metabolite present at elevated levels in the TME owing to increased secretion by metabolically hyperactive tumor cells, inhibits lactate export by effector T cells[114], dampens T

cell signaling mediated by nuclear factor of activated T cells (NFAT)[115] and diminishes lactate dehydrogenase-mediated NAD recycling[116], whereas it preferentially activated expansion of T_{reg} cells, which does not depend on heightened glycolysis[116]. Tumor-cell-secreted lactic acid can also polarize macrophages towards an immunosuppressive M2 phenotype[117]. Furthermore, the acidic TME caused by lactic acid secretion also directly contributes to the blunting of effector T cell functions by reducing the production of cytokines, perforin and to a lesser extent granzyme B, which can be partially reversed by neutralizing intratumoral acidity through treatment with proton pump inhibitors[118] or bicarbonate therapy[119]. The myriad of ways in which metabolism directly affects T cell fitness suggests that reprogramming T cells to calibrate their metabolic fluxes — which can be accomplished via both genetic and pharmaceutical means — may be a fruitful approach to enhancing T cell function in the TME[120,121].

Moving forward

Advances in adoptive T-cell immunotherapy have opened up the possibility of treating a broad spectrum of refractory cancers, spearheaded by the clinical success of anti-CD19 CAR-T cell therapies. However, major challenges must be overcome before adoptive T-cell immunotherapy can be effectively used to target the majority of tumors. In the remaining chapters of this dissertation, I describe cellular engineering strategies to develop smarter and stronger next-generation CAR-T cells. I first introduce an engineering framework in Chapter 2 that tackles challenges associated with target antigen choice by engineering T cells to target intracellular antigens; here, we aimed to enable smarter T-cell recognition of cancer cells by reimagining how T cells kill. Next, I delve into the analysis of functionally divergent high- and low-performing CAR-T cells with the objective of uncovering potent T-cell subtypes and drivers of intrinsic CAR-T cell dysfunction in Chapter 3. I collaborated with a senior PhD student, Ximin Chen, on a project where my conceptions towards rational CAR protein design significantly improved *in vivo* CAR-T cell efficacy in Chapter 4; in particular, I investigate how differences in antigen-independent CAR-T

cell signaling impacts *in vivo* tumor-killing efficacy. Collectively, my dissertation leverages synthetic and systems biological methods towards advancing CAR-T cell therapy by enabling T cells to outsmart and outmuscle cancer cells.

REFERENCES

1. Maude, S. L. *et al.* Chimeric Antigen Receptor T Cells for Sustained Remissions in Leukemia. *N. Engl. J. Med.* **371**, 1507–1517 (2014).
2. Sadelain, M., Brentjens, R. & Rivière, I. The Basic Principles of Chimeric Antigen Receptor Design. *Cancer Discov.* **3**, 388 LP – 398 (2013).
3. Scheller, L., Strittmatter, T., Fuchs, D., Bojar, D. & Fussenegger, M. Generalized extracellular molecule sensor platform for programming cellular behavior. *Nat. Chem. Biol.* **14**, 723–729 (2018).
4. Morsut, L. *et al.* Engineering Customized Cell Sensing and Response Behaviors Using Synthetic Notch Receptors. *Cell* **164**, 780–791 (2016).
5. Schwarz, K. A., Daringer, N. M., Dolberg, T. B. & Leonard, J. N. Rewiring human cellular input–output using modular extracellular sensors. *Nat. Chem. Biol.* **13**, 202 (2016).
6. Rapoport, A. P. *et al.* NY-ESO-1–specific TCR–engineered T cells mediate sustained antigen-specific antitumor effects in myeloma. *Nat. Med.* **21**, 914 (2015).
7. Seubert, N. *et al.* Active and Inactive Orientations of the Transmembrane and Cytosolic Domains of the Erythropoietin Receptor Dimer. *Mol. Cell* **12**, 1239–1250 (2003).
8. Roybal, K. T. *et al.* Engineering T Cells with Customized Therapeutic Response Programs Using Synthetic Notch Receptors. *Cell* **167**, 419-432.e16 (2016).
9. Hinrichs, C. S. & Restifo, N. P. Reassessing target antigens for adoptive T cell therapy. *Nat. Biotechnol.* **31**, 999–1008 (2013).
10. Rosenberg, S. A. Finding suitable targets is the major obstacle to cancer gene therapy. *Cancer Gene Ther.* **21**, 45–47 (2014).
11. Yu, J. X., Upadhaya, S., Tatake, R., Barkalow, F. & Hubbard-Lucey, V. M. Cancer cell therapies: the clinical trial landscape. *Nat. Rev. Drug Discov.* (2020) doi:10.1038/d41573-020-00099-9.

12. Davila, M. L. *et al.* Efficacy and Toxicity Management of 19-28z CAR T Cell Therapy in B Cell Acute Lymphoblastic Leukemia. *Sci. Transl. Med.* **6**, 224ra25-224ra25 (2014).
13. Lee, D. W. *et al.* T cells expressing CD19 chimeric antigen receptors for acute lymphoblastic leukaemia in children and young adults: a phase 1 dose-escalation trial. *The Lancet* **385**, 517–528 (2015).
14. Sadelain, M., Brentjens, R., Rivière, I. & Park, J. CD19 CAR Therapy for Acute Lymphoblastic Leukemia. *Am. Soc. Clin. Oncol. Educ. Book* e360–e363 (2015) doi:10.14694/EdBook_AM.2015.35.e360.
15. Johnson, L. A. *et al.* Gene therapy with human and mouse T-cell receptors mediates cancer regression and targets normal tissues expressing cognate antigen. *Blood* **114**, 535–546 (2009).
16. Parkhurst, M. R. *et al.* T Cells Targeting Carcinoembryonic Antigen Can Mediate Regression of Metastatic Colorectal Cancer but Induce Severe Transient Colitis. *Mol. Ther.* **19**, 620–626 (2011).
17. Lamers, C. H. J. *et al.* Treatment of Metastatic Renal Cell Carcinoma With Autologous T-Lymphocytes Genetically Retargeted Against Carbonic Anhydrase IX: First Clinical Experience. *J. Clin. Oncol.* **24**, e20–e22 (2006).
18. Morgan, R. A. *et al.* Cancer Regression and Neurological Toxicity Following Anti-MAGE-A3 TCR Gene Therapy. *J. Immunother.* **36**, 133–151 (2013).
19. Linette, G. P. *et al.* Cardiovascular toxicity and titin cross-reactivity of affinity-enhanced T cells in myeloma and melanoma. *Blood* **122**, 863–871 (2013).
20. Cameron, B. J. *et al.* Identification of a Titin-Derived HLA-A1–Presented Peptide as a Cross-Reactive Target for Engineered MAGE A3–Directed T Cells. *Sci. Transl. Med.* **5**, 197ra103-197ra103 (2013).

21. Morgan, R. A. *et al.* Case Report of a Serious Adverse Event Following the Administration of T Cells Transduced With a Chimeric Antigen Receptor Recognizing ERBB2. *Mol. Ther.* **18**, 843–851 (2010).
22. Chang, K., Pai, L. H., Batra, J. K., Pastan, I. & Willingham, M. C. Characterization of the antigen (CAK1) recognized by monoclonal antibody K1 present on ovarian cancers and normal mesothelium. *Cancer Res.* **52**, 181–186 (1992).
23. Morello, A., Sadelain, M. & Adusumilli, P. S. Mesothelin-Targeted CARs: Driving T Cells to Solid Tumors. *Cancer Discov.* **6**, 133–146 (2016).
24. Maus, M. V. *et al.* T Cells Expressing Chimeric Antigen Receptors Can Cause Anaphylaxis in Humans. *Cancer Immunol. Res.* **1**, 26–31 (2013).
25. Beatty, G. L. *et al.* Mesothelin-Specific Chimeric Antigen Receptor mRNA-Engineered T Cells Induce Antitumor Activity in Solid Malignancies. *Cancer Immunol. Res.* **2**, 112–120 (2014).
26. Haas, A. R. *et al.* Phase I Study of Lentiviral-Transduced Chimeric Antigen Receptor-Modified T Cells Recognizing Mesothelin in Advanced Solid Cancers. *Mol. Ther.* **27**, 1919–1929 (2019).
27. Adusumilli, P. S. *et al.* Regional delivery of mesothelin-targeted CAR T cells for pleural cancers: Safety and preliminary efficacy in combination with anti-PD-1 agent. *J. Clin. Oncol.* **37**, 2511–2511 (2019).
28. Annunziata, C. M. *et al.* Feasibility and preliminary safety and efficacy of first-in-human intraperitoneal delivery of MCY-M11, anti-human-mesothelin CAR mRNA transfected into peripheral blood mononuclear cells, for ovarian cancer and malignant peritoneal mesothelioma. *J. Clin. Oncol.* **38**, 3014–3014 (2020).
29. Chmielewski, M., Hombach, A., Heuser, C., Adams, G. P. & Abken, H. T Cell Activation by Antibody-Like Immunoreceptors: Increase in Affinity of the Single-Chain Fragment Domain above Threshold Does Not Increase T Cell Activation against Antigen-Positive Target Cells but Decreases Selectivity. *J. Immunol.* **173**, 7647–7653 (2004).

30. Liu, X. *et al.* Affinity-Tuned ErbB2 or EGFR Chimeric Antigen Receptor T Cells Exhibit an Increased Therapeutic Index against Tumors in Mice. *Cancer Res.* **75**, 3596–3607 (2015).
31. Caruso, H. G. *et al.* Tuning Sensitivity of CAR to EGFR Density Limits Recognition of Normal Tissue While Maintaining Potent Antitumor Activity. *Cancer Res.* **75**, 3505–3518 (2015).
32. Stone, J. D., Aggen, D. H., Schietinger, A., Schreiber, H. & Kranz, D. M. A sensitivity scale for targeting T cells with chimeric antigen receptors (CARs) and bispecific T-cell Engagers (BiTEs). *OncoImmunology* **1**, 863–873 (2012).
33. Posey, A. D. *et al.* Engineered CAR T Cells Targeting the Cancer-Associated Tn-Glycoform of the Membrane Mucin MUC1 Control Adenocarcinoma. *Immunity* **44**, 1444–1454 (2016).
34. He, Y. *et al.* Multiple cancer-specific antigens are targeted by a chimeric antigen receptor on a single cancer cell. *JCI Insight* **4**, (2019).
35. Sharma, P. *et al.* Structure-guided engineering of the affinity and specificity of CARs against Tn-glycopeptides. *Proc. Natl. Acad. Sci.* **117**, 15148–15159 (2020).
36. Kloss, C. C., Condomines, M., Cartellieri, M., Bachmann, M. & Sadelain, M. Combinatorial antigen recognition with balanced signaling promotes selective tumor eradication by engineered T cells. *Nat. Biotechnol.* **31**, 71–75 (2013).
37. Srivastava, S. *et al.* Logic-Gated ROR1 Chimeric Antigen Receptor Expression Rescues T Cell-Mediated Toxicity to Normal Tissues and Enables Selective Tumor Targeting. *Cancer Cell* **35**, 489-503.e8 (2019).
38. Choe, J. H. *et al.* SynNotch-CAR T cells overcome challenges of specificity, heterogeneity, and persistence in treating glioblastoma. *Sci. Transl. Med.* **13**, eabe7378 (2021).
39. Fedorov, V. D., Themeli, M. & Sadelain, M. PD-1– and CTLA-4–Based Inhibitory Chimeric Antigen Receptors (iCARs) Divert Off-Target Immunotherapy Responses. *Sci. Transl. Med.* **5**, 215ra172-215ra172 (2013).
40. Cho, J. H., Collins, J. J. & Wong, W. W. Universal Chimeric Antigen Receptors for Multiplexed and Logical Control of T Cell Responses. *Cell* **173**, 1426-1438.e11 (2018).

41. Death by a Thousand Cuts: Granzyme Pathways of Programmed Cell Death | Annual Review of Immunology. https://www.annualreviews.org/doi/10.1146/annurev.immunol.26.021607.090404?url_ver=Z39.88-2003&rfr_id=ori%3Arid%3Acrossref.org&rfr_dat=cr_pub++0pubmed.
42. Ho, P., Ede, C. & Chen, Y. Y. Modularly Constructed Synthetic Granzyme B Molecule Enables Interrogation of Intracellular Proteases for Targeted Cytotoxicity. *ACS Synth. Biol.* **6**, 1484–1495 (2017).
43. Tumor Hypoxia: Definitions and Current Clinical, Biologic, and Molecular Aspects | JNCI: Journal of the National Cancer Institute | Oxford Academic. https://academic.oup.com/jnci/article/93/4/266/2906460?login=true.
44. Ede, C., Chen, X., Lin, M.-Y. & Chen, Y. Y. Quantitative Analyses of Core Promoters Enable Precise Engineering of Regulated Gene Expression in Mammalian Cells. *ACS Synth. Biol.* **5**, 395–404 (2016).
45. Juillerat, A. *et al.* An oxygen sensitive self-decision making engineered CAR T-cell. *Sci. Rep.* **7**, 39833 (2017).
46. Chapuis, A. G. *et al.* Transferred WT1-Reactive CD8+ T Cells Can Mediate Antileukemic Activity and Persist in Post-Transplant Patients. *Sci. Transl. Med.* **5**, 174ra27-174ra27 (2013).
47. Chapuis, A. G. *et al.* T cell receptor gene therapy targeting WT1 prevents acute myeloid leukemia relapse post-transplant. *Nat. Med.* **25**, 1064–1072 (2019).
48. Kageyama, S. *et al.* Adoptive Transfer of MAGE-A4 T-cell Receptor Gene-Transduced Lymphocytes in Patients with Recurrent Esophageal Cancer. *Clin. Cancer Res.* **21**, 2268–2277 (2015).
49. Maus, M. V. *et al.* An MHC-restricted antibody-based chimeric antigen receptor requires TCR-like affinity to maintain antigen specificity. *Mol. Ther. - Oncolytics* **3**, (2016).
50. Akahori, Y. *et al.* Antitumor activity of CAR-T cells targeting the intracellular oncoprotein WT1 can be enhanced by vaccination. *Blood* **132**, 1134–1145 (2018).

51. Schumacher, T. N. & Schreiber, R. D. Neoantigens in cancer immunotherapy. *Science* **348**, 69–74 (2015).

52. Nielsen, M. *et al.* NetMHCpan, a Method for Quantitative Predictions of Peptide Binding to Any HLA-A and -B Locus Protein of Known Sequence. *PLOS ONE* **2**, e796 (2007).

53. Fritsch, E. F. *et al.* HLA-Binding Properties of Tumor Neoepitopes in Humans. *Cancer Immunol. Res.* **2**, 522–529 (2014).

54. Peng, S. *et al.* Sensitive Detection and Analysis of Neoantigen-Specific T Cell Populations from Tumors and Blood. *Cell Rep.* **28**, 2728-2738.e7 (2019).

55. Carreno, B. M. *et al.* A dendritic cell vaccine increases the breadth and diversity of melanoma neoantigen-specific T cells. *Science* **348**, 803–808 (2015).

56. Ott, P. A. *et al.* An immunogenic personal neoantigen vaccine for patients with melanoma. *Nature* **547**, 217–221 (2017).

57. Ahmadzadeh, M. *et al.* Tumor antigen–specific CD8 T cells infiltrating the tumor express high levels of PD-1 and are functionally impaired. *Blood* **114**, 1537–1544 (2009).

58. Klebanoff, C. A., Gattinoni, L. & Restifo, N. P. Sorting through subsets: Which T cell populations mediate highly effective adoptive immunotherapy? *J. Immunother. Hagerstown Md 1997* **35**, 651–660 (2012).

59. Yamamoto, T. N., Kishton, R. J. & Restifo, N. P. Developing neoantigen-targeted T cell–based treatments for solid tumors. *Nat. Med.* **25**, 1488–1499 (2019).

60. Alexandrov, L. B. *et al.* Signatures of mutational processes in human cancer. *Nature* **500**, 415–421 (2013).

61. Lu, Y.-C. *et al.* Efficient Identification of Mutated Cancer Antigens Recognized by T Cells Associated with Durable Tumor Regressions. *Clin. Cancer Res.* **20**, 3401–3410 (2014).

62. Linnemann, C. *et al.* High-throughput epitope discovery reveals frequent recognition of neo-antigens by CD4+ T cells in human melanoma. *Nat. Med.* **21**, 81–85 (2015).

63. Davila, M. L. *et al.* Efficacy and Toxicity Management of 19-28z CAR T Cell Therapy in B Cell Acute Lymphoblastic Leukemia. *Sci. Transl. Med.* **6**, 224ra25 LP-224ra25 (2014).
64. Rossi, J. *et al.* Preinfusion polyfunctional anti-CD19 chimeric antigen receptor T cells are associated with clinical outcomes in NHL. *Blood* **132**, 804 LP – 814 (2018).
65. Fraietta, J. A. *et al.* Determinants of response and resistance to CD19 chimeric antigen receptor (CAR) T cell therapy of chronic lymphocytic leukemia. *Nat. Med.* **24**, 563–571 (2018).
66. Singer, M. *et al.* A Distinct Gene Module for Dysfunction Uncoupled from Activation in Tumor-Infiltrating T Cells. *Cell* **166**, 1500-1511.e9 (2016).
67. Chihara, N. *et al.* Induction and transcriptional regulation of the co-inhibitory gene module in T cells. *Nature* **558**, 454–459 (2018).
68. Sukumar, M. *et al.* Mitochondrial Membrane Potential Identifies Cells with Enhanced Stemness for Cellular Therapy. *Cell Metab.* **23**, 63–76 (2016).
69. McLane, L. M., Abdel-Hakeem, M. S. & Wherry, E. J. CD8 T Cell Exhaustion During Chronic Viral Infection and Cancer. *Annu. Rev. Immunol.* **37**, 457–495 (2019).
70. Pauken, K. E. *et al.* Epigenetic stability of exhausted T cells limits durability of reinvigoration by PD-1 blockade. *Science* **354**, 1160–1165 (2016).
71. Satpathy, A. T. *et al.* Massively parallel single-cell chromatin landscapes of human immune cell development and intratumoral T cell exhaustion. *Nat. Biotechnol.* **37**, 925–936 (2019).
72. Khan, O. *et al.* TOX transcriptionally and epigenetically programs CD8+ T cell exhaustion. *Nature* **571**, 211–218 (2019).
73. Scott, A. C. *et al.* TOX is a critical regulator of tumour-specific T cell differentiation. *Nature* **571**, 270–274 (2019).
74. Yao, C. *et al.* Single-cell RNA-seq reveals TOX as a key regulator of CD8+ T cell persistence in chronic infection. *Nat. Immunol.* **20**, 890–901 (2019).
75. Alfei, F. *et al.* TOX reinforces the phenotype and longevity of exhausted T cells in chronic viral infection. *Nature* **571**, 265–269 (2019).

76. Chen, J. *et al.* NR4A transcription factors limit CAR T cell function in solid tumours. *Nature* **567**, 530–534 (2019).

77. LaFleur, M. W. *et al.* PTPN2 regulates the generation of exhausted CD8 + T cell subpopulations and restrains tumor immunity. *Nat. Immunol.* **20**, 1335–1347 (2019).

78. Wiede, F. *et al.* PTPN2 phosphatase deletion in T cells promotes anti-tumour immunity and CAR T-cell efficacy in solid tumours. *EMBO J.* **39**, e103637 (2020).

79. Chen, Z. *et al.* TCF-1-Centered Transcriptional Network Drives an Effector versus Exhausted CD8 T Cell-Fate Decision. *Immunity* **51**, 840-855.e5 (2019).

80. Siddiqui, I. *et al.* Intratumoral Tcf1+PD-1+CD8+ T Cells with Stem-like Properties Promote Tumor Control in Response to Vaccination and Checkpoint Blockade Immunotherapy. *Immunity* **50**, 195-211.e10 (2019).

81. Beltra, J.-C. *et al.* Developmental Relationships of Four Exhausted CD8+ T Cell Subsets Reveals Underlying Transcriptional and Epigenetic Landscape Control Mechanisms. *Immunity* **52**, 825-841.e8 (2020).

82. Lynn, R. C. *et al.* c-Jun overexpression in CAR T cells induces exhaustion resistance. *Nature* **576**, 293–300 (2019).

83. Feucht, J. *et al.* Calibration of CAR activation potential directs alternative T cell fates and therapeutic potency. *Nat. Med.* **25**, 82–88 (2019).

84. Cherkassky, L. *et al.* Human CAR T cells with cell-intrinsic PD-1 checkpoint blockade resist tumor-mediated inhibition. *J. Clin. Invest.* **126**, 3130–3144 (2016).

85. Rafiq, S. *et al.* Targeted delivery of a PD-1-blocking scFv by CAR-T cells enhances anti-tumor efficacy in vivo. *Nat. Biotechnol.* **36**, 847–856 (2018).

86. Grosser, R., Cherkassky, L., Chintala, N. & Adusumilli, P. S. Combination Immunotherapy with CAR T Cells and Checkpoint Blockade for the Treatment of Solid Tumors. *Cancer Cell* **36**, 471–482 (2019).

87. Bruggner, R. V, Bodenmiller, B., Dill, D. L., Tibshirani, R. J. & Nolan, G. P. Automated identification of stratifying signatures in cellular subpopulations. *Proc. Natl. Acad. Sci.* **111**, E2770 LP-E2777 (2014).

88. Aghaeepour, N. *et al.* Early immunologic correlates of HIV protection can be identified from computational analysis of complex multivariate T-cell flow cytometry assays*. *Bioinformatics* **28**, 1009–1016 (2012).

89. Pavlova, N. N. & Thompson, C. B. The Emerging Hallmarks of Cancer Metabolism. *Cell Metab.* **23**, 27–47 (2016).

90. Heiden, M. G. V., Cantley, L. C. & Thompson, C. B. Understanding the Warburg Effect: The Metabolic Requirements of Cell Proliferation. *Science* **324**, 1029–1033 (2009).

91. Chang, C.-H. *et al.* Metabolic Competition in the Tumor Microenvironment Is a Driver of Cancer Progression. *Cell* **162**, 1229–1241 (2015).

92. Menk, A. V. *et al.* Early TCR Signaling Induces Rapid Aerobic Glycolysis Enabling Distinct Acute T Cell Effector Functions. *Cell Rep.* **22**, 1509–1521 (2018).

93. Chang, C.-H. *et al.* Posttranscriptional Control of T Cell Effector Function by Aerobic Glycolysis. *Cell* **153**, 1239–1251 (2013).

94. Ho, P.-C. *et al.* Phosphoenolpyruvate Is a Metabolic Checkpoint of Anti-tumor T Cell Responses. *Cell* **162**, 1217–1228 (2015).

95. Qiu, J. *et al.* Acetate Promotes T Cell Effector Function during Glucose Restriction. *Cell Rep.* **27**, 2063-2074.e5 (2019).

96. Renner, K. *et al.* Restricting Glycolysis Preserves T Cell Effector Functions and Augments Checkpoint Therapy. *Cell Rep.* **29**, 135-150.e9 (2019).

97. Cascone, T. *et al.* Increased Tumor Glycolysis Characterizes Immune Resistance to Adoptive T Cell Therapy. *Cell Metab.* **27**, 977-987.e4 (2018).

98. Bengsch, B. *et al.* Bioenergetic Insufficiencies Due to Metabolic Alterations Regulated by the Inhibitory Receptor PD-1 Are an Early Driver of CD8+ T Cell Exhaustion. *Immunity* **45**, 358–373 (2016).

99. Fisicaro, P. *et al.* Targeting mitochondrial dysfunction can restore antiviral activity of exhausted HBV-specific CD8 T cells in chronic hepatitis B. *Nat. Med.* **23**, 327–336 (2017).

100. Dumauthioz, N. *et al.* Enforced PGC-1α expression promotes CD8 T cell fitness, memory formation and antitumor immunity. *Cell. Mol. Immunol.* 1–11 (2020) doi:10.1038/s41423-020-0365-3.

101. Ligtenberg, M. A. *et al.* Coexpressed Catalase Protects Chimeric Antigen Receptor–Redirected T Cells as well as Bystander Cells from Oxidative Stress–Induced Loss of Antitumor Activity. *J. Immunol.* **196**, 759–766 (2016).

102. Vardhana, S. A. *et al.* Impaired mitochondrial oxidative phosphorylation limits the self-renewal of T cells exposed to persistent antigen. *Nat. Immunol.* 1–12 (2020) doi:10.1038/s41590-020-0725-2.

103. Gemta, L. F. *et al.* Impaired enolase 1 glycolytic activity restrains effector functions of tumor-infiltrating CD8+ T cells. *Sci. Immunol.* **4**, (2019).

104. Chakraborty, P. *et al.* Pro-Survival Lipid Sphingosine-1-Phosphate Metabolically Programs T Cells to Limit Anti-tumor Activity. *Cell Rep.* **28**, 1879-1893.e7 (2019).

105. O'Sullivan, D. *et al.* Memory CD8+ T Cells Use Cell-Intrinsic Lipolysis to Support the Metabolic Programming Necessary for Development. *Immunity* **41**, 75–88 (2014).

106. Mellor, A. L. & Munn, D. H. Ido expression by dendritic cells: tolerance and tryptophan catabolism. *Nat. Rev. Immunol.* **4**, 762–774 (2004).

107. Li, H. *et al.* Metabolomic adaptations and correlates of survival to immune checkpoint blockade. *Nat. Commun.* **10**, 4346 (2019).

108. Long, G. V. *et al.* Epacadostat plus pembrolizumab versus placebo plus pembrolizumab in patients with unresectable or metastatic melanoma (ECHO-301/KEYNOTE-252): a phase 3, randomised, double-blind study. *Lancet Oncol.* **20**, 1083–1097 (2019).

109. Triplett, T. A. *et al.* Reversal of indoleamine 2,3-dioxygenase–mediated cancer immune suppression by systemic kynurenine depletion with a therapeutic enzyme. *Nat. Biotechnol.* **36**, 758–764 (2018).

110. Beavis, Paul. A., Stagg, J., Darcy, P. K. & Smyth, M. J. CD73: a potent suppressor of antitumor immune responses. *Trends Immunol.* **33**, 231–237 (2012).

111. Zhang, B. *et al.* High expression of CD39/ENTPD1 in malignant epithelial cells of human rectal adenocarcinoma. *Tumor Biol.* **36**, 9411–9419 (2015).

112. Leone, R. D. & Emens, L. A. Targeting adenosine for cancer immunotherapy. *J. Immunother. Cancer* **6**, 57 (2018).

113. Beavis, P. A. *et al.* Targeting the adenosine 2A receptor enhances chimeric antigen receptor T cell efficacy. *J. Clin. Invest.* **127**, 929–941 (2017).

114. Fischer, K. *et al.* Inhibitory effect of tumor cell–derived lactic acid on human T cells. *Blood* **109**, 3812–3819 (2007).

115. Brand, A. *et al.* LDHA-Associated Lactic Acid Production Blunts Tumor Immunosurveillance by T and NK Cells. *Cell Metab.* **24**, 657–671 (2016).

116. Angelin, A. *et al.* Foxp3 Reprograms T Cell Metabolism to Function in Low-Glucose, High-Lactate Environments. *Cell Metab.* **25**, 1282-1293.e7 (2017).

117. Colegio, O. R. *et al.* Functional polarization of tumour-associated macrophages by tumour-derived lactic acid. *Nature* **513**, 559–563 (2014).

118. Calcinotto, A. *et al.* Modulation of Microenvironment Acidity Reverses Anergy in Human and Murine Tumor-Infiltrating T Lymphocytes. *Cancer Res.* **72**, 2746–2756 (2012).

119. Pilon-Thomas, S. *et al.* Neutralization of Tumor Acidity Improves Antitumor Responses to Immunotherapy. *Cancer Res.* **76**, 1381–1390 (2016).

120. Yang, W. *et al.* Potentiating the antitumour response of CD8+ T cells by modulating cholesterol metabolism. *Nature* **531**, 651–655 (2016).

121. Patel, C. H. & Powell, J. D. Targeting T cell metabolism to regulate T cell activation, differentiation and function in disease. *Curr. Opin. Immunol.* **46**, 82–88 (2017).

TABLES

Antigen target	CAR/ TCR	Tumor type(s)	Cross-reactivity	Description of toxicities	Clinical trial identifier
MART-1[7]	TCR	Metastatic melanoma	Melanocytes in the skin, eye, and ear	Epidermal melanocyte toxicity, uveitis, synechiae, hearing loss	NCT00509288
gp100[7]	TCR	Metastatic melanoma	Melanocytes in the skin, eye, and ear	Epidermal melanocyte toxicity, uveitis, synechiae, hearing loss	NCT00509496
CEA[8]	TCR	Metastatic colorectal cancer	Gastrointestinal epithelium	Severe transient inflammatory colitis	NCT00923806
CAIX[9]	CAR	Metastatic renal carcinoma	Bile duct epithelium	Liver toxicity	DDHK97-29/P00.0040C
MAGE-A3[10]	TCR	Metastatic cancer, metastatic renal cancer, and metastatic melanoma	Brain	Lethal neurotoxicity	NCT01273181
MAGE-A3[11]	TCR	Metastatic melanoma	Myocardium	Lethal cardiac toxicity	NCT01350401
MAGE-A3[11]	TCR	Advanced myeloma	Myocardium	Lethal cardiac toxicity	NCT01352286
HER2[13]	CAR	Metastatic cancer	Lung epithelium	Lethal pulmonary toxicity	NCT00924287

Table 1-1. Clinical outcomes of T-cell therapy trials with on-target, off-tumor toxicities. Abbreviations. CAR, chimeric antigen receptor; TCR, T-cell receptor; MART-1, melanoma

antigen recognized by T cells 1; gp100, glycoprotein 100; CEA, carcinoembryonic antigen; CAIX, carboxy-anhydrase-IX; HER2, human epidermal growth factor receptor 2

Antigen target	Number of unique CARs in active clinical trials	CAR generation		Clinical trial phases		Clinical trial identifiers
AXL	2	**3rd Generation**	1	**I**	1	NCT03198052, NCT03393936
		Unspecified	1	**I/II**	1	
B7-H3	7	**2nd Generation**	3	**I**	5	NCT03198052, NCT04385173, NCT04185038, NCT04077866, NCT04483778, NCT04483778, NCT04432649
		3rd Generation	1			
		4th Generation	1	**I/II**	2	
		Unspecified	2			
CD147	2	**Unspecified**	2	**I**	2	NCT03993743, NCT04045847
CD171	3	**2nd Generation**	2	**I**	3	NCT02311621, NCT02311621, NCT02311621
		3rd Generation	1			
CD20	1	**Unspecified**	1	**I**	1	NCT03893019
CD44v6	2	**4th Generation**	2	**I/II**	2	NCT04430595, NCT04427449
CD70	2	**Unspecified**	2	**I**	1	NCT02830724, NCT04438083
				I/II	1	
CEA	6	**Unspecified**	6	**I**	4	NCT03818165, NCT04348643, NCT03682744, NCT02850536, NCT04513431, NCT04037241
				I/II	1	
				II/III	1	
CLDN18.2	3	**Unspecified**	3	**I**	3	NCT04404595, NCT04467853, NCT03874897
CLDN6	1	**Unspecified**	1	**I/II**	1	NCT04503278
DLL3	1	**Unspecified**	1	**I**	1	NCT03392064
DR5	2	**Unspecified**	2	**I/II**	2	NCT03638206, NCT03941626
EGFR	6	**2nd Generation**	3	**I**	6	NCT03198052, NCT03638167, NCT03542799, NCT03618381, NCT03618381, NCT04153799
		3rd Generation	1			
		4th Generation	2			
EGFRvIII	2	**Unspecified**	2	**I/II**	2	NCT03638206, NCT03941626
EpCAM	4	**2nd Generation**	1	**I**	2	NCT03563326, NCT03013712, NCT02915445, NCT04151186
		3rd Generation	1	**I/II**	1	
		Unspecified	2	**N/A**	1	
ErbB	1	**2nd Generation**	1	**I/II**	1	NCT01818323
FRα	2	**2nd Generation**	1	**I**	1	NCT03585764, NCT03185468
		4th Generation	1	**I/II**	1	

GD2	13	**2nd Generation**	2	**I**	9	NCT03356795, NCT04196413, NCT04539366, NCT02761915, NCT03373097, NCT02765243, NCT04099797, NCT03635632, NCT04430595, NCT03721068, NCT02992210, NCT01953900, NCT01822652
		3rd Generation	2			
		4th Generation	6	**I/II**	4	
		Unspecified	3			
gp100 (MHC-1)	1	**2nd Generation**	1	**I**	1	NCT03649529
GPC3	10	**2nd Generation**	1	**I**	10	NCT03198052, NCT04506983, NCT03198546, NCT03198546, NCT04121273, NCT04377932, NCT02905188, NCT02932956, NCT03980288, NCT03884751
		3rd Generation	2			
		4th Generation	3			
		Unspecified	4			
HER2	7	**2nd Generation**	3	**I**	6	NCT03198052, NCT03500991, NCT03696030, NCT04430595, NCT02442297, NCT04511871, NCT00902044
		3rd Generation	1			
		4th Generation	1	**I/II**	1	
		Unspecified	2			
IL13Rα2	2	**2nd Generation**	2	**I**	2	NCT04510051, NCT02208362
LeY	2	**2nd Generation**	1	**I**	2	NCT03851146, NCT03198052
		3rd Generation	1			
LFA-I	1	**3rd Generation**	1	**I**	1	NCT04420754
MMP-2	1	**2nd Generation**	1	**I**	1	NCT04214392
MSLN	18	**2nd Generation**	3	**I**	11	NCT03198052, NCT03638206, NCT03356795, NCT03941626, NCT04503980, NCT04489862, NCT03747965, NCT03814447, NCT03916679, NCT03638193, NCT03799913, NCT03545815, NCT03497819, NCT03323944, NCT03615313, NCT03054298, NCT02414269, NCT02792114
		3rd Generation	1	**I/II**	6	
		4th Generation	4	**N/A**	1	
		Unspecified	10			
MUC1	5	**3rd Generation**	1	**I**	1	NCT03198052, NCT03356795, NCT03633773, NCT03706326, NCT03525782
		Unspecified	4	**I/II**	4	
MUC1*	1	**2nd Generation**	1	**I**	1	NCT04020575
MUC16	1	**4th Generation**	1	**I**	1	NCT03907527

MUC16ecto	1	**4th Generation**	1	**I**	1	NCT02498912
NECTIN4	1	**4th Generation**	1	**I**	1	NCT03932565
NKG2D	1	**2nd Generation**	1	**I**	1	NCT03692429
NKG2DL	2	**2nd Generation**	1	**I**	2	NCT04270461, NCT04107142
		Unspecified	1			
PSCA	3	**1st Generation**	1	**I**	2	NCT03198052, NCT03873805, NCT02744287
		2nd Generation	1	**I/II**	1	
		3rd Generation	1			
PSMA	6	**4th Generation**	4	**I**	3	NCT03356795, NCT04053062, NCT04227275, NCT03089203, NCT03185468, NCT04429451
		Unspecified	2	**I/II**	3	
ROR1	1	**Unspecified**	1	**I**	1	NCT02706392
ROR2	2	**Unspecified**	2	**I**	1	NCT03960060, NCT03393936
				I/II	1	
TM4SF1	1	**Unspecified**	1	**N/A**	1	NCT04151186
TnMUC1	1	**Unspecified**	1	**I**	1	NCT04025216
Unspecified	6	**4th Generation**	2	**I**	1	NCT03356782, NCT04085159, NCT04433221, NCT03184753, NCT03170141, NCT03356808
		Unspecified	4	**I/II**	5	

Table 1-2. Clinical outcomes of T cell therapy trials with on-target, off-tumour toxicity. Abbreviations: CAIX, carboxy-anhydrase IX; CAR, chimeric antigen receptor; CEA, carcinoembryonic antigen; gp100, glycoprotein 100; HER2, human epidermal growth factor receptor 2; MART1, melanoma antigen recognized by T cells 1; TCR, T cell receptor.

Chapter 2. Engineering intracellular oncoprotein-responsive CAR-T cells

ABSTRACT

Adoptively transferred T cells recognize tumor cells by recognition of surface-bound tumor-associated antigens (TAAs) through the T-cell receptor (TCR) or chimeric antigen receptor (CAR). However, vital cells may also express TAAs at low levels and can consequently be targeted by engineered T cells, leading to a phenomenon known as “on-target, off-tumor” toxicity that poses a large risk to patient safety. To circumvent the limitations of “on-target, off-tumor” toxicity, we propose to engineer T cells that kill target cells based on detection of both a surface-bound TAA in addition to an intracellular oncoprotein through a system termed cytoplasmic oncoprotein verifier and response trigger (COVERT). The COVERT system involves T-cell mediated delivery of an intracellular oncoprotein-responsive cytotoxic switch into the target cell after surface-bound recognition of a TAA. In this chapter, we optimize T-cell engineering strategies to remove T cells of their constitutive killing machinery. Next, we explore rational design and high-throughput protein engineering strategies towards developing an oncoprotein-responsive protein switch. Finally, we test the efficacy of COVERT-equipped T cells in animal models.

INTRODUCTION

The use of engineered tumor-targeting T cells has been successful at treating hematological malignancies, but such success has yet to be translated into the context of solid tumors. Engineered T cells typically express a T-cell receptor (TCR) or chimeric antigen receptor (CAR) that targets surface-bound tumor-associated antigens (TAA). However, tumor-associated antigens are rarely tumor-exclusive. Thus, engineered T cells can accidentally attack healthy and vital cells that share expression of the TAA, leading to an effect known as "on-target, off-tumor" toxicity (**Fig. 2-1A**). The difficulty in identifying the appropriate antigen to target is a major limitation in adoptive T-cell therapies[1].

To address this major limitation, our lab has proposed a system whereby CAR-T cells are engineered to detect intracellular oncoproteins within a target cell prior to CAR-T cell cytolysis[2]. In this system, T-cell recognition of a surface-bound tumor-associated antigen leads to the delivery of an oncoprotein-responsive payload into the target cell; this oncoprotein-responsive payload interrogates the target cell's intracellular proteome and executes apoptotic pathways depending on the presence or absence of an oncoprotein of interest (**Fig. 2-1B**). We termed these oncoprotein-responsive payload molecules as cytoplasmic oncoprotein verifier and response trigger (COVERT) molecules.

Granzyme B (GrB) is the primary mechanism of T-cell cytolysis[3]. GrB is stored within T-cell lytic granules in an inactive form that subsequently gets released through the immunological synapse and into the target cell through with the help of perforin upon T-cell recognition of a target cell[3]. Given that GrB naturally has the capacity to penetrate a target cell, we hypothesized that GrB is a suitable chassis to protein engineer an oncoprotein-responsive switch. In fact, our lab has demonstrated a proof-of-concept, onco-protein responsive GrB switch termed SUMO-GrB[2]. SUMO-GrB was engineered to respond to tumor-associated protease SUMO Specific Peptidase 1 (SENP1). The next step is to expand the repertoire of ligands COVERT molecules can respond to. In addition to engineering COVERT molecules that can respond to oncoproteins other than

proteases, the endogenous killing machinery in T cells needs to be disrupted for COVERT molecules to selectively kill based on interrogation of the intracellular proteome.

Throughout this chapter, we explore strategies to 1) disarm endogenous T-cell killing and 2) engineer oncoprotein-responsive COVERT molecules. We we use CRISPR/Cas9 to knockout one or multiple cytolysis genes and demonstrate reduction in T-cell killing efficacy. We also explore rational protein design and high-throughput strategies in developing new COVERT molecules. Finally, we combine cellular engineering with SUMO-GrB and evaluate whether engineered CAR-T cells can achieve differential killing in a pre-clinical animal model.

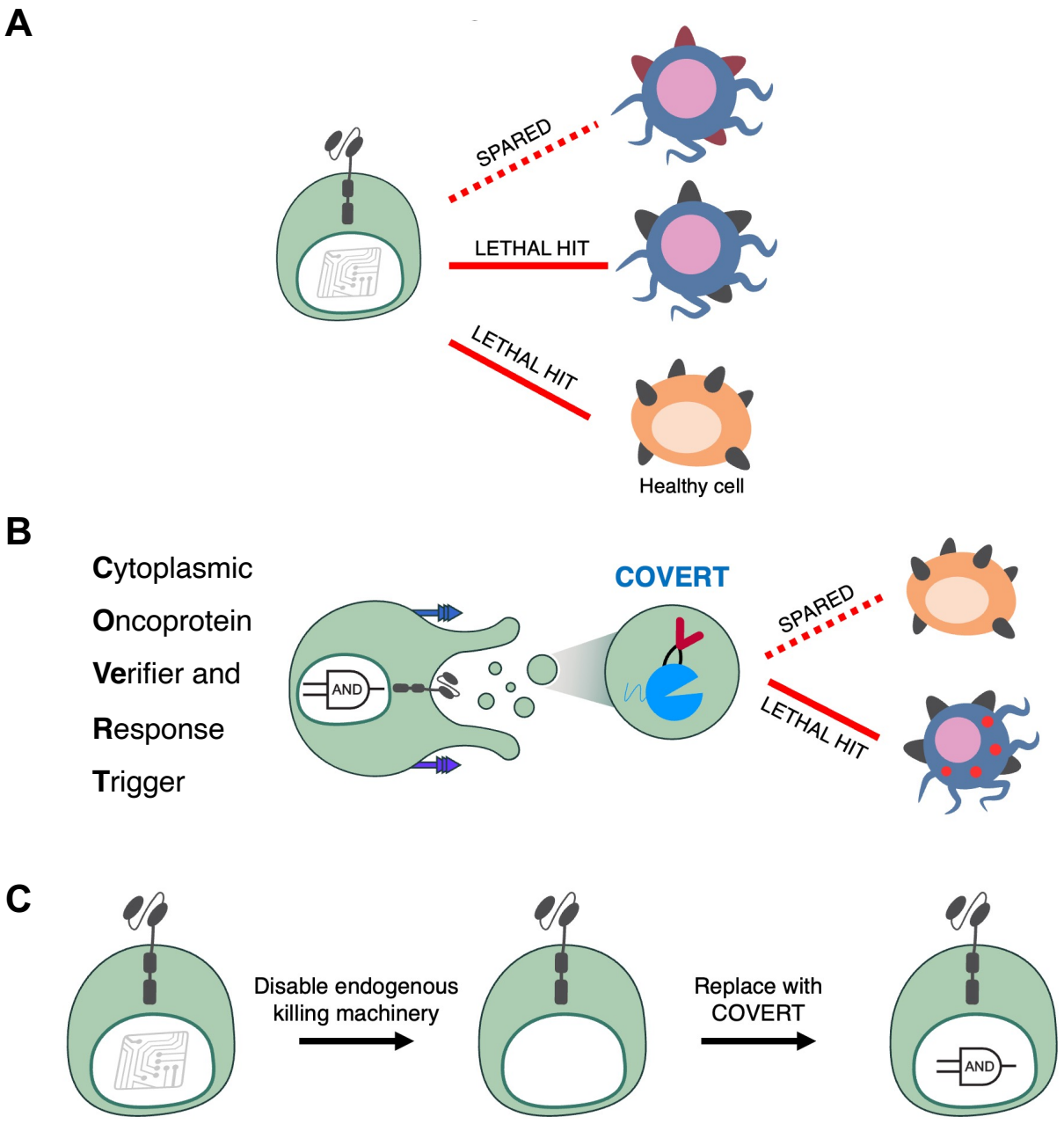

Figure 2-1: Reprogramming T cells to target intracellular antigens with COVERT. (**A**) Pictorial representation of on-target, off-tumor toxicity wherein CAR-T cells targeting tumor-associated antigen (in black) are present on both tumor and normal healthy cells. (**B**) Equipping T cells with intracellular antigen-responsive, Granzyme B-based COVERT molecules for AND-gate targeting of tumor cells. In the schematic, an mCherry-targeting ligand-binding domain is internally inserted into Granzyme B, enabling mCherry-specific killing only when inside a tumor cell. (**C**) An outline of the T-cell engineering process required in pairing COVERT with T-cell immunotherapies.

METHODS

DNA Constructs. The MSCV retroviral vector and pHIT60 and RD114 retroviral packaging vectors were generous gifts from Dr. Steven Feldman (National Cancer Institute). CD19 and CD20 CARs were constructed as previously reported and were cloned into the MSCV backbone[4]. The sequence of GrB is from the human QPY variant, with an S183A mutation serving as the inactive GrB control[2]. DNA sequences for mCherry binding nanobody LaM4 and GFP-binding nanobodies GBe and GBP6 were derived from literature[5,6]. The pEXPR-CAG-BxbI vector (which expresses mammalian codon-optimized BxBI integrase) and the payload pENTR-attB(BxbI) vector were generous gifts from Dr. Timothy K. Lu (Massachusetts Institute of Technology). DNA constructs were assembled using standard molecular biology cloning techniques assembling chemically synthesized oligonucleotides or gBlocks by Integrated DNA Technologies (Coralville, IA).

Cell Lines. HEK293T cells were obtained in 2011 from ATCC (Manassas, VA). Raji, K562, and TM-LCL cells were generous gifts from Dr. Michael C. Jensen (Seattle Children's Research Institute), which were originally obtained from ATCC in 2003. Landing pad CHO-K1 cells were generous gifts from Dr. Timothy K. Lu (Massachusetts Institute of Technology). Cells were cultured in either DMEM (HEK293T), RPMI-1640 (Raji, K562, TM-LCL), or F-12K Media (CHO-K1) supplemented with 10% heat-inactivated FBS (HI-FBS). All mammalian cell cultures were maintained at 37°C and 5% CO_2.

Primary Human T-cell Isolation and Culture. Primary human $CD3^+$ and $CD8^+$ T cells were isolated from healthy donor blood samples obtained from the UCLA Blood & Platelet Center using the RosetteSep Human T Cell or $CD8^+$ Enrichment Cocktail (Stemcell Technologies) according to the manufacturer's protocol. Peripheral blood mononuclear cells (PBMCs) were isolated from a Ficoll-Paque PLUS (GE Healthcare) density gradient using SepMate™ PBMC Isolation Tubes

(Stemcell Technologies) per manufacturer's instructions. CD14–/CD25–/CD62L+ naïve/memory T cells (Tnm) were enriched from PBMCs using magnetic-activated cell sorting (Miltenyi). T cells were either kept in culture or cryopreserved at 10-50 x 10^6 cells/mL in complete T-cell media (RPMI-1640 supplemented with 10% HI-FBS) supplemented with 10% DMSO post-isolation. Thawed T cells were seeded at 1-2 x 10^6 cells/mL in complete T-cell media. T cells were activated with anti-CD3/CD28 Dynabeads (Life Technologies, Carlsbad, CA) at 1:1 or 3:1 cell-to-bead ratios. T-cell cultures were supplemented with 50 U/mL IL-2 (Life Technologies, Carlsbad, CA) and 1 ng/mL IL-15 (Peprotech) every 48-72 hours unless otherwise specified.

Retrovirus Production and Transduction. HEK293T cells were seeded at 3-6 x 10^6 cells/9 mL/dish in 10 cm tissue-culture dishes. Tissue culture dishes were coated with 0.1 mg/mL poly-d-lysine for one hour and washed with phosphate buffered saline (PBS) prior to HEK293T seeding. Culture medium was replaced with fresh DMEM + 10% HI-FBS prior to the transfection of 3.8 μg retroviral construct, 3.8 μg pHIT60, and 2.4 μg RD114 via linear PEI. 14 to 18 hours post-transfection, cells were washed with PBS supplemented with 2% HI-FBS and cultured in DMEM supplemented with 10% HI-FBS, 20 mM HEPES, and 10 mM sodium butyrate for 8 hours. After 8 hours, cells were washed with PBS supplemented with 2% HI-FBS before media change to DMEM supplemented with 10% HI-FBS and 20 mM HEPES. Retrovirus-containing supernatant was harvested on each of the two subsequent days post-media change and filtered through a 0.45 μm, low-protein–binding filter and stored at -80 °C. At 48 and 72 hours post-Dynabead activation, 1 x 10^6 T activated T cells were transduced with 2 mL of retroviral supernatant supplemented with 5 μg/mL polybrene (Sigma-Aldrich) by spinfection at 800 x g for 90 minutes at 30 °C. Retroviral supernatant was removed immediately post-spinfection and replenished with fresh T-cell media.

Generation of CRISPR-edited Primary Human T cells. Primary human $CD3^+$, $CD8^+$, and Tnm cells were isolated and activated as previously described. CAR-T cells were transduced on days 2 and 3 prior to CRISPR-editing as previously described. Chemically synthesized single-guide RNAs (sgRNAs) were ordered with 2'-O-methyl analogs and 3' phosphorothioate internucleotide linkages at the 3 bases on both 5' and 3' ends of each sgRNA (Synthego). The following sgRNA sequences were ordered for Granzyme B (GCCAGGGCAGACAUGCAGUG), Granzyme A (CAGAAAAACCAUCUGUGCUG), Fas ligand (AUAUCCCCAGAUCUACUGGG), TRAIL (GCUAUGAUGGAGGUCCAGGG), and Negative Control sgRNA #1 (GCACUACCAGAGCUAACUCA). The sgRNA were resuspended at 100 μM or 300 μM in nuclease-free Tris-HCl pH 8.0 and stored at -20 °C. Prior to CRISPR/Cas9 RNP complexing, 3 μL thawed sgRNA was mixed with 4.5 μL nuclease-free water and 5 μL of in-house SpCas9 protein (10 mg/mL) was mixed with 2.5 μL Cas9 storage buffer. CRISPR/Cas9 RNP complexes were formed by gently mixing the diluted sgRNA with SpCas9 protein and incubating at room temperature for at least 10 minutes. 5 x 10^6 total T cells were washed three times with PBS prior to resuspension in 100 μL Ingenio® electroporation buffer (Mirus Bio) on either days 4 or 5 of the T-cell cycle. The CRISPR/Cas9 RNP complex was gently added to the resuspended T cells prior to transferring to 0.2 cm Ingenio® cuvettes (Mirus Bio). Cells were electroporated using Program T-017 of the Nucleofector™ 2b Device (Lonza) following the manufacturer's protocol. Cells were immediately recovered with 500 μL pre-warmed complete RPMI and transferred into T-cell media supplemented with 50 U/mL IL-2 (Life Technologies) and 1 ng/mL IL-15 (Peprotech).

TIDE analysis. Genomic DNA was isolated from T cells using the Qiagen DNeasy Blood & Tissue kit following manufacturer's protocol. The CRISPR/Cas9 genomic cut site was amplified by PCR using flanking oligos for subsequent Sanger sequencing (Retrogen). The TIDE calculator online resource (www.tide.deskgen.com) was used to calculate % indel formation, which accepts Sanger sequencing chromatograms as input.

***In Vivo* Studies.** Six- to eight-week-old NOD/SCID/IL-2Rγnull (NSG) mice were obtained from UCLA Department of Radiation and Oncology with animal protocol approval by the UCLA Institutional Animal Care and Used Committee. Mice were engrafted with EGFP-firefly luciferase (ffluc)-expressing Raji through tail-vein intravenous injection. Mice were also engrafted with EGFP-ffluc-expressing K562 cells either subcutaneously or through tail-vein injections. CAR-T cells were subsequently injected intravenously at the teil-vein. In disseminated tumor models, tumor progression/regression was monitored with an IVIS Illumina III LT Imaging System (PerkinElmer). In the subcutaneous tumor model, tumor volume was calculated by tumor length and width caliper measurements with the following equation: $Tumor\ volume = \frac{1}{2}(length \times width^2)$. Mice were euthanized at the humane endpoint.

Retroviral Cytotoxicity Assay. Retrovirus was prepared for each cytotoxic construct of interest as previously described, with only the first viral harvest, skipping cell filtration, and with everything scaled down to 12-well format. Fresh HEK293T cells were seeded for transduction at 0.1 x 10^6 cells per 12-well one day before transduction. On the day of transduction, spent media was aspirated from seeded HEK293T cells and the complete retrovirus culture was added to the seeded cells. HEK293T cells were incubated in the presence of retrovirus for 48-72 hours prior to flow cytometric analysis.

Flow Cytometry and Cell Permeabilization. Flow cytometry experiments performed in this report was run on a MACSQuant VYB cytometer (Miltenyi Biotec). Truncated epidermal growth factor receptor (EGFRt) surface expression was probed with Erbitux (Bristol-Myers Squibb) that was biotinylated in-house (EZ-link Sulfo-NHS-Biotin, Pierce) followed by PE-conjugated streptavidin (Jackson ImmunoResearch). Granzyme B intracellular staining was probed with

Pacific Blue™-conjugated anti-human/mouse Granzyme B antibody (BioLegend) after cell permeabilization. Cells were fixed by resuspending cells in complete media supplemented with 1.5% formaldehyde for 30 minutes at room temperature; cells were subsequently permeabilized by resuspension in 4 °C methanol for 30 minutes on ice.

COVERT Transposition Library Cloning. A transposition reaction was set up with 100 ng of linearized MuA-BsaI transposon and 50 ng of staging plasmid (i.e., host GrB plasmid) with 1 μL MuA Transposase in MuA Transposition Buffer (ThermoFisher Scientific) at 30 °C for 4 hours followed by transposase inactivation at 75 °C for 20 minutes. The reaction was cleaned up using DNA Clean and Concentrator (Zymo Research) following manufacturer's instructions, eluting in 6 μL sterile water. 2 μL of the transposition eluate was mixed with 20 μL of thawed NEB® 10-beta electrocompetent E. coli (New England Biolabs) on ice and subsequently transferred into pre-chilled in 1 mm Thermo Scientific™ electroporation cuvettes (ThermoFisher Scientific) and electroporated using the "E. coli" protocol in a MicroPulser™ electroporator (Bio-Rad). Electroporated cells were immediately recovered with 900 μL pre-warmed SOC media and recovered at 37 °C while shaking at 190 rpm for 1 hour. A small fraction of cells (< 10 μL) were plated onto 15 μg/mL chloramphenicol LB agar plates to quantify transformation efficiency. Remaining cells were inoculated into liquid LB culture containing 15 μg/mL chloramphenicol for propagation. Additional manipulations to the COVERT library were made using conventional molecular biology techniques as previously described.

Landing Pad CHO-K1 Transfection and Library Screen. 6 x 10^6 landing pad CHO-K1 cells were seeded in 10 cm dishes per 9 mL media the day prior to plasmid library transfection. Culture medium was replaced with fresh F-12K + 10% HI-FBS prior to transfection with 8.44 μg payload plasmid DNA (either in single plasmid or library format) and 5.06 μg pEXPR-CAG-BxbI with linear

PEI at a 1:3 DNA:PEI ratio. 14 to 18 hours after transfection, cells were washed with PBS + 2% HI-FBS and fresh F-12K + 10% HI-FBS was replenished. 3 days after transfection, puromycin (MilliporeSigma) was added to cell cultures at a concentration of 200 μg/mL. Media was changed as necessary and puromycin was supplemented daily. After 9 days of puromycin selection, the remaining CHO-K1 cells were trypsinized. A small fraction of trypsinized cells were analyzed via flow cytometry and genomic DNA was isolated from the bulk of the remaining cells using the Qiagen DNeasy Blood & Tissue kit following manufacturer's protocol.

Amplicon Seq Library Preparation and Sequencing. The COVERT library was amplified by PCR from genomic DNA using primers flanking the landing pad site. DNA library amplicons were first sonicated in 0.1 mL Bioruptor® Pico Microtubes following manufacturer's protocol (Diagenode); DNA amplicons were subject to 30 cycles of (30 seconds ON/30 seconds OFF) shearing. NGS DNA amplicon libraries were subsequently prepared using the NEB Next Ultra II FS Kit (New England Biolabs) following manufacturer's protocol. DNA amplicon libraries were sequenced via NextSeq 500 SBS, 2x75 paired-end.

Amplicon Sequencing Analysis. Amplicon sequencing data shown were analyzed using the domain-insertion profiling sequencing (DIPseq; https://github.com/SavageLab/dipseq)[7] pipeline on UCLA's Hoffman2 computational cluster. Custom scripts in Python (2.7) were used to further parse raw DIPseq data output. Custom scripts in R were used to calculate set scores, enrichment, and permissivity. The base unit for counting was counts per million (CPM; i.e., the number of times a given variant appears normalized by the total number of reads present in a given library).

Western Blot. Cellular lysates were obtained by incubating cells in cell lysis buffer (150 mM NaCl, 20 mM Tris pH 7.2, 1% (v/v) Triton-X) on ice for 45 minutes. Cell debris was separated from the lysate supernatant by centrifugation at 20,000 x g for 10 minutes. Protein concentration was

quantified by Bradford assay (ThermoFisher Scientific). Protein samples were run on 4-12% Bis-Tris SDS-PAGE gels, transferred onto nitrocellulose membranes, and subsequently stained using anti-GrB (clone 2C5, Santa Cruz Biotech) as the primary antibody and a horseradish peroxidase (HRP)-conjugated anti-mouse secondary antibody (Jackson Immunoresearch). Western blots were developed using SuperSignal West Pico Chemilumniescent Substrate (ThermoFisher Scientific).

GrB/COVERT Protein Expression and Purification. 9-12 x 10^6 HEK293T cells were seeded per 20 mL media in T-150 flasks the day before transfection. On the day of transfection, culture media was replenished, and cells were transfected with His-tagged COVERT-expressing plasmids using the linear PEI method. 14-18 hours after transfection, cells were gentl washed with PBS and replenished with complete media. Supernatants were collected 48-72 hours after transfection and filtered through a 0.45 μm filter to remove debris. His-tagged proteins in supernatant were bound to Ni-NTA agarose beads (Genesee) following manufacturer's protocols; in brief, supernatant was incubated with Ni-NTA beads on ice for 1 hour while shaking, washed over a chromatography column with binding buffer, and eluted using imidazole. Eluted proteins were buffer-exchanged and concentrated into enterokinase digestion buffer using 10 kDa cutoff Amicon protein concentration tubes (EMD Millipore). Purified GrB/COVERT molecules were activated by enterokinase (P8070, New England BioLabs) following manufacturer's protocol.

Ac-IEPD-pNA Granzyme B Enzymatic Activity Assay. Protein concentration of purified and enterokinase-digested GrB/COVERT molecules were quantified by Bradford assay. 25 nmol GrB/COVERT were added to 100 uL Ac-IEPD-pNA substrate buffer (50 mM HEPES pH 7.5, 10% (w/v) sucrose, 0.05 % (w/v) CHAPS, 5 mM DTT) containing 200 μM Ac-IEPD-pNA substrate

(ENZO Life Sciences) in clear 96-well flat-bottom wells per literature[8]. EONC microplate reader (BioTek) was used to measure 405 nm absorbance at 405 every minute for 200 minutes.

Repeated Antigen Challenge Assay. Engineered EGFP-expressing Raji and TM-LCL cells were seeded at 1-2 x 10^5 cells/well in a tissue-culture 48-well plate and co-incubated with primary human CAR T cells at varying effector-to-target ratios. Specifically, the number of effector cells refers to the number of CAR-expressing T cells within the population. Media culture conditions were monitored throughout the course of the experiment, and when necessary, media changes were performed to maintain nutrient availability of the culture. Resuspended aliquots of challenge cultures were harvested every 48-72 hours to quantify the number of $EGFP^+$ Raji cells and CAR-expressing T cells. The same number of fresh $EGFP^+$ Raji cells, were added to each culture post-aliquot harvest, thereby constituting a new challenge.

Statistics. Statistical tests used two-tailed, unpaired, two-sample Student's t test with Sidak correction for multiple comparisons.

RESULTS

CRISPR-mediated Granzyme B knockout modestly reduces CAR-T cell cytotoxicity

To re-engineer how CAR-T cells kill using COVERT molecules that sense-and-respond to intracellular oncoproteins, the endogenous killing capacity of CAR-T cells must first be disabled in order to prevent constitutive, antigen-dependent killing (**Fig. 1C**). Given that GrB is the dominant mechanism of killing used by cytotoxic T cells, we reasoned that knocking out the GrB pathway would ablate CAR-T cell cytotoxicity. CRISPR-mediated knockout of Granzyme B using an established lab protocol resulted in ~80% knockout efficacy (**Supp Fig. 2-1A**) that led to the inability of GrB knockout, CD19-BBz $CD3^+$ CAR-T cells to control Raji lymphoma outgrowth after repeated antigen challenges (RAC) *in vitro* (**Fig. 2-2A**). Of note, GrB knockout CAR-T cells

retained the capacity to control target cell outgrowth during the earlier rounds of RAC (**Fig. 2-2A**). This may be due to residual GrB stores that have yet to be released. However, after several rounds of antigen stimulation, depletion of GrB within CAR-T cells was found to be substantially reduced *in vitro* (**Fig. 2-2B**).

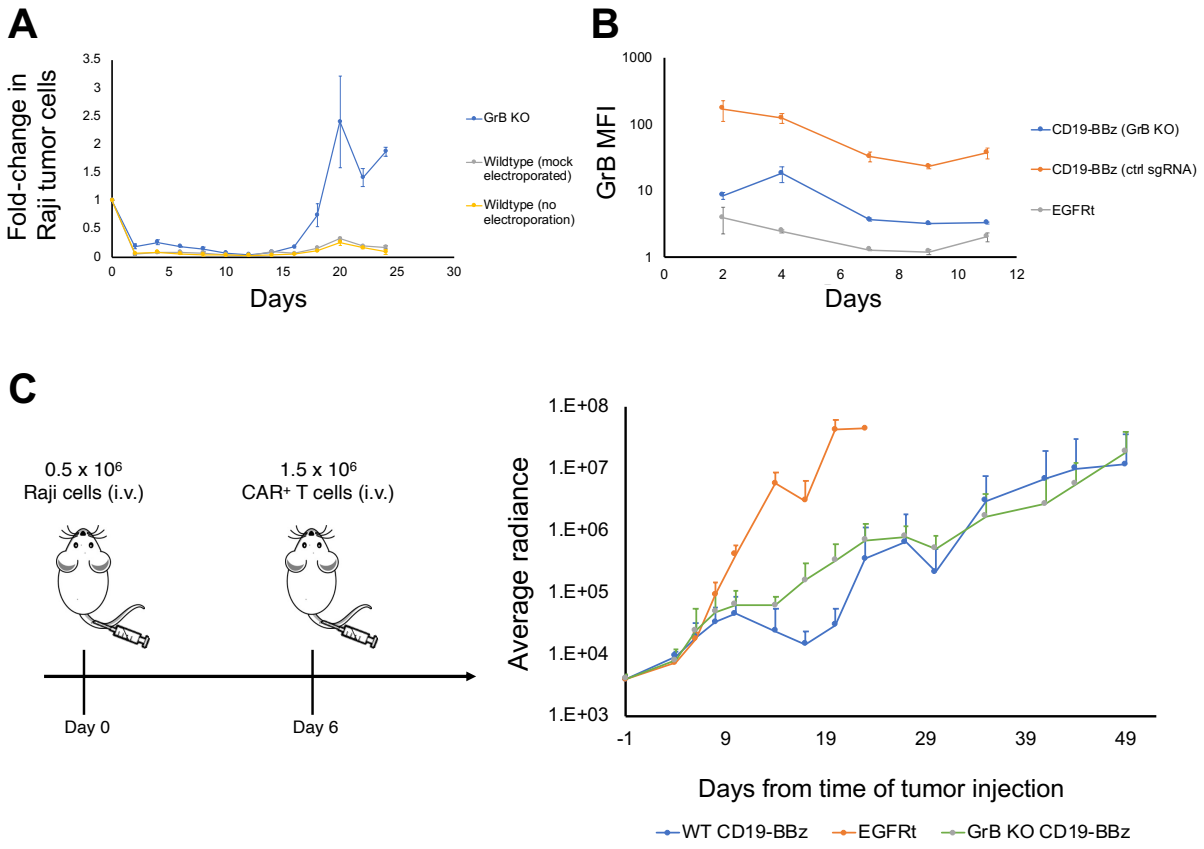

Figure 2-2: Modest reduction in CAR-T cell lysis with Granzyme B CRISPR knockout. (A) CAR-T–cell cytotoxicity upon repeated antigen challenge. CD19-BBz CD3+ CAR-T cells were challenged with Raji tumor cells at a 2:1 effector-to-target (E:T) ratio every 2 days, and the number of viable Raji was quantified by flow cytometry. (**B**) GrB MFI upon cytotoxicity upon repeated antigen challenge. CD19-BBz Tnm CAR-T cells were challenged with Raji tumor cells at a 2:1 effector-to-target (E:T) ratio every 2-3 days, and GrB expression was quanitifed using intracellular flow cytometry. (**C**) Schematic of *in vivo* experiment; n = 6 mice per group. NOD/scid/$\gamma^{-/-}$ (NSG) mice were injected intravenously with ffLuc-expressing Raji cells followed by a single dose of CAR^+ T cells (left). Tumor progression was monitored by bioluminescence imaging (top). Radiance (in photons/sec/cm^2/sr) of individual animals are shown for each group (right).

Having established that GrB can be effectively knocked-out during *in vitro* testing, we sought to evaluate whether GrB knockout was sufficient to ablate CAR-T cell killing in a pre-

clinical *in vivo* setting. We transitioned from using $CD8^+$ and $CD3^+$ T cell subtypes during *in vitro* testing in favor of a more potent, clinically relevant, naïve/memory T (Tnm) cell subtype[9]. GrB knockout CAR-T cells were less effective at controlling tumor outgrowth compared to control CAR-T cells CRISPR-edited with a scrambled sgRNA (wildtype; WT) early in the *in vivo* study (**Fig. 2-2C**). However, both WT and GrB knockout CAR-T cells lost the ability to effectively control the tumor after 29 days (**Fig. 2-2C**). Of note, GrB knockout CAR-T cells were more effective at tumor control than T cells expressing a non-signaling, truncated epidermal growth factor receptor (EGFRt) negative control (**Fig. 2-C**). These data show that GrB knockout CAR-T cells are still able to exert some degree of anti-tumor efficacy, and that there is a lack of tumor-killing persistence by mock CRISPR-edited CD19 CAR-T cells.

We reasoned that the residual level of anti-tumor efficacy mediated by GrB knockout CD19 CAR-T cells can be explained by 1) incomplete GrB knockout, 2) alternative modes of CAR-T cell killing, or a combination of both. We observed that the conventional lab CRISPR protocol resulted in less efficacious knockout of GrB when using Tnm cells (**Supp Fig. 2-1A**), with non-zero levels of GrB present in cells at the end of T-cell culture (**Supp Fig. 2-1B**). Thus, incomplete GrB knockout in Tnm cells can partially account for residual CAR-T cell killing.

Systematic CRISPR optimization enhances Granzyme B knockout efficacy in Tnm cells

Since Tnm cells, by definition, are more naïve in differentiation state compared to bulk $CD8^+$ or $CD3^+$ T cells, we hypothesize that the genomic accessibility to GrB may be a contributing factor for the decreased efficacy in knocking out GrB. Thus, we reasoned that experimental parameters related to the activation status of Tnm cells could improve GrB knockout efficiency. To that end, we varied the day at which CRISPR editing occurs and the initial strength of T-cell activation, in addition to increasing sgRNA concentrations in our first round of CRISPR optimization (**Fig. 2-3A**). We found that all three variables tested – the day of CRISPR editing, the strength of activation, and sgRNA concentration – led to substantial improvement in GrB

knockout efficacy as quantified by TIDE analysis (**Fig. 2-3B**). While increased sgRNA concentration increased CRISPR-editing efficacy, the presence of additional sgRNA contributed to cellular toxicity as evidenced by poor T-cell expansion following CRISPR knockout (**Fig. 2-3C**). In sharp contrast, editing T cells one day earlier alone substantially increased knockout efficacy while improving T-cell recovery and expansion (**Fig. 2-3C**). T-cell expansion is an important metric not only because it effects final cell yield, but also because greater T-cell expansion provides T cells more opportunity to dilute residual GrB stores during cell division. We carried out another iteration of CRISPR optimization, varying additional test parameters coupled with an earlier day of CRISPR editing (**Fig. 2-3D**). A combination of varying all three parameters (condition G) resulted in the highest GrB knockout efficacy and T-cell fold-expansion and was thus adopted as the "optimized" CRISPR editing protocol for Tnm cells (**Fig. 2-3E–F**). The optimized CRISPR protocol was able to reliably increase GrB knockout efficacy, thereby resolving a factor contributing to residual CAR-T cell killing in GrB knockout Tnm cells (**Fig. 2-3G–I**).

A

A. Day 4 CRISPR, 3:1 cell:bead, 1:1 sgRNA:Cas9
B. Day 5 CRISPR, 1:1 cell:bead, 1:1 sgRNA:Cas9
C. Day 5 CRISPR, 3:1 cell:bead, 1:1 sgRNA:Cas9
D. Day 5 CRISPR, 3:1 cell:bead, 3:1 sgRNA:Cas9
E. Day 5 CRISPR, 3:1 cell:bead, 5:1 sgRNA:Cas9

D

A. Day 5 CRISPR, 3:1 cell:bead, 1:1 sgRNA:Cas9
B. Day 4 CRISPR, 3:1 cell:bead, 1:1 sgRNA:Cas9
C. Day 5 CRISPR, 3:1 cell:bead, 3:1 sgRNA:Cas9
D. Day 5 CRISPR, 1:1 cell:bead, 1:1 sgRNA:Cas9
E. Day 4 CRISPR, 3:1 cell:bead, 3:1 sgRNA:Cas9
F. Day 4 CRISPR, 1:1 cell:bead, 1:1 sgRNA:Cas9
G. Day 4 CRISPR, 1:1 cell:bead, 3:1 sgRNA:Cas9

B

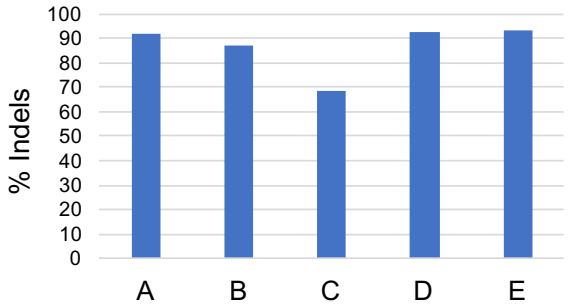

E

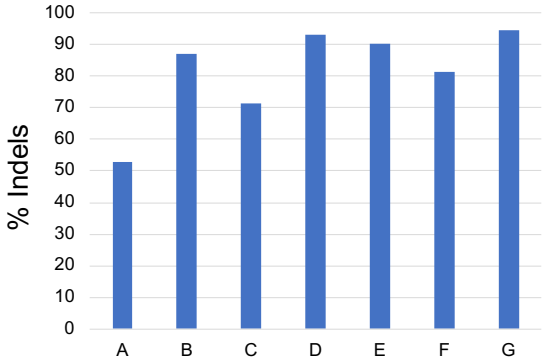

C

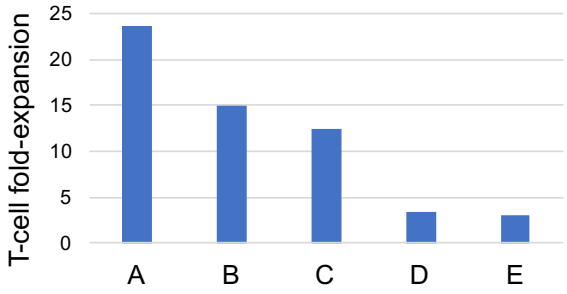

F

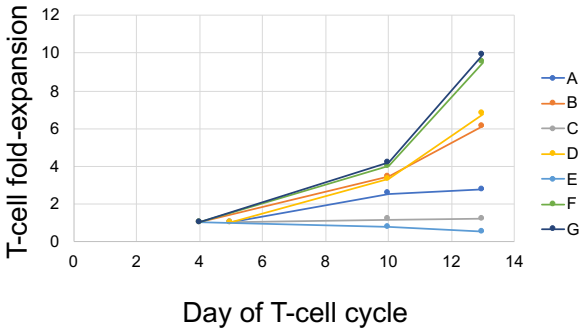

G

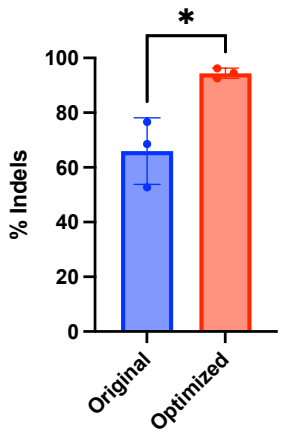

I

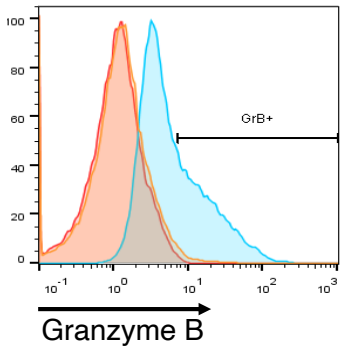

Isotype
CD19-28z GrB KO
CD19-28z WT

Figure 2-3: GrB CRISPR knockout optimization in Tnm cells. (A–C) CRISPR optimization strategy toggling the day of CRISPR editing, activation strength, and sgRNA-to-Cas9 ratio individually. Data are from one Tnm donor. (**A**) Overview of CRISPR editing conditions tested; the parameters from the original, unoptimized CRISPR protocol is underlined as test group C. (**B**) Granzyme B knockout quantified by TIDE analysis. Genomic DNA was isolated from T cells on day 10 and knockout was evaluated by TIDE analysis. (**C**) T-cell fold-expansion comparing the total number of T cells present on day 14 normalized to the number of T cells electroporated per condition. (**D–F**) Expansion of CRISPR optimization strategy toggling the day of CRISPR editing, activation strength, and sgRNA-to-Cas9 ratio individually. Data are from one Tnm donor. (**D**) Overview of CRISPR editing conditions tested; the parameters from the original, unoptimized CRISPR protocol is underlined as test group A. (**E**) Granzyme B knockout quantified by TIDE analysis. Genomic DNA was isolated from T cells on day 10 and knockout was evaluated by TIDE analysis. (**F**) T-cell fold-expansion comparing the total number of T cells present on each day normalized to the number of T cells electroporated per condition. (**G**) Granzyme B knockout quantified by TIDE analysis. Genomic DNA was isolated from T cells on day 10 and knockout was evaluated by TIDE analysis. Data are from 3 Tnm donors. $*p < 0.05$. (**I**) Granzyme B expression in Granzyme B knockout CD19-28z CAR-T cells on day 13 using the optimized protocol evaluated by intracellular flow cytometry.

Multiplexed CRISPR editing of cytolysis genes further ablates CAR-T cell killing

Despite achieving near-complete GrB knockout with the optimized CRISPR protocol (**Fig. 2-3**), GrB single-knockout T cells still exhibited substantial levels of background killing against $OKT3^+$ TM-LCL target cells during *in vitro* RAC (**Fig. 2-4A–B**). We thus sought to further knockout additional modes of T-cell killing in a multiplexed fashion in targeting cytolysis genes Granzyme A (GrA)[3], Fas Ligand (FasL)[10], and tumor necrosis factor-related apoptosis-inducing ligand (TRAIL)[11]. With the exception of the GrB/GrA/FasL/TRAIL quadruple-knockout, all multiplexed CRISPR-editing conditions maintained high efficacy in GrB knockout (**Fig. 2-4C–E**), with substantial knockout of the multiplexed gene targets (**Supp Fig. 2-2A–C**). In line with theoretical expectations, the GrB/GrA/FasL/TRAIL quadruple-knockout condition resulted in the strongest ablation of T-cell killing in one Tnm donor (**Fig. 2-4A**), but the variable GrB knockout efficacy with the quadruple-knockout in a second Tnm donor led to substantial levels of residual T-cell killing (**Fig. 2-4B–C**). Therefore, the GrB/GrA/FasL triple-knockout condition was selected as the strategy to ablate endogenous T-cell killing in light of its reproducibility in multiplexed CRISPR knockout of cytolysis genes and its consistency in being one of the best multiplexed knockout

conditions in reducing T-cell cytotoxicity. Cytolysis knockout T cells in the remainder of this chapter will refer to CRISPR-mediated GrB/GrA/FasL triple-knockout T cells.

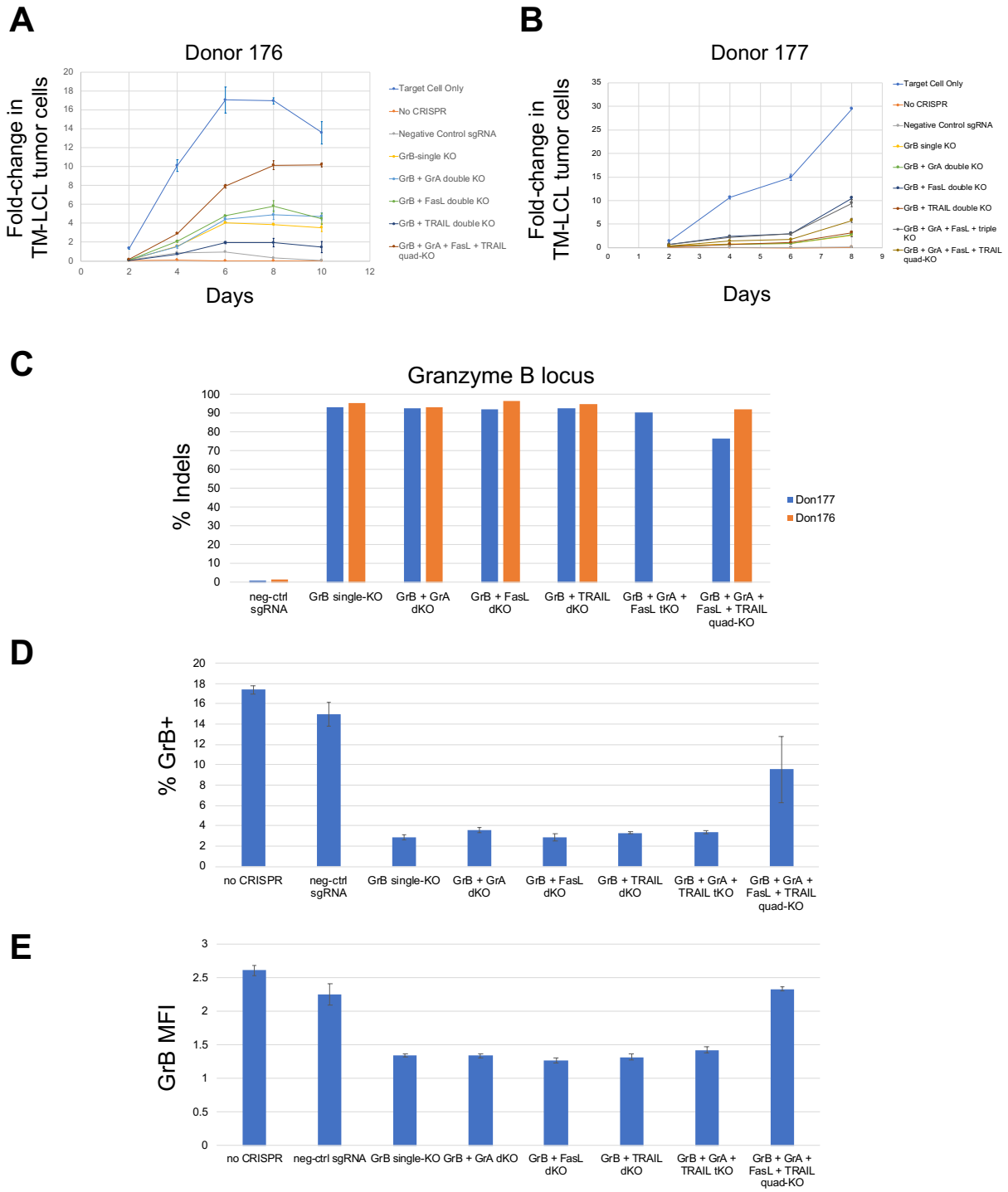

Figure 2-4: Multiplexed CRISPR knockout of multiple T-cell cytolysis genes in Tnm cells. (A–B) T-cell cytotoxicity of multiplex CRISPR-edited Tnm cells upon repeated antigen challenge

in Donor 176 (**A**) and Donor 177 (**B**). T cells were challenged with OKT3^{+} TM-LCL target cells at a 2:1 effector-to-target (E:T) ratio every 2 days, and the number of viable TM-LCL cells was quantified by flow cytometry. (**C**) Granzyme B knockout quantified by TIDE analysis after multiplexed CRISPR editing. Genomic DNA was isolated from T cells on day 10 and knockout was evaluated by TIDE analysis. (**D–E**) Granzyme B expression in multiplex CRISPR-edited T cells on day 14 by flow cytometry. (**D**) Percent GrB positivity and (**E**) GrB MFI.

Retroviral cytotoxicity assay identifies Granzyme B peptide insertion sites for rational protein design

A second piece of the puzzle in reprogramming T cells to kill based on detection of intracellular oncoproteins is the oncoprotein-responsive, GrB-based COVERT molecule itself (**Fig. 2-1**). Specifically, COVERT molecules are engineered GrB molecules that turns ON or OFF its enzymatic activity depending on interactions with an oncoprotein of interest. We envisioned two modes of allosteric by rational protein design – 1) auto-inhibition that is relieved in the presence of oncoprotein (**Fig. 2-5A**) and 2) oncoprotein-induced blockade or conformational alteration of the enzymatic active site (**Fig. 2-5B**). If a peptide could be internally inserted within GrB, then one could fuse a C-terminal cognate ligand-binding domain to induce auto-inhibition, which can subsequently be displaced by nature of oncoprotein competition to the ligand-binding domain (**Fig. 2-5A**). Second, if an oncoprotein ligand-binding domain could be inserted within GrB without significantly disrupting enzymatic activity, oncoprotein binding to COVERT could result in inhibition of GrB enzymatic activity, for instance, through steric blockade of the active site (**Fig. 2-5B**). Therefore, the identification of amino acid sites within GrB permissive to peptide insertion sites is valuable as a foundation for rational COVERT switch design.

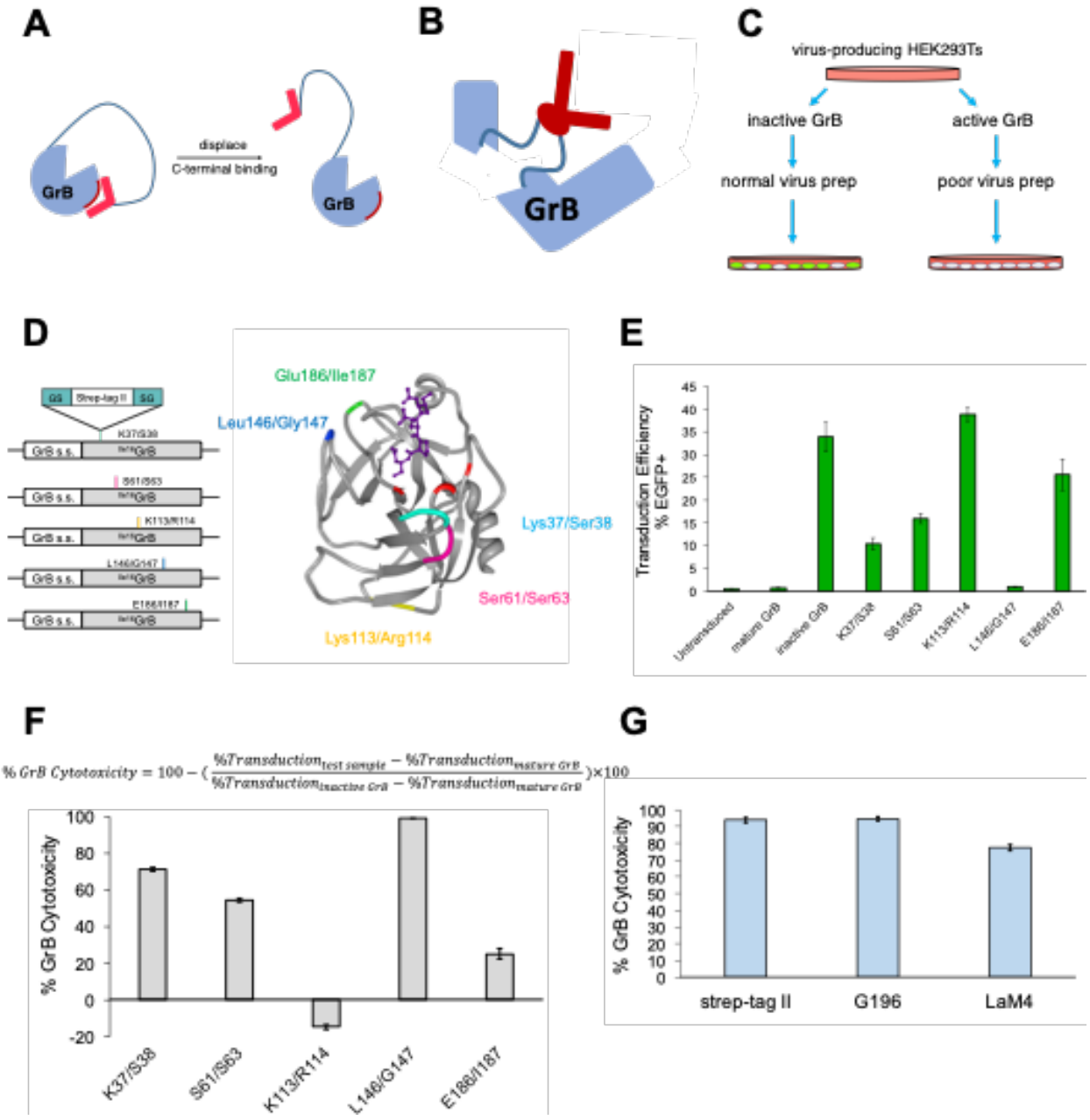

Figure 2-5: Retroviral cytotoxicity assay identifies amino acid residues within Granzyme B amenable to peptide insertion. (**A**–**B**) Schematic representations of putative COVERT designs. (**A**) An auto-inhibitory COVERT molecule comprising of an internal peptide tag insertion (shown as a red arc) and a C-terminal cognate ligand-binding domain. Oncoprotein competition with the C-terminal ligand-binding domain unlocks COVERT from its auto-inhibited state. (**B**) An oncoprotein-responsive COVERT wherein a ligand-binding domain is inserted within Granzyme B, either switching Granzyme B cytotoxicity ON or OFF. (**C**) Pictorial representation of retroviral cytotoxicity assay. HEK293T cells that package retroviral vectors co-expressing GFP (or any transduction marker) with inactive Granzyme B will result in high transduction (left). In contrast, HEK293T cells transfected with retroviral vectors co-expressing active Granzyme B will lead to poor transduction (right), because HEK293T cells that express active Granzyme B will die. (**D**)

Schematic of DNA constructs with strep-tag II, an eight-residue minimal peptide sequence (YSHPQFEK), inserted at various sites within GrB flanked by GS and SG residues (left). Crystal structure of mature GrB (PDB ID: 1IAU) with the catalytic triad (red), tetrapeptide (purple), Lys37/Ser38 (light blue), Ser61/Ser63 (magenta), Lys113/Arg114 (yellow), Leu146/Gly147 (dark blue), and Glu186/Ile187 (green) highlighted (right). Insertion sites all belong to solvent exposed, unstructured loops. (**E**) Transduction efficiencies of HEK293T cells 2 days post-transduction as quantified by flow cytometry. (**F**) The relative cytotoxicity of engineered GrB. Error bars indicate the range among biological triplicates. (**G**) The relative cytotoxicity of synthetic GrB variants with strep-tag II (8 amino acids), G196 (5 amino acids), and a mCherry-binding nanobody (LaM4; 130 amino acids) inserted between L146/G147. Retroviral transduction efficiencies of HEK293T cells were assessed 2 days post-transduction. Error bars indicate the range among biological triplicates.

In order to facilitate higher-throughput testing of putative COVERT switch variants, we developed a novel cell-based cytotoxicity screening assay, termed retroviral cytotoxicity assay (RVCA), in lieu of lower throughout biochemical assays (**Fig. 2-5C**). RVCA leveraged the observation that we were unable to produce retrovirus for constructs that express an active form of GrB (data not shown). This is likely due to the fact retroviral producer HEK293T cells also express active GrB during the viral packaging process and subsequently succumb to GrB-mediated cytotoxicity, thereby preventing any meaningful production of retrovirus. Thus, the relative cytotoxicity of a given COVERT variant can be quantified by how well the virus transduces a fresh set of HEK293T cells.

Since internal insertion of a small peptide is more likely to preserve GrB functionality compared to insertion of a large peptide, we used a short eight amino acid strep-tag II peptide[12], with several known binding partners, as a starting point to identify permissive insertion sites within GrB. We identified five solvent-exposed, unstructured loops within GrB by studying the protein structure and tested their tolerance for peptide insertion (**Fig. 2-5D**). The panel of strep-tag II insertion COVERT constructs co-expressed enhanced green fluorescent protein (EGFP) as a transduction marker. Using RVCA, we quantified the transduction efficacy of each strep-tag II variant (**Fig. 2-5E**) and subsequently calculated the relative cytotoxicity of each molecule (**Fig. 2-5F**). While not all solvent-exposed, unstructured loops were amenable to strep-tag II insertion, we

identified L146/G147 as a permissive insertion site (**Fig. 2-5F**). Additionally, the L146/G147 site tolerates the insertions of a five amino acid G196 peptide[13] and LaM4, a 130 amino acid mCherry-binding nanobody (**Fig. 2-5G**).

Lack of oncoprotein-responsive COVERT switches identified through rational design

The auto-inhibitory COVERT architecture requires an internal peptide insertion and a cognate ligand-binding domain fused to the C-terminal end (**Fig. 2-5A**). G196 is a short peptide with a known G196 single-chain variable fragment (scFv) binding partner[13]; Strep-tag II is another short peptide with strep-tag II scFv[12] and monomeric streptavidin 2 (mSA2)[14] as known binding partners. We cloned a panel of auto-inhibitory COVERT variants, with G196 or strep-tag II as internal peptide tags inserted at the L146/G147 site, paired with either a G196 scFv, strep-tag II scFv, or mSA2 as C-terminal binding partners (**Fig. 2-6A**). C-terminal binding moieties were fused to GrB with a 25, 37, or 50 amino acid flexible GST linker (**Fig. 2-6A**); linker lengths were determined by measuring the distance from GrB's C-terminal end to the L146/G147 site, whereby 25 amino acids provides sufficient slack to bridge the binding domains (data not shown). We observed little-to-no reduction in GrB cytotoxicity among all auto-inhibitory variants tested per RVCA (**Fig. 2-6A**). To determine whether increasing binding avidity could enhance the auto-inhibitory effect, we fused three tandem copies of strep-tag II in tandem, connected with flexible (G4S)2 linkers (**Fig. 2-6B**). Unfortunately, increasing the avidity of strep-tag II and strep-tag II scFv binding interactions did not yield an increase in the auto-inhibitory effect (**Fig. 2-6B**). Collectively, these data demonstrate that such the auto-inhibitory architecture is ineffective at effectively ablating GrB activity.

A

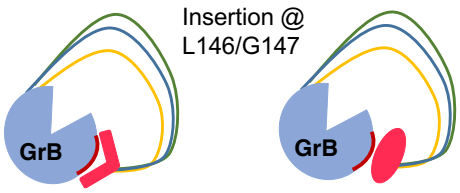

Internal ligand: G196 or strep-tag II

Ligand-binding domains: G196 scFv or strep-tag II scFv

Internal ligand: strep-tag II

Ligand-binding domain: monomeric streptavidin 2 (mSA2)

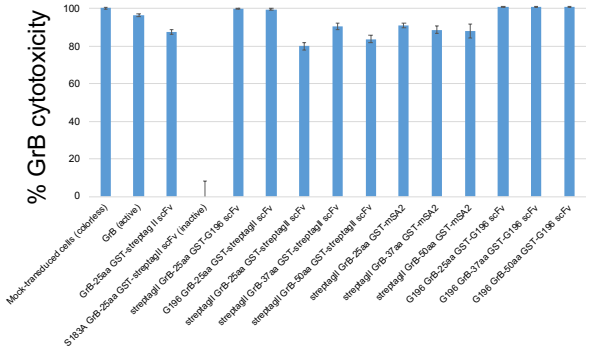

B

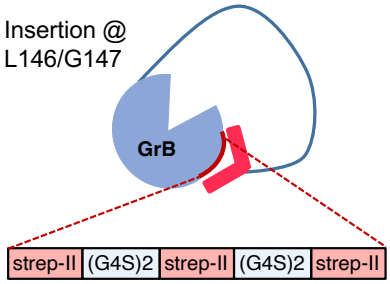

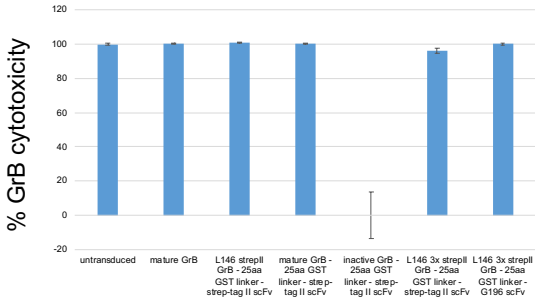

C

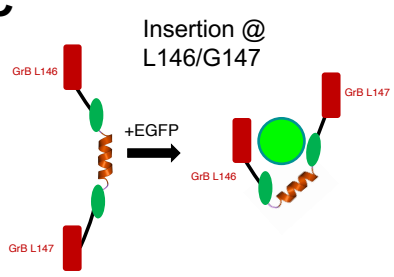

pYC1968	MBP inserted atGrB L146/G147
pYC1969	MBP inserted at GrB L146/G147 flanked with (EK)3
pYC1970	[GBe - alpha helix - GBP6] inserted at GrB L146/G147
pYC1971	[GBP6 - alpha helix - GBe] inserted at GrB L146/G147
pYC1972	[EAAAK1 - GBe - alpha helix - GBP6 - EAAAK1] inserted at GrB L146/G147
pYC1973	[EAAAK1 - GBP6 - alpha helix - GBe - EAAAK1] inserted at GrB L146/G147
pYC1974	GBe inserted at GrB L146/G147 (no additional linkers)
pYC1975	GBP6 inserted at GrB K97/N98 and GBe inserted at GrB L146/G147
pYC1976	GBe inserted at GrB L146/G147 and GBP6 inserted at GrB Y175/D176

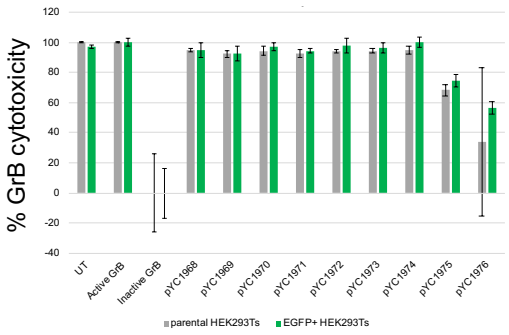

D

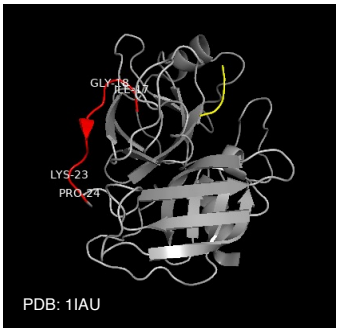

Insertion @ I17/G18

pYC1680	Mature GrB
pYC1681	Inactive GrB
pYC2041	17-GBe-GrB
pYC2049	I17-GBe-(G4S)1-KSYQQQLAK-(G4S)1-GBP6-GrB
pYC2050	I17- GBP6-(G4S)1-KSYQQQLAK-(G4S)1-GBe -GrB
pYC2051	I17-(EAAAK)1-GBe-(G4S)1-KSYQQQLAK-(G4S)1-GBP6-(EAAAK)1-GrB
pYC2052	I17-(EAAAK)1-GBP6-(G4S)1-KSYQQQLAK-(G4S)1-GBe-(EAAAK)1-GrB

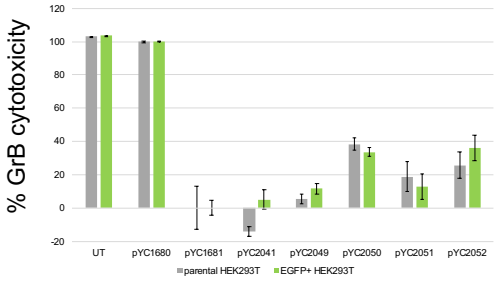

Figure 2-6: Rational COVERT designs demonstrate limited potential for oncoprotein-responsive switch behavior. (A) Evaluation of auto-inhibitory COVERT variants, schematics shown on the left. Relative cytotoxicity of COVERT variants shown on the right. Retroviral transduction efficiencies of HEK293T cells were assessed 2 days post-transduction. Error bars indicate the range among biological triplicates. (**B**) Follow-up evaluation of auto-inhibitory COVERT variants, with 3 tandem insertions of strep-tag II. Relative cytotoxicity of COVERT variants shown on the right. Retroviral transduction efficiencies of HEK293T cells were assessed 2 days post-transduction. Error bars indicate the range among biological triplicates. (**C**) Schematic of maltose-binding protein (MBP)-inspired GFP-binding hinge (left). Two GFP-binding nanobodies that bind to distinct epitopes, GBe and GBP6, sandwich an alpha helical motif; upon GFP-binding, the GFP-binding hinge is expected to clamp around GFP thereby altering local Granzyme conformation at L146/G147. The key for constructs tested are shown (middle) and the relative cytotoxicity of COVERT variants in the presence or absence of EGFP are shown on the right. Retroviral transduction efficiencies of HEK293T cells were assessed 2 days post-transduction. Error bars indicate the range among biological triplicates. (**D**) Crystal structure of mature Granzyme B (PDB ID: 1IAU) with an unstructured stretch of sequences highlighted in red. MBP-inspired, GFP-binding hinge (as shown in (C)) are inserted at I17/G18. The key for constructs tested are shown (middle) and the relative cytotoxicity of COVERT variants in the presence or absence of EGFP are shown on the right. Retroviral transduction efficiencies of HEK293T cells were assessed 3 days post-transduction. Error bars indicate the range among biological triplicates.

Periplasmic binding proteins are a family of proteins found in *E. coli* that adopt large conformational changes in response to ligand, serving as a natural inspiration for a variety of biosensors and synthetic allosteric molecules[15]. Maltose binding protein (MBP) is a canonical periplasmic binding protein, characterized by its ability to clamp around its ligand upon binding[15]. Inspired by MBP, we cloned a panel of COVERT variants with EGFP-binding clamps. We identified two GFP-binding nanobodies, GBe and GBP6[16], that bind to non-overlapping epitopes and use them as our ligand-binding “clamping” moieties. In one EGFP clamp architecture, the GFP-binding nanobodies were joined by the alpha helical sequence that serves as the clamping pivot point in MBP[17] (**Fig. 2-6C**). In a second EGFP clamp architecture, we inserted one GFP-binding nanobody at L146/G147, and a second GFP-binding nanobody at distal to L146/G147 at positions K97/N98 or Y175/D176. All the COVERT molecules with the first EGFP architecture retained high levels of GrB cytotoxicity in the presence or absence of EGFP, demonstrating that the presence of EGFP was insufficient to inhibit GrB function (**Fig. 2-6C**). While the second EGFP

clamp architecture was able to reduce GrB cytotoxicity, this effect was observed irrespective of the presence of EGFP, yielding a lack of OFF switch behavior (**Fig.2-6C**).

GrB is a zymogen with an auto-inhibitory N-terminal Gly-Glu peptide; GrB requires cathepsin C to cleave the N-terminal Gly-Glu peptide to free the N-terminal Ile16 residue from conformational strain such that it can fold into the active site to form a salt bridge with Asp194 for functional enzymatic activity[2]. Seeking inspiration from natural GrB regulation, we inserted GBe or our panel of EGFP-binding clamps, flanked by flexible G4S or rigid EAAAAK linkers, in the unstructured N-terminal region in GrB (**Fig.2-6D**). Here, we expect that ligand binding would induce conformational strain such that Ile16 cannot properly fold into the active site. In contrast to all the previously tested constructs, insertion of peptides at the N-terminal end substantially reduced GrB cytotoxicity across the board (**Fig. 2-6D**). However, only modest EGFP-dependent switch behavior was observed across these constructs with low dynamic range (**Fig.2-6D**). Collectively, none of the rationally designed COVERT variants yielded any allosteric switches, echoing the difficulty in predicting protein function from protein sequence in the space of protein design.

Development of a COVERT library screen enables high-throughput testing of COVERT transposition libraries

Thus far, we have been unable to reliably identify any COVERT molecules with switch behavior through rational design, pointing to the necessity of screening COVERT variants in high-throughput fashion. Per protein sector theory, induction of allostery requires a propagation of forces and strains that alter the conformation of the enzymatic active site upon ligand-binding[18,19]. Therefore, the position at which a ligand-binding domain is inserted plays large role in engaging allosteric conformational changes. To that end, we generated COVERT libraries where LaM4 was randomly inserted throughout the GrB DNA sequence via transposition cloning[7,20] (**Fig. 2-7A**). Since the desired output of an ideal COVERT molecule is ligand-dependent cell death, we

pursued a cell-based screening process to explore the LaM4 COVERT library search space. To ensure that the phenotype of a given cell is directly tied to a single COVERT variant, we designed the library screen around CHO-K1 cells engineered to have a single copy of a DNA landing pad integrated, herein referred to as landing pad CHO-K1 cells[21]. In the landing pad CHO-K1 system, co-transfection of a BxBI integrase with a COVERT library payload plasmid facilitates single-copy integration of the payload plasmid into the CHO-K1 genome (**Fig. 2-7A**).

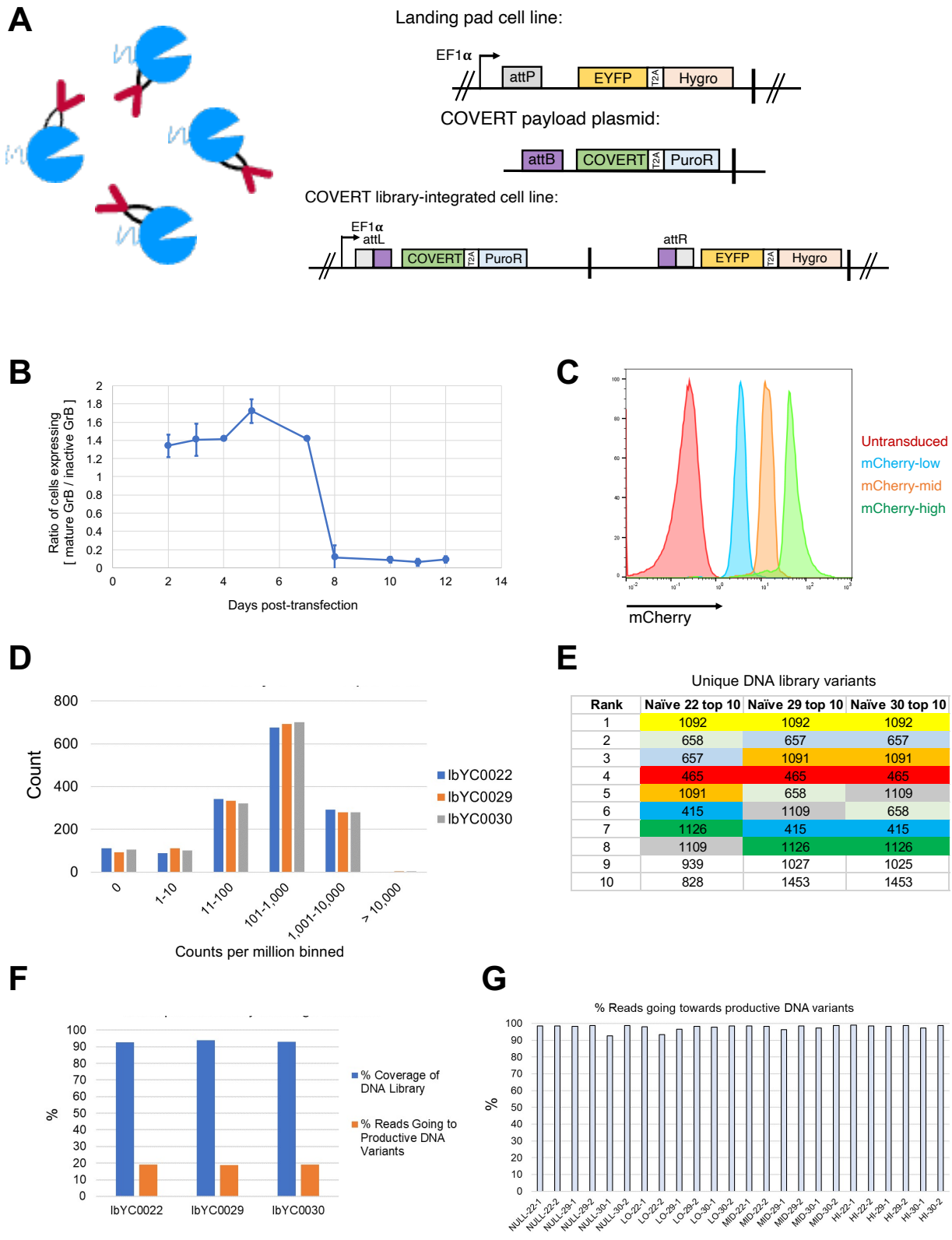

Rank	Naïve 22 top 10	Naïve 29 top 10	Naïve 30 top 10
1	1092	1092	1092
2	658	657	657
3	657	1091	1091
4	465	465	465
5	1091	658	1109
6	415	1109	658
7	1126	415	415
8	1109	1126	1126
9	939	1027	1025
10	828	1453	1453

Figure 2-7: COVERT transposition library design and screening. (**A**) Schematic representation of a COVERT transposition library, where LaM4 is inserted randomly throughout

Granzyme B (left). Landing pad CHO-K1 cells have been integrated with a single-copy of the "landing pad" DNA cassette to facilitate single-copy integration of a cognate "payload" DNA cassette; Landing pad CHO-K1 cells co-transfected with plasmids expressing BxBI integrase and containing the "payload" cassette will result in DNA recombination that introduces the "payload" sequence into the landing pad site (right). attP and attB are recombination motifs that are recognized by BxBI integrase for recombination. Successful recombination leads to loss of EYFP and hygromycin resistance gene expression in landing pad CHO-K1 cells. In its place, a single-copy of COVERT and puromycin resistance gene is expressed. (**B**) The ratio of landing pad CHO-K1 cells expressing mature vs. inactive Granzyme B over time. (**C**) Representative mCherry expression histograms in landing pad CHO-K1 cells engineered to express no, low, mid, or high levels of mCherry. (**D**) The distribution of normalized read counts (in counts per million) for unique DNA library variants prior to library screening in three replicate DNA libraries. (**E**) The 10 most abundant unique DNA library variants present in three replicate DNA libraries. (**F**) Characterization of DNA library variants in each naïve library. The theoretical fraction of reads going to productive DNA variants (i.e., forward and in-frame) is 1/6. (**G**) Fraction of DNA library variants corresponding to productive DNA library variants after library screening. Data are shown for libraries recovered from all four landing pad CHO-K1 cell lines across two independent experiments.

For the cell-based library screen to work, the CHO-K1 cells must succumb to GrB-mediated cell death and be able to co-localize the oncoprotein of interest (i.e., mCherry) with LaM4 COVERT. We confirmed that single-copy expression of active GrB is sufficient to induce CHO-K1 cell death 8 days after transfection (**Fig. 2-7B**). We also generated mCherry-low, mCherry-mid, and mCherry-high expressing CHO-K1 cell lines to study any oncoprotein concentration-dependent effects on LaM4 COVERT switchability (**Fig. 2-7C**). Of note, mCherry was fused to a GrB signal sequence to ensure co-localization with COVERT molecules, which are also fused to a GrB signal sequence necessary for mature GrB expression. By nature of transposition cloning, there is a 5/6 chance that LaM4 is unproductively inserted into GrB – by being inserted out-of-frame or in the reverse orientation; any non-productive insertion results in a premature stop codon within LaM4, thereby preventing the puromycin gene from being properly translated. Altogether, the LaM4 COVERT library screening workflow consists of generation of LaM4 libraries, transfection of libraries into landing pad CHO-K1 cells, expansion and selection in the presence of puromycin (to weed out non-productive insertions), recovery of cellular genomic DNA (gDNA), and next-generation sequencing (NGS) analysis of COVERT amplicons (**Supp Fig. 2-3A**).

Amplicon NGS analysis of the naïve libraries (i.e., the COVERT library prior to library screening) show a normal distribution in the frequency at which a unique COVERT library is present (**Fig.2-7D**). However, upon closer examination, the same library variants show up as being the most abundant across three independent replicate libraries, suggesting that there is a DNA sequence-dependent effect on how frequent a given variant is present in the naïve library (**Fig. 2-7E**). Nevertheless, we were able to generate LaM4 COVERT libraries that cover the vast majority of the theoretical search space, with the expected 1/6 of the library consisting of productively inserted COVERT variants (**Fig.2-7F**). We further validated that only productive DNA variants survive the selection and screening process with puromycin treatment (**Fig. 2-7G**). Collectively, these data validate the COVERT screening methodology as a cell-based screening platform for exploring COVERT transposition libraries.

COVERT library screening identifies putative LaM4 switches but yields poor activity *in vitro*

Our first library screen consisted of three replicate LaM4-inserted COVERT libraries screened in two independent experiments. We developed a scoring system to grade the consistency in which a unique COVERT library variant behaves as a switch for both ON or OFF switches (**Supp Fig. 2-3B–C**). However, none of the COVERT variants in the initial library screen yielded any variants with convincing switch behavior (**Supp Fig. 2-3D**).

We speculated that the lack of linkers flanking LaM4 could render it difficult for proper folding of LaM4, so we subsequently generated LaM4 transposition libraries where LaM4 was flanked by 2, 4, or 8 flexible linkers. Permissivity analysis of the amplicon NGS data show that the most permissive insertion sites are centered around GrB's C-terminus (**Fig. 2-8A**), acting as an internal positive control that enzymatically active GrB variants can be identified in the library screening process. Using the same scoring system (**Supp Fig. 2-3B–C**), we identified three putative COVERT OFF switches that (**Fig.2-8B**). Intriguingly, all three putative switches inserted

LaM4 around GrB's substrate binding pocket, suggesting steric hinderance or occlusion of the active site as the mode of turning OFF GrB activity (**Fig.2-8C**). To functionally validate the activity of these putative switches, we purified each COVERT molecule from HEK293T cells after confirming protein expression (**Supp Fig. 2-4**). Despite showing promise in mCherry-inducible OFF switch behavior, none of the purified LaM4 COVERT molecules had enzymatic activity *in vitro* in the absence of mCherry (**Fig. 2-8D**). Altogether, we were unfortunately unable to identify any ligand-responsive GrB switches through rational design and high-throughput screening.

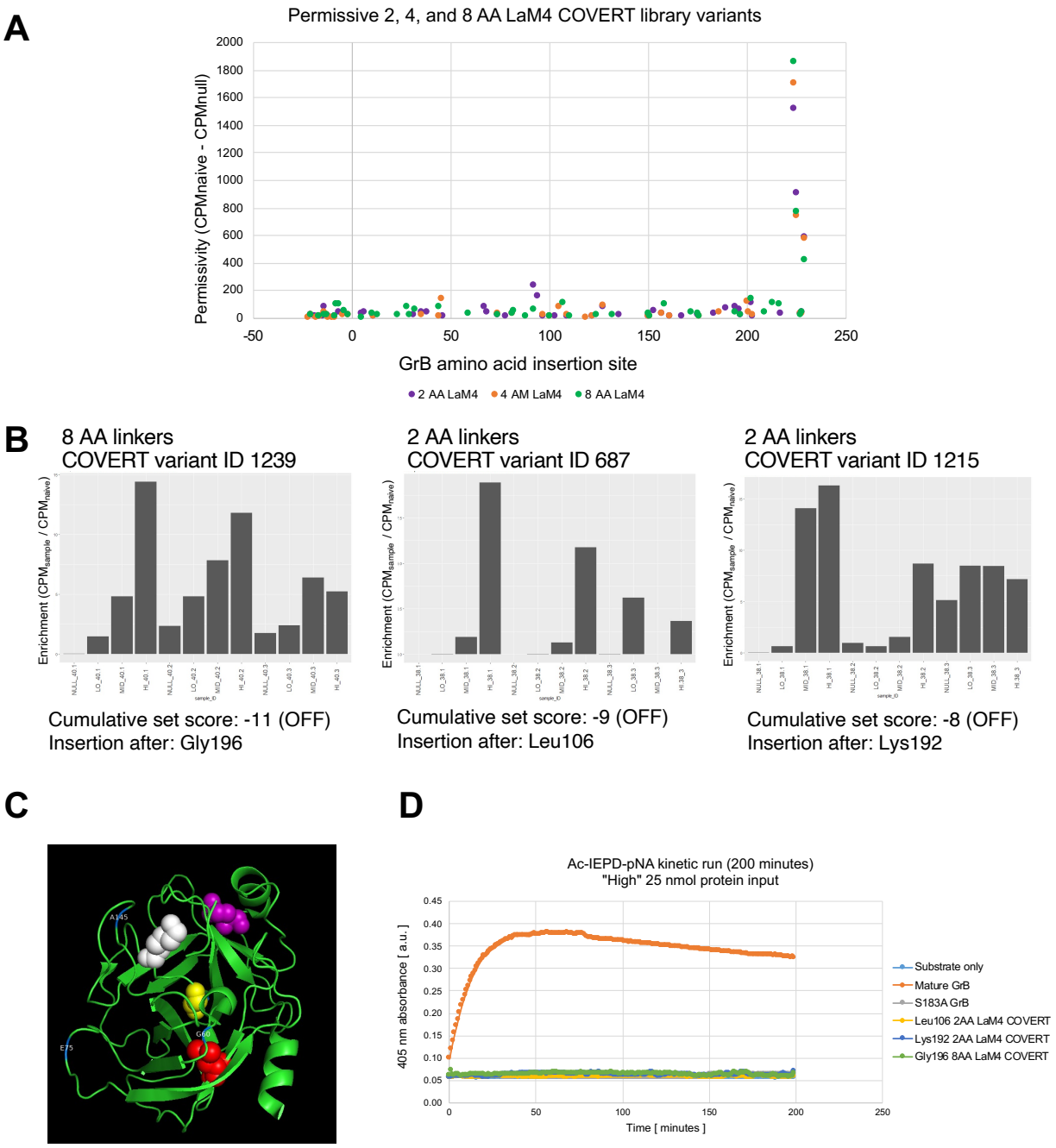

Figure 2-8: Expanding the LaM4 COVERT library search space by varying LaM4 flanking linkers. (**A**) Permissivity analysis for evaluating the tolerability of an insertion at a given amino acid insertion site. (**B**) Three COVERT library variants with OFF switch behavior. (**C**) Crystal structure of mature Granzyme B (PDB ID: 1IAU) with an unstructured stretch of sequences highlighted in red. The insertion sites of each COVERT library variant is mapped onto the crystal structure in bubbles, all surrounding the active site. (**D**) Enzymatic activity of LaM4 COVERT molecules in the absence of mCherry by Ac-IEPD-pNA assay.

Combining cytolysis-knockout CAR-T cells with SUMO-GrB shows lack of differential killing

Given that we were unable to identify any mCherry-responsive COVERT molecules, we moved forward with pairing cytolysis knockout CAR-T cells with a known GrB switch. Our lab had previously developed a SUMO-GrB switch molecule that responds to a tumor-associated protease; a peptide cleavage motif for SENP1 is fused to GrB's N-terminus, and only upon protease cleavage will SUMO-GrB become activated[2]. Our lab had engineered a pair of SENP1-low (by CRISPR-mediated SENP1 knockout) and SENP1-high (through overexpression) K562 leukemia cells. We engrafted SENP1-low and SENP1-high $CD19^+$ K562 cells on opposing flanks to evaluate whether differential killing by cytolysis knockout, SUMO-GrB CD19 CAR-T cells can be achieved (**Fig. 2-9A**). No differential killing of SENP1-low vs. SENP1-high K562 tumors were seen at all three dosages (**Fig. 2-9B**). In fact, there is limited tumor control even when targeting SENP1-high K562 cells when compared to the EGFRt control (**Fig.2-9B**). We hypothesized that the subcutaneously engrafted K562 model may be too difficult for CAR-T cells to clear. To address this, we repeated the experiment and administered CAR-T cells 4 days after tumor engraftment – the point where the tumors have successfully engrafted based on bioluminescence imaging but yet to be palpable; CAR-T cells administered at the highest dose were unable to control tumor in this modified model as well (data not shown). We further attempted to establish a disseminated K562 model in which an equal mixture of SENP1-low and SENP1-high cells were administered intravenously (**Supp Fig. 2-6A**), with the thinking that a liquid tumor model would be easier to clear than a solid tumor model. While we found that tumor control can be achieved in the disseminated model (**Supp Fig. 2-6B**), the highly uneven engraftment of K562 cells introduced intravenously precludes the ability to carry out a well-controlled full-scale animal study (**Supp Fig. 2-6C**).

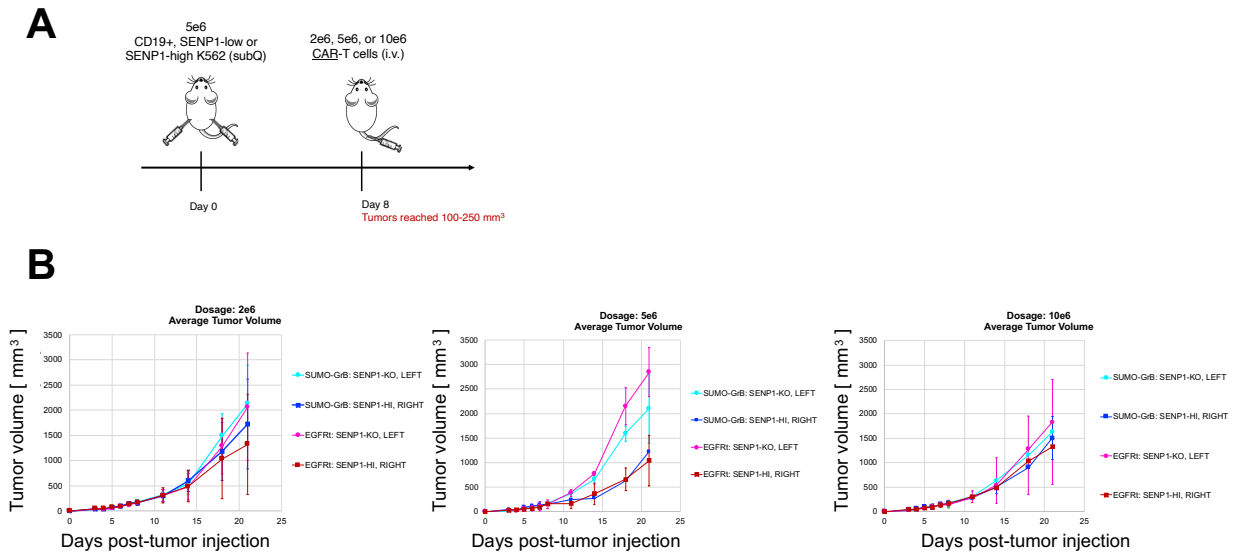

Figure 2-9: Lack of differential killing *in vivo* by cytolysis-knockout, SUMO-Granzyme B CAR-T cells against SENP1-low vs. SENP1-high tumors *in vivo*. (**A**) Schematic of *in vivo* experiment; n = 3 mice per group. NOD/scid/$\gamma^{-/-}$ (NSG) mice were subcutaneously injected with ffLuc-expressing SENP1-low and SENP1-high K562 cells on left and right flanks, respectively, followed by a single dose of CAR-T cells administered intravenously. (**B**)Tumor progression was monitored by caliper measurement.

DISCUSSION

In this chapter, we explored the possibility of re-engineering T cells to kill not based on pattern recognition of surface-bound, tumor-associated antigens, but rather on the presence of intracellular oncoproteins. This addresses the problem of “on-target, off-tumor” toxicities that are associated with T-cell based immunotherapies. We propose that T cells must recognize two tumor-associated signals prior to killing the tumor cell – one signal based on detection of a membrane-bound antigen and a subsequent second signal based on detection of an intracellular oncoprotein within the target cell. In particular, CAR-mediated recognition of a tumor-associated antigen would trigger delivery of an oncoprotein-responsive GrB switch into the target cell, where the presence or absence of the oncoprotein of interest would activate or inhibit GrB-mediated apoptosis. Throughout this exploration, we laid out a roadmap to follow in order to achieve such reprogramming of T-cell killing.

First, the endogenous killing capacity of CAR-T cells must be eliminated to prevent constitutive killing upon CAR antigen stimulation. To that end, we first evaluated whether knocking out a T cell's primary mechanism of killing, through GrB-mediated apoptosis, would be sufficient to prevent CAR-T cells from effectively killing target cells. We found that knocking out GrB alone was insufficient to prevent CAR-T cell cytotoxicity, even with near-perfect CRISPR knockouts, pointing to the presence of compensatory killing mechanisms. This finding was not entirely surprising given the fact that T cells are known to kill through multiple mechanisms. We optimized a multiplexed-CRISPR editing protocol in order to knockout additional cytolysis genes and found that up to three gene targets, including GrB, can be effectively knocked-out. Based on *in vitro* lysis experiments, we identified GrB, GrA, and FasL as a combination of knockouts that best ablated endogenous T-cell killing. However, it should be noted that these findings were based off of T-cell killing of TM-LCL cells, and the best combination of cytolysis genes may depend on the target cell of interest. Maximal ablation of endogenous T-cell killing against a certain cell line will require testing of different combinations of multiplexed CRISPR knockouts against cytolysis genes.

Second, an oncoprotein-responsive switch must be packaged by CAR-T cells and delivered into target cells upon CAR antigen stimulation. GrB naturally fulfills these criteria for CAR-T cell packaging and delivery and was thus used as the starting point for oncoprotein-responsive COVERT switches. Strategies for protein engineering are broadly characterized as rational protein design or directed evolution. Rational protein design, as the name suggests, hinges on the premise that one can rationalize how changes in protein sequences and motifs can influence protein function. This rationalization of protein design narrows down the protein search space and does not necessitate high-throughput screening processes. Throughout this chapter, we explored various rationally designed COVERT architectures, largely drawn from natural inspiration, ranging from auto-inhibitory strategies to mimicking MBP clamping. In fact, additional rational design strategies such as kinase-responsive COVERT molecules or small molecule-

induced intein splicing within GrB were explored (data not shown). Unfortunately, none of the rationally designed COVERT architectures yielded any ligand-inducible switching in GrB enzymatic activity. Broadly, the COVERT architectures tested were either unable to reduce appreciable GrB activity (such as the case of L146/G147 insertions) or substantially reduced GrB activity irrespective of the ligand. These efforts underscore the challenge in predicting novel protein function based on protein sequence alone and reasoned that a high-throughput screen would give us better odds of finding a switch.

In this chapter, we further pursued COVERT protein engineering using directed evolution and adapted a transposition-based library cloning process and developed a high-throughput library screening workflow. Transposition-based library generation enabled us to sample a search space where our ligand-binding domain LaM4 was randomly inserted throughout the whole GrB sequence – an incredibly difficult and time-consuming task if cloned through conventional molecular biology techniques. However, it should be noted that transposition libraries are inherently skewed in the frequency at which a unique variant is present due to DNA sequence-based preferences of the transposase. Therefore, it is important to incorporate appropriate analysis strategies, such as calculating relative enrichment, to control for cloning-associated biases. Even though positive and negative controls behaved as expected during vetting of the library screening process, putative COVERT switches that were identified were unable to translate into functional switches in the wet lab. In fact, all identified OFF switches (i.e., should be active in the absence of cognate ligand) had no enzymatic activity in the absence of mCherry. This indicates that there is a mismatch in what the screening process is screening for compared to our expectations. One potential explanation is a species-associated difference in our library screening process. While CHO-K1 cells are commonly used in producing recombinant therapeutics, differences in post-translational modifications could account for differences in protein function. Furthermore, it is important to note that our screen relies on cell death as a direct readout of GrB activity. While GrB activity results in apoptosis, cell death may also occur for other biological

reasons. Moving forward, implementing direct readouts of GrB activity in the appropriate target cell types would be instrumental in enhancing the validity of the library screening results.

Finally, we engineered our multiplexed CRISPR-edited CAR-T cells to express a SENP1-responsive SUMO-GrB molecule and evaluated whether appreciable differential killing could be observed in a pre-clinical setting. We used a matching pair of CD19+ K562 leukemia cells that with low and high levels of SENP1 expression. Our lab had previously found that K562 cells were the only cell line that could grow normally with a SENP1 knockout and overexpression, presumably because SENP1 is central to controlling a host of key biological processes. We found that the cytolysis knockout CAR-T cells were unable to mediate any effective tumor control in the K562 model, precluding any comparison of tumor control based on SENP1 expression. This may be due to the fact that K562 cells are harder to kill than other liquid tumor cell lines (data not shown), that multiplex CRISPR-edited T cells have decreased fitness, or a combination of both. A less aggressive tumor model should be used to showcase the ability of cytolysis knockout, SUMO-GrB CAR-T cells to differentially kill *in vivo*. This may be achieved by identifying a different tumor cell line that can be engineered to have low and high levels of SENP1 expression, by identifying a method for even engraftment of K562 cells as disseminated tumor model, or by increasing the CAR-T cell treatment dosage. The finding that cytolysis knockout CAR-T cells cannot effectively clear tumors highlights a key consideration for the proposed COVERT system – that cytolysis CRISPR-edited T cells are inherently have a weaker capacity in killing tumor cells. Therefore, in order for the COVERT system to work in a clinically relevant setting, the engineered COVERT molecule of interest must be highly cytotoxic in the ON state.

Altogether, this chapter presents a framework for engineering T cells to kill based on the detection of intracellular oncoproteins. While no oncoprotein-responsive switch was ultimately identified, the work presented in this chapter provides methods that can be incorporated into other T-cell engineering efforts. We now have a methodology for simultaneously target three gene targets in primary human CAR-T cells. Furthermore, we demonstrate that the combination of

transposition library cloning with single-cell library integration can facilitate cell-based library screens in high-throughput fashion.

ACKNOWLEDGEMENTS

We would like to thank Patrick Ho for his vision in the COVERT platform, for establishing the CRISPR methodology that served as our starting point for optimization, and for adapting the transposition library cloning methodology used in this chapter together with Vinya Bhuvan. We also thank Dr. Timothy K. Lu for providing the landing pad CHO-K1 cell lines and corresponding plasmids that helped us enable single-copy COVERT library integration. We also thank Dr. Adam Savage and Avi Flamholz for the development of DIPseq and their assistance with troubleshooting. We also thank Nicholas Rochette from the UCLA Collaboratory for his assistance in setting up the DIPseq pipeline on UCLA's Hoffman2 computational cluster. We finally would like to thank Marco Morselli from the UCLA Collaboratory for his assistance in DNA sonication and discussions regarding DNA amplicon sequencing library preparation.

REFERENCES

1. Hou, A. J., Chen, L. C. & Chen, Y. Y. Navigating CAR-T cells through the solid-tumour microenvironment. *Nat. Rev. Drug Discov.* **20**, 531–550 (2021).
2. Ho, P., Ede, C. & Chen, Y. Y. Modularly Constructed Synthetic Granzyme B Molecule Enables Interrogation of Intracellular Proteases for Targeted Cytotoxicity. *ACS Synth. Biol.* **6**, 1484–1495 (2017).
3. Cullen, S. P., Brunet, M. & Martin, S. J. Granzymes in cancer and immunity. *Cell Death Differ.* **17**, 616–623 (2010).
4. Zah, E., Lin, M.-Y., Silva-Benedict, A., Jensen, M. C. & Chen, Y. Y. T Cells Expressing CD19/CD20 Bispecific Chimeric Antigen Receptors Prevent Antigen Escape by Malignant B Cells. *Cancer Immunol. Res.* **4**, 498 LP – 508 (2016).
5. Fridy, P. C. *et al.* A robust pipeline for rapid production of versatile nanobody repertoires. *Nat. Methods* **11**, 1253–1260 (2014).
6. Tang, J. C. Y. *et al.* A Nanobody-Based System Using Fluorescent Proteins as Scaffolds for Cell-Specific Gene Manipulation. *Cell* **154**, 928–939 (2013).
7. Nadler, D. C., Morgan, S.-A., Flamholz, A., Kortright, K. E. & Savage, D. F. Rapid construction of metabolite biosensors using domain-insertion profiling. *Nat. Commun.* **7**, 12266 (2016).
8. Ewen, C. L., Kane, K. P. & Bleackley, R. C. A quarter century of granzymes. *Cell Death Differ.* **19**, 28–35 (2012).
9. Zah, E. *et al.* Systematically optimized BCMA/CS1 bispecific CAR-T cells robustly control heterogeneous multiple myeloma. *Nat. Commun.* **11**, 2283 (2020).
10. Charles A Janeway, J., Travers, P., Walport, M. & Shlomchik, M. J. T cell-mediated cytotoxicity. *Immunobiol. Immune Syst. Health Dis. 5th Ed.* (2001).
11. Wang, S. & El-Deiry, W. S. TRAIL and apoptosis induction by TNF-family death receptors. *Oncogene* **22**, 8628–8633 (2003).

12. Schmidt, T. G. & Skerra, A. The Strep-tag system for one-step purification and high-affinity detection or capturing of proteins. *Nat. Protoc.* **2**, 1528–1535 (2007).
13. Tatsumi, K. *et al.* G196 epitope tag system: a novel monoclonal antibody, G196, recognizes the small, soluble peptide DLVPR with high affinity. *Sci. Rep.* **7**, 43480 (2017).
14. Lim, K. H., Huang, H., Pralle, A. & Park, S. Stable, high-affinity streptavidin monomer for protein labeling and monovalent biotin detection. *Biotechnol. Bioeng.* **110**, 57–67 (2013).
15. Dwyer, M. A. & Hellinga, H. W. Periplasmic binding proteins: a versatile superfamily for protein engineering. *Curr. Opin. Struct. Biol.* **14**, 495–504 (2004).
16. Chang, Z. L. *et al.* Rewiring T-cell responses to soluble factors with chimeric antigen receptors. *Nat. Chem. Biol.* **14**, 317–324 (2018).
17. Kim, J. R. & Ostermeier, M. Modulation of effector affinity by hinge region mutations also modulates switching activity in an engineered allosteric TEM1 β-lactamase switch. *Arch. Biochem. Biophys.* **446**, 44–51 (2006).
18. Pincus, D., Resnekov, O. & Reynolds, K. A. An evolution-based strategy for engineering allosteric regulation. *Phys. Biol.* **14**, 025002 (2017).
19. Reynolds, K. A., McLaughlin, R. N. & Ranganathan, R. Hot Spots for Allosteric Regulation on Protein Surfaces. *Cell* **147**, 1564–1575 (2011).
20. Oakes, B. L. *et al.* Profiling of engineering hotspots identifies an allosteric CRISPR-Cas9 switch. *Nat. Biotechnol.* **34**, 646–651 (2016).
21. Gaidukov, L. *et al.* A multi-landing pad DNA integration platform for mammalian cell engineering. *Nucleic Acids Res.* **46**, 4072–4086 (2018).

SUPPLEMENTARY INFORMATION

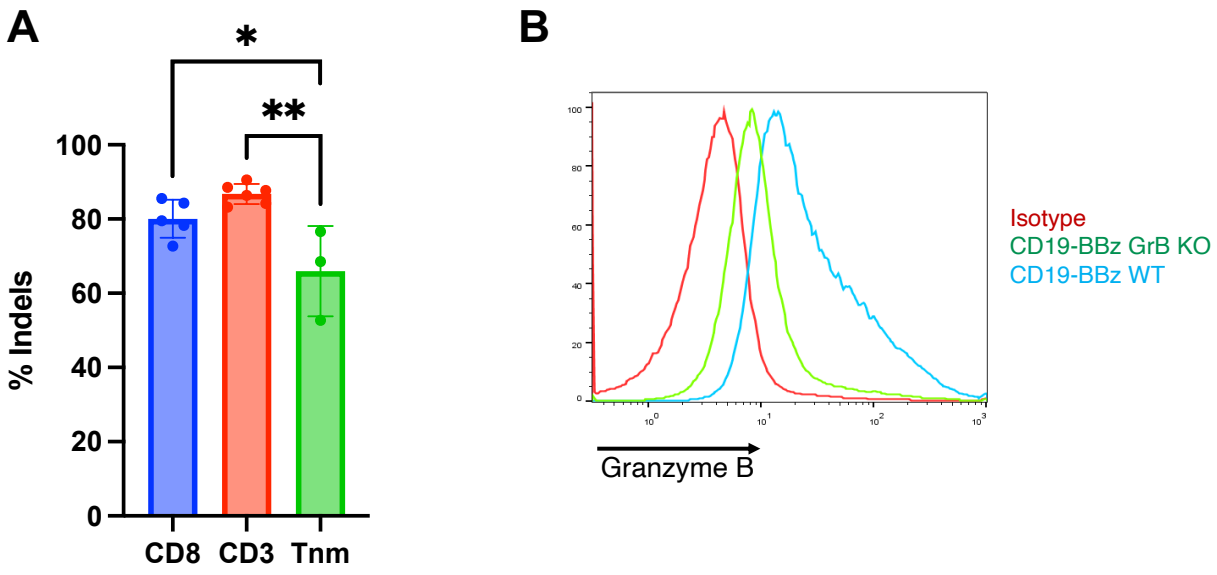

Supplementary Figure 2-1: GrB knockout using the original, unoptimized CRISPR editing protocol. (**A**) The extent of Granzyme B knockout mediated by the original, unoptimized CRISPR knockout protocol tested on $CD8^+$, $CD3^+$, or Tnm T cells. Genomic DNA was isolated from T cells on day 10 and knockout was evaluated by TIDE analysis. *$p < 0.05$, **$p < 0.01$ (**B**) Granzyme B expression in Granzyme B knockout CD19-BBz CAR-T cells on day 13 using the optimized protocol evaluated by intracellular flow cytometry.

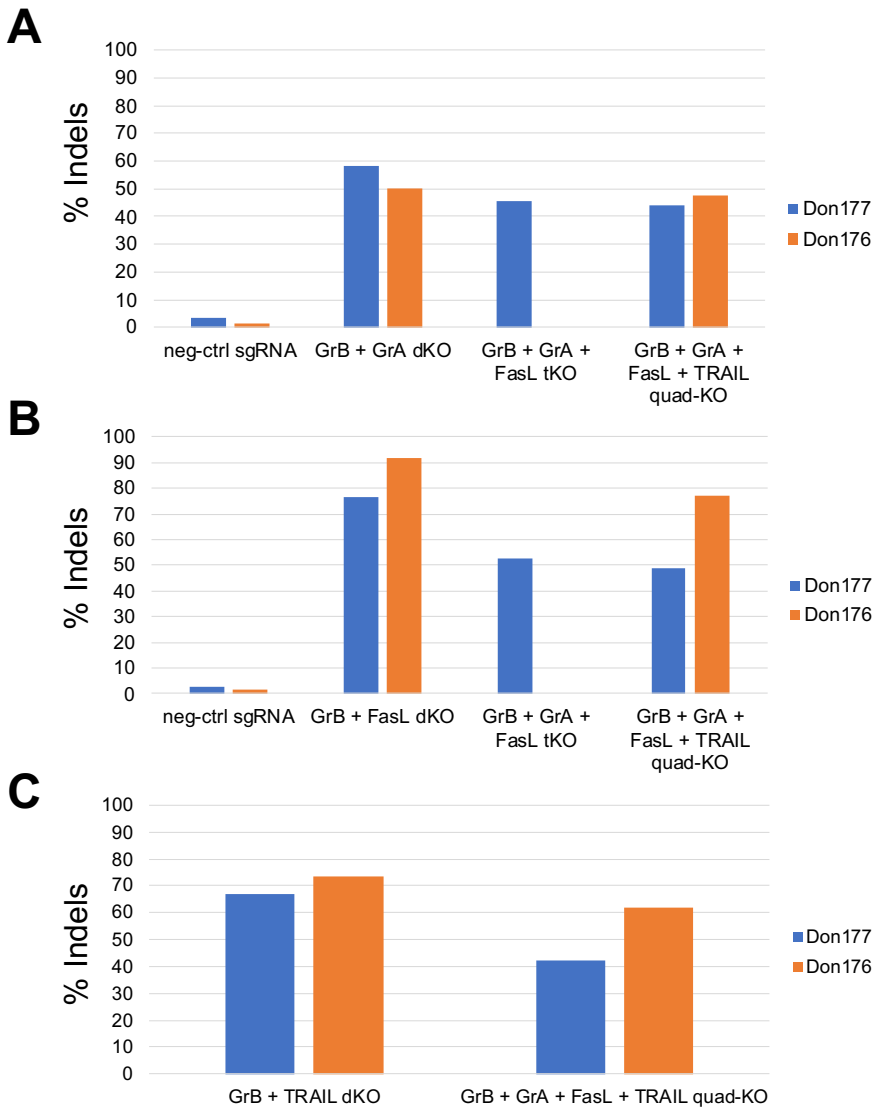

Supplementary Figure 2-2: Quantification of multiplexed CRISPR editing efficacy by TIDE analysis. (**A**) Granzyme A, (**B**) Fas ligand, and (**C**) Tumor necrosis factor-related apoptosis-inducing ligand (TRAIL) knockout quantified by TIDE analysis. Genomic DNA was isolated from T cells on day 10 and knockout was evaluated by TIDE analysis.

A

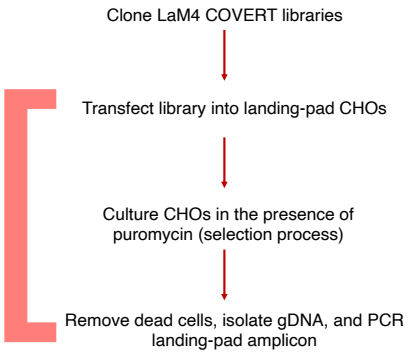

B

If NULL > HI → set score = 4

- If NULL < LO, then penalize the score (–1)
- If NULL < MID, then penalize the score (–1)
- If LO < MID, then penalize the score (–1)
- If LO < HI, then penalize the score (–1)
- If MID < HI, then penalize the score (–1)

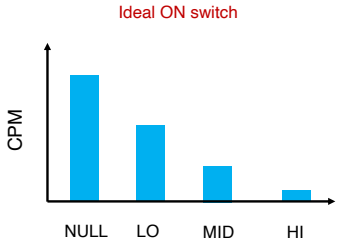

Note: the "highest" score per set is 4, the "lowest" score per set is 1

C

If NULL < HI → set score = –4

- If NULL > LO, then penalize the score (+1)
- If NULL > MID, then penalize the score (+1)
- If LO > MID, then penalize the score (+1)
- If LO > HI, then penalize the score (+1)
- If MID > HI, then penalize the score (+1)

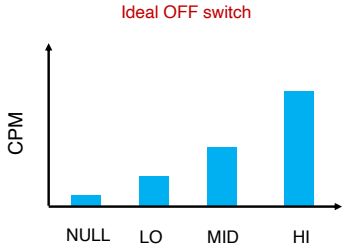

Note: the "highest" score per set is –4, the "lowest" score per set is –1

D

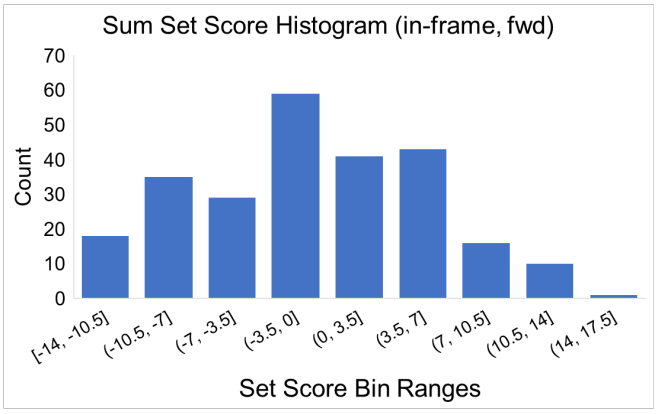

Supplementary Figure 2-3: COVERT transposition library screening processes. (**A**) LaM4 COVERT library screening workflow. (**B–C**) Computational logic in calculating "set scores" for each COVERT library variant to evaluate switch behavior for ON switch behavior (**B**) or OFF switch behavior (**C**). (**D**) The distribution of "set scores" after library screening. Set scores for an ideal ON switch is +24 and an ideal OFF switch is –24 since there were three replicate libraries, screened in two independent experiments.

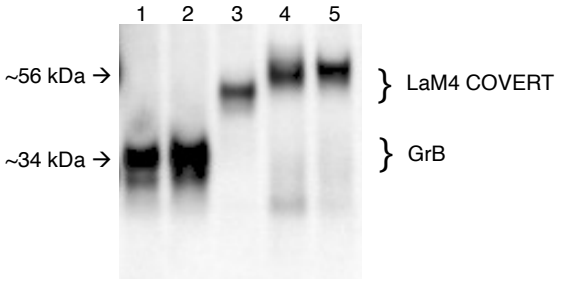

1. Mature GrB
2. S183A GrB (inactive)
3. Leu106 2AA LaM4 COVERT
4. Lys192 2AA LaM4 COVERT
5. Gly196 8AA LaM4 COVERT

Supplementary Figure 2-4: Confirmation of LaM4 COVERT protein expression. Anti-Granzyme B western blot staining of cell lysate from HEK293T cells transfected to express mature Granzyme B, inactive Granzyme B, and LaM4 COVERT OFF switches.

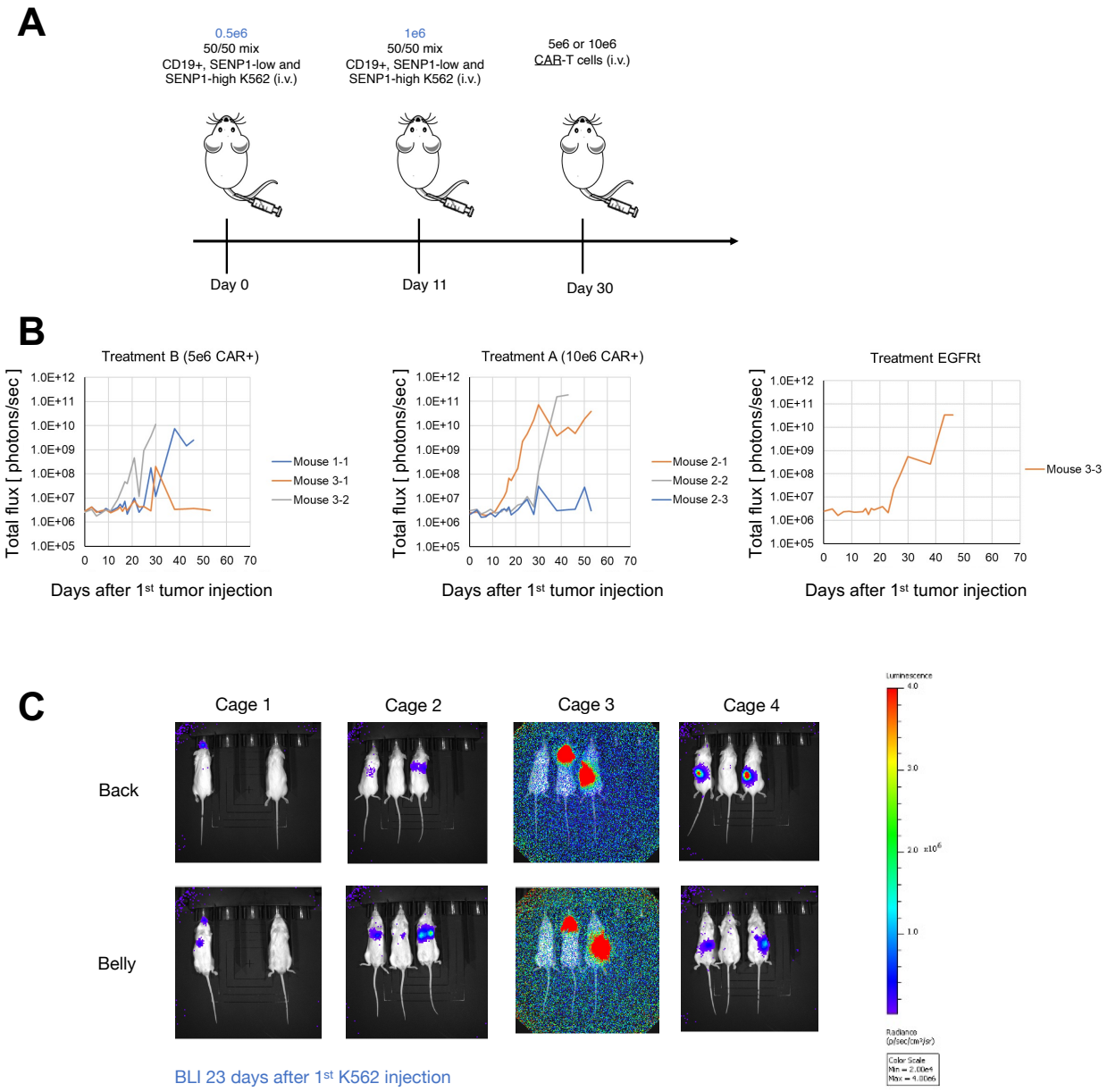

Supplementary Figure 2-6: Inconsistent engraftment of K562 cells when administered intravenously. (**A**) Schematic of *in vivo* experiment; n = 1-3 mice per group. NOD/scid/$\gamma^{-/-}$ (NSG) mice were injected intravenously with two doses of 1:1 mixture of SENP1-low and SENP1-high, ffLuc-expressing K562 cells, followed by a single dose of CAR^{+} T cells. (**B**) Total flux (in photons/sec) of individual animals are shown for each group. (**C**) Radiance (in photons/sec/cm^{2}/sr) of individual animals are shown for each cage 23 days after the first dose of tumor cells.

Chapter 3. Transcriptomic-guided enrichment strategies of high-performing CAR T cells and targeted ablation of CAR-T cell dysfunction

ABSTRACT

The success of adoptive T-cell therapy hinges in part on the sustained output of robust anti-tumor functions from engineered T cells. However, T cells become exhausted upon repeated antigen stimulation and can enter a dysfunctional state, preventing any further control of the tumor. Therefore, the ability to engineer T cells with enhanced persistence and ability to resist exhaustion and dysfunction will improve the potency of adoptively transferred CAR-T cells. Here, We systematically compare high-performing vs. low-performing CAR T cells with the objectives of developing engineering strategies that 1) enrich for robust CAR T cell subpopulations during cell manufacturing and 2) counteract T-cell dysfunction–related processes for enhanced functionality and persistence.

INTRODUCTION

While significant advances have been made in the design of synthetic receptors and genetic T-cell therapeutic genetic programs[1,2], the ability for T cells to robustly sustain therapeutic output remains an indispensable prerequisite for clinical success. T cells can enter a dysfunctional state when challenged with prolonged antigen stimulation, such as while fighting tumor cells, due to exhaustion and consequently exhibit defective anti-tumor functions[3]. While studies have shown that T-cell responses can be reinvigorated through checkpoint inhibitory blockade, a large fraction of patients remain non-responsive, suggesting additional dysfunction-inducing mechanisms are at play and that there is a need for other avenues of T-cell reinvigoration[4–6]. Our lab has previously reported the observation that CAR-T cells undergo population bifurcation upon antigen stimulation, wherein one population, termed CAR^{hi}, displayed robust anti-tumor functions while the other population, termed CAR^{lo}, was dysfunctional[7]. A systematic comparison of CAR^{hi} and CAR^{lo} cells can provide a framework for studying immune checkpoint-independent dysfunction, as the CAR^{hi} population comprises of robust CAR T cells that upregulate PD-1[8]. We reason that understanding the causes and symptoms of T-cell dysfunction can guide the development of therapeutic strategies that prevent or counteract loss of T-cell function due to exhaustion. Broadly speaking, two categories of approaches may be taken to generate more uniform, high-performing T-cell products. First, one could attempt to identify and generate therapeutic products from specific T-cell subtypes with higher anti-tumor potential. Second, if the mechanism of T-cell dysfunction is well understood, one could attempt to introduce genetic or pharmaceutical interventions to prevent dysfunction.

We propose to address the challenge of engineering T cells capable of sustained anti-tumor responses by exploring strategies that 1) enrich for robust CAR^{hi} cells during CAR T-cell manufacturing and 2) targeted ablation of pathways contributing to CAR T-cell dysfunction. We hypothesize that the transcriptomic comparison of functionally heterogeneous CAR^{hi} and CAR^{lo}

cells 1) can identify intrinsic surface markers on unactivated T cells destined to become CAR^{hi} and 2) can elucidate intrinsic mechanisms of CAR-T–cell dysfunction upon antigen stimulation. An understanding of CAR-T–cell dysfunction mechanisms can subsequently be used to guide the development of cellular engineering strategies that counteract CAR T-cell exhaustion/dysfunction. In this chapter, we present transcriptomics-based exploratory strategies that can guide the identification of sortable surface markers for potent T-cell subtypes and exhaustion/dysfunction-inducing biological pathways. We further explore the validity of the transcriptomic data-guided insights through empirical *in vitro* testing.

METHODS

DNA Constructs. DNA constructs were assembled using standard molecular biology cloning techniques assembling chemically synthesized oligonucleotides or gBlocks by Integrated DNA Technologies (Coralville, IA). The MSCV retroviral vector and pHIT60 and RD114 retroviral packaging vectors were generous gifts from Dr. Steven Feldman (National Cancer Institute). CD19 and CD20 CARs were constructed as previously reported and were cloned into the MSCV backbone[9].

Cell Lines. HEK293T cells were obtained in 2011 from ATCC (Manassas, VA). Raji cells were generous gifts from Dr. Michael C. Jensen (Seattle Children's Research Institute), which were originally obtained from ATCC in 2003. Cells were cultured in either DMEM (HEK293T) or RPMI-1640 (Raji) supplemented with 10% heat-inactivated FBS (HI-FBS). All mammalian cell cultures were maintained at 37°C and 5% CO_2.

Primary Human T-cell Isolation and Culture. Primary human CD3+, CD4+, and CD8+ T cells were isolated from healthy donor blood samples obtained from the UCLA Blood & Platelet Center using the RosetteSep Human T Cell, $CD4^+$ T Cell, or $CD8^+$ Enrichment Cocktail (Stemcell

Technologies, Vancounver, Canada) according to the manufacturer's protocol. T cells were either kept in culture or cryopreserved at 10-50 x 10^6 cells/mL in complete T-cell media (RPMI-1640 supplemented with 10% HI-FBS) supplemented with 10% DMSO post-isolation. Thawed T cells were seeded at 1-2 x 10^6 cells/mL in complete T-cell media. T cells were activated with anti-CD3/CD28 Dynabeads (Life Technologies, Carlsbad, CA) at 1:1 or 3:1 cell-to-bead ratios. T-cell cultures were supplemented with 50 U/mL IL-2 (Life Technologies, Carlsbad, CA) and 1 ng/mL IL-15 (Peprotech, Rocky Hill, NJ) every 48-72 hours unless otherwise specified. T cells were expanded in complete T-cell media supplemented with 0.25 μM PXD101, 1.58 μM SAHA, or 0.50 μM SAHA after retroviral transduction.

Retrovirus Production and Transduction. HEK293T cells were seeded at 3-6 x 10^6 cells/9 mL/dish in 10 cm tissue-culture dishes. Tissue culture dishes were coated with 0.1 mg/mL poly-d-lysine for one hour and washed with phosphate buffered saline (PBS) prior to HEK293T seeding. Culture medium was replaced with fresh DMEM + 10% HI-FBS prior to the transfection of 3.8 μg retroviral construct, 3.8 μg pHIT60, and 2.4 μg RD114 via linear PEI. 14 to 18 hours post-transfection, cells were washed with PBS supplemented with 2% HI-FBS and cultured in DMEM supplemented with 10% HI-FBS, 20 mM HEPES, and 10 mM sodium butyrate for 8 hours. After 8 hours, cells were washed with PBS supplemented with 2% HI-FBS before media change to DMEM supplemented with 10% HI-FBS and 20 mM HEPES. Retrovirus-containing supernatant was harvested on each of the two subsequent days post-media change and filtered through a 0.45 μm, low-protein–binding filter and stored at -80 °C. At 48 and 72 hours post-Dynabead activation, 1 x 10^6 T activated T cells were transduced with 2 mL of retroviral supernatant supplemented with 5 μg/mL polybrene (Sigma-Aldrich, St. Louis, MO) by spinfection at 800 x g for 90 minutes at 30 °C. Retroviral supernatant was removed immediately post-spinfection and replenished with fresh T-cell media.

Flow Cytometry and FACS. Unless otherwise noted, flow cytometry experiments performed in this report was run on a MACSQuant VYB cytometer (Miltenyi Biotec). CAR expression was determined by antibody staining for FLAG-tag (clone M2; BioLegend). Truncated epidermal growth factor receptor (EGFRt) surface expression was probed with Erbitux (Bristol-Myers Squibb) that was biotinylated in-house (EZ-link Sulfo-NHS-Biotin, Pierce) followed by PE-conjugated streptavidin (Jackson ImmunoResearch). A flow-cytometric screen of the surface proteome was carried out using LEGENDScreen™ Human PE Kit (BioLegend) according to manufacturer's protocol. T cells were assessed for surface expression of epitopes using fluorescently labelled monoclonal antibodies for CD194 (clone L291H4, BioLegend), CD62L (clone DREG-56, BioLegend), CD49d (clone 9F10, BioLegend), CD192 (clone K036C2, BioLegend), CD14 (clone M5E2, BioLegend), and CD25 (clone BC96, BioLegend) and corresponding isotype controls. Flow data compensation and data analysis were performed using FlowJo Data Analysis software (TreeStar, Ashland, OR). Data shown were derived from biological triplicates unless otherwise specified.

RNA Isolation and RNA Sequencing. Total RNA from sorted cells were isolated via Qiagen RNeasy Mini Kit immediately post-FACS and cryopreserved at -80 °C. Total RNA from CAR^{hi}, CAR^{lo}, and unstimulated cells were prepared following a non-stranded mRNA protocol (TruSeq RNA Library Prep Kit v2) for RNA sequencing on the HiSeq 4000 with SR50 cycles by the IGM Genomics Center at UC San Diego.

RNAseq Processing and Analysis. Raw RNAseq data was processed using the Toil-RNAseq pipeline[10]. Reads were mapped to the Genome Reference Consortium's GRCh38.p10 using STAR. The Hugo ID output was used for downstream weighted gene co-expression network analysis (WGCNA)[11]. Genes that were lowly expressed (i.e., average TPM within group < 10)

were filtered out and TPM counts were log transformed (log_2(TPM+1)) prior to WGCNA analysis. Briefly, 11 signed WGCNA modules were clustered using a soft thresholding power ß = 18 with a minimum module size of 30 genes and a cutHeight of 0.13 was used to merge modules. Quantitative "CAR_status" trait values were assigned to CARhi, unstimulated (unstim), and CARlo samples of 2, 1, and 0 respectively. Module membership scores were calculated using the WGCNA R Software. Gene set enrichment analysis (GSEA) and gene ontology analysis were performed through MSigDB[12,13] and Enrichr[14]. The relationship between WGCNA modules and published gene signatures was quantified using gene set hypergeometric overlap with the following MSigDB gene signature sets: GSE13738, GSE13887, GSE28726, GSE15324, and GSE44649[15–19]. Differentially-expressed genes were identified using DESeq2[20] ($a < 0.01$, abs(log2FC) > 1.5). Principal component analysis (PCA) was also carried out in DESeq2[20]. K562 gene signatures were detected among differentially-expressed genes via Enrichr using the ARCHS4 Cell-lines database[14].

Repeated Antigen Challenge Assay. Engineered EGFP-expressing Raji cells were seeded at 1-2 x 10^5 cells/well in a tissue-culture 48-well plate and co-incubated with primary human CAR T cells at varying effector-to-target ratios. Specifically, the number of effector cells refers to the number of CAR-expressing T cells within the population. Media culture conditions were monitored throughout the course of the experiment, and when necessary, media changes were performed to maintain nutrient availability of the culture. Resuspended aliquots of challenge cultures were harvested every 48-72 hours to quantify the number of $EGFP^+$ Raji cells and CAR-expressing T cells. The same ratio of fresh $EGFP^+$ Raji cells, after being adjusted for the fraction removed for analysis, were added to each culture post-aliquot harvest, thereby constituting a new challenge.

RESULTS

Isolating functionally heterogeneous CAR^{hi} and CAR^{lo} cells post-population bifurcation

Our lab has previously reported on the observation that primary human CAR-T cells undergo population bifurcation upon antigen stimulation, leading to distinct, functionally heterogeneous CAR^{hi} and CAR^{lo} populations[7]. CAR^{hi} cells are identified by CAR^{hi}/CD25^{+} surface expression, can elicit robust anti-tumor functions, and are resistant to PD-1–associated dysfunction despite upregulating PD-1 expression[7]. On the other hand, CAR^{lo} cells are identified by CAR^{lo}/CD25^{-} surface expression and display symptoms of T–cell dysfunction[7]. As such, comparing the transcriptomes of CAR^{hi} vs. CAR^{lo} cells provides a framework to 1) identify sortable surface markers on unactivated T cells that demarcate T-cell subtypes that preferentially bifurcate into CAR^{hi} T cells upon antigen stimulation and 2) to study biological pathways associated with CAR-T–cell dysfunction.

In order to isolate RNA from CAR^{hi} and CAR^{lo} cells, primary human CD4^{+} T cells expressing CD19 CARs, paired with a 4-1BB co-stimulatory domain, were generated from four healthy donors. CD19 CAR T cells were challenged with CD19^{+} K562 cells at a 1:1 effector-to-target (E:T) ratio for 16-20 hours and subsequently sorted for bifurcated CAR^{hi} and CAR^{lo} populations via FACS (**Fig. 1A, Fig. S1**). As a control, “unstimulated” CAR-T cells that had not been exposed to target cells were co-incubated with CD19– K562 cells at the same E:T ratio and sorted via FACS.

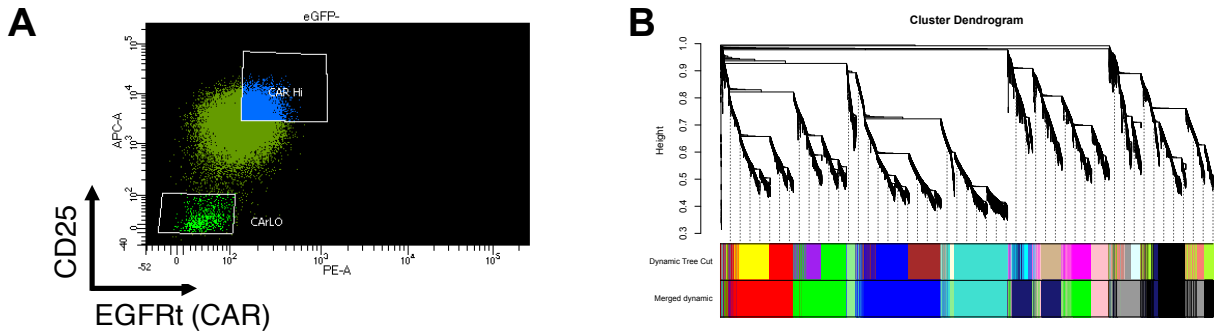

Figure 3-1: Derivation of WGCNA modules from *in vitro*-derived CAR^{hi} and CAR^{lo} T cells. **(A)** Representative CAR^{hi} vs. CAR^{lo} FACS gating. **(B)** WGCNA clustering of RNAseq data. A soft thresholding power β = 18 with a minimum module size of 30 genes and a cutHeight of 0.13 was used to merge modules.

Transcriptomic co-expression analysis coupled with T-cell surface proteomic analysis identifies candidate CAR^{hi} enrichment markers

Gene expression data from CAR^{hi}, CAR^{lo}, and unstimulated cells were clustered into distinct gene modules based on network co-expression patterns using weighted gene co-expression network analysis (WGCNA)[11]. Genes belonging to the same WGCNA module are predicted to be co-expressed, and each co-expression module may represent a true biological function or noise, requiring further downstream analysis to assign biological relevance to each module[11]. Eleven WGCNA modules were extrapolated from bulk RNAseq data, and each module's relationship to the CAR^{hi} and CAR^{lo} phenotypes was scored (**Fig. 1B, Fig. S2**). A module-trait correlation of 1 implies that the module is correlated with CAR^{hi} and a correlation of -1 implies that the module is correlated with CAR^{lo}.

In order to identify candidate sorting markers that would enrich for the CAR^{hi} population during CAR T-cell biomanufacturing, a flow-cytometry–based screen (LEGENDScreen^{TM} Human PE Kit, BioLegend) probing the unactivated CD4 surface proteome was carried out and candidate WGCNA modules with high anti-tumor potential were identified. The flow-cytometry–based screen identified 65 surface markers that (i) produced asymmetric or multimodal expression patterns and (ii) were expressed on at least 25% of unactivated CD4s (data not shown), two criteria that a marker should meet to be sortable for CAR^{hi} enrichment purposes. To further narrow down the list of candidate sorting markers, WGCNA modules were evaluated based on their correlation to the CAR^{hi} phenotype and, importantly, their overlap (or lack thereof) with T-cell activation gene signatures. Of the CAR^{hi}-associated modules (blue, red, and turquoise), the turquoise and blue modules had the highest enrichment for T-cell activation signatures, an important transcriptomic metric for productive and robust CAR-T cell activation, while the red

module was the least enriched for T-cell activation signatures among the CAR^{hi}-associated modules (**Fig. 2A**)[15–19]. However, surface markers within the red module failed to meet the two criteria described above and are thus less useful as sorting markers. As an alternative, the green module was evaluated further due to its high correlation with the red module (**Fig. 2B**). Candidate sorting markers were co-stained across 3 donors to remove surface proteins that marked redundant subpopulations (data not shown); altogether, a short list of candidate sorting markers was established (**Supplementary Table 1**).

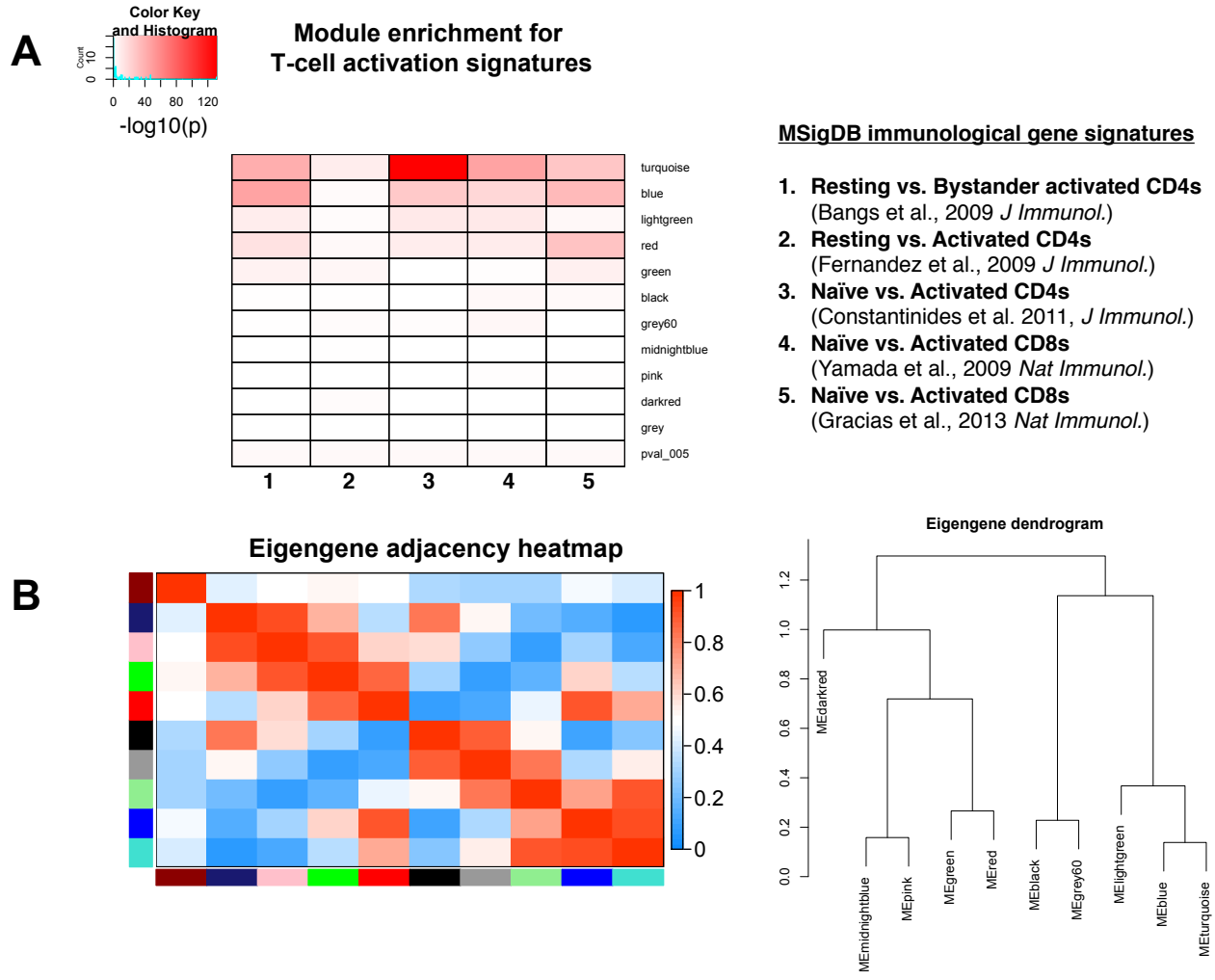

Figure 3-2: Identification of WGCNA modules associated with T-cell activation. (A) WGCNA module enrichment of activated T-cell gene signatures. P-values determined by hypergeometric test. **(B)** Eigengene adjacency heatmap (left) and the module eigengene dendrogram (right) generated based on eigengene adjacency matrix generated using WGCNA[11]. Large vertical distances indicate dissimilarity and short vertical distances in the eigengene dendrogram indicate similarity between modules.

Anti-tumor therapeutic output among sorted CAR T-cell subpopulations proved difficult to discern

T cells were sorted via FACS following the previously defined guidelines (**Supplementary Table 1**) prior to activation. The majority of the sorting strategies enriched for less-differentiated T-cell phenotypes among CD3 T cells, with the exception of CD49d enrichment, which skewed enriched for terminal effector T cells (**Fig. 3A-B**). CD19-41BB CAR T cells generated from the various sorted T-cell subpopulations were subjected to repeated antigen challenge (RAC) against Raji cells, and their ability to lyse target cells and proliferate upon antigen stimulation were quantified by flow cytometry. The results indicated that CD194-enriched cells had poorer anti-tumor functions compared to the others (**Fig. 3C-D**), consistent with the notion that differentiated T-cell phenotypes have poorer anti-tumor potential than relatively naïve-like T-cell phenotypes[21]. Sorting by the other markers tested did not result in significant changes in the resulting T cells' anti-tumor function (**Fig. 3C-D**). During the course of this study, a different group reported on the identification of sorting markers that enriched for T cells with higher anti-tumor capacity using a similar strategy combining transcriptomics and T cell surface proteomics[22]. Given that pre-sorted CAR-T cells did not exhibit significantly improved *in vitro* lysis upon repeated antigen challenge and the presence of a competing manuscript already in press, the surface marker sorting aspect of the project was discontinued shortly after.

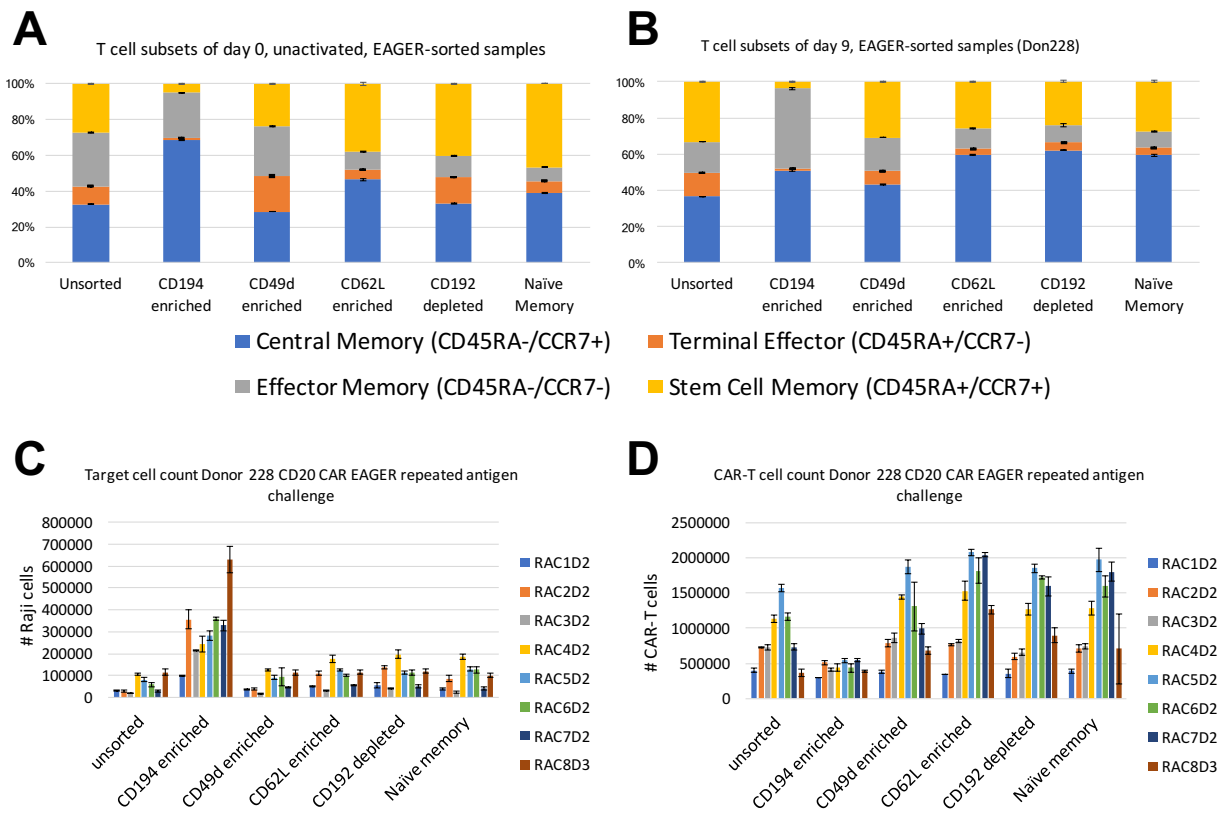

Figure 3-3: CAR-T cells generated from T cells that were marker-sorted prior to dynabead activation. $CD3^+$ T-cell subtype distribution among sorted cells **(A)** immediately post-sorting, prior to Dynabead activation and **(B)** 9 days after T-cell isolation. CAR T cells generated from the sorted T-cell subtypes were subject to repeated antigen challenge against $EGFP^+$ Raji cells at a 2:1 effector-to-target ratio. Target cell counts **(C)** and CAR T-cell counts **(D)** were tracked at each challenge.

Exploration of gene expression signatures associated with CAR-T–cell dysfunction

We hypothesize that an understanding of underlying biological pathways associated with CAR-T–cell dysfunction can provide actionable strategies to counteract exhaustion/dysfunction. Exploratory analysis of CAR^{lo}-associated modules highlights two epigenetic regulators as drivers of CAR^{lo} dysfunction. Gene set enrichment analysis (GSEA) through MSigDB[12,13] showed that CAR^{lo} modules were heavily annotated with differentiation-like programs (**Supplementary Table 2**), and given the enrichment of differentiation-like programs, it was unsurprising that genes within CAR^{lo} were also annotated to be regulated by epigenetic factors enhancer of zeste 2 (EZH2) and histone deacetylases (HDACs) (**Supplementary Table 3**). Specifically, EZH2 activity is

downregulated and HDAC activity is upregulated in CAR^{lo} cells relative to unstimulated and CAR^{hi} cells. A second GSEA approach using Enrichr[14] also showed heightened HDAC activity in the midnightblue, CAR^{lo}-associated module (**Fig. S3**). The fact that 1) EZH2 activity has been shown to promote anti-tumor immunity and 2) EZH2 restriction by tumor cells mediates effector T-cell dysfunction provides credence to the exploratory findings[23–25]. Altogether, the analysis suggests that enforcement of EZH2 activity or repression of HDAC activity during CAR-T cell antigen stimulation may counteract CAR^{lo} dysfunction. Because HDAC repression is more easily achieved than conditional EZH2 upregulation, we proceeded to evaluate the effects of HDAC repression on CAR T-cell anti-tumor functions.

HDAC repression during *ex vivo* expansion did not significantly improve CAR T-cell anti-tumor functionality *in vitro*

Targeted ablation of HDAC activity during CAR-T cell antigen stimulation can be achieved through pharmaceutical inhibition using HDACi, which are FDA-approved drugs for cancer treatment[26,27]. Culturing $CD3^+$ T cells in the presence of HDACi limited *ex vivo* T-cell expansion, irrespective of the integrated construct or the type of inhibitor used (**Fig. 4A**). HDACi priming (i.e., culturing T cells in the presence of HDACi) of $CD3^+$ T cells slightly enriched for central memory T cells, concomitant with a smaller fraction of effector-memory T cells relative to vehicle control (**Fig. 4B**). Furthermore, HDACi priming of $CD3^+$ T cells did not skew the specific outgrowth of $CD4^+$ or $CD8^+$ T cells (**Fig. S4**). Importantly, HDACi-primed CAR T cells did not demonstrate superior anti-tumor functionality in the context of *in vitro* RAC compared to CAR-T cells expanded in the absence of HDACi, both in terms of target-cell cytotoxicity and CAR T-cell proliferation (**Fig. 4C-D**)

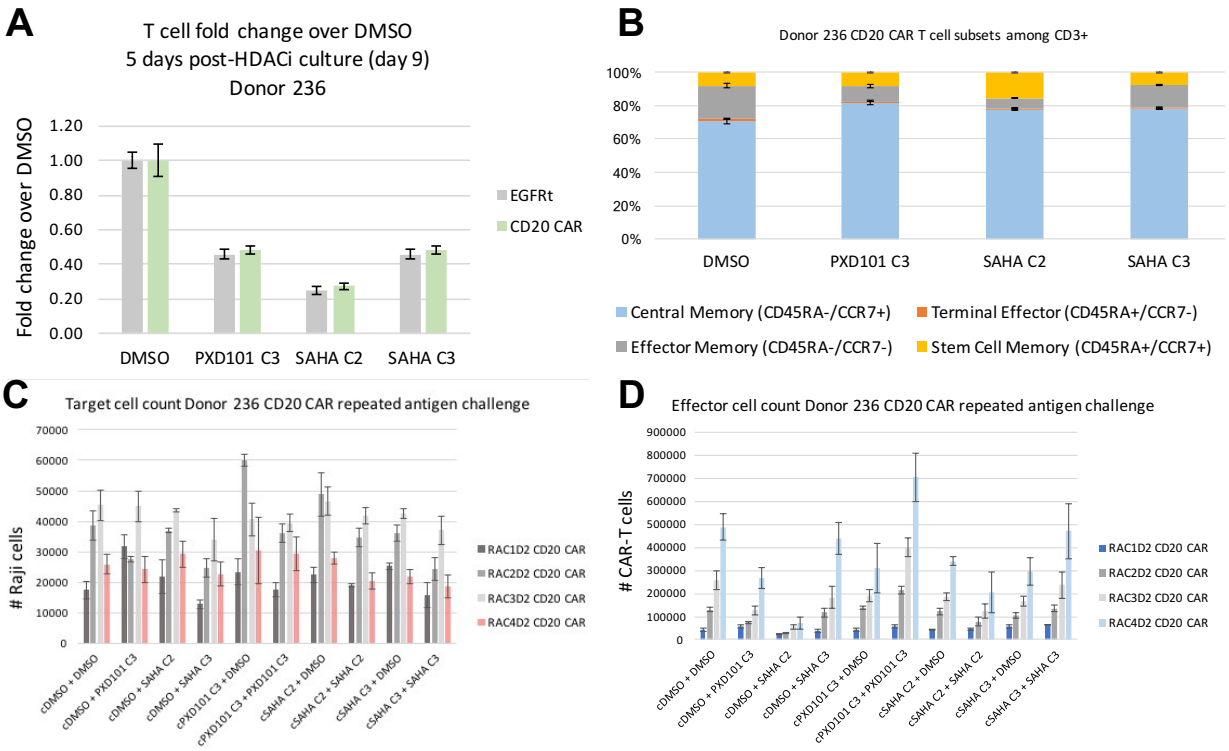

Figure 3-4: HDAC inhibition of CAR-T cells during *ex vivo* expansion and repeated antigen stimulation. Over the course of HDACi priming of CD3$^+$ T cells, **(A)** *ex vivo* T-cell expansion and **(B)** T-cell subtype distributions were evaluated 9 days post T-cell isolation or thawing. CAR T cells generated from HDACi-primed T cells (cPXD101 C3 = 0.25 μM PXD101, cSAHA C2 = 1.58 μM SAHA, cSAHA C3 = 0.50 μM SAHA) or vehicle-primed T cells (cDMSO = spiked in with equal volume DMSO) were subject to repeated antigen challenge, while cultured in the presence or absence of corresponding HDACi, against EGFP$^+$ Raji cells at a 2:1 effector-to-target ratio. Target cell counts **(C)** and CAR T-cell counts **(D)** were tracked at each challenge. Results are representative across n=2 donors.

Benefits of targeted ablation of HDAC activity during CAR T-cell antigen stimulation were not generalizable *in vitro*

Addition of the HDACi suberoylanilide hydroxamic acid (SAHA) during CD8$^+$ CD20 CAR T-cell repeated antigen challenge (at a 2:1 effector-to-target ratio) preserved CAR–T-cell cytotoxicity and resulted in superior T-cell proliferation, whereas a mock-treated arm lost the ability to control tumor-cell growth (**Fig. 5A-B**). Although the RNAseq data presented above had been generated from CD4$^+$ CD19 CAR-T cells, we chose to perform HDACi testing on CD20 CAR-T cells, which are known to have weaker anti-tumor activities (and thus greater room for

functional improvement) compared to CD19 CAR-T cells. However, while the beneficial effects of HDACi is detectable in $CD8^+$ CD20 CAR-T cells under certain conditions, these effects were not recapitulated in $CD3^+$ or $CD4^+$ CD20 CAR-T cells (**Fig. 5C-F**). Furthermore, the benefits of HDACi treatment during CAR T-cell challenge was only evident at a 2:1 effector-to-target ratio and became obfuscated at a different ratio (**Fig. S5**). Altogether, the improved anti-tumor functions of SAHA-treated CAR T cells on $CD8^+$ CD20 CAR T are not generalizable across different T-cell subtypes, CARs, and target-cell challenge conditions.

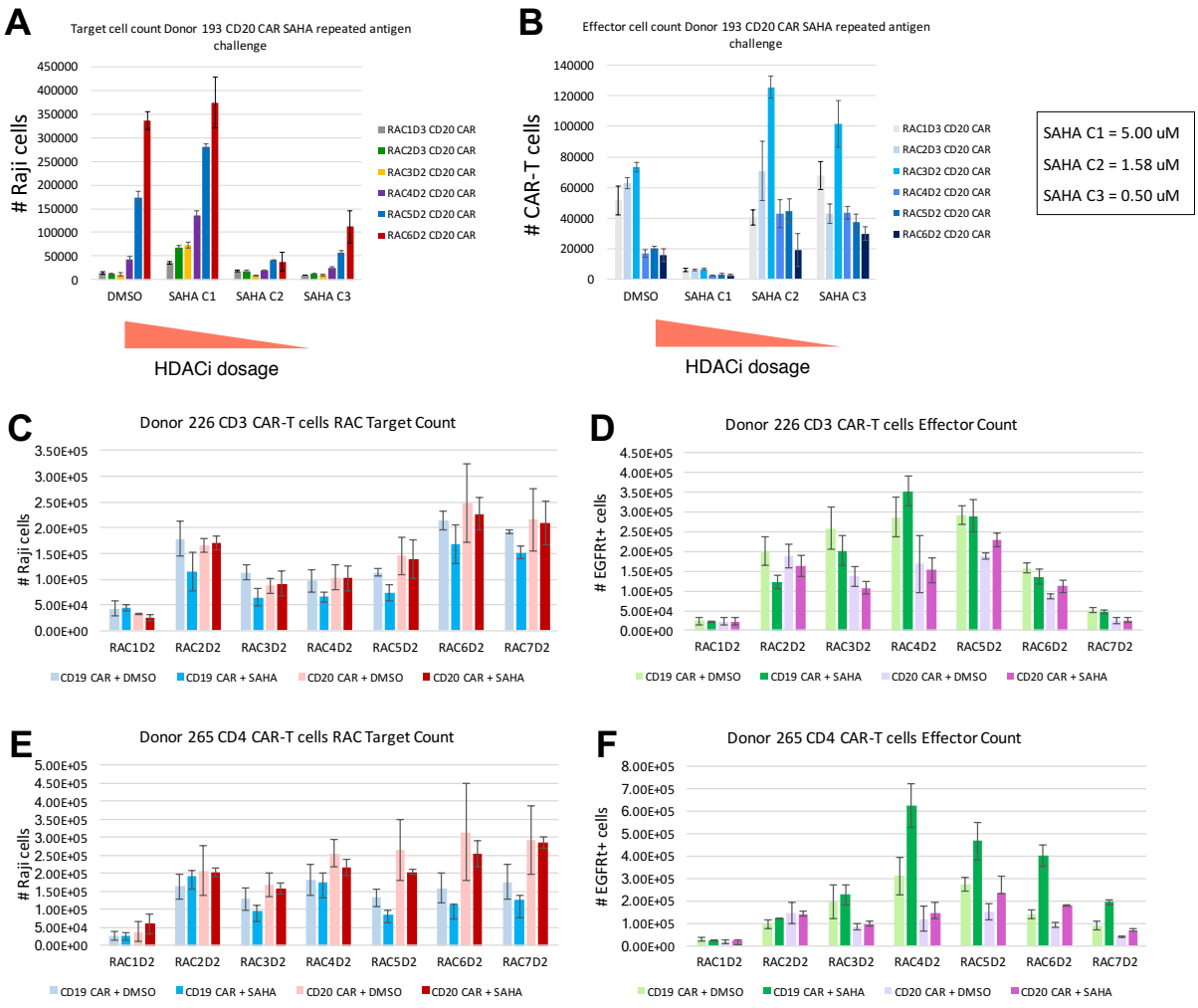

Figure 3-5: Effects of HDAC inhibition of CAR-T cells during repeated antigen stimulation across different CARs and T-cell subtypes. CD20 CAR-expressing $CD8^+$ T cells were subject to repeated antigen challenge at a 2:1 effector-to-target ratio, where Raji target-cell counts (**A**) and CAR T-cell counts (**B**) were tracked at each challenge. Results shown in (A) and (B) are consistent across two healthy donors. CD19- and CD20-CAR–expressing $CD3^+$ (**C-D**) and $CD4^+$ (**E-F**) T cells were subject to repeated antigen challenge at a 1:2 effector-to-target ratios, cultured

either in the presence of DMSO or 0.50 μM SAHA, where Raji target-cell counts (**C, E**) and CAR T-cell counts (**D, F**) were tracked at each challenge.

DISCUSSION

Much effort and attention in cancer immunotherapy has been directed towards reinvigorating T cell responses by using checkpoint inhibitors, such as anti-PD-1 therapy [5,6,28]. However, a large fraction of patients remains unresponsive to checkpoint inhibitor therapy, and thus there is a need for other avenues of T-cell reinvigoration[4–6]. A systematic comparison of CAR^{hi} and CAR^{lo} cells provides a framework for studying the heterogeneity of CAR T cell anti-tumor responses. In particular, bulk RNAseq was able to highlight the vast difference between the CAR^{hi} and CAR^{lo} populations (**Fig. S6**), with 5,540 differentially-expressed genes detected (false discovery rate a < 0.01 and absolute log2(fold change) > 1.5; data not shown)—a large number of differentially-expressed genes given strict criteria.

Gene set enrichment analysis of CAR^{hi} modules (i.e., blue, red, and turquoise in **Figure 1B**) illustrate many metabolic characteristics of productively activated effector T cells (**Supplementary Table 4**). In particular, CAR^{hi} modules are associated with oxidative phosphorylation, glycolysis, PI3K/AKT/mTOR signaling, and reactive oxidative species (ROS), which are all metabolic traits associated with productive T-cell activation and effector function. Interestingly, CAR^{hi} modules are also enriched for fatty acid metabolism across the blue, red, and turquoise modules (p-values all < 1.5 e-6). Memory T cells, a persistent T cell subset capable of long term survival, have a quiescent metabolic state that is associated with fatty acid metabolism[29]. Furthermore, the blue and red modules are enriched for gene signatures related to Myc signaling (p-values both < 1.16e-38). Thus, CAR^{hi} cells have both superior effector function as well as persistence relative to CAR^{lo} cells, consistent with experimental data and expectations. Gene ontology biological process analysis of CAR^{lo} modules (i.e., black, midnightblue, and grey60 in **Supplementary Table 4**) using MSigDb reveal strong signatures of cell differentiation

(**Supplementary Table 5**), which is consistent with the notion that T cells approaching terminal differentiation have diminished ability to sustain robust anti-tumor functions[30].

While bulk RNAseq is useful in highlighting differentially regulated biological pathways and connecting the observed phenotype to published gene signatures[12], it is difficult to distinguish using transcriptomic data alone whether the expression of certain surface markers or biological pathways have a causal impact on functional CAR-T cell activation (i.e., polarize into CAR^{hi} cells) as opposed to correlation to phenotypes of interest. While algorithms, such as Ingenuity Pathway Analysis Software[31], may suggest potential upstream regulators given a gene expression dataset, such algorithms are inherently predictive by nature and require experimental validation for hypothesis testing. As such, the methods by which hypotheses are tested are as important as the hypothesis-generating exploratory methods. Throughout the course of this study, we relied on stress-testing CAR-T cells *in vitro* using RAC assays to determine whether improvements in anti-tumor efficacy could be achieved via surface marker sorting or HDAC inhibition. The lack of significant improvement in tumor-cell lysis or CAR-T cell expansion *in vitro* led us to reason that our cell sorting and HDAC inhibition strategies yielded minimal benefits. However, in retrospect, our lab has learned that *in vitro* RAC assays do not accurately represent how well CAR-T cells eventually perform once adoptively transferred into animal models[32] – the most important metric in pre-clinical testing. Thus, we may have overlooked the potential benefits of surface marker sorting and HDAC inhibition given how much weight we assigned to the *in vitro* RAC assays. In fact, a report was published after we stopped pursuing the research in this chapter describing how HDAC inhibition can promote effector $CD8^+$ T polarization into memory subsets[33].

In the HDAC inhibition paper by Wang et al., the authors applied HDAC inhibition during repeated *ex vivo* expansion of differentiated T cells in order to dedifferentiate expanded $CD8^+$ T cells[33]. The benefits of HDAC inhibition came in the form of reprogramming differentiated T cells into memory subsets, with only minor emphases on T-cell lytic capacity. Overall, it can be seen that HDAC inhibition of T cells has beneficial effects in the context of adoptive T-cell therapy that

we had initially overlooked. This suggests that a more comprehensive set of assays should be used in determining whether novel CAR-T cell strategies truly provide an additional benefit. In particular, *in vivo* experiments should be performed to gauge any enhanced anti-tumor efficacy, using *in vitro* lysis data to weed out any conditions that significantly hinder CAR-T cell efficacy. Furthermore, immunostaining or transcriptomics-based experiments should be used to analyze the state of CAR-T cells to determine what specific effects may be induced.

Nevertheless, the validation of HDAC inhibition reported independently by a different research group provides confidence in the hypothesis-generating capacity of the transcriptomic methods used in this chapter. Moving forward, we apply the framework of transcriptomic analysis used in this chapter in analyzing additional CAR-T cell RNAseq datasets in Chapters 4 and 5. We further take the lessons learned from this chapter (i.e., to evaluate anti-tumor efficacy *in vivo* and to comprehensively analyze T-cell states) and successfully demonstrate novel strategies in improving anti-tumor efficacy and its associated underlying mechanisms.

REFERENCES

1. Sadelain, M., Brentjens, R. & Rivière, I. The Basic Principles of Chimeric Antigen Receptor Design. *Cancer Discov.* **3**, 388 LP – 398 (2013).

2. Geering, B. & Fussenegger, M. Synthetic immunology: modulating the human immune system. *Trends Biotechnol.* **33**, 65–79 (2015).

3. Wherry, E. J. & Kurachi, M. Molecular and cellular insights into T cell exhaustion. *Nat. Rev. Immunol.* **15**, 486 (2015).

4. Legat, A., Speiser, D., Pircher, H., Zehn, D. & Fuertes Marraco, S. Inhibitory Receptor Expression Depends More Dominantly on Differentiation and Activation than “Exhaustion” of Human CD8 T Cells . *Frontiers in Immunology* vol. 4 455 (2013).

5. Jiang, Y., Li, Y. & Zhu, B. T-cell exhaustion in the tumor microenvironment. *Cell Death Amp Dis.* **6**, e1792 (2015).

6. La-Beck, N. M., Jean, G. W., Huynh, C., Alzghari, S. K. & Lowe, D. B. Immune Checkpoint Inhibitors: New Insights and Current Place in Cancer Therapy. *Pharmacother. J. Hum. Pharmacol. Drug Ther.* **35**, 963–976 (2015).

7. Chang, Z. L., Silver, P. A. & Chen, Y. Y. Identification and selective expansion of functionally superior T cells expressing chimeric antigen receptors. *J. Transl. Med.* **13**, 161 (2015).

8. Chang, Z. L. *et al.* Rewiring T-cell responses to soluble factors with chimeric antigen receptors. *Nat. Chem. Biol.* **14**, 317 (2018).

9. Zah, E., Lin, M.-Y., Silva-Benedict, A., Jensen, M. C. & Chen, Y. Y. T Cells Expressing CD19/CD20 Bispecific Chimeric Antigen Receptors Prevent Antigen Escape by Malignant B Cells. *Cancer Immunol. Res.* **4**, 498 LP – 508 (2016).

10. Vivian, J. *et al.* Toil enables reproducible, open source, big biomedical data analyses. *Nat. Biotechnol.* **35**, 314–316 (2017).

11. Langfelder, P. & Horvath, S. WGCNA: an R package for weighted correlation network analysis. *BMC Bioinformatics* **9**, 559 (2008).

12. Subramanian, A. *et al.* Gene set enrichment analysis: A knowledge-based approach for interpreting genome-wide expression profiles. *Proc. Natl. Acad. Sci.* **102**, 15545 LP – 15550 (2005).

13. Liberzon, A. *et al.* The Molecular Signatures Database Hallmark Gene Set Collection. *Cell Syst.* **1**, 417–425 (2015).

14. Kuleshov, M. V *et al.* Enrichr: a comprehensive gene set enrichment analysis web server 2016 update. *Nucleic Acids Res.* **44**, W90–W97 (2016).

15. Bangs, S. C. *et al.* Human CD4⁺ Memory T Cells Are Preferential Targets for Bystander Activation and Apoptosis. *J. Immunol.* **182**, 1962 LP – 1971 (2009).

16. Fernandez, D. R. *et al.* Activation of Mammalian Target of Rapamycin Controls the Loss of TCRζ in Lupus T Cells through HRES-1/Rab4-Regulated Lysosomal Degradation. *J. Immunol.* **182**, 2063 LP – 2073 (2009).

17. Yamada, T., Park, C. S., Mamonkin, M. & Lacorazza, H. D. Transcription factor ELF4 controls the proliferation and homing of CD8+ T cells via the Krüppel-like factors KLF4 and KLF2. *Nat. Immunol.* **10**, 618 (2009).

18. Constantinides, M. G., Picard, D., Savage, A. K. & Bendelac, A. A Naive-Like Population of Human CD1d-Restricted T Cells Expressing Intermediate Levels of Promyelocytic Leukemia Zinc Finger. *J. Immunol.* **187**, 309 LP – 315 (2011).

19. Gracias, D. T. *et al.* The microRNA miR-155 controls CD8+ T cell responses by regulating interferon signaling. *Nat. Immunol.* **14**, 593 (2013).

20. Love, M. I., Huber, W. & Anders, S. Moderated estimation of fold change and dispersion for RNA-seq data with DESeq2. *Genome Biol.* **15**, 550 (2014).

21. Gattinoni, L., Klebanoff, C. A. & Restifo, N. P. Paths to stemness: building the ultimate antitumour T cell. *Nat. Rev. Cancer* **12**, 671 (2012).

22. Fraietta, J. A. *et al.* Determinants of response and resistance to CD19 chimeric antigen receptor (CAR) T cell therapy of chronic lymphocytic leukemia. *Nat. Med.* **24**, 563–571 (2018).

23. Yang, X.-P. *et al.* EZH2 is crucial for both differentiation of regulatory T cells and T effector cell expansion. *Sci. Rep.* **5**, 10643 (2015).

24. Zhao, E. *et al.* Cancer mediates effector T cell dysfunction by targeting microRNAs and EZH2 via glycolysis restriction. *Nat. Immunol.* **17**, 95 (2015).

25. He, S. *et al.* Ezh2 phosphorylation state determines its capacity to maintain CD8+ T memory precursors for antitumor immunity. *Nat. Commun.* **8**, 2125 (2017).

26. Bolden, J. E., Peart, M. J. & Johnstone, R. W. Anticancer activities of histone deacetylase inhibitors. *Nat. Rev. Drug Discov.* **5**, 769 (2006).

27. Suraweera, A., O'Byrne, K. J. & Richard, D. J. Combination Therapy With Histone Deacetylase Inhibitors (HDACi) for the Treatment of Cancer: Achieving the Full Therapeutic Potential of HDACi . *Frontiers in Oncology* vol. 8 92 (2018).

28. Tumeh, P. C. *et al.* PD-1 blockade induces responses by inhibiting adaptive immune resistance. *Nature* **515**, 568 (2014).

29. Sukumar, M., Kishton, R. J. & Restifo, N. P. Metabolic reprograming of anti-tumor immunity. *Curr. Opin. Immunol.* **46**, 14–22 (2017).

30. Henning, A. N., Roychoudhuri, R. & Restifo, N. P. Epigenetic control of CD8+ T cell differentiation. *Nat. Rev. Immunol.* **18**, 340 (2018).

31. Krämer, A., Pollard Jr, J., Green, J. & Tugendreich, S. Causal analysis approaches in Ingenuity Pathway Analysis. *Bioinformatics* **30**, 523–530 (2013).

32. Zah, E. *et al.* Systematically optimized BCMA/CS1 bispecific CAR-T cells robustly control heterogeneous multiple myeloma. *Nat. Commun.* **11**, 2283 (2020).

33. Wang, J. *et al.* Histone Deacetylase Inhibitors and IL21 Cooperate to Reprogram Human Effector CD8+ T Cells to Memory T Cells. *Cancer Immunol. Res.* **8**, 794–805 (2020).

SUPPLEMENTARY INFORMATION

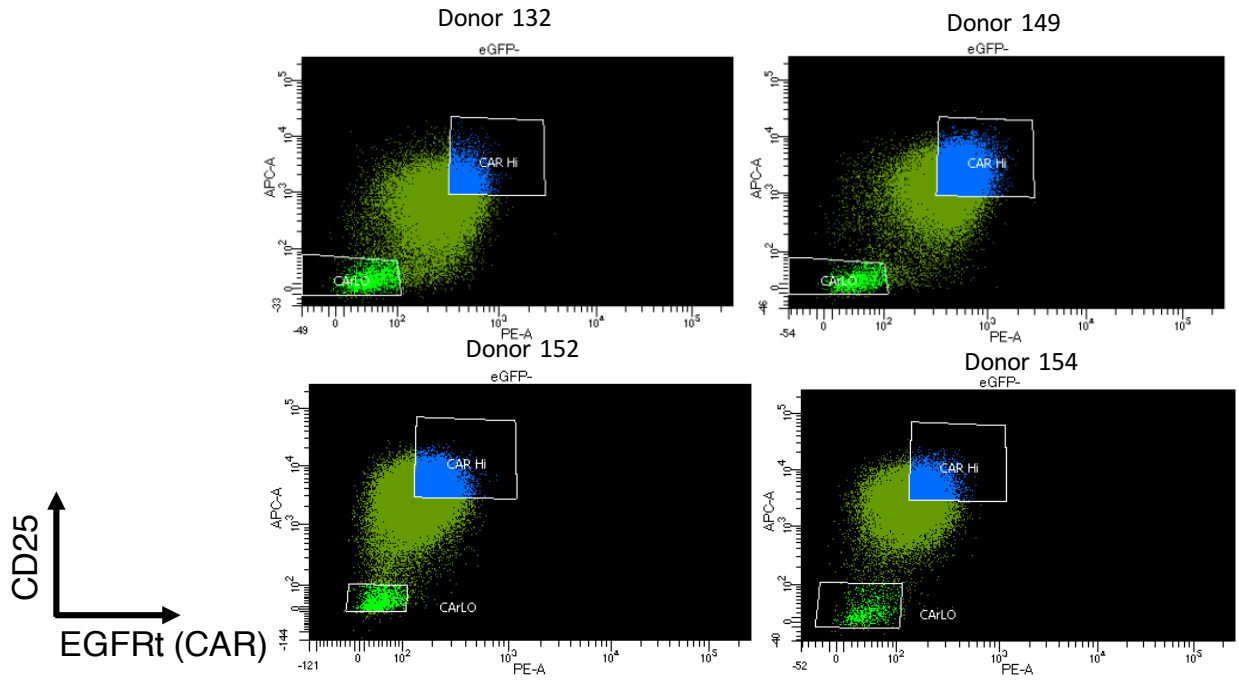

Supplementary Figure 3-1: Fluorescent-activated cell sorting (FACS) gating of sorted CAR^{hi} and CAR^{lo} populations.

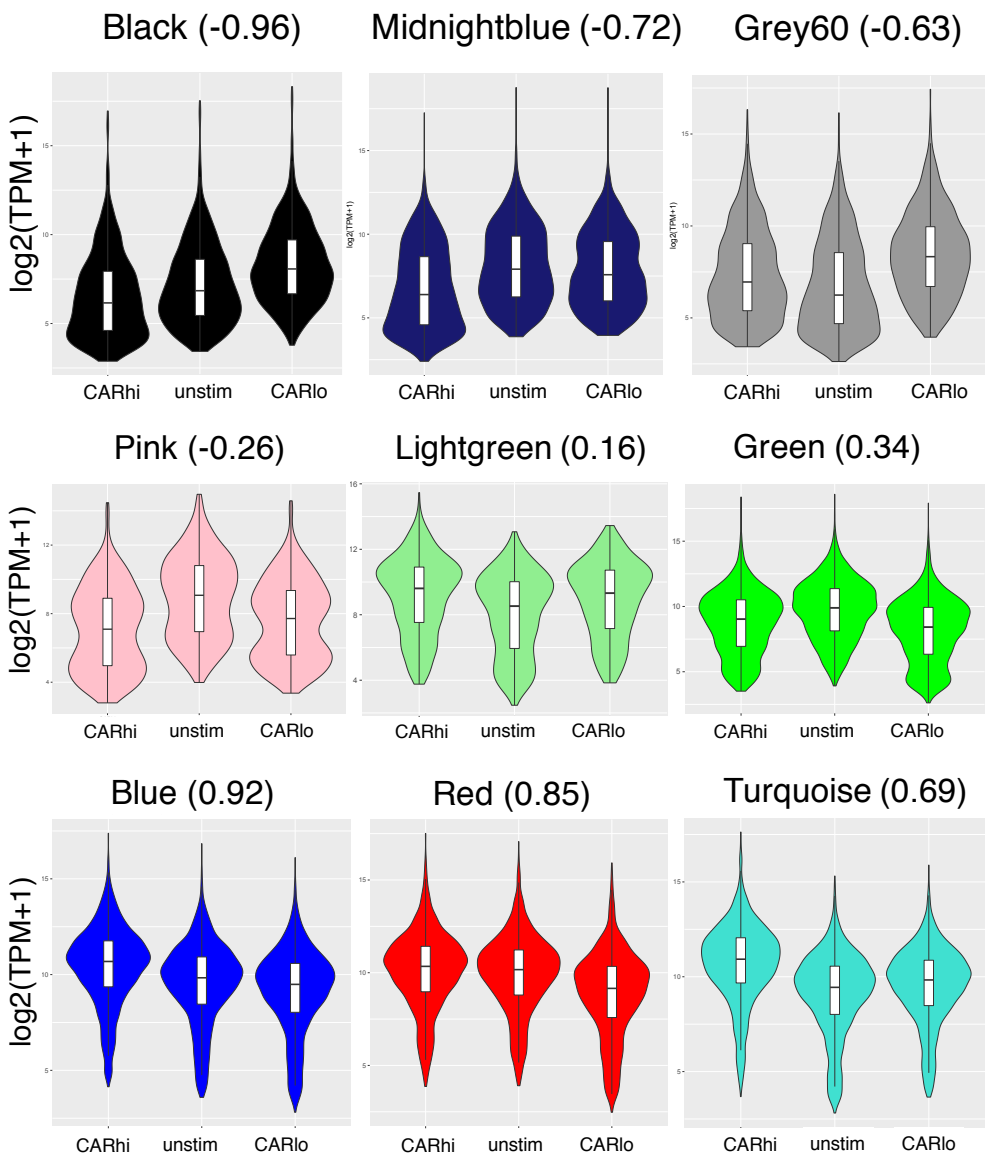

Supplementary Figure 3-2: Violin plots of genes belonging to each WGCNA module labelled with corresponding module-trait correlation scores.

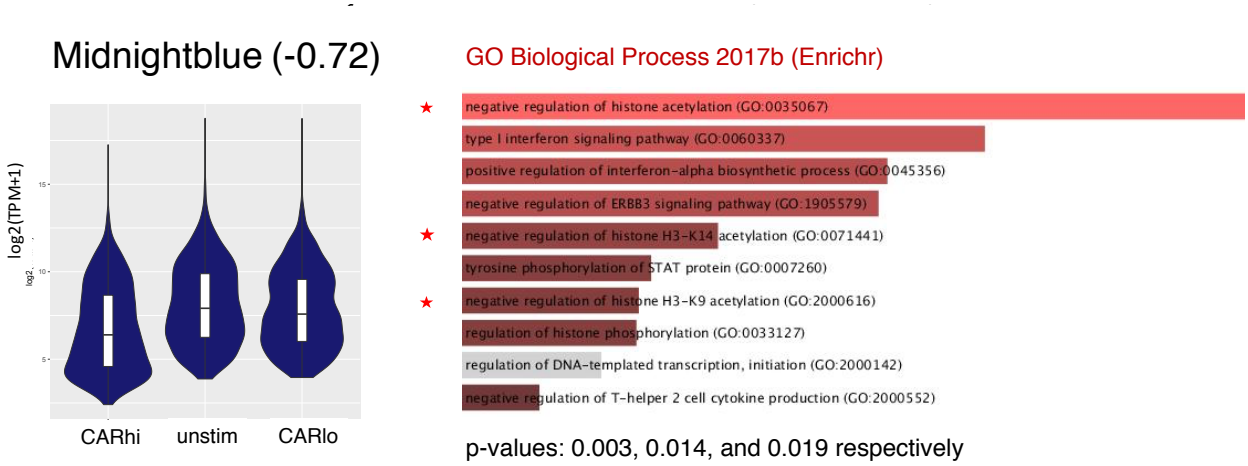

Supplementary Figure 3-3: Biological process gene ontology (GO) analysis shows increased HDAC activity to be associated with the midnightblue module via Enrichr.

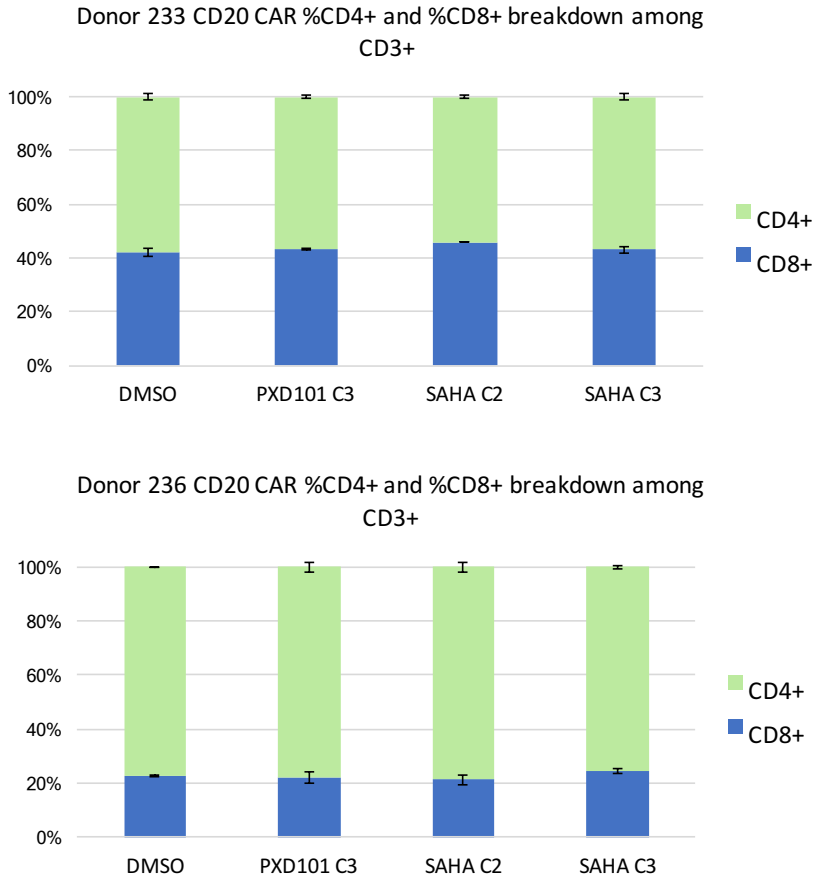

Supplementary Figure 3-4: T-cell subtype breakdown upon HDACi treatment. $CD4^+$ and $CD8^+$ T-cell distributions distribution among HDACi-primed $CD3^+$ T cells (cPXD101 C3 = 0.25 μM PXD101, cSAHA C2 = 1.58 μM SAHA, cSAHA C3 = 0.50 μM SAHA) or vehicle-primed T cells (cDMSO = spiked in with equal volume DMSO)

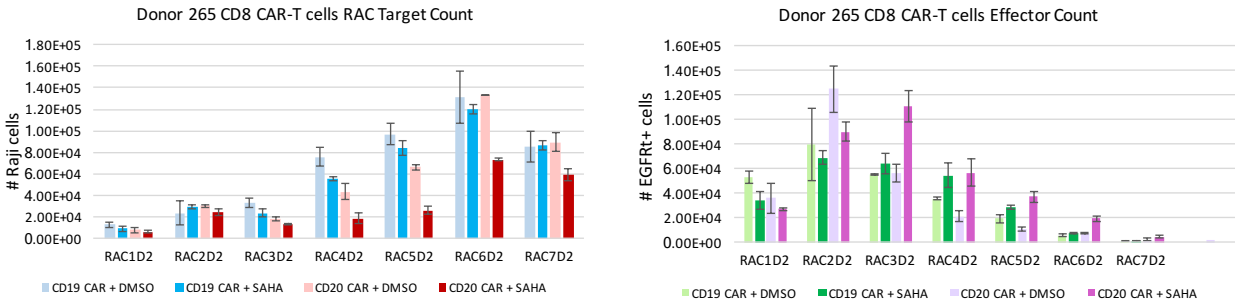

Supplementary Figure 3-5: Repeated antigen challenge of CD8$^+$ CAR-T cells in the presence or absence of HDACi. CD19- and CD20-CAR–expressing CD8$^+$ T cells were subject to repeated antigen challenge at a 1:1 effector-to-target ratio, cultured in the presence of DMSO or 0.50 μM SAHA, where Raji target-cell counts (left) and CAR T-cell counts (right) were tracked at each challenge.

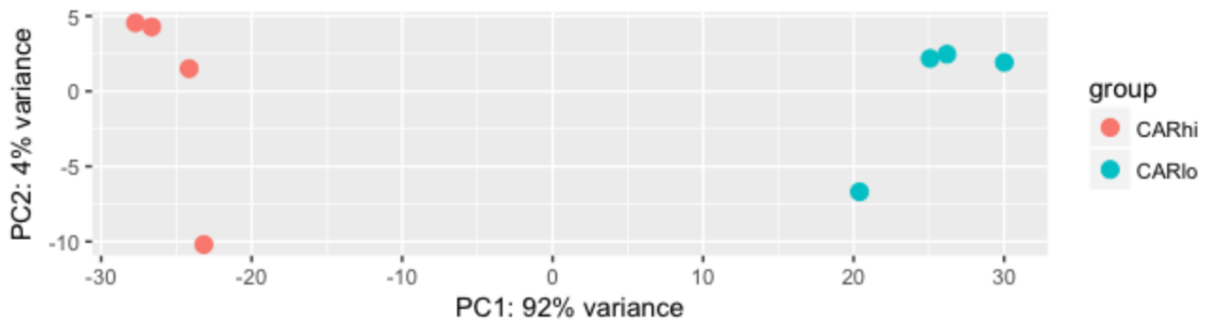

Supplementary Figure 3-6: Principal component analysis (PCA) comparing the transcriptomes of CAR^{hi} and CAR^{lo} populations.

Surface Marker	Module	Module-trait score	Sorting strategy
CD62L	Green	0.34	CAR^{hi} enrichment
CD49d	Green	0.34	CAR^{hi} enrichment
CD194	Blue	0.92	CAR^{hi} enrichment
CD192	Grey60	-0.63	CAR^{lo} depletion

Supplementary Table 3-1: Outline of surface marker sorting strategy based on combined transcriptomic and surface proteomic analyses.

Module	module-trait correlation	Gene set	Gene Set Name	p-value	FDR q-value
Black	-0.96	GO BP	GO_REGULATION_OF_MULTICELLULAR_ORGANISMAL_DEVELOPMENT	1.92E-22	8.51E-19
Black	-0.96	GO BP	GO_TISSUE_DEVELOPMENT	4.25E-22	9.43E-19
Black	-0.96	GO BP	GO_REGULATION_OF_CELL_DIFFERENTIATION	7.62E-20	6.76E-17
Black	-0.96	GO BP	GO_CELL_DEVELOPMENT	1.66E-19	1.23E-16
Black	-0.96	GO BP	GO_REGULATION_OF_ANATOMICAL_STRUCTURE_MORPHOGENESIS	1.66E-18	1.05E-15
Black	-0.96	GO BP	GO_EMBRYO_DEVELOPMENT	6.38E-18	3.14E-15
Black	-0.96	GO BP	GO_MOVEMENT_OF_CELL_OR_SUBCELLULAR_COMPONENT	8.04E-18	3.57E-15
Black	-0.96	GO BP	GO_ORGAN_MORPHOGENESIS	1.88E-17	7.56E-15
Black	-0.96	GO BP	GO_ANATOMICAL_STRUCTURE_FORMATION_INVOLVED_IN_MORPHOGENESIS	2.00E-15	7.39E-13
Black	-0.96	GO BP	GO_REGULATION_OF_NERVOUS_SYSTEM_DEVELOPMENT	8.72E-15	2.97E-12
Black	-0.96	GO BP	GO_EPITHELIUM_DEVELOPMENT	1.26E-13	3.11E-11
Black	-0.96	GO BP	GO_REGULATION_OF_CELL_MORPHOGENESIS	1.89E-13	4.24E-11
Midnightblue	-0.72	GO BP	GO_REGULATION_OF_ANATOMICAL_STRUCTURE_MORPHOGENESIS	3.72E-13	9.70E-11
Grey60	-0.63	GO BP	GO_REGULATION_OF_MULTICELLULAR_ORGANISMAL_DEVELOPMENT	3.67E-40	1.63E-36
Grey60	-0.63	GO BP	GO_REGULATION_OF_CELL_DIFFERENTIATION	4.20E-33	6.46E-30
Grey60	-0.63	GO BP	GO_POSITIVE_REGULATION_OF_MULTICELLULAR_ORGANISMAL_PROCESS	4.37E-33	6.46E-30
Grey60	-0.63	GO BP	GO_REGULATION_OF_CELL_PROLIFERATION	9.39E-29	1.04E-25
Grey60	-0.63	GO BP	GO_POSITIVE_REGULATION_OF_DEVELOPMENTAL_PROCESS	1.42E-28	1.26E-25
Grey60	-0.63	GO BP	GO_TISSUE_DEVELOPMENT	5.88E-27	3.26E-24
Grey60	-0.63	GO BP	GO_POSITIVE_REGULATION_OF_CELLULAR_COMPONENT_ORGANIZATION	3.88E-26	1.72E-23
Grey60	-0.63	GO BP	GO_REGULATION_OF_CELLULAR_COMPONENT_MOVEMENT	5.84E-25	1.99E-22

Supplementary Table 3-2: CAR^{lo}-associated gene modules are enriched for differentiation-like signatures. Differentiation-related gene set enrichments of CARlo modules from MSigDB. Genes with high module membership scores (≥ 0.80) were considered for analysis.

Module	module-trait correlation	Gene set	Gene Set Name	p-value	FDR q-value
Black	-0.96	C2: curated gene sets	MEISSNER_BRAIN_HCP_WITH_H3K4ME3_AND_H3K27ME3	3.00E-21	1.42E-17
Black	-0.96	C2: curated gene sets	BENPORATH_EED_TARGETS	1.20E-20	2.84E-17
Black	-0.96	C2: curated gene sets	SENESE_HDAC3_TARGETS_DN	1.06E-18	1.00E-15
Black	-0.96	C2: curated gene sets	HELLER_HDAC_TARGETS_SILENCED_BY_METHYLATION_UP	2.83E-17	2.24E-14
Black	-0.96	C2: curated gene sets	BENPORATH_SUZ12_TARGETS	3.44E-14	9.06E-12
Black	-0.96	C2: curated gene sets	SENESE_HDAC1_TARGETS_DN	2.09E-13	5.13E-11
Midnightblue	-0.72	C2: curated gene sets	NUYTTEN_NIPP1_TARGETS_UP	1.00E-20	5.28E-18
Midnightblue	-0.72	C2: curated gene sets	NUYTTEN_EZH2_TARGETS_UP	7.11E-16	1.87E-13
Grey60	-0.63	C2: curated gene sets	NUYTTEN_EZH2_TARGETS_UP	1.23E-33	1.94E-30
Grey60	-0.63	C2: curated gene sets	MEISSNER_BRAIN_HCP_WITH_H3K4ME3_AND_H3K27ME3	5.90E-32	6.99E-29
Grey60	-0.63	C2: curated gene sets	HELLER_HDAC_TARGETS_SILENCED_BY_METHYLATION_UP	8.74E-25	4.14E-22

Supplementary Table 3-3: CAR^{lo}-associated gene modules are affected by epigenetic regulators. Curated gene set (C2) enrichments of CARlo modules from MSigDB. Genes with high module membership scores (≥ 0.80) were considered for analysis.

Module	module-trait correlation	Gene set	Gene Set Name	Description	p-value	FDR q-value
Blue	0.92	C2: curated gene sets	DANG_BOUND_BY_MYC	Genes whose promoters are bound by MYC [GeneID=4609], according to MYC Target Gene Database	1.46E-73	4.95E-71
Blue	0.92	H: Hallmark gene sets	HALLMARK_MYC_TARGETS_V1	A subgroup of genes regulated by MYC - version 1 (v1).	4.71E-36	2.36E-34
Blue	0.92	H: Hallmark gene sets	HALLMARK_OXIDATIVE_PHOSPHORYLATION	Genes encoding proteins involved in oxidative phosphorylation.	6.14E-19	6.14E-18
Blue	0.92	H: Hallmark gene sets	HALLMARK_GLYCOLYSIS	Genes encoding proteins involved in glycolysis and gluconeogenesis.	2.03E-14	1.69E-13
Blue	0.92	H: Hallmark gene sets	HALLMARK_MTORC1_SIGNALING	Genes up-regulated through activation of mTORC1 complex.	5.07E-13	3.62E-12
Blue	0.92	H: Hallmark gene sets	HALLMARK_FATTY_ACID_METABOLISM	Genes encoding proteins involved in metabolism of fatty acids.	7.40E-08	2.85E-07
Blue	0.92	H: Hallmark gene sets	HALLMARK_IL2_STAT5_SIGNALING	Genes up-regulated by STAT5 in response to IL2 stimulation.	1.81E-07	6.48E-07
Blue	0.92	H: Hallmark gene sets	HALLMARK_PI3K_AKT_MTOR_SIGNALING	Genes up-regulated by activation of the PI3K/AKT/mTOR pathway.	6.31E-06	1.62E-05
Red	0.85	C2: curated gene sets	DANG_BOUND_BY_MYC	Genes whose promoters are bound by MYC [GeneID=4609], according to MYC Target Gene Database	1.16E-38	3.44E-36
Red	0.85	H: Hallmark gene sets	HALLMARK_PI3K_AKT_MTOR_SIGNALING	Genes up-regulated by activation of the PI3K/AKT/mTOR pathway.	5.65E-08	4.71E-07
Red	0.85	H: Hallmark gene sets	HALLMARK_OXIDATIVE_PHOSPHORYLATION	Genes encoding proteins involved in oxidative phosphorylation.	1.17E-07	7.29E-07
Red	0.85	H: Hallmark gene sets	HALLMARK_FATTY_ACID_METABOLISM	Genes encoding proteins involved in metabolism of fatty acids.	4.19E-07	1.70E-06
Red	0.85	H: Hallmark gene sets	HALLMARK_GLYCOLYSIS	Genes encoding proteins involved in glycolysis and gluconeogenesis.	4.43E-07	1.70E-06
Red	0.85	H: Hallmark gene sets	HALLMARK_MTORC1_SIGNALING	Genes up-regulated through activation of mTORC1 complex.	4.43E-07	1.70E-06
Red	0.85	H: Hallmark gene sets	HALLMARK_REACTIVE_OXIGEN_SPECIES_PATI	Genes up-regulated by reactive oxigen species (ROS).	6.76E-05	1.69E-04
Turquoise	0.69	H: Hallmark gene sets	HALLMARK_MYC_TARGETS_V1	A subgroup of genes regulated by MYC - version 1 (v1).	6.98E-77	3.49E-75
Turquoise	0.69	H: Hallmark gene sets	HALLMARK_E2F_TARGETS	Genes encoding cell cycle related targets of E2F transcription factors.	3.22E-51	8.04E-50
Turquoise	0.69	H: Hallmark gene sets	HALLMARK_MYC_TARGETS_V2	A subgroup of genes regulated by MYC - version 2 (v2).	3.04E-42	5.07E-41
Turquoise	0.69	H: Hallmark gene sets	HALLMARK_MTORC1_SIGNALING	Genes up-regulated through activation of mTORC1 complex.	5.15E-42	6.44E-41
Turquoise	0.69	H: Hallmark gene sets	HALLMARK_OXIDATIVE_PHOSPHORYLATION	Genes encoding proteins involved in oxidative phosphorylation.	1.71E-34	1.71E-33
Turquoise	0.69	H: Hallmark gene sets	HALLMARK_GLYCOLYSIS	Genes encoding proteins involved in glycolysis and gluconeogenesis.	2.62E-15	1.19E-14
Turquoise	0.69	H: Hallmark gene sets	HALLMARK_PI3K_AKT_MTOR_SIGNALING	Genes up-regulated by activation of the PI3K/AKT/mTOR pathway.	2.74E-07	8.57E-07
Turquoise	0.69	H: Hallmark gene sets	HALLMARK_FATTY_ACID_METABOLISM	Genes encoding proteins involved in metabolism of fatty acids.	1.50E-06	4.18E-06

Supplementary Table 3-4: Significant metabolic gene set enrichments of strong CAR^{hi} modules using MSigDB. Genes with high module membership (MM >= 0.80) were used for gene set enrichment analysis.

Module	module-trait correlation	Gene set	Gene Set Name	p-value	FDR q-value
Black	-0.96	GO BP	GO_REGULATION_OF_MULTICELLULAR_ORGANISMAL_DEVELOPMENT	1.92E-22	8.51E-19
Black	-0.96	GO BP	GO_TISSUE_DEVELOPMENT	4.25E-22	9.43E-19
Black	-0.96	GO BP	GO_REGULATION_OF_CELL_DIFFERENTIATION	7.62E-20	6.76E-17
Black	-0.96	GO BP	GO_CELL_DEVELOPMENT	1.66E-19	1.23E-16
Black	-0.96	GO BP	GO_REGULATION_OF_ANATOMICAL_STRUCTURE_MORPHOGENESIS	1.66E-18	1.05E-15
Black	-0.96	GO BP	GO_EMBRYO_DEVELOPMENT	6.38E-18	3.14E-15
Black	-0.96	GO BP	GO_MOVEMENT_OF_CELL_OR_SUBCELLULAR_COMPONENT	8.04E-18	3.57E-15
Black	-0.96	GO BP	GO_ORGAN_MORPHOGENESIS	1.88E-17	7.56E-15
Black	-0.96	GO BP	GO_ANATOMICAL_STRUCTURE_FORMATION_INVOLVED_IN_MORPHOGENESIS	2.00E-15	7.39E-13
Black	-0.96	GO BP	GO_REGULATION_OF_NERVOUS_SYSTEM_DEVELOPMENT	8.72E-15	2.97E-12
Black	-0.96	GO BP	GO_EPITHELIUM_DEVELOPMENT	1.26E-13	3.11E-11
Black	-0.96	GO BP	GO_REGULATION_OF_CELL_MORPHOGENESIS	1.89E-13	4.24E-11
Midnightblue	-0.72	GO BP	GO_REGULATION_OF_ANATOMICAL_STRUCTURE_MORPHOGENESIS	3.72E-13	9.70E-11
Grey60	-0.63	GO BP	GO_REGULATION_OF_MULTICELLULAR_ORGANISMAL_DEVELOPMENT	3.67E-40	1.63E-36
Grey60	-0.63	GO BP	GO_REGULATION_OF_CELL_DIFFERENTIATION	4.20E-33	6.46E-30
Grey60	-0.63	GO BP	GO_POSITIVE_REGULATION_OF_MULTICELLULAR_ORGANISMAL_PROCESS	4.37E-33	6.46E-30
Grey60	-0.63	GO BP	GO_REGULATION_OF_CELL_PROLIFERATION	9.39E-29	1.04E-25
Grey60	-0.63	GO BP	GO_POSITIVE_REGULATION_OF_DEVELOPMENTAL_PROCESS	1.42E-28	1.26E-25
Grey60	-0.63	GO BP	GO_TISSUE_DEVELOPMENT	5.88E-27	3.26E-24
Grey60	-0.63	GO BP	GO_POSITIVE_REGULATION_OF_CELLULAR_COMPONENT_ORGANIZATION	3.88E-26	1.72E-23
Grey60	-0.63	GO BP	GO_REGULATION_OF_CELLULAR_COMPONENT_MOVEMENT	5.84E-25	1.99E-22

Supplementary Table 3-5: Significant differentiation-related gene set enrichments of CAR^{lo} modules using MSigDB. Genes with high module membership (MM >= 0.80) were used for gene set enrichment analysis.

Chapter 4: Modulating antigen-independent CAR-T cell signaling to enhance tumor-killing efficacy

Chapter 4 is partially adapted from our manuscript submission, titled Rational protein design boosts CAR-T cell efficacy and reveals non-linear relationship between tonic signaling and CAR-T cell function, to *Cancer Immunology Research*, which is currently undergoing peer review at the time of this writing with author contributions as follows –

Authors: Ximin Chen[†], Laurence C. Chen[†], Mobina Khericha, Aliya Lakhani, Xiangzhi Meng, Emma Salvestrini, Neha Iyer, Amanda Shafer, Anya Alag, Yunfeng Ding, Demetri Nicolaou, Junyoung O. Park, and Yvonne Y. Chen[*] († denotes co-first authorship, * denotes corresponding author)

As a preface to this chapter – this project was started by a senior PhD student in our lab, Ximin Chen, where she spearheaded the efforts on protein engineering CD20 CARs. The majority of the data demonstrating improved functionality of CD20 CAR variants shown in Fig. 4-1 and Fig. 4-2 were carried out by Ximin Chen. The RNAseq data shown in Fig. 4-3 were generated by Ximin Chen, providing the initial dataset for me to begin digging into underlying molecular signaling pathways. I am grateful to Ximin Chen as these data served the foundation in which I could study the relationship between CAR tonic signaling and *in vivo* anti-tumor efficacy, which is the focal point of this chapter.

ABSTRACT

Chimeric antigen receptors (CARs) are fusion proteins whose functional domains are often connected in a plug-and-play manner to generate multiple CAR variants. However, CARs with highly similar sequences can nonetheless exhibit dramatic differences in function, and approaches to rationally optimize CAR proteins are critical to the development of effective CAR-T cell therapies. Using tonic signaling as a guide in rational protein design, we demonstrate juxtamembrane alanine insertion and single-chain variable fragment (scFv) sequence hybridization as two strategies that can be combined to maximize CAR-T cell efficacy. Precise changes in the CAR sequence drive dramatically different transcriptomic profiles in the presence and absence of antigen stimulation. We identified phosphoinositide 3-kinase/protein kinase B (PI3K/AKT) signaling as the primary driver of CD20 CAR tonic signaling through transcriptomic analyses. Pharmacological modulation of CAR tonic signaling demonstrated a causal role between high levels of CAR tonic signaling and poor *in vivo* anti-tumor efficacy. In fact, anti-tumor efficacy can be enhanced through pharmacological minimization of CAR tonic signaling, irrespective of whether the CAR has a high or low proclivity for tonic signaling. Finally, we propose a working model wherein strong tonic signaling induces oxidative stress, which induces an antioxidant response through NF-κB and sterol regulatory-element binding proteins (SREBP), that drives heightened T-cell activity in the absence of antigen stimulation.

INTRODUCTION

The adoptive transfer of chimeric antigen receptor (CAR)-T cells has shown remarkable efficacy in treating advanced B-cell malignancies[1]. A major appeal of CARs as a tumor-targeting moiety is their modularity in composition—i.e., the CAR protein comprises well-defined functional domains that are often reused or recombined to form new CARs[2]. Studies over the past decades have revealed several design parameters that influence CAR-T cell function[2–4]. These include the CAR's binding affinity for the targeted antigen[5,6], the size and rigidity of the CARs' extracellular domains to provide structural support for optimal target-cell engagement[7–9], the number and identity of co-stimulatory domains that booster T-cell activation upon antigen stimulation[10–12], and the number of signaling-competent motifs in the CD3ζ domain incorporated in the CAR[13]. With the exception of extracellular spacer modifications, CAR engineering efforts generally focus on domains and properties that are directly involved in ligand binding or receptor signaling. However, substantial literature in protein engineering and directed evolution has demonstrated that small sequence variations at positions with no obvious functional roles can nonetheless have major impacts on protein activity[14]. A deeper understanding of how CAR protein sequence—including residues with no annotated function—impacts CAR-T cell efficacy can significantly enhance our ability to rationally design robust CAR-T cell therapies for cancer.

For a completely unbiased exploration of the CAR sequence space, one could pursue a library-screening approach in which functionally superior clones are isolated from a pool of fully randomized sequences through high-throughput screening. Recent studies have applied a scaled-down version of the library-screening approach to evaluate new signaling domains for CARs[15,16]. In these studies, 40–89 different signaling domains were used to construct up to ~700,000 CAR variants, and functional clones were identified through *in vitro* T-cell activation or proliferation assays. However, scaling such an approach to a fully randomized CAR sequence would require libraries containing 20^{300} variants or more, an impractically large number to subject to meaningful functional screening.

An alternative approach is rational protein design, in which deliberate choices are made on protein sequences to achieve desired functions. Protein design is only “rational” to the extent that information is available on the relationship between protein sequence and function. To explore the effect of CAR protein segments and residues that are not directly implicated in specific functions, one has to rely on indirectly related properties to guide the protein design. Here, we examine antigen-independent signaling—also known as tonic signaling—as a means by which to guide CAR protein engineering.

Several studies have observed the phenomenon of tonic signaling (i.e., antigen-independent signaling) in CARs targeting various antigens, with the majority concluding that tonic signaling is detrimental to CAR-T cell function[9,17–21]. Different factors have been proposed as the cause of CAR tonic signaling. CARs commonly incorporate a single-chain variable fragment (scFv) as the ligand-binding domain, and two independent studies concluded that CAR tonic signaling is attributable to scFvs that self-aggregate, leading to CAR macrocluster formation on the T-cell surface, which in turn results in tonic signaling and premature T-cell exhaustion[17,18]. To that end, sequence changes introduced to stabilize the scFvs were shown to prevent CAR clustering, eliminate tonic signaling, and improve CAR-T cell function[18]. Separately, replacing CD28 with 4-1BB as the co-stimulatory domain has also been shown to reduce tonic signaling and enhance CAR-T cell efficacy[17,21]. These studies suggest tonic signaling is not exclusively triggered by a single component of the CAR, but it could potentially serve as a quantifiable property by which to guide CAR protein design, with the majority of existing reports indicating the minimization of tonic signaling would be the desirable outcome.

In this chapter, we demonstrate that tonic signaling can occur even when CARs do not self-aggregate, and that the intensity of tonic signaling can be calibrated through sequence changes in non-signaling domains. We generated CD20 CAR variants in which minute changes in CAR protein residues, introduced through rational protein design, were observed to greatly alter CAR-T cell phenotype, metabolism, and effector function, leading to significant improvements in

in vivo anti-tumor efficacy. Using tonic signaling as a guide for protein design, we built a novel CD20 CAR, termed RFR-LCDR.AA, that outperformed the gold-standard CD19 CAR in a Raji lymphoma animal model. Furthermore, we used our protein engineered CD20 CAR panel to examine the relationship between CAR tonic signaling and anti-tumor efficacy using multi-omics assay approaches. We found that CD20 CAR tonic signaling was driven in part by phosphoinositide 3-kinase/protein kinase B (PI3K/AKT) signaling. Pharmacological inhibition of PI3K/AKT signaling nodes on rituximab CAR-T cells demonstrated that high levels of CAR tonic signaling leads to poor *in vivo* responses. Additional characterization of PI3K/AKT pathway-inhibited rituximab CAR-T cells show that high levels of tonic signaling are amplified through the nuclear factor kappa B (NF-κB) pathway. Minimization of CAR tonic signaling through AKT or mechanistic target of rapamycin (mTOR) inhibition provided a straightforward means to enhance CAR-T cell efficacy. However, contrary to our expectations, our results also indicate that CAR-T cell optimization is not only achieved by simple minimization of tonic signaling, but rather by programming T cells to effectively transition from their resting state to a productively stimulated state, characterized by enrichment of highly functional memory T cells upon antigen exposure. Collectively, our findings demonstrate (a) protein engineering and pharmacological modulation of CAR-T cells are parallel means to modulate CAR-T cell tonic signaling, (b) that CAR tonic signaling is driven predominantly by PI3K/AKT and can be further amplified in part by NF-κB, and (c) high levels of CAR tonic signaling worsens anti-tumor responses.

METHODS

Construction of anti-CD20 scFvs and CARs. Plasmids encoding scFv sequences of rituximab were generous gifts from Dr. Anna M. Wu (UCLA and City of Hope)[22]. Plasmid encoding scFv derived from the leu16 monoclonal antibody (mAb) was a generous gift from Dr. Michael C. Jensen (Seattle Children's Research Institute)[23]. Anti-CD20 CARs were constructed by assembling an scFv (in V_L-V_H orientation), an extracellular IgG4 hinge-CH2-CH3 spacer

containing the L235E N297Q mutation[24], CD28 transmembrane and cytoplasmic domain, CD3ζ cytoplasmic domain, and a T2A "self-cleaving" sequence followed by a truncated epidermal growth factor receptor (EGFRt) with the MSCV backbone. EGFRt was used as a transduction and sorting marker. The abovementioned anti-CD20 CAR constructs were used as templates to generate CAR-HaloTag fusion proteins for microscopy imaging of CAR clustering.

Cell line generation and maintenance. HEK 293T and Raji cells were obtained from ATCC. Leu16, rituximab and RFR-LCDR (hybrid) scFv-expressing HEK293T cell lines were generated by retroviral transduction of HEK293T cells to express each scFv fused with EGFP via a 2A peptide, and EGFP+ cells were sorted by fluorescence-activated cell sorting (FACS) on a FACSAria (II) cell sorter (BD Bioscience) at the UCLA Flow Cytometry Core Facility. K562 cells were a gift from Dr. Michael C. Jensen (Seattle Children's Research Institute). $CD20^+$ K562 cells were generated by transduction of K562 cells with a retroviral construct encoding full-length CD20. K562 cells with varying CD20 expression levels were generated by FACS sorting of $CD20^+$ K562 into bins of different antigen densities. Luciferase-expressing CHLA-255 cell line (CHLA-255-Luc) was a gift from Dr. Shahab Asgharzadeh (Children's Hospital of Los Angeles). CHLA-255-Luc-EGFP cells were generated by retroviral transduction of CHLA-255-Luc to express EGFP, and EGFP+ cells were enriched by FACS. HEK 293T cells were cultured in DMEM (HyClone) supplemented with 10% heat-inactivated FBS (HI-FBS; ThermoFisher). CHLA-255-Luc-EGFP cells were cultured in IMDM (ThermoFisher) with 10% HI-FBS. Primary human T cells, Raji, and K562 cells were cultured in RPMI-1640 (Lonza) with 10% HI-FBS. For CAR-T cells used in metabolomics studies, T cells were cultured in RPMI-1640 containing 2 g/L of 1,2-^{13}C-glucose with 10% heat-inactivated dialyzed FBS (HI-dFBS).

Retrovirus production and generation of human primary CAR-T cells. Retroviral supernatants were produced by transient co-transfection of HEK 293T cells with pRD114/pHIT60

virus-packaging plasmids (gifts from Dr. Steven Feldman of National Cancer Institute) and plasmids encoding CARs or control constructs using linear polyethylenimine (PEI, 25 kDa; Polysciences). Supernatants were collected 48 and 72 hours later and pooled after removal of cell debris by a 0.45 μm membrane filter. Healthy donor blood was obtained from the UCLA Blood and Platelet Center. $CD8^+$ T cells were isolated using RosetteSep Human $CD8^+$ T Cell Enrichment Cocktail (StemCell Technologies) following manufacturer's protocol. Peripheral blood mononuclear cells (PBMCs) were isolated from a Ficoll-Paque PLUS (GE Healthcare) density gradient. $CD14^-/CD25^-/CD62L^+$ naïve/memory T cells ($T_{N/M}$) were enriched from PBMCs using magnetic-activated cell sorting (MACS; Miltenyi). $T_{N/M}$ cells were stimulated with CD3/CD28 Dynabeads (ThermoFisher) at a 3:1 cell-to-bead ratio on Day 0 (day of isolation) and transduced with retroviral supernatant on Day 2 and Day 3. Dynabeads were removed on Day 7. T cells were cultured in T-cell media (RPMI-1640 supplemented with 10% HI-FBS) and fed with recombinant human IL-2 (ThermoFisher) and IL-15 (Miltenyi) every 2 days to final concentrations of 50 U/mL and 1 ng/mL, respectively. For CAR-T cells used in RNA-seq and metabolomics studies, T cells were enriched for CAR^+ expression by magnetic cell sorting via staining of EGFRt with biotinylated cetuximab (Eli Lilly; biotinylated in-house) followed by anti-biotin microbeads (Miltenyi).

For experiments shown in Fig. 4-4 through Fig. 4-6, starting on Day 8, T cells were cultured in T-cell media with cytokine support in the presence of 1 μM PI3Kδ isoform inhibitor (CAL-101, Apex Biotechnology #A300520)), 1 μM AKT inhibitor (AZD5363, Selleckchem #S8019), 100 nM mTORC1 inhibitor (Rapamycin, LC Laboratories #R-5000), 2 μM c-Myc inhibitor (MYCi975, MedChemExpress #HY-129601), SREBP inhibitor (Betulin, MilliporeSigma #92648), or DMSO as a vehicle control. Each inhibitor molecule was solubilized in DMSO. For experiments shown in Fig. 4-7 through Fig. 4-9 and Supp Fig. 4-3, CAR^+ T cells were magnetically sorted via staining of EGFRt as described above on day 8 prior to pharmacological inhibition.

Cytokine production quantification by ELISA. In 96-well U-bottom plates, 5 x 10^5 CAR^+ T cells were incubated with 2.5 x 10^5 EGFP-expressing parental K562 ($CD19^-CD20^-$) or $CD19^+CD20^+$ K562 target cells at a 2:1 effector-to-target (E:T) ratio. To control for cell density while accounting for differences in transduction efficiency, untransduced T cells were added as necessary to reach the same number of total T cells per well. After a 48-hour co-incubation, cells were spun down at 300 x g for 2 min. Supernatant was harvested and cytokine levels were quantified by ELISA (BioLegend).

Proliferation assay. T cells were stained with 1.25 μM CellTrace Violet (ThermoFisher) and 4 x 10^5 CAR^+ T cells were seeded in each well in 96-well U-bottom plates. Untransduced T cells were added to wells as needed to normalize for differing transduction efficiencies and ensure the total number of T cells per well was consistent throughout. Cultures were passaged as needed, and CTV dilution was analyzed on a MACSQuant VYB flow cytometer after a 4-day co-incubation.

Cytotoxicity assay with repeated antigen challenge. CAR^+ T cells were seeded at 4 x 10^5 cells/well in 24-well plate and coincubated with target cells at a 2:1 E:T ratio. Untransduced T cells were added to wells as needed to normalize for differing transduction efficiencies and ensure the total number of T cells per well was consistent throughout. Cell counts were quantified by a MACSQuant VYB flow cytometer every 2 days prior to addition of fresh target cells (2 x 10^5 cells/well).

Cytotoxicity assay with Raji cells. Raji cells were seeded at 2 x 10^5 cells/well in 96-well U-bottom plate and coincubated with CAR^+ T cells at 1:1, 3.33:1, and 10:1 E:T ratios. Untransduced T cells were added to wells as needed to normalize for differing transduction efficiencies and ensure the total number of T cells per well was consistent throughout. Remaining target cells were quantified by MACSQuant VYB flow cytometer 24-hr post co-incubation.

Antibody staining for flow-cytometry analysis. EGFRt expression was measured with biotinylated cetuximab (Eli Lilly; biotinylated in-house), followed by PE-conjugated streptavidin (Jackson ImmunoResearch #016-110-084). CAR expression was quantified by surface epitope staining using anti-Fc (Alexa Fluor 488, Jackson ImmunoResearch #709-546-098). Antigen-independent activation-marker expression of CAR-T cells was evaluated by antibody staining for CD137 (PE/Cy7, clone 4B4-1, BioLegend #309818), and PD-1 (FITC, clone EH12.2H7, BioLegend #329904) on Days 18 (i.e., 18 days after Dynabead addition and 11 days after Dynabead removal) and after 5-6 days of inhibitor culture (Fig. 4-4, Fig. 4-6). T-cell subtype of CAR-T cells was evaluated by antibody staining for CD45RO (VioBlue®, clone REA611, Miltenyi #130-119-620) and CD62L (APC, clone DREG56, Invitrogen #17-0629-42) after 5-6 days of inhibitor culture (Fig. 4-4, Fig. 4-6). T-cell persistence *in vivo* was monitored by antibody staining of retro-orbital blood, liver, and spleen samples. Samples were treated with red blood cell lysis solution (10X, Miltenyi) following manufacturer's protocol. The remaining cellular content was stained with anti-human CD45 (PacBlue or PECy7, clone HI30, BioLegend #304029 or #304016) and biotinylated cetuximab, followed by PE-conjugated streptavidin. All samples were analyzed on a MACSQuant VYB flow cytometer (Miltenyi), and the resulting data were analyzed using the FlowJo software (TreeStar).

Confocal microscopy. The initial imaging experiment shown in Supplementary Figure 4-1A was done using CAR-expressing Jurkat cells stained with anti-Fc antibody conjugated to DyLight 405 (Jackson ImmunoResearch #109-477-008). The follow-up experiment shown in Supplementary Figure 4-1B was done using Jurkat cells transduced with CAR-HaloTag fusion protein stained with the red fluorescent dye tetramethylrhodamine (TMR) ligand. In both experiments, CAR-expressing Jurkat cells were seeded at 1 x 10^5 cells per well in 50 µL RPMI-1640 + 10% HI-FBS in one well of a 48-well flat-bottom glass plate (MatTek) without antigen stimulation. Scanning

confocal imaging was acquired with a Zeiss LSM 880 laser scanning confocal microscope with AiryScan and a 63X 1.4 NA oil objective.

***In vivo* studies.** Six- to eight-week-old NOD/SCID/IL-2Rγ^{null} (NSG) mice were obtained from UCLA Department of Radiation and Oncology. The protocol was approved by UCLA Institutional Animal Care and Used Committee. Mice were injected with EGFP^{+} firefly luciferase (ffLuc)-expressing Raji lymphoma cells or CHLA-255 neuroblastoma cells by tail-vein injection, and subsequently treated with CAR-T cells or cells expressing EGFRt only (negative control) via tail-vein injection. Details of the dose and timing of tumor injection, T-cell injection, and tumor re-challenge are indicated in the text and figures. Tumor progression/regression was monitored with an IVIS Illumina III LT Imaging System (PerkinElmer). Blood samples were harvested via retro-orbital bleeding 3 days post T-cell injection and every 10-13 days thereafter. Mice were euthanized at the humane endpoint. Bone marrow, spleen and liver were collected after euthanasia. Tissues were ground and passed through a 100-μm filter followed by red-blood-cell lysis prior to flow-cytometry analysis.

Bulk RNA-seq for CAR-T cells cultured *ex vivo.* CD14^{-}/CD25^{-}/CD62L^{+} naïve/memory T cells ($T_{N/M}$) were isolated, activated, retrovirally transduced as described above. On day 16 or 18 post activation, T cells were MACS-sorted with Dead Cell Removal kit (Miltenyi) to remove apoptotic population and enriched for EGFRt^{+} subpopulation for Fig. 4-3. CAR-T cells were directly lysed for RNA extraction on day 14 post activation for the dataset shown in Fig. 4-7 through Fig. 4-9. Total RNA was extracted from MACS-sorted CAR-T cells using Qiagen RNeasy Plus Mini kit.

RNA library preparation and sequencing for the dataset shown in Fig. 4-3 are as follows: mRNAs were isolated using NEBNext Poly(A) mRNA Magnetic Isolation Module (New England BioLabs). RNA-seq libraries were generated using NEBNext Ultra II Directional RNA Library Prep Kit (New

England BioLabs) following manufacturer's protocol. Libraries were sequenced on the Illumina NovaSeq S1 platform at the High Throughput Sequencing core at UCLA Broad Stem Cell Research Center with 50-bp paired-end reads. RNA library preparation and sequencing for the dataset shown in Fig. 4-7 through Fig. 4-9 are as follows: Libraries for RNA-Seq were prepared with KAPA Stranded mRNA-Seq Kit (Roche, Cat.KK8420). The workflow consists of mRNA enrichment and fragmentation, first strand cDNA synthesis using random priming followed by second strand synthesis converting cDNA:RNA hybrid to double-stranded cDNA (dscDNA), and incorporates dUTP into the second cDNA strand. cDNA generation is followed by end repair to generate blunt ends, A-tailing, adaptor ligation and PCR amplification. Different adaptors were used for multiplexing samples in one lane. Sequencing was performed on Illumina NovaSeq 6000 for PE 2x50 run. Data quality check was done on Illumina SAV. Demultiplexing was performed with Illumina Bcl2fastq v2.19.1.403 software.

Fastq files from RNA-seq were quality-examined by FastQC (Linux, v0.11.8). Reads were processed by cutadapt (Linux, v1.18) to remove reads with low quality (quality score < 33) and to trim adapters. Trimmed reads were mapped to hg38 genome by Tophat2. Fragments assigned to each gene were counted by *featureCounts* function in subread package (Linux, v1.6.3) with ensembl 38 gene sets as references. Genes without at least 8 reads mapped in at least one sample were considered below reliable detection limit and eliminated. Read counts were normalized by Trimmed Mean of M-values method (TMM normalization method in edgeR running on R v3.6.3) to yield FPKM (fragments per millions per kilobases) values.

Gene set enrichment analysis (GSEA), Enrichr analysis, principal component analysis (PCA), and regulon network inference analysis. ANOVA cluster genes were assigned using hierarchical clustering via the centroid method, with the cutHeight set at 2.8. GO analysis was performed using GSEA software (v4.1.0, Broad Institute) (*61*). Expression values of differentially

expressed genes were input to the program and using a curated list of 2493 T-cell–relevant gene sets selected from current Molecular Signatures Database (MSigDB; 2020 version) gene set, namely the Hallmark and Kyoto Encyclopedia of Genes and Genomes (KEGG; 2021 version) gene databases. Differentially expressed genes were used to perform KEGG (2021 version) and MSigDB Hallmark (2020 version) pathway enrichment using Enrichr[25]. Top 3 pathways with adjusted *p* value that were less than 0.05 were chosen to display. Heatmaps for differentially expressed genes were generated using *heatmap.plus, pheatmap* and *ggplot2* packages in R (version 3.6.3). Volcano plots and GSEA dot plots were generated using *ggplot2* in R (version 3.6.3). PCA analysis was conducted using pcaExplorer (version 3.15)[26]. Regulon network inference analysis was performed in collaboration with Katherine Sheu, a former MSTP in Alex Hoffmann's Lab. 46 samples from GSE136891 were used to infer the transcriptomic network using ARACNE[27]. LogFC from differential gene expression data, obtained from *in vivo* antigen stimulated CD20 CAR-T cells (data not shown), were used to determine gene ranks using VIPER[28].

Metabolite extraction and analysis. Metabolite data collected in Fig. 4-1 are as follows: Cell culture media were collected from each cell line every 24 hours to evaluate nutrient uptake and consumption. Four volumes of 100% HPLC-grade methanol were added to one volume of media and centrifuged at 17,000 x g and 4°C for 5 minutes to precipitate cell debris. Clear supernatants were harvested and analyzed by liquid chromatography followed by mass spectrometry (LC-MS). To provide accurate estimation of nutrient uptake and consumption, partial media change was performed every 24 hours to avoid nutrient depletion. Methanol-treated media samples were analyzed by reversed-phase ion-pairing liquid chromatography (Vanquish UPLC; Thermo Fisher Scientific) coupled to a high-resolution orbitrap mass spectrometer (Q-Exactive plus Orbitrap; Thermo Fisher Scientific) at the Molecular Instrumentation Center (MIC) in UCLA. Metabolites were identified by comparing mass-to-charge (m/z) ratio and retention time to previously validated

standards. Samples were detected in both negative-ion mode and positive-ion mode. Negative-ion mode was separated into two subgroups—nlo and nhi—to obtain data with m/z ratio from 60 to 200 and 200 to 2000, respectively. LC-MS data were processed using Metabolomic Analysis and Visualization Engine (MAVEN)[29]. Labeling fractions were corrected for the naturally occurring abundance of ^{13}C. Concentration of metabolites in culture media was quantified at 24 and 72 hours by normalizing ion counts from LC-MS measurement to controls with known concentrations. Uptake and secretion rates were calculated by subtracting sample concentration from fresh media and normalizing to viable cell count (positive values indicated secretion and negative values indicated uptake). A mole balance was performed to account for media change from cell cultures. Calculation accounted for 10–20% of media evaporation every 24 hours.

Metabolite data collected in Supp. Fig. 4-3 are as follows: 0.5 x 10^6 CAR-T cells were seeded in 0.5 mL RPMI 1640 + 10% HI-dFBS in the presence of IL-2 and IL-15. Cell culture media was collected after 46-49 hours to evaluate nutrient uptake and consumption. Cell culture media was spun down at 300 x g for 10 minutes to remove any cellular debris. 20 µL culture medium was extracted with 500 µL 80% MeOH. The cleared extract was dried under vacuum at 30 °C and stored at –80°C until LC-MS analysis. Dried metabolites were resuspended in 50 µL 50% ACN:water and 5 µL was loaded onto a Luna NH2 3 µm 100A (150 × 2.0 mm) column (Phenomenex) using a Vanquish Flex UPLC (Thermo Scientific). The chromatographic separation was performed with mobile phases A (5 mM NH4AcO pH 9.9) and B (ACN) at a flow rate of 300 µL/min. A linear gradient from 25% A to 95% A over 6 min was followed by 4 min isocratic flow at 95% A and reequilibration to 25% A. Metabolites were detection with a Thermo Scientific Q Exactive mass spectrometer run with polarity switching (+3.5 kV/− 3.5 kV) in full scan mode using a range of 70-975 m/z and 70.000 resolution. Maven (v 8.1.27.11)[29] was used to quantify the targeted polar metabolites by AreaTop, using expected retention time and accurate mass measurements (< 5 ppm) for identification. Uptake and secretion rates were calculated by

subtracting sample concentration from fresh media and normalizing to viable cell count (positive values indicated secretion and negative values indicated uptake).

Statistical Analysis. Statistical tests including two-tailed, unpaired, two-sample Student's *t* test with Sidak correction for multiple comparisons, log-rank Mentel-Cox test with Holm-Sidak correction for multiple comparisons, and Mann-Whitney U test with Holm-Sidak correction for multiple comparisons were performed using GraphPad Prism V8. One-way ANOVA test and pairwise differential gene expression analysis in RNA-seq was performed with *glmQLFTest* function in edgeR. Fisher's exact test and the Benjamini-Hochberg method were used to calculate *p* values and adjusted *p* values, respectively, in Enrichr.

RESULTS

Rituximab-based CD20 CAR-T cells tonically signal and have limited anti-tumor efficacy

To elucidate the effect of CAR protein sequence on CAR-T cell function, we focus on a CAR with strong translational potential but also substantial room for improvement in anti-tumor efficacy—i.e., a CD20 CAR containing a rituximab-based scFv and CD28 co-stimulatory domain (**Fig. 4-1A**). CD20 CAR-T cell therapy has gained increasing interest in recent years, in part due to frequent antigen-negative relapse seen in patients treated with CD19 CAR-T cell therapy[30]. Emerging evidence suggests CD20 may be more resistant to antigen escape than CD19, even under selective pressure from immunotherapy[31,32]. Given that rituximab, an anti-CD20 monoclonal antibody, is the front-line treatment option for a variety of B-cell malignancies[33], we generated a rituximab-based CD20 CAR as a clinically relevant starting point to understand the relationship between CAR sequence and function. For comparison, we also generated an FMC63-based CD19 CAR equipped with identical transmembrane and signaling domains as the rituximab CAR (**Fig. 4-1A**). Of note, a long spacer (IgG4 hinge-CH2-CH3) was used for the CD20 CAR while a

short IgG4 hinge was used for the CD19 CAR, based on prior studies indicating different structural requirements for optimal CD19 and CD20 antigen targeting[24,34]. Each CAR was connected via a self-cleaving T2A peptide to a non-signaling, truncated epidermal growth factor receptor (EGFRt) as transduction marker, and T cells transduced with EGFRt alone served as negative controls throughout this study.

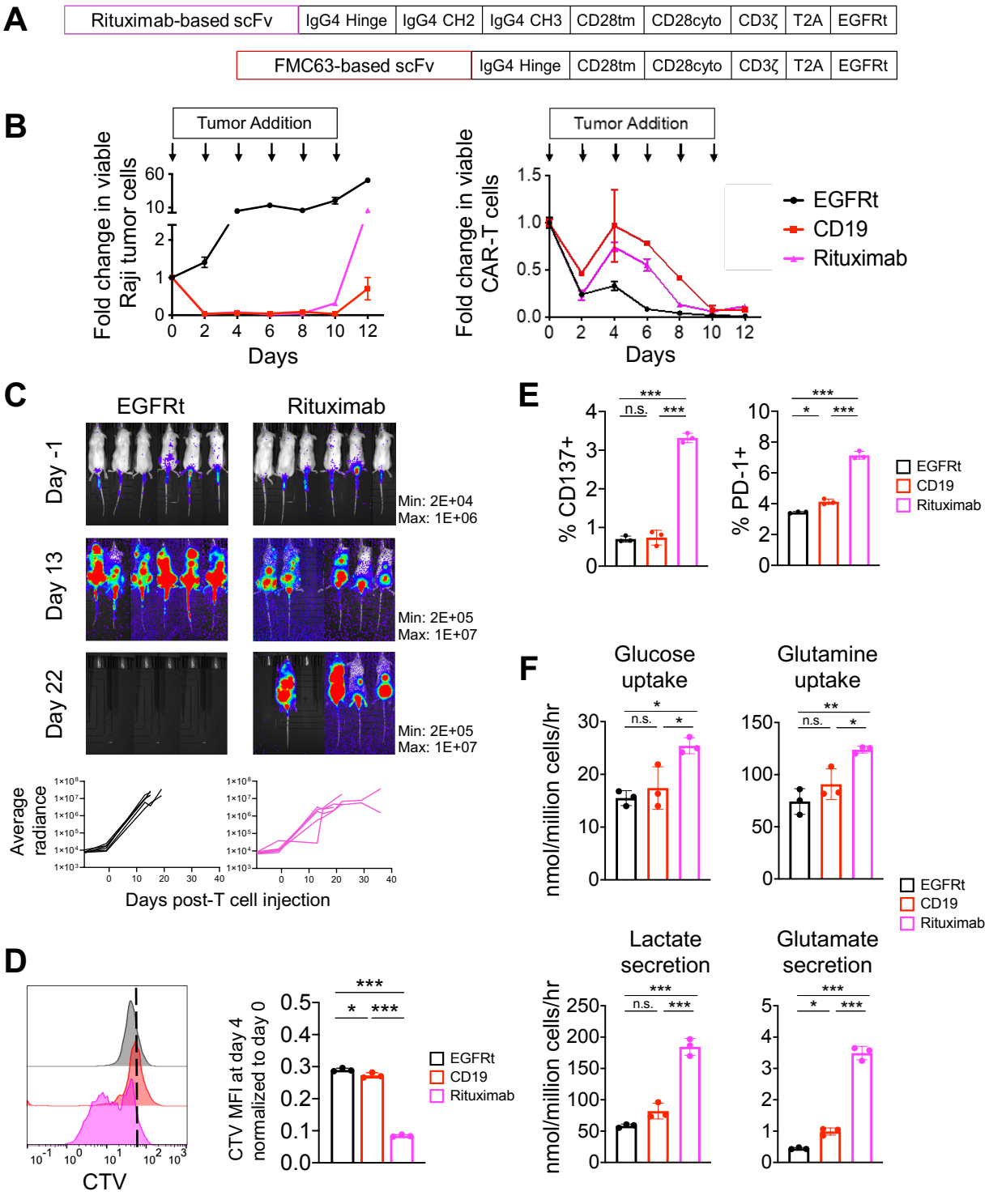

Figure 4-1: Rituximab-based CD20 CAR-T cells have limited anti-tumor efficacy and tonically signal. (**A**) Schematic of rituximab-based CD20 CAR and FMC63-based CD19 CAR. (**B**) CAR-T cell cytotoxicity and proliferation upon repeated antigen challenge. Rituximab-based CD20 CAR-T cells, FMC63-based CD19 CAR-T cells, or control T cells (transduced to express only the transduction marker, truncated epidermal growth factor receptor—EGFRt) were

challenged with $CD19^+CD20^+$ Raji tumor cells at a 2:1 effector-to-target (E:T) ratio every two days, and the number of viable Raji and CAR-T cell was quantified by flow cytometry. Data shown are the means of technical triplicates with error bars indicating ± 1 standard deviation (S.D.). Results are representative of three independent experiments using T cells from three different healthy donors. (**C**) NOD/scid/$\gamma^{-/-}$ (NSG) mice were injected intravenously with 0.5 x 10^6 firefly-luciferase (ffLuc)-expressing Raji cells followed by two doses of 1.35 x 10^6 CAR-T cells each at 6 and 11 days post tumor injection; n = 6 mice per group. Tumor progression was monitored by bioluminescence imaging (top). Radiance (in photons/sec/cm^2/sr) of individual animals are shown for each group (bottom). (**D**) Proliferation of CAR^+ T cells stained with CellTrace Violet (CTV) dye was assayed after a 4-day culture in the absence of target cells or exogenous cytokines. CTV histogram on Day 4 (left) and fold-change of CTV MFI from Day 0 to Day 4 are shown (right). Results are representative of five independent experiments using T cells from five different healthy donors. (**E**) Activation and exhaustion marker expression by CAR^+ T cells in the absence of antigen stimulation. Data bars indicate the means of technical triplicates ± 1 S.D. Results are representative of two independent experiments using T cells from two different healthy donors. (**F**) Metabolic analysis of CAR-T cells in culture in the absence of antigen stimulation. CAR-T cells were cultured for 72 hours in RPMI supplemented with 10% heat-inactivated, dialyzed fetal bovine serum (HI-dFBS), IL-2, and IL-15. Data bars indicate the means of technical triplicates ± 1 S.D. Results are representative of four independent experiments using T cells from four different healthy donors. Statistical significance in panels (D)–(F) was determined by two-tailed Student's *t* test with Sidak correction for multiple comparisons. *p<0.05, **p<0.01, ***p<0.001, n.s. not statistically significant. **Experimental data collected in panels (B) and (D–F) were collected by co-first author of the submitted manuscript, Ximin Chen.**

The rituximab and CD19 CARs both expressed well and exhibited even distribution on the T-cell surface (**Supp. Fig. 4-1A–B**). Compared to CD19 CAR-T cells, rituximab CAR-T cells showed reduced tumor-cell lysis and T-cell expansion upon repeated challenge with Raji cells *in vitro* (**Fig. 4-1B**). Furthermore, rituximab CAR-T cells failed to control Raji lymphoma xenografts *in vivo* (**Fig. 4-1C**). Analysis of rituximab CAR-T cells during *ex vivo* culture revealed antigen-independent T-cell proliferation (**Fig. 4-1D**). Furthermore, compared to mock-transduced and CD19 CAR-T cells, rituximab CAR-T cells showed elevated expression of both activation and exhaustion markers (**Fig. 4-1E**), as well as increased metabolic flux (**Fig. 4-1F**), in the absence of antigen stimulation. Taken together, these data indicate strong tonic signaling and poor anti-tumor efficacy by rituximab CAR-T cells.

Rational CAR protein design through torsional engineering and scFv sequence hybridization yields functionally superior CAR variant

Given that Raji cells highly express both CD19 and CD20[35] and that the CD19 and CD20 CARs contain identical signaling domains as well as high-affinity scFv sequences for each antigen[36,37], we reasoned that portions of the CD20 CAR not directly involved in ligand-binding or signaling must nonetheless impact the CAR's capability to signal and trigger T-cell effector function. The signaling cascades downstream of CD28 and CD3ζ are mediated by adaptor proteins and kinases whose interactions depend on the protein conformation and physical accessibility of receptor chains[38]. Receptor conformation is, in turn, a function of the overall protein sequence, not just domains that directly engage in ligand binding or signaling. CARs typically contain an α-helical transmembrane domain, such as the CD28 transmembrane domain used in our CARs (UniProt P10747, subcellular location). Alanine insertion is a well-established method to form or extend α-helices, with each alanine expected to cause a ~109° turn in the protein structure[39–41]. For example, EAAAK is a frequently used rigid linker due to its stable α-helical conformation[42,43]. We thus hypothesized that inserting alanine residues immediately after the transmembrane domain of a CAR could alter the receptor's conformation by extending the transmembrane helix, providing a means to calibrate CAR signaling without directly altering signaling domains of the CAR. A panel of receptors was generated to allow varying alignments between each CAR's extracellular ligand-binding domain and cytoplasmic signaling domains (**Fig. 4-2; Supp. Fig. 4-2A**). We observed that alanine-insertion rituximab CAR variants decreased activation- and exhaustion-marker expression (**Supp. Fig. 4-2B**), in addition to antigen-independent T-cell proliferation (**Supp. Fig. 4-2C**), indicating that torsional engineering of the CAR through juxtamembrane alanine insertions reduced rituximab CAR tonic signaling.

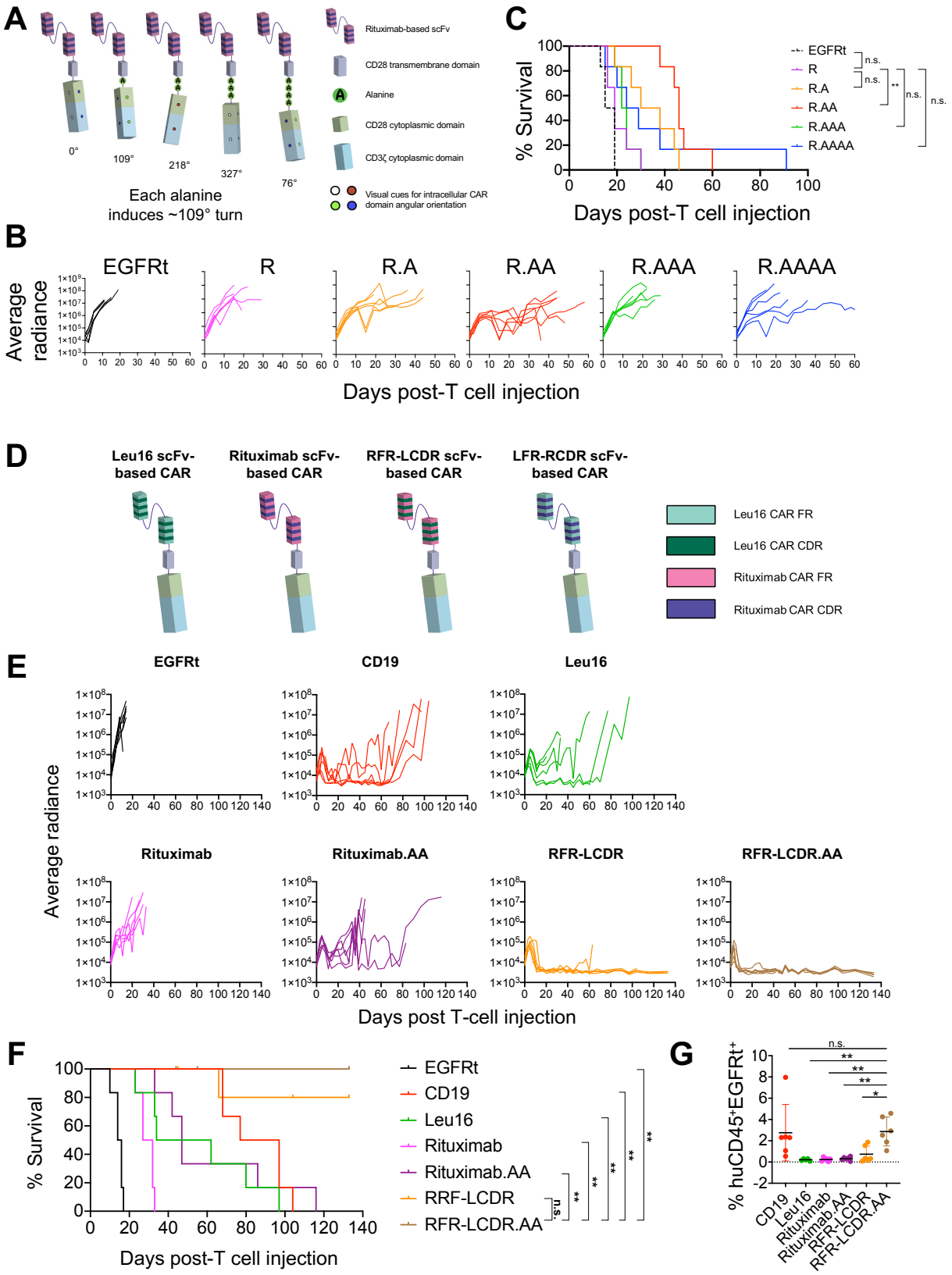
A
0°
109°
218°
327°
76°
Each alanine induces ~109° turn
Rituximab-based scFv
CD28 transmembrane domain
Alanine
CD28 cytoplasmic domain
CD3ζ cytoplasmic domain
Visual cues for intracellular CAR domain angular orientation
C
% Survival
Days post-T cell injection
EGFRt
R
R.A
R.AA
R.AAA
R.AAAA
n.s.
**
B
EGFRt
R
R.A
R.AA
R.AAA
R.AAAA
Average radiance
Days post-T cell injection
D
Leu16 scFv-based CAR
Rituximab scFv-based CAR
RFR-LCDR scFv-based CAR
LFR-RCDR scFv-based CAR
Leu16 CAR FR
Leu16 CAR CDR
Rituximab CAR FR
Rituximab CAR CDR
E
EGFRt
CD19
Leu16
Rituximab
Rituximab.AA
RFR-LCDR
RFR-LCDR.AA
Average radiance
Days post T-cell injection
F
% Survival
Days post-T cell injection
EGFRt
CD19
Leu16
Rituximab
Rituximab.AA
RRF-LCDR
RFR-LCDR.AA
n.s.
**
G
% huCD45+EGFRt+
CD19
Leu16
Rituximab
Rituximab.AA
RFR-LCDR
RFR-LCDR.AA
n.s.
**
*

Figure 4-2: Protein engineered CD20 CARs enhance tumor-killing efficacy in the Raji lymphoma animal model. (**A**) Schematic of rituximab-based CAR constructs with zero to four alanines inserted between the CD28 transmembrane and cytoplasmic domains. (B,C) NSG mice were injected intravenously with 0.5 x 10^6 ffLuc–expressing Raji cells followed by two doses of CAR^+ T cells 6 days (1.35 x 10^6 cells) and 12 days (1.5 x 10^6 cells) later; n = 6 mice per group. (**B**) Tumor progression was monitored by bioluminescence imaging and tumor radiance (in photons/sec/cm^2/sr) of individual animals are shown for each group. The end point of each trace indicates the humane end point of each animal. (**C**) Kaplan-Meier survival curve. Statistical significance was determined by log-rank (Mantel-Cox) test with Holm-Sidak correction for multiple comparisons. $^{**}p$ 0.01, n.s. not statistically significant. (**D**) Schematic of scFv sequence hybridization in CAR molecules. The framework regions (FR) and complementarity-determining regions (CDRs) of Leu16- and rituximab-derived scFvs were intermixed to yield two hybrid CAR variants. (**E**) Tumor signal (in photons/sec/cm^2/sr) in individual animals as quantified by bioluminescence imaging. (**F**) Kaplan-Meier survival curve. Log-rank (Mantel-Cox) test was performed with Holm-Sidak correction for multiple comparisons. $^{*}p<0.05$, $^{**}p<0.01$, $^{***}p<0.001$, n.s. not statistically significant. (**G**) Frequency of human $CD45^+EGFRt^+$ cell in peripheral blood collected from mice on day 23 after first dose of T-cell infusion. Statistical significance was determined by two-tailed Student's *t* test with Sidak correction for multiple comparisons. $p<0.05$, $^{**}p<0.01$, $^{***}p<0.001$, n.s. not statistically significant. **Of note, I contributed to the conception of the juxtamembrane alanine insertion CAR protein design strategy. The scFv hybridization strategy was conceived by Yvonne Chen and Ximin Chen. The reduction to practice and collection of experimental data shown in this figure were executed by Ximin Chen with the help of co-authors listed in our manuscript.**

In vivo, T cells expressing rituximab-based CARs containing 1, 2, or 4 inserted alanines showed significantly improved control of Raji xenografts compared to parental rituximab CAR-T cells, whereas 3-alanine insertion provided no benefit (**Fig. 4-2B**). In particular, the 2-alanine CAR increased median survival period by 2.1 folds compared to the original rituximab CAR (55 days vs. 26 days; **Fig. 4-2C**), indicating a small change in CAR protein sequence—and possibly changes in tonic signaling—can exert significant impact on *in vivo* tumor-killing efficacy.

Given that juxtamembrane engineering altered rituximab CAR tonic signaling, and reduced tonic signaling correlated with *in vivo* efficacy, we reasoned that we could use tonic signaling as a guide to protein engineer novel CD20 CARs. As an alternative approach, we applied a concept similar to DNA shuffling in protein evolution[44], and recombined sequences from two different anti-CD20 scFvs that exhibit different tonic signaling levels when incorporated into CAR molecules. This hybridization approach allows exploration of novel CAR sequence space while maximizing the probability of success, as the parent sequences are already "solutions" (i.e.,

functional in CD20 binding). An scFv molecule comprises a light chain and a heavy chain, and each chain can be further subdivided into four FRs flanking three complementarity-determining regions (CDRs) (**Fig. 4-2D**). CDRs closely interact with the target antigen while FRs primarily provide structural support for the variable chains; this division of labor underpins the practice of humanizing antibodies by grafting murine CDRs onto human FRs[45].

As a partner for rituximab, we chose Leu16, an anti-CD20 antibody that has been incorporated into CAR constructs evaluated in the clinic[46–48], and whose V_L and V_H sequences are 91% and 92% identical to those of rituximab, respectively (**Supp. Fig. 4-2D**). We constructed hybrid CARs whose scFv comprised the FRs of rituximab and CDRs of Leu16 (RFR-LCDR), or vice versa (LFR-RCDR) (**Fig. 4-2D**). The RFR-LCDR and LFR-RCDR hybrids differ from the rituximab CAR in 11 and 9 amino acid residues, respectively. Even though both hybrid CARs expressed well on the cell surface, at levels comparable to those of the parental Leu16 and rituximab CARs, the RFR-LCDR hybrid CAR variant was the only functional CAR as evaluated by *in vitro* Raji lysis (data not shown). Henceforth, the LFR-RCDR hybrid CAR variant was excluded from further analysis and the term "hybrid CAR" refers to the RFR-LCDR variant. We further built a hybrid CAR variant with a two-alanine juxtamembrane insertion, termed RFR-LCDR.AA or "hybrid.AA CAR".

In contrast to the strongly tonically signaling rituximab CAR, the Leu16 CAR showed no sign of tonic signaling as measured by antigen-independent T-cell proliferation, cytokine production, activation and exhaustion marker expression, and metabolic flux (**Supp. Fig. 4-2E–H**). Intriguingly, hybrid CAR variants exhibited intermediate tonic signaling intensity compared to the two parental constructs (**Supp. Fig. 4-2E–H**). We next performed head-to-head comparisons of the hybrid CAR against each of its parent construct and the CD19 CAR *in vivo* (**Fig. 4-2E-F**). In contrast to both Leu16 and rituximab-based CAR-T cells, RFR-LCDR and RFR-LCDR.AA CAR-T cells efficiently rejected both the original tumor as well as a tumor re-challenge applied 55 days after initial T-cell treatment (**Fig. 4-2E-F**), with the RFR-LCDR.AA CAR driving superior *in vivo* T-

cell persistence compared to all other CD20 CAR constructs tested (**Fig. 4-2G**). Notably, the co-first author of the submitted manuscript, Ximin Chen, excluded scFv binding affinity, antigen-detection threshold, and off-target cross-reactivity as mechanisms contributing towards the hybrid CARs' enhanced functionality (data not shown; data can be found in the submitted manuscript or Ximin Chen's doctoral dissertation). Taken together, these results indicate that the functionality of a CAR can be significantly improved by small changes to the scFv sequence, without altering the target antigen or antigen-detection threshold. Taken together, these results indicate that minute changes in CAR protein sequence—as few as two extra alanine residues inserted between transmembrane and cytoplasmic domains, or residue changes in the framework region of the single-chain variable fragment (scFv) of the CAR—can significantly alter CAR-T cell phenotype, metabolism, and effector function, yielding marked improvements in *in vivo* anti-tumor efficacy.

CAR expression differentially activates PI3K/AKT signaling and downstream T-cell functions

The panel of protein engineered CD20 CARs provides an intriguing window to examine the relationship between CAR tonic signaling and *in vivo* efficacy. We noted with interest that rituximab CAR-T cells exhibit strong T-cell activation in the absence of antigen stimulation, whereas Leu16 CAR-T cells appear completely quiescent at rest (**Fig. 4-3A**). By comparison, hybrid CAR-T cells show an intermediate level of antigen-independent activation, but far outperform both parental constructs in tumor control *in vivo* (**Fig. 4-3A**). These observations led us to speculate whether an intermediate level of antigen-independent activation may be key to the hybrid CAR-T cells' ability to productively respond to tumor challenge *in vivo*. If a causal relationship between tonic signaling and *in vivo* efficacy can be made, then one can in principle use tonic signaling as the primary design parameter in developing novel CARs, circumventing the

need to carry out time- and resource-intensive *in vivo* experiments in determining functional efficacy.

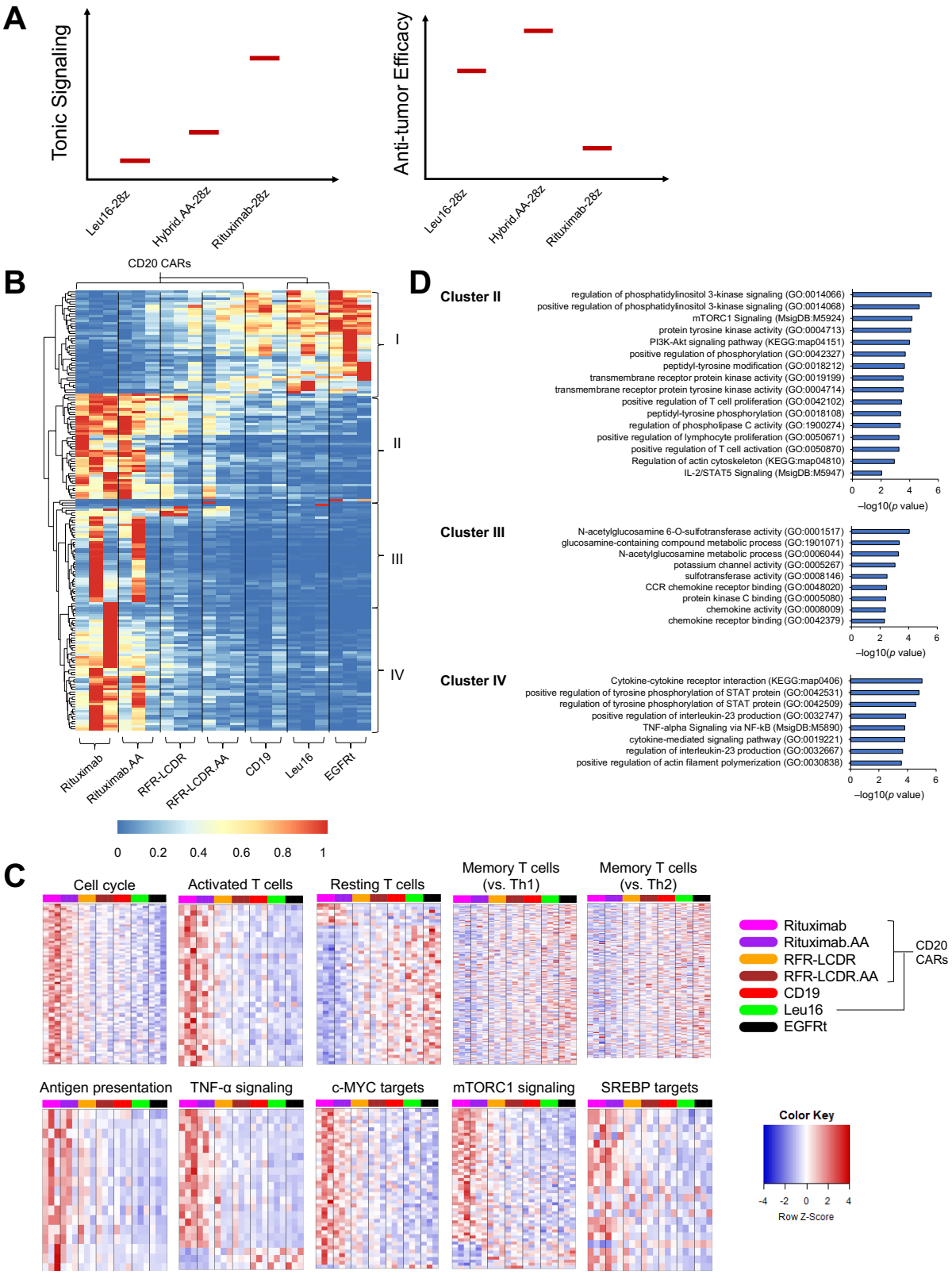

Figure 4-3. CAR sequences differentially impact basal CAR-T cell activity without antigen stimulation. (**A**) Pictorial representation of the correlation between tonic signaling and *in vivo*

anti-tumor efficacy of high-performing (hybrid.AA) and poorer-performing (leu16, rituximab) CAR-T cells. (**B–D**) T cells expressing the indicated CAR constructs or the transduction marker EGFRt were cultured in the absence of CD20 antigen stimulation for 16–18 days prior to RNA extraction for bulk RNA-seq analysis. (B) Heatmap of differentially expressed genes (FDR < 0.05) identified through ANOVA. Each column represents one donor. Each row is scaled to a maximum of 1 and minimum of 0 to highlight relative expression of each gene. (C) Heatmap showing genes associated with resting, activated, or memory T cells; antigen presentation; cell-cycle activity; and signaling pathways associated with TNF-α, c-MYC, mTORC1, and SREBP targets. Complete list of genes shown in each heatmap is provided in Data S1. (D) Enriched pathways associated with the different DGE clusters, with *p* values shown in –log10 scale. Only pathways with statistically significant adjusted *p* value (<0.05) using the Benjamini-Hochberg method are included. No pathways in the GO Biological Process, GO Molecular Function, KEGG and MSigDB Hallmarks were found to be statistically significant for Cluster I. RNA samples, RNAseq count data, and the heatmap for panel (B) were generated by Ximin Chen in collaboration with the help of co-authors listed in our manuscript.

To understand the molecular pathways underlying CD20 CAR tonic signaling, transcriptional analyses were performed on unstimulated CD20 CAR-T cells at the end of the CAR-T cell manufacturing cycle. Consistent with *in vitro* measurements, RNA-seq data indicate the hybrid CAR-T cells exhibit intermediate transcriptomic profile compared to T cells expressing the rituximab and Leu16 parental constructs (**Fig. 4-3B–C**). Gene ontology (GO) and pathway analyses indicate unstimulated rituximab CAR-T cells significantly upregulate signaling pathways related to PI3K, phospholipase C (PLC), and mechanistic target of rapamycin complex 1 (mTORC1), as well as T-cell activation and proliferation (Cluster II, **Fig. 4-3D**). Furthermore, unstimulated rituximab CAR-T cells exhibit an increase in metabolic processes and cytokine signaling relative to other CD20 CAR-T cells (Cluster III/IV, **Fig. 4-3C–D**). Together, these transcriptomic signatures indicate rituximab CAR signaling through the CD3ζ and CD28 domains despite lack of antigen stimulation[49]. Although a number of genes were enriched in CD19, Leu16, and EGFRt-only samples (Cluster I), these genes did not correspond to any pathway with statistical significance.

The strong antigen-independent activation of rituximab CAR-T cells revealed by transcriptomic analysis was corroborated at the functional level with increased cell division, TNF-α production, activation-marker expression, and elevated metabolic flux, all in the absence of

antigen stimulation (**Supp. Fig. 4-2E–H**). In contrast, unstimulated Leu16 CAR-T cells were enriched in resting and memory T-cell phenotypes (**Fig. 4-3C**), and exhibited minimal antigen-independent cell proliferation, cytokine production, activation-marker expression, and metabolic flux (**Supp. Fig. 4-2E–H**). In fact, among all the CAR-T cell lines tested (including CD19 CAR-T cells), Leu16 CAR-T cells were the most similar to mock-transduced (EGFRt-only) T cells and exhibited a nearly complete lack of antigen-independent T-cell activation (**Fig. 4-3B–C, Supp. Fig. 4-2E–H**). These results demonstrate that (a) CAR expression alone, without antigen stimulation, can drive divergent CAR-T cell phenotype, likely through the PI3K/AKT signaling axis; (b) slight alterations in CAR sequences can lead to dramatic changes in CAR-T cell function; and (c) strong antigen-independent activation may be detrimental to CAR-T cell function, but minimizing basal activation does not necessarily maximize anti-tumor-efficacy.

Pharmacological inhibition of PI3K/AKT and mTOR signaling modestly enhances anti-tumor efficacy in tonic signaling rituximab CAR-T cells

The functional and transcriptomic data detailed above revealed that RFR-LCDR.AA, a novel CAR obtained through scFv sequence hybridization combined with alanine insertion, exhibits intermediate levels of T-cell activation at rest and, upon antigen stimulation *in vivo*, enables T cells to exhibit robust effector functions while enriching for the memory T-cell phenotype. We next sought to understand whether the intermediate level of antigen-independent signaling and strong antigen-dependent effector function are a mere coincidence, or if antigen-independent activation level is a parameter that one could productively tune to enhance CAR-T cell function. To do so, we explored the use of small-molecule inhibitors of signaling pathways identified through our transcriptomic analysis of unstimulated CAR-T cells (**Fig. 4-3**). If proven effective, such a pharmacological modulation approach would be easily implementable during the manufacturing of clinical CAR-T cell products, without necessitating a change in the CAR protein construct.

To maximize clinical adaptability, we identified small-molecule inhibitors targeting PI3K, AKT, mTORC1, c-MYC, and SREBP that have undergone pre-clinical testing or have already been FDA-approved for human use (**Fig. 4-4A**)[50–54]. Rituximab CAR-T cells treated with PI3Kδ (CAL-101) and AKT (AZD5363) inhibitors significantly reduced antigen-independent expression of activation and exhaustion markers, TNF-α production, and cell division compared to vehicle (DMSO)-treated rituximab CAR-T cells (**Fig. 4-4B–D**). In contrast, inhibition of c-Myc (MYCi975) and SREBP (betulin) increased most measures of antigen-independent CAR-T cell activation (**Fig. 4-4B–D**). Concordantly, PI3Kδ (CAL-101)- and AKT (AZD5363)-inhibited rituximab CAR-T cells preserved a greater fraction of naïve and stem-cell memory T (Tn/scm) cells compared to their vehicle-treated counterpart, whereas c-Myc (MYCi975) and SREBP inhibition (betulin) accelerated T-cell differentiation (**Fig. 4-4E**). Interestingly, mTORC1 inhibition by rapamycin led to reduced CD137 and PD-1 expression as well as enrichment of Tn/scm cells, but it had insignificant impact on CD69 expression while increasing TNF-α production in the absence of antigen stimulation (**Fig. 4-4B–E**), suggesting a branching of regulatory pathways controlling these different outputs upstream of mTOR signaling. Notably, mTORC1 (rapamycin) and SREBP (betulin) inhibition led to substantial decreases and increases in antigen-independent CAR-T cell metabolic activity, respectively (**Supp Fig. 4-3**), indicating that modulating mTORC1 signaling or amplifying tonic signaling impacts antigen-independent metabolic activity. However, all pharmacologically inhibited rituximab CAR-T cells were unable to expand as effectively *ex vivo* (**Fig. 4-4F**), highlighting a limitation when using drug inhibitors.

A

Inhibitor	Target	Inhibitor concentration
CAL-101	PI3Kδ Isoform	1 μM
AZD5363	Pan-AKT	1 μM
Rapamycin	mTORC1	100 nM
MYCi975	c-Myc	2 μM
Betulin	SREBP	10 μM

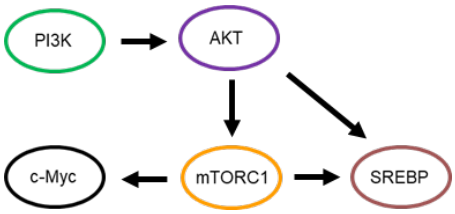

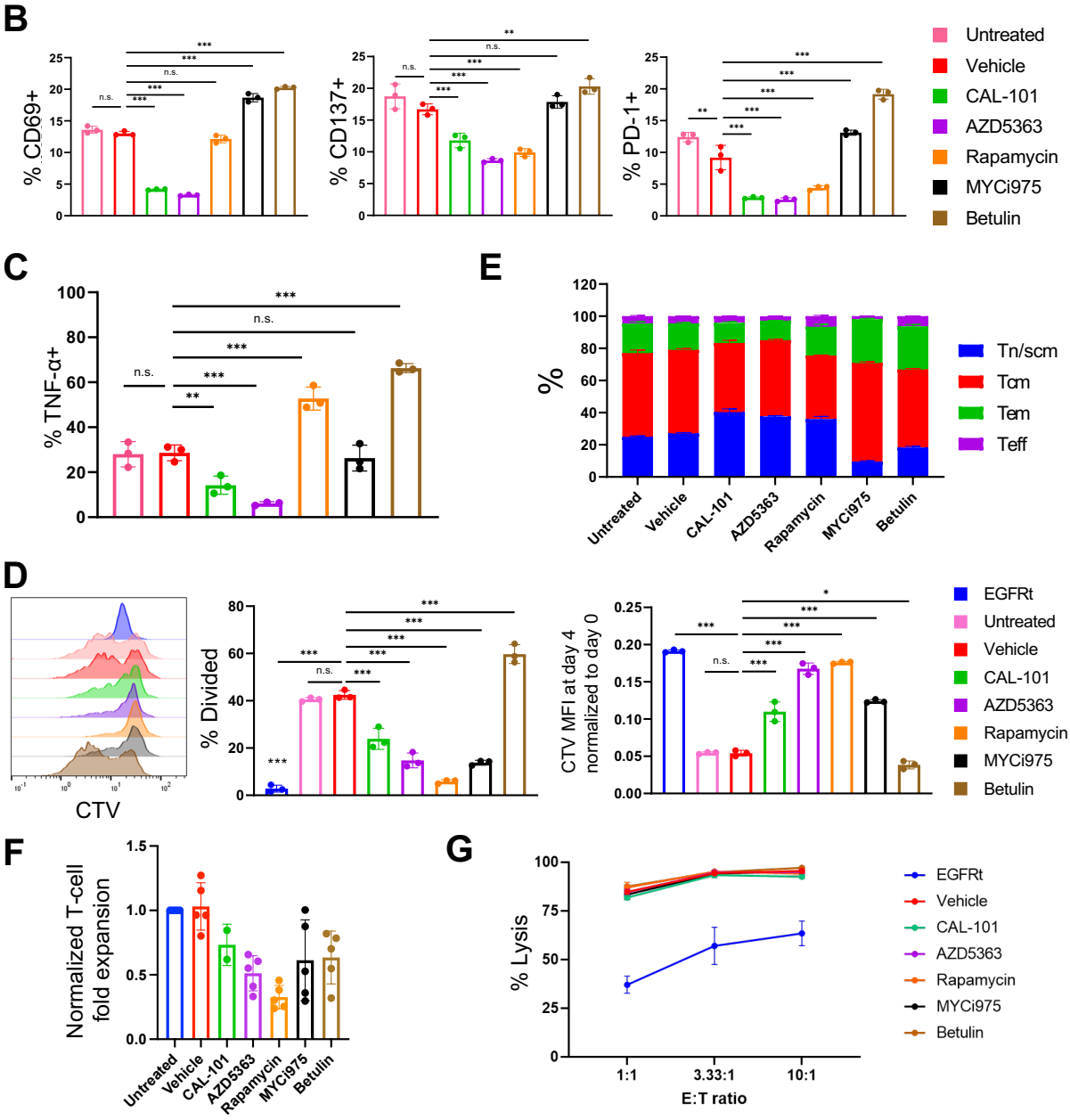

Figure 4-4. Pharmacological inhibition of PI3K/AKT pathway modulates antigen-independent CAR-T cell activation. (**A**) Table of pharmacological inhibitors used during *ex vivo*

expansion of rituximab CAR-T cells (left). Simplified schematic of the PI3K/AKT signaling axis where black arrows represent activation (right). (**B**) Activation marker expression by CAR^+ T cells in the absence of antigen stimulation after 5 days of pharmacological modulation. Data bars indicate the means of technical triplicates ± 1 S.D. (**C**) TNF-α production CAR^+ T cells in the absence of antigen stimulation as quantified by intracellular flow cytometry. Data bars indicate the means of technical triplicates ± 1 S.D. (**D**) Proliferation of CAR^+ T cells stained with CellTrace Violet (CTV) dye was assayed after a 4-day culture in the absence of target cells or exogenous cytokines. Data shown in the histogram correspond to one of technical triplicates shown in the bar graph. (**E**) % distribution of T-cell subtypes in CAR^+ T cells after 5 days of pharmacological modulation. Data bars indicate the means of technical triplicates ± 1 S.D. (**F**) Rituximab CAR-T cell fold expansion after 6 days of inhibitor culture was tracked. T-cell fold expansion was normalized to the untreated control with each data point representing biological replicates collected from healthy donors. (**G**) A 24-hr lysis assay of CD20 CAR-T cells against Raji target cells at three effector-to-target (E:T) ratios. Data bars indicate the means of technical triplicates ± 1 S.D. Percent lysis was normalized to cell counts in target-only wells. In (B)–(F), results are representative two independent experiments using cells from of two heathy donors. Statistical significance in panels B, C, and D was determined by two-tailed Student's *t* test with Sidak correction for multiple comparisons. **p*<0.05, ***p*<0.01, ****p*<0.001, n.s. not statistically significant.

All inhibitor-treated rituximab CAR-T cells lysed Raji tumor cells as well as their vehicle-treated counterpart, indicating that *ex vivo* culture modulation did not impair CAR-T cell function (**Fig. 4-4G**). We next evaluated whether the change in antigen-independent T-cell activation induced by temporary pharmacological modulation during *ex vivo* T-cell manufacturing would translate to changes in *in vivo* anti-tumor efficacy. NSG mice bearing Raji tumor xenografts were treated with rituximab CAR-T cells preconditioned with various modulators (**Fig. 4-4A**). Since each group was treated with T cells expressing the same CAR, this comparison was not subject to confounding effects of CAR protein sequence variation. Results showed PI3Kδ (CAL-101)-, AKT (AZD5363)-, and mTORC1 (rapamycin)-preconditioned rituximab CAR-T cells delayed tumor outgrowth and prolonged median survival compared to vehicle (DMSO)-treated rituximab CAR-T cells by 1.5, 1.6, and 1.8 folds, respectively (**Fig. 4-5A–B**). Furthermore, AKT (AZD5363)- and mTORC1 (rapamycin)-inhibited rituximab CAR-T cells showed significantly increased *in vivo* expansion compared to the control (**Fig. 4-4C**), coinciding with their prolonged suppression of tumor outgrowth (**Fig. 4-5A**). In contrast, animals treated with c-Myc (MYCi975)- and SREBP (betulin)-preconditioned rituximab CAR-T cells, which exhibited increased antigen-independent activation in culture, resulted in accelerated tumor progression compared to the control group (**Fig.**

4-5A–B). These results support the concept that tuning the level of antigen-independent activity can indeed impact CAR-T cell function. Specifically, for a CAR that triggers strong basal T-cell activation, dampening antigen-independent activation enhances *in vivo* anti-tumor efficacy while further increasing activation diminishes *in vivo* function (**Fig. 4-6A**).

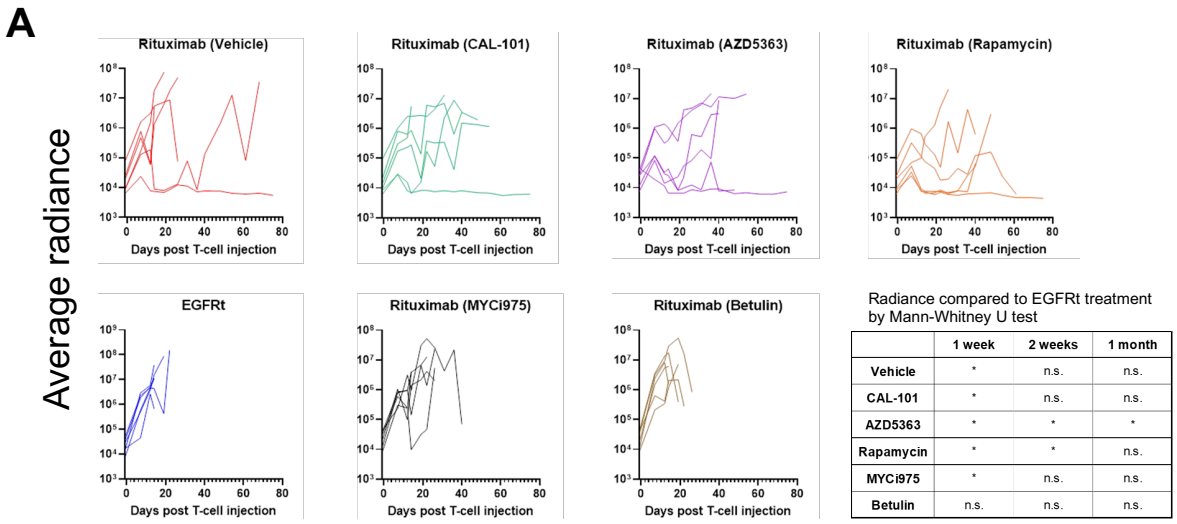

Radiance compared to EGFRt treatment by Mann-Whitney U test

	1 week	2 weeks	1 month
Vehicle	*	n.s.	n.s.
CAL-101	*	n.s.	n.s.
AZD5363	*	*	*
Rapamycin	*	*	n.s.
MYCi975	*	n.s.	n.s.
Betulin	n.s.	n.s.	n.s.

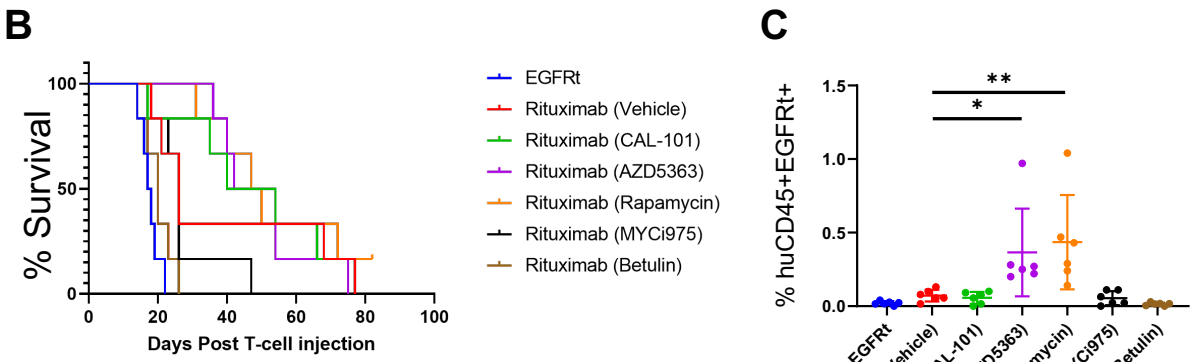

	EGFRt	Rituximab (Vehicle)	Rituximab (CAL-101)	Rituximab (AZD5363)	Rituximab (Rapamycin)	Rituximab (MYCi975)	Rituximab (Betulin)
Median survival period (days)	17	26	40	42	47	26	20

Figure 4-5. Modulation of antigen-independent rituximab CAR-T cell activation leads to divergent anti-tumor efficacy *in vivo*. NSG mice were injected intravenously with 0.5 x 10^6 ffLuc-expressing Raji cells followed by two doses of 1.35 x 10^6 CAR-T cells at 7 and 12 days post tumor injection. (**A**) Tumor signal (in photons/sec/cm2/sr) in individual animals as quantified by bioluminescence imaging. Table of statistical differences in tumor signal compared to EGFRt-treated animals 1 week, 2 weeks, or 1 month after the 2nd T-cell injection. Statistical significance was determined by Mann-Whitney U test with Holm-Sidak correction for multiple comparisons. *p<0.05, n.s. not statistically significant. (**B**) Kaplan-Meier survival curve (top) and table of median survival period in days (bottom). (**C**) Frequency of human CD45+EGFRt+ cell in peripheral blood collected from mice on day 8 after first dose of T-cell infusion. Statistical significance was

determined by two-tailed Student's *t* test with Sidak correction for multiple comparisons. *$p<0.05$, **$p<0.01$.

Pharmacological inhibition of mTOR signaling modestly decreases tonic signaling and enhances anti-tumor efficacy in Leu16 CAR-T cells

The panel of PI3K/AKT pharmacological inhibitors allowed us to decrease or increase baseline antigen-independent activation of a strong tonic signaling CAR, providing evidence that high levels of tonic signaling causes CAR-T cell dysfunction, which can be rescued by minimization of tonic signaling (**Fig. 4-6A**). We wanted to further test our hypothesis that the enhanced anti-tumor functionality of hybrid.AA CAR-T cells were due to the low but intermediate levels of tonic signaling. In order to do so, we reasoned that we could repurpose inhibitors of c-MYC (MYCi975) and SREBPs (betulin), which increased tonic signaling in rituximab CAR-T cells, to elevate Leu16 CAR-T cell tonic signaling (**Fig. 4-6B**). If the hypothesis were true, we would expect Leu16 CAR-T cell *in vivo* efficacy to improve, concomitant with minimal benefits towards tumor-killing efficacy with mTORC1 (rapamycin) inhibition (**Fig. 4-6B**).

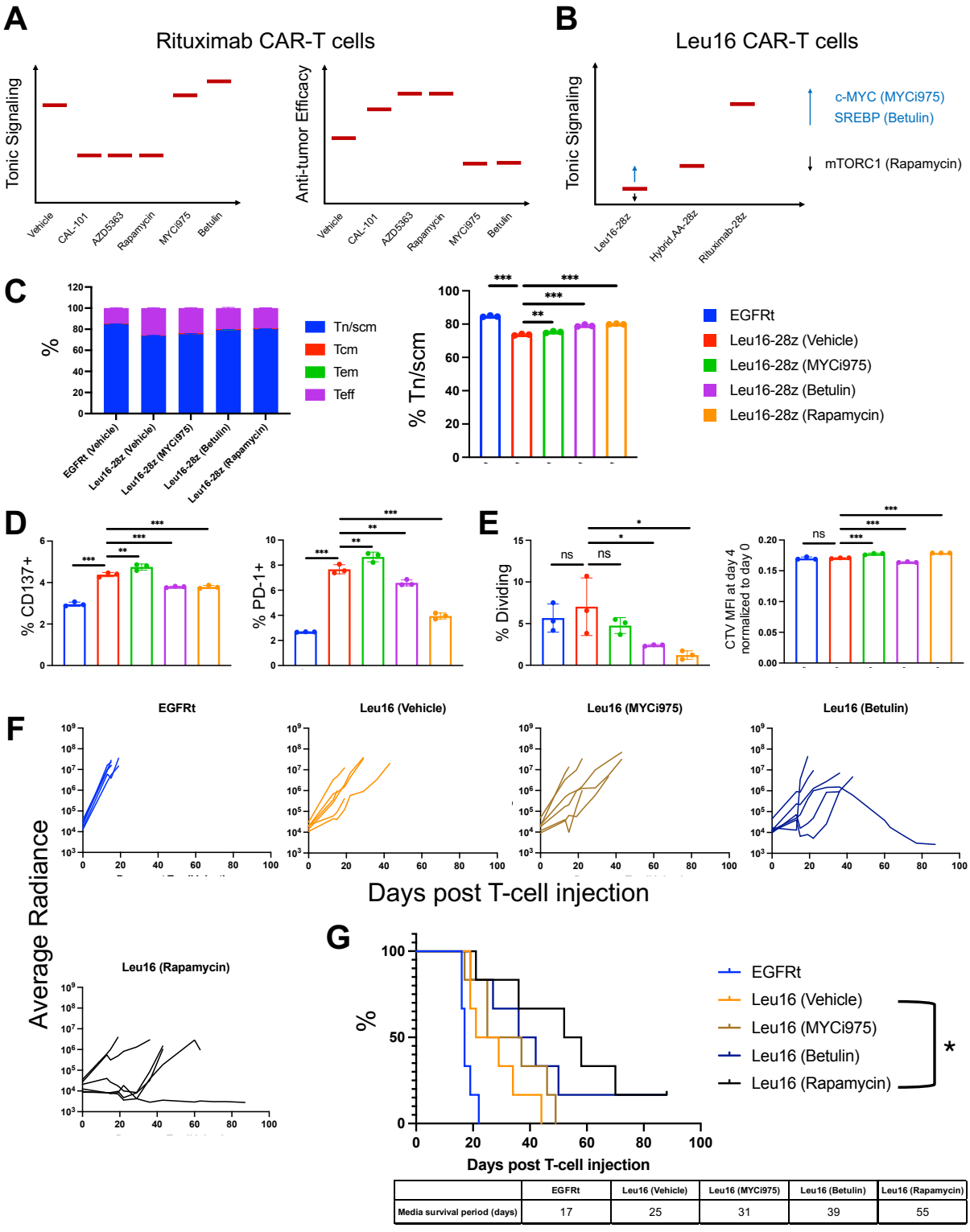

	EGFRt	Leu16 (Vehicle)	Leu16 (MYCi975)	Leu16 (Betulin)	Leu16 (Rapamycin)
Media survival period (days)	17	25	31	39	55

Figure 4-6. Pharmacological modulation of Leu16 CAR-T cells modestly dampens tonic signaling while enhancing anti-tumor efficacy. (**A**) Pictorial representation of the correlation between tonic signaling-modulated rituximab CAR-T cells and *in vivo* anti-tumor efficacy. (**B**) Pictorial representation of pharmacological modulation strategy aimed to either increase or

decrease Leu16 CAR tonic signaling; c-MYC (MYCi975) and SREBP (betulin) inhibition increased tonic signaling whereas mTORC1 (rapamycin) inhibition decreased tonic signaling in rituximab CAR-T cells. (**C**) % distribution of T-cell subtypes in CAR^+ T cells after 6 days of pharmacological modulation (left) and Tn/scm enrichment (right). (**D**) Activation and exhaustion marker expression by CAR^+ T cells in the absence of antigen stimulation after 6 days of pharmacological modulation. (**E**) Proliferation of CAR^+ T cells stained with CellTrace Violet (CTV) dye was assayed after a 4-day culture in the absence of target cells or exogenous cytokines. (**F**) NSG mice were injected intravenously with 0.5×10^6 ffLuc-expressing Raji cells followed by two doses of 1.35×10^6 CAR-T cells at 7 and 12 days post tumor injection. (**F**) Tumor signal (in photons/sec/cm2/sr) in individual animals as quantified by bioluminescence imaging. (**G**) Kaplan-Meier survival curve. Log-rank (Mantel-Cox) test was performed with Holm-Sidak correction for multiple comparisons. *p<0.05, **p<0.01, ***p<0.001, n.s. not statistically significant. Data bars indicate the means of technical triplicates ± 1 S.D. *p<0.05, **p<0.01, ***p<0.001, ns not statistically significant.

In contrast to what we observed in rituximab CAR-T cells, which have a high basal level of tonic signaling, pharmacological inhibition of Leu16 CAR-T cells targeting c-MYC (MYCi975), SREBPs (betulin), and mTORC1 (rapamycin) dampened tonic signaling Leu16 CAR-T cells, which have a very low basal level of tonic signaling, when treated at equivalent concentrations as shown in **Fig. 4-4A**. Inhibition by MYCi975, betulin, and rapamycin resulted in increased enrichment of Tn/scm cells relative to their vehicle counterpart (**Fig. 4-6C**), with rapamycin preserving the largest pool of Tn/scm cells. Similarly, all pharmacological inhibitors tested leds to significant decreases in activation and exhaustion marker expression (**Fig. 4-6D**). Furthermore, inhibition of mTORC1 by rapamycin significantly ablated antigen-independent proliferation in Leu16 CAR-T cells (**Fig. 4-6E**). It should be noted, however, that while the differences in T-cell subtype, exhaustion and activation marker expression, and antigen-independent proliferation were significant, the absolute differences between vehicle and drug-inhibited groups are, on an absolute scale, minute. This is likely due to the fact that Leu16 CAR-T cells tonic signal minimally, leaving a small dynamic range to be modulated. In fact, the pharmacologically induced modulation in tonic signaling led to no significant differences in TNF-α production (**Supp. Fig. 4-4A**). Despite modest changes in antigen-independent Leu16 CAR-T cell behavior, mTORC1-inhibited Leu16 CAR-T cells were unable to expand as effectively as its vehicle counterpart (**Supp. Fig. 4-4B**).

Pharmacologically modulated Leu16 CAR-T cells lysed Raji tumor cells equally well as well as their vehicle-treated counterpart, demonstrating no overt impairment of CAR-T cell

function (**Supp. Fig. 4-4C**). We proceeded to evaluate whether the modest changes observed in Leu16 CAR tonic signaling would potentiate differences in anti-tumor responses in a Raji lymphoma animal model. To our surprise, we found that mTORC1 (rapamycin)-inhibited Leu16 CAR-T cells had superior *in vivo* functionality compared to its vehicle treated counterpart (**Fig. 4-6F–G**). Taken together, these results suggest that further reducing tonic signaling in an already minimally tonic signaling CAR can further augment anti-tumor efficacy, but suggest that factors other than minimization of tonic signaling alone may be at play.

Inhibition of PI3K/AKT signaling in rituximab CAR-T cells does not fully recapitulate the hybrid.AA CAR-T cell phenotype

To better understand the changes in molecular pathways in response to pharmacological inhibition of the PI3K/AKT signaling pathway, we conducted RNAseq analysis on unstimulated inhibitor-treated rituximab CAR-T cells at the end of the manufacturing cycle. We observed that inhibition of AKT (AZD5363) abated expression of PI3K/AKT genes (**Fig. 4-7A**), a custom PI3K/AKT gene signature we derived from cluster II which stratified tonic signaling CD20 CARs (**Fig. 4-3B**); inhibition of mTORC1 (rapamycin) partially inhibited PI3K/AKT gene expression (**Fig. 4-7A**), which is consistent with the fact that mTORC1 signals downstream of PI3K/AKT. Expectedly, both AKT (AZD5363) and mTORC1 (rapamycin) inhibition dampened mTORC1, c-MYC, and SREBP pathway expression (**Fig. 4-4A, Fig. 4-7A**). The data show that inhibition of c-MYC was achieved, albeit weakly, with a concomitant slight decrease in SREBP pathway expression, suggesting cross-talk between c-MYC and SREBP pathways in rituximab CAR-T cells (**Fig. 4-7A**). Curiously, SREBP inhibition by betulin *increased* SREBP target gene expression (**Fig. 4-7A**), highlighting a potential need for rituximab CAR-T cells to engage in SREBP pathway feedback loop to compensate for pharmacological inhibition of SREBP.

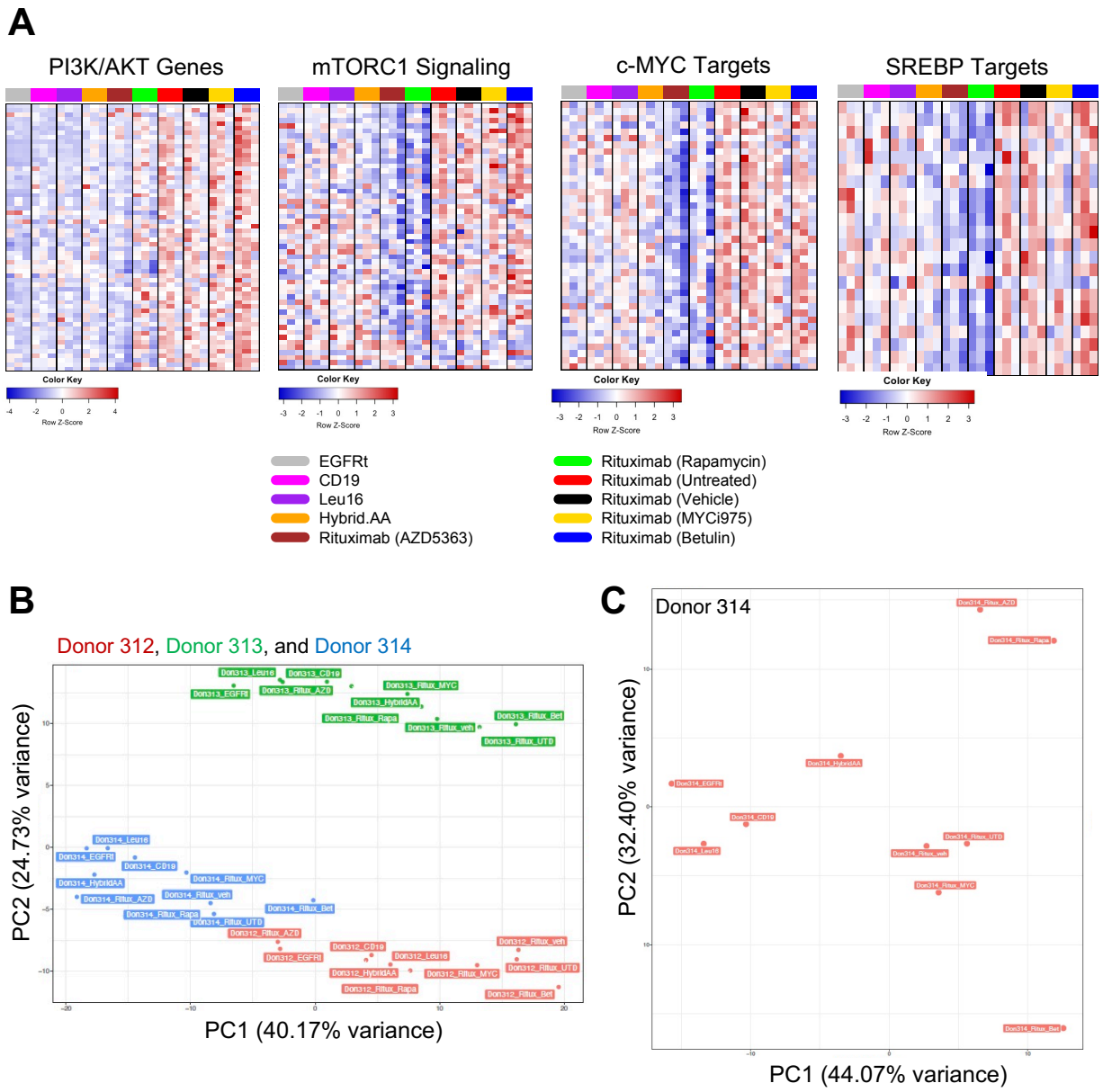

Figure 4-7. Pharmacological inhibitors of PI3K/AKT ablate respective signaling nodes in rituximab CAR-T cells do not recapitulate the hybrid.AA CAR-T cell phenotype. CAR-T cells expressing the indicated CAR constructs, the transduction marker EGFRt, or rituximab CAR-T cells treated with the indicated inhibitors were cultured in the absence of CD20 antigen stimulation for 14 days prior to RNA extraction for bulk RNA-seq analysis. (**A**) Heatmap showing genes associated with PI3K/AKT genes (cluster II from Fig. 4-3B and signaling pathways associated with mTORC1, c-MYC, and SREBP targets. Complete list of genes shown in each heatmap is provided in Data S1. (**B**) Principal component analysis (PCA) of all RNAseq library samples, spanning 10 CAR-T cell lines as indicated, with there healthy donors as biological replicates. Samples are colored by donor. (**C**) PCA analysis within a given representative donor. Abbreviations: Ritux_UTD – Rituximab (Untreated), Ritux_veh – Rituximab (Vehicle), Ritux_AZD – Rituximab (AZD5363), Ritux_Rapa – Rituximab (Rapamycin), Ritux_MYC – Rituximab (MYCi975), Ritux_Bet – Rituximab (Betulin).

Despite successful ablation of PI3K/AKT signaling in rituximab CAR-T cells through inhibition of AKT (AZD5363), rituximab (AZD5363) CAR-T cells do not recapitulate the transcriptional phenotype of hybrid.AA CAR-T cells (**Fig. 4-7B, 4-7C, Supp Fig. 4-5**). Principal component analysis (PCA) of all RNAseq samples show that the samples are predominantly stratified by donor-to-donor variation (**Fig. 4-7B)**, something that we have observed repeatedly in other omics datasets generated by our lab (data not shown). To exclude variation introduced by donor-to-donor variability, we proceeded to conduct PCA analysis for distinct CAR-T cell lines within a given donor. Consistent with prior expectations, we observed that minimally tonic signaling T cells (EGFRt, CD19, and Leu16 CAR-T cells) clustered closely together (**Fig. 4-7C, Supp. Fig. 4-5**). Untreated, vehicle treated, and MYCi975 treated rituximab CAR-T cells also clustered closely together, consistent with our *in vitro* data wherein minimal changes were induced by vehicle treatment and c-MYC inhibition (MYCi975) slightly elevated tonic signaling (**Fig. 4-7C, Supp. Fig. 4-5**). However, tonic signaling-dampened rituximab CAR-T cells (i.e., rituximab (AZD5363) and rituximab (rapamycin) exhibited distinct transcriptomes from hybrid.AA CAR-T cells (**Fig. 4-7C, Supp. Fig. 4-5**). Collectively, the data indicate that matching the extent of PI3K/AKT signaling alone is insufficient to recapitulate hybrid.AA CAR-T cell biology. Furthermore, the data indicate that the enhanced anti-tumor efficacy of hybrid.AA CAR-T cells extends beyond fine-tuning of CAR tonic signaling.

Rituximab tonic signaling is correlated with increased cellular responses to oxidative stress

Although the collective data disproved our hypothesis that hybrid.AA CAR-T cells have superior function *in vivo* due to their intermediate levels of tonic signaling, the functional *in viv*o data do point to minimizing tonic signaling as a design strategy to optimize CAR efficacy, irrespective of its predilection for tonic signaling. Therefore, if we can understand the detrimental

effects of tonic signaling, as opposed to simply using tonic signaling as a design guide, we could design novel strategies that directly target the problem that comes with tonic signaling. In order to do so, we took a deep dive into the transcriptomes of pharmacologically modulated rituximab CAR-T cells. This panel provides a unique opportunity to study the direct relationship between tonic signaling and anti-tumor efficacy because it excludes minor differences in CAR protein sequence as a confounding factor. Analysis of differentially expressed genes among the different CAR-T cell lines highlight cluster 3 as a group of genes wherein its expression correlated with *in vitro* measures of tonic signaling, indicating that this is another contributor of tonic signaling observed in rituximab CAR-T cells. Gene ontology (GO) of cluster 3 showed significant enrichment of nuclear factor kappa B (NF-κB) signaling (**Fig. 4-8**), indicating that the differences in tonic signaling among PI3K/AKT modulated rituximab CAR-T cells are correlated with NF-κB activity. Whether the correlation between NF-κB activity and tonic signaling is causal, coincidental, or in response to strong basal levels of rituximab CAR tonic signaling remains to be further explored.

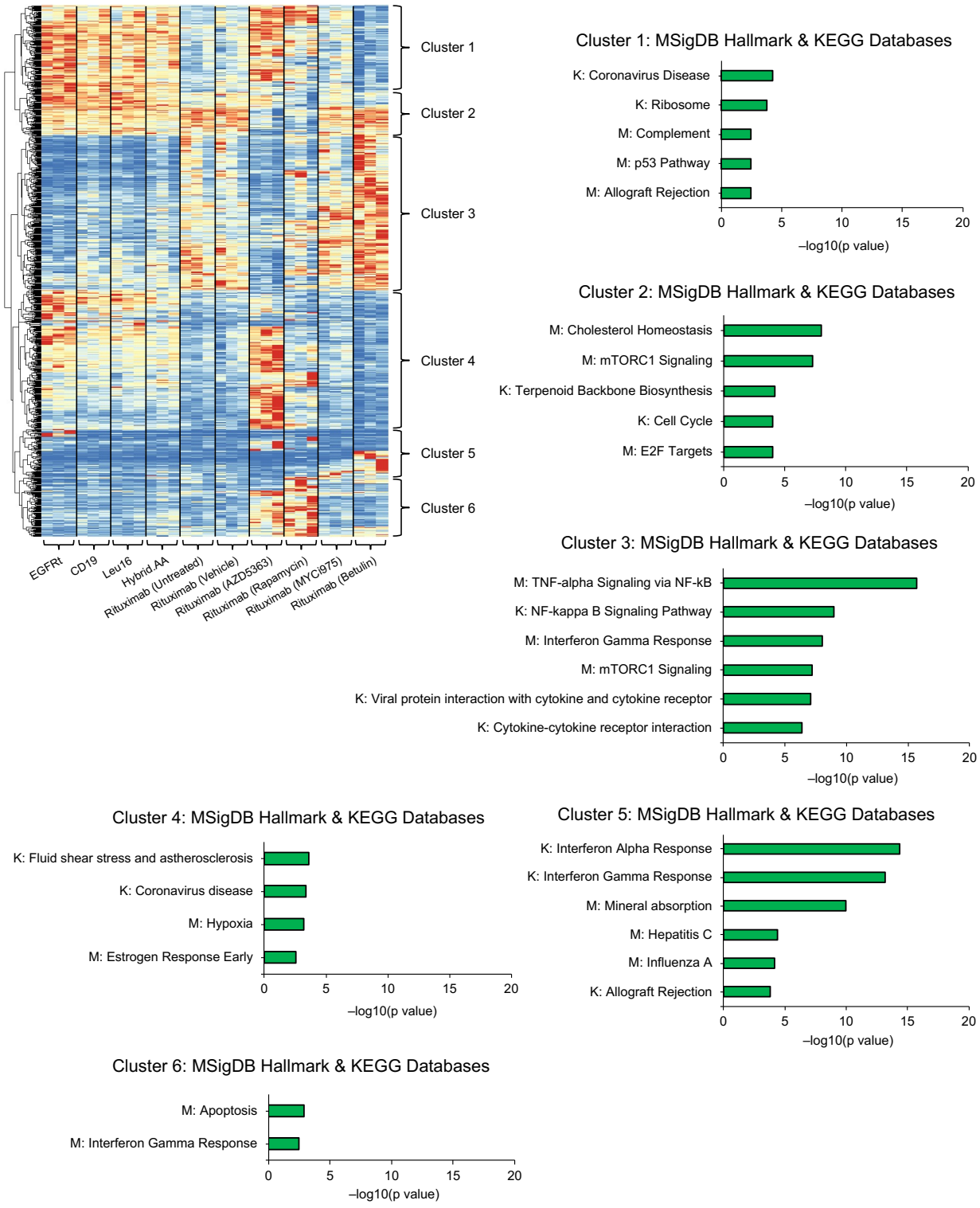

Figure 4-8. Tonic signaling in rituximab CAR-T cells is further amplified by NF-KB signaling. CAR-T cells expressing the indicated CAR constructs, the transduction marker EGFRt, or rituximab CAR-T cells treated with the indicated inhibitors were cultured in the absence of CD20 antigen stimulation for 14 days prior to RNA extraction for bulk RNA-seq analysis. (Top) Heatmap of differentially expressed genes (FDR < 0.05) identified through ANOVA. Each column

represents one donor. Each row is scaled to a maximum of 1 and minimum of 0 to highlight relative expression of each gene. (Bottom) Enriched pathways associated with the different DGE clusters, as assigned through hierarchical clustering, with *p* values shown in –log10 scale. All pathways shown are statistically significant adjusted *p* value (<0.05) using the Benjamini-Hochberg method. Only the top three most statistically significant pathways from the Molecular Signatures Database (MSigDB; 2020 version) and Kyoto Encyclopedia of Genes and Genomes (KEGG; 2021 version) from each cluster are shown; M and K denote gene sets originating from the MSigDB and KEGG datasets, respectively.

The comparison between vehicle-treated and betulin-treated rituximab CAR-T cells provides a unique window in studying the effects of tonic signaling in light of the direct relationship between amplified tonic signaling via SREBP inhibition and reduced anti-tumor efficacy (**Fig. 4-4, Fig. 4-5**). Differential gene expression (DGE) analysis highlighted a group of genes encoding for metallothionines that were highly upregulated in response to SREBP inhibition (**Fig. 4-9A**). We note with particular interest that metallothionines are heavy metal-binding proteins that protect cells from heavy metal toxicity and oxidative stresses[55,56]. Given that there is no reason for *in vitro* cultured CAR-T cells to be exposed to heavy metals, we reasoned that the upregulation of metallothionines is a response to oxidative stress. This correlation between high tonic signaling and the antioxidant metallothionine response led us to hypothesize that strong tonic signaling induces oxidative stress. If this hypothesis were true, one would expect to see hints of oxidative stress in rituximab CAR-T cells compared to tonic signaling-dampened rituximab CAR-T cells.

Using gene set enrichment analysis (GSEA), we found that vehicle-treated rituximab CAR-T cells, when compared against rituximab (AZD5363) or rituximab (rapamycin) CAR-T cells, had enhanced activity in c-Myc activity, oxidative stress, and oxidative stress response gene sets, including DNA repair, G2M checkpoint, an unfolded protein response, that are associated with cellular damage[56] (**Fig. 4-9A–B**). We found additional support in examining the RNAseq dataset comparing protein engineered CD20 CAR variants, wherein oxidative stress response gene sets were found to be significantly elevated in rituximab CAR-T cells when compared against Leu16 CAR-T cells (**Supp Fig. 4-6A**) or against Hybrid.AA CAR-T cells (**Supp Fig. 4-6B**). In contrast, we found that tonic signaling-dampened rituximab (AZD5363) and rituximab (rapamycin) CAR-T

cells, when compared to rituximab (vehicle) CAR-T cells through separate GSEA comparisons, collectively saw enhanced activity in only one gene set, indicating that the action of AZD5363 and rapamycin dampens cellular activity instead of rerouting it (rituximab (AZD5363) data not shown, **Supp Fig. 4-7**). This indicates that the addition of AZD5363 and rapamycin lessened the need for an oxidative stress response, providing additional support to our hypothesis that tonic signaling induces oxidative stress. Taken together, the strong correlation between tonic signaling and oxidative stress responses leads us to hypothesize that tonic signaling induces oxidative stresses, leading to cellular damage.

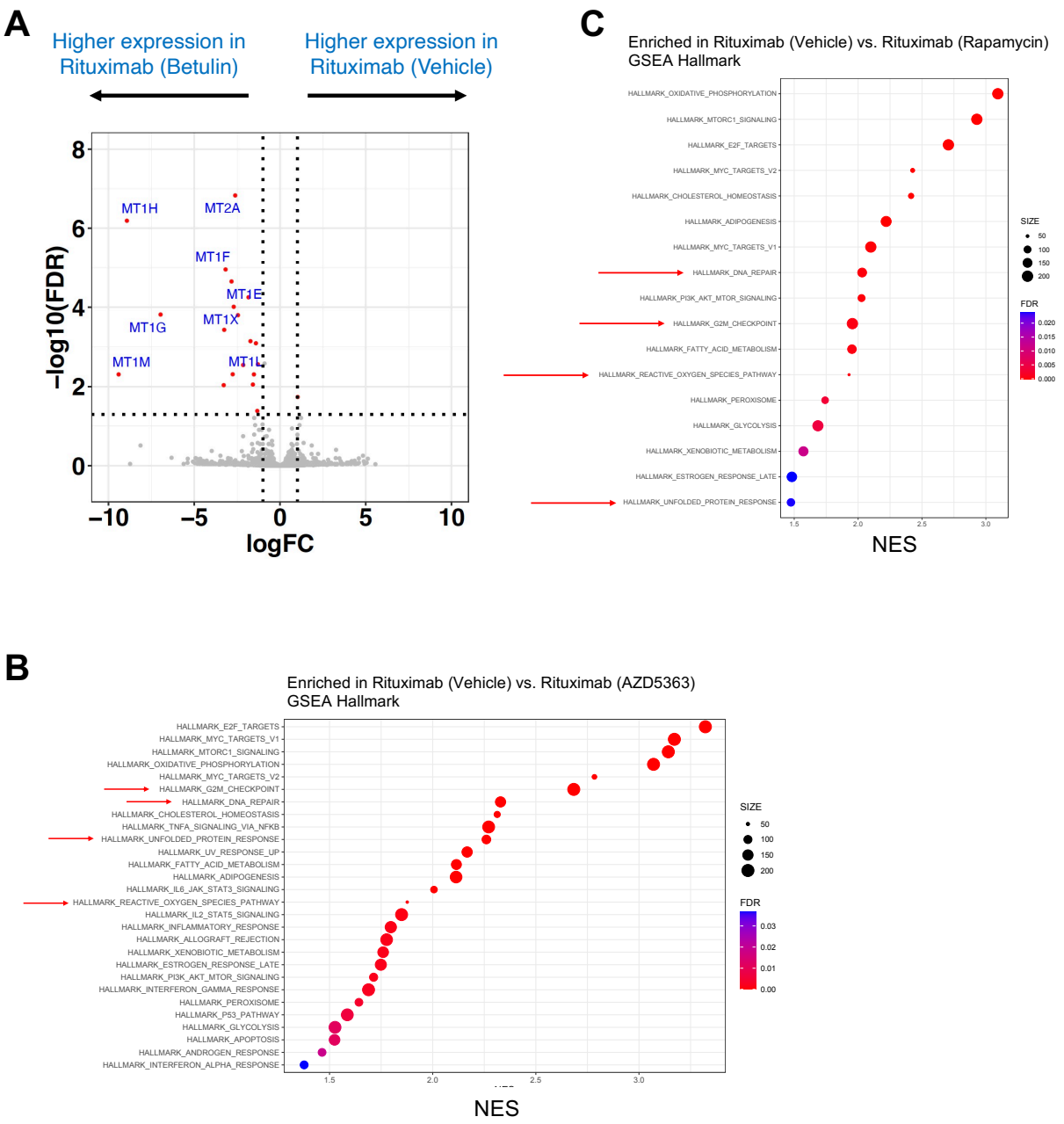

Figure 4-9. Strong tonic signaling in rituximab CAR-T cells is correlated with increased oxidative stress. CAR-T cells expressing the indicated CAR constructs, the transduction marker EGFRt, or rituximab CAR-T cells treated with the indicated inhibitors were cultured in the absence of CD20 antigen stimulation for 14 days prior to RNA extraction for bulk RNA-seq analysis. (**A**) Volcano plot showing differentially expressed genes between rituximab CAR-T cells treated with SREBP inhibitor (betulin) or vehicle control. Differentially expressed genes are defined as genes with an FDR < 0.05 and an absolute log2 fold-change greater than 1; black dotted lines are shown to indicate thresholding. Each dot represents a gene and red dots are statistically significant genes. Genes of interest are further annotated in blue. (**B**) Statistically significant gene sets quantified by gene set enrichment analysis (GSEA), comparing Rituximab (Vehicle) vs. Rituximab (AZD5363) CAR-T cells, in the Molecular Signatures Database (MSigDB) Hallmark set are plotted;

positive NES value indicates enrichment in Rituximab (vehicle). (**C**) Statistically significant gene sets quantified by GSEA, comparing Rituximab (Vehicle) vs. Rituximab (Rapamycin) CAR-T cells, in the Molecular Signatures Database (MSigDB) Hallmark set are plotted; positive NES value indicates enrichment in Rituximab (vehicle). Red arrows highlight noteworthy gene sets of interest.

Hybrid.AA CAR-T cells are elevated in MXD4 activity which may confer protection against PI3K/AKT signaling-induced oxidative stress

Given the correlation between strong antigen-independent PI3K/AKT signaling, we reasoned that Hybrid.AA CAR-T cells would have elevated c-Myc activity, oxidative stress, and associated oxidative stress responses. In contrast to our expectations, Leu16 CAR-T cells exhibited increased activity in c-Myc activity and oxidative stress, with modest but statistically insignificant elevation in oxidative stress responses (**Fig. 4-10A–B**; **Supp. Fig. 4-8**). This suggests that Hybrid.AA CAR-T cells may have a mechanism towards counteracting the induction of oxidative stress by PI3K/AKT signaling. Protein regulon network inference analyses, via ARACNE[27] and VIPER[28], identified MAX dimerization protein 4 (MXD4), a repressor of c-Myc by competing for MAX heterodimerization[57], as being the regulon with the strongest activity in Hybrid.AA CAR-T cells compared to Leu16 CAR-T cells (**Fig. 4-10C**). Moreover, Hybrid.AA were also found to have significantly elevated MXD4 activity compared to Rituximab CAR-T cells (**Fig. 4-10C**). This suggests that c-Myc may be an inducer of oxidative stress, and that Hybrid.AA CAR-T cells may be engaging in MXD4 activity to counteract PI3K/AKT/mTORC-1/c-Myc–induced oxidative stresses (**Fig. 4-10D**).

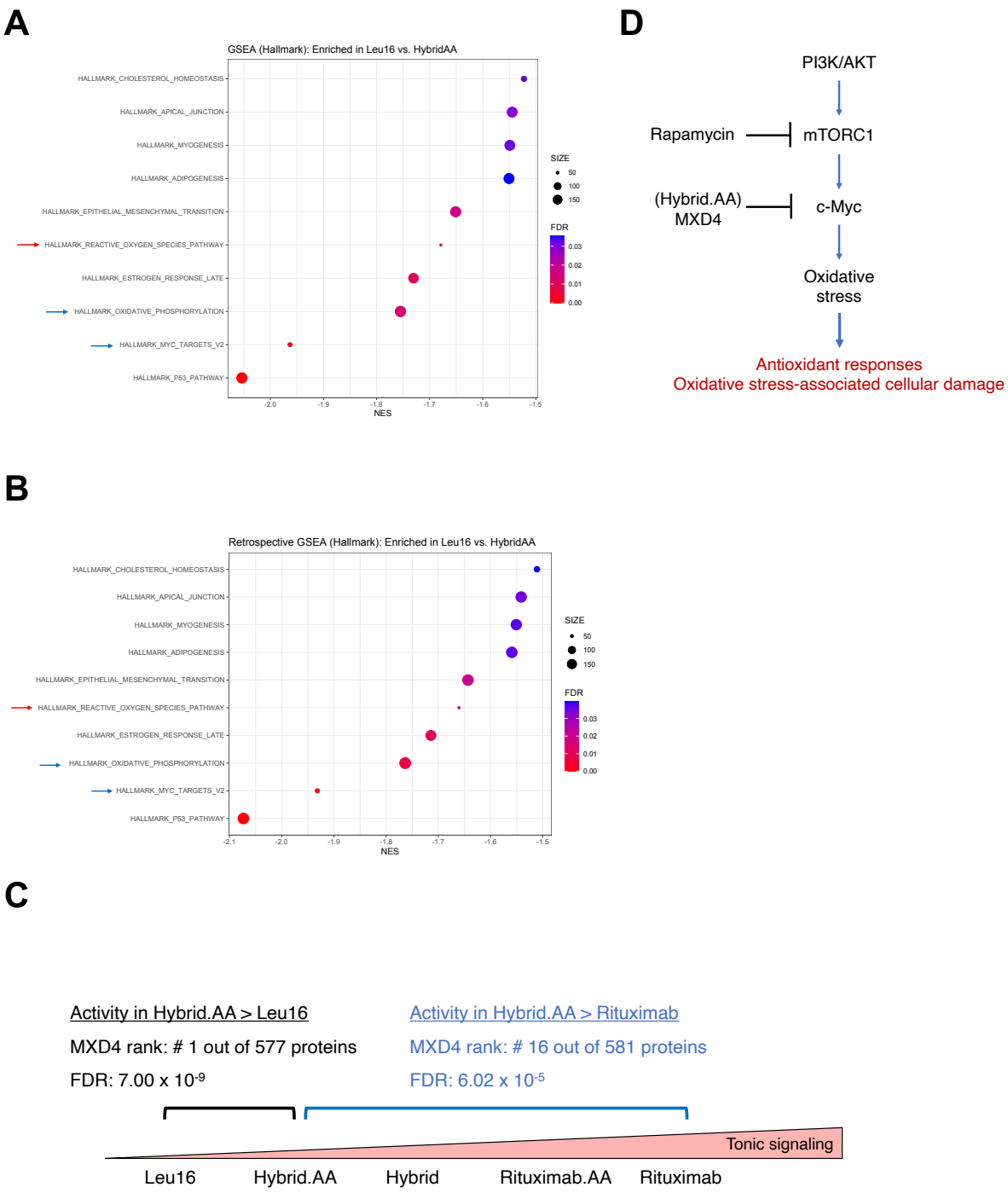

Figure 4-10. Hybrid.AA CAR-T cells are better protected from oxidative stresses compared to Leu16 CAR-T cells. CAR-T cells expressing the indicated CAR constructs, the transduction marker EGFRt, or rituximab CAR-T cells treated with the indicated inhibitors were cultured in the absence of CD20 antigen stimulation for 14 days prior to RNA extraction for bulk RNA-seq analysis. (**A**) Statistically significant gene sets quantified by GSEA, comparing Rituximab vs. Leu16 CAR-T cells from the pharmacological modulation RNAseq dataset, in the Molecular Signatures Database (MSigDB) Hallmark set are plotted; negative NES value indicates enrichment in Leu16 CAR-T cells. Arrows highlight noteworthy gene sets of interest. (**B**) Statistically significant gene sets quantified by GSEA, comparing Rituximab vs. Leu16 CAR-T

cells from the protein engineered CD20 CAR panel, in the Molecular Signatures Database (MSigDB) Hallmark set are plotted; negative NES value indicates enrichment in Leu16 CAR-T cells. Arrows highlight noteworthy gene sets of interest.

DISCUSSION

In this study, we used tonic signaling both as a guide to explore different protein-engineering strategies and as a target to modulate with the objective of improving CAR-T cell function. Through this process, a new CD20 CAR, termed RFR-LCDR.AA, that incorporated scFv sequence hybridization and alanine insertion to enable robust *in vivo* anti-tumor efficacy was developed by Ximin Chen, a senior PhD student and co-first author of the project. Of note, the RFR-LCDR.AA CAR is 98% identical to both the rituximab CAR (differing in 13 out of 661 residues) and the Leu16 CAR (differing in 11 out of 661 residues), underscoring the criticality of the *precise* CAR protein sequence to CAR-T cell function.

Although we began our investigation with the assumption that minimizing tonic signaling would result in optimized CAR-T cell function, our results suggest a more nuanced relationship between tonic signaling and anti-tumor efficacy. Through transcriptomic as well as functional analyses, we observed that rituximab CAR-T cells exhibit strong T-cell activation in the absence of antigen stimulation, whereas Leu16 CAR-T cells appear completely quiescent at rest. By comparison, hybrid CAR-T cells show an intermediate level of antigen-independent activation, but far outperform both parental constructs in tumor control *in vivo*. These observations led us to speculate whether an intermediate level of antigen-independent activation may be key to the hybrid CAR-T cells' ability to productively respond to antigen stimulation, resulting in robust effector outputs and an enrichment of memory phenotype. Tonic signaling—for both 28z and BBz CARs—has been described by multiple studies as a major contributor to T-cell dysfunction[9,17–21]. However, a recent study on CD22.BBz CARs reported that CARs with stronger tonic signaling exhibited greater efficacy, concluding that tonic signaling could be beneficial in certain situations[58]. Confounding these somewhat contradictory observations in prior literature is the fact that different

groups use CARs targeting different antigens as well as different measures for tonic signaling, precluding a direct comparison of results across studies. In this work, we circumvented these challenges by generating a panel of CD20 CARs with identical signaling domains and similar antigen-binding affinities.

To test our hypothesis that intermediate levels of tonic signaling are beneficial for CAR-T cells, we needed test systems wherein minor differences in amino acid sequence would not serve as confounding factors. Transcriptomic analyses of CD20 CAR variants led us to hypothesize that PI3K/AKT signaling was the primary driver of CD20 CAR tonic signaling. Pharmacological modulation of PI3K/AKT signaling nodes using pre-clinically tested inhibitors confirmed this hypothesis. Furthermore, pharmacological tuning of antigen-independent CAR signaling is an attractive cell engineering strategy as it is straightforward to implement and obviates the need of rational protein design, a non-trivial task. We found that inhibitors targeting upstream signaling targets—namely PI3K, AKT, and mTORC1— dampened tonic signaling while enhancing *in vivo* efficacy. To our surprise, inhibitors targeting downstream signaling pathways, c-MYC and SREBP, further amplified tonic signaling in rituximab CAR-T cells, which worsened tumor-killing efficacy. This demonstrated a causal relationship between strong tonic signaling and worsened anti-tumor efficacy.

Inhibition of tonic signaling in rituximab CAR-T cells confirmed that minimizing tonic signaling was beneficial. However, to further test our hypothesis that intermediate levels of tonic signaling are beneficial, we sought to increase tonic signaling in the Leu16 CAR that tonic signals minimally to an intermediate tonic signaling state. To our surprise, c-MYC and SREBP inhibitors that increased rituximab CAR-T cell tonic signaling modestly decreased tonic signaling in Leu16 CAR-T cells, as did mTORC1 inhibition. Functionally, mTORC1-inhibited Leu16 CAR-T cells, which saw the largest decrease in tonic signaling, led to significant tumor-killing improvements compared to vehicle-treated Leu16 CAR-T cells. Although not statistically significant, SREBP-inhibited Leu16 CAR-T cells, which saw a reduction smaller reduction in tonic signaling compared

to mTORC1 inhibition, also modestly improved tumor control and survival. Collectively, the Leu16 data disproves the hypothesis that maintaining intermediate levels of CAR tonic signaling as to why hybrid.AA CAR-T cells are superior to rituximab and Leu16 CAR-T cells *in vivo*. Furthermore, the data show that the outcomes of pharmacological PI3K/AKT modulation is contingent on whether the CAR expressed has high or low levels of tonic signaling.

Transcriptomic analyses of PI3K/AKT modulated rituximab CAR-T cells further highlighted the fact that the hybrid.AA CAR-T cell phenotype is distinct from PI3K/AKT-dampened rituximab CAR-T cells. This suggests that hybrid.AA CAR-T may be engaging in qualitatively distinct antigen-independent signaling pathways compared to rituximab CAR-T cells as opposed to differing only in magnitude. Furthermore, this points to the need to study differences in antigen-dependent CAR-T cell behavior as tuning tonic signaling does not capture the full story.

Nevertheless, the panel of tonic signaling dampened or amplified rituximab CAR-T cells provided a unique window in studying the consequences of modulating CAR tonic signaling. In particular, if the root of the problem associated with tonic signaling can be identified, one could further identify a refined design parameter for testing novel CAR constructs as opposed to tonic signaling and develop solutions that directly address the biological problem. To that end, we dissected the transcriptomes of pharmacologically modulated rituximab CAR-T cells and found that tonic signaling was further driven by NF-κB signaling, suggesting that *in* vitro measures of CAR tonic signaling is an amalgamation of multiple signaling pathways. This is in concordance with the fact that CD137, whose expression is regulated in part by NF-κB[59], is an *in vitro* activation marker that is consistently correlated with transcriptomic measures of tonic signaling.

Importantly, we discovered that strong tonic signaling rituximab CAR-T cells have significantly enhanced oxidative stress responses when compared to tonic signaling dampened rituximab CAR-T cells, suggesting that oxidative stress and associated cellular damage could be the root of the problem for tonic signaling CAR-T cell. In fact, we found that vehicle-treated rituximab CAR-T cells had significant elevation of gene signatures associated with oxidative

stress-induced toxicities[56], including DNA damage, DNA repair, and an unfolded protein response, compared to AKT- and mTORC1-inhibited rituximab CAR-T cells. We found additional support of this in the protein engineered CD20 CAR RNAseq dataset, where rituximab CAR-T cells had significantly enhanced oxidative stress-response gene sets when compared to weakly tonic signaling Leu16 and hybrid.AA CAR-T cells. The surprising finding was that Leu16 CAR-T cells had elevated c-Myc and oxidative stress pathway activity when compared to Hybrid.AA CAR-T cells. This finding suggests that hybrid.AA CAR-T cells may have a method towards antagonizing c-Myc–induced oxidative stresses, which we putatively identify as MXD4 through regulon network inference analyses. Furthermore, this may also explain why Leu16 CAR-T cells saw such a significant improvement in tumor control survival when treated with rapamycin; given that Leu16 CAR-T cells had such minimal levels of tonic signaling, simple minute minimization of tonic signaling alone likely does not completely capture the underlying effects of rapamycin treatment. Based on our proposed model of PI3K/AKT/mTORC1/c-Myc–induced oxidative stress, we hypothesize that rapamycin reduced c-Myc activity by reducing mTORC1 activity, which thereby reduced oxidative stress in Leu16 CAR-T cells.

We noted with interest that SREBP inhibition amplified rituximab tonic signaling in rituximab CAR-T cells but not in Leu16 CAR-T cells, suggesting that the amplification in tonic signaling may be dependent on the strong tonic signaling characteristic of the rituximab CAR. In turn, we speculate that the SREBP response to tonic signaling protects rituximab CAR-T cells from oxidative stress given the necessity for cells to further enhance SREBP pathway activity during pharmacological inhibition. This is consistent with the fact that SREBP-inhibited rituximab CAR-T cells strongly upregulated metallothionein expression indicating a cellular need to reduce oxidative stress[60]. Moreover, the increased SREBP activity and accumulation of lipids via lipid biosynthesis (lipidomic data not shown) in tonic signaling CAR-T cells is reminiscent of reports wherein cancer cells upregulate lipid biosynthesis through SREBP to protect against oxidative stress[61,62]. Given the correlation between NF-κB and tonic signaling, we speculate that NF-κB,

whose signaling activity can be induced in response to oxidative stress[63,64], is an adaptive antioxidant response by tonic signaling CAR-T cell, triggering additional cascades of antigen-independent immune responses as a byproduct.

The scope of this study is confined to studying tonic signaling in the context of second generation CD20-targeting CARs containing a CD28 co-stimulatory domain. It is possible that CARs containing distinct or additional co-stimulatory domains could engage in different types of antigen-independent CAR signaling. Furthermore, the working model wherein tonic signaling induces oxidative stress was based on transcriptomic data alone. Through transcriptomic analysis, we found strong correlations between tonic signaling, oxidative stress, and antioxidant pathways. Functional experiments will be required to validate this proposed working model.

In this study, we demonstrated that judicial design of CAR protein sequences is critical to CAR-T cell function, and even minute changes in amino-acid sequences can lead to significant alterations in CAR-T cell function in the absence of antigen stimulation and upon *in vivo* antigen challenge. We observed a correlation between intermediate levels of tonic signaling with heightened *in vivo* efficacy among a panel of protein engineered CD20 CARs. We identified PI3K/AKT as the primary driver of tonic signaling through functionally validated transcriptomic analyses. We further demonstrated that minimizing tonic signaling, as opposed to maintaining an intermediate level of tonic signaling, enhanced *in vivo* anti-tumor efficacy. Finally, we propose a working model wherein strong tonic signaling induces oxidative stress, which when unbalanced, leads to cellular damage to the detriment of anti-tumor efficacy.

REFERENCES

1. Majzner, R. G. & Mackall, C. L. Clinical lessons learned from the first leg of the CAR T cell journey. *Nat. Med.* **25**, 1341–1355 (2019).
2. Chang, Z. L. & Chen, Y. Y. CARs: Synthetic Immunoreceptors for Cancer Therapy and Beyond. *Trends Mol. Med.* **23**, 430–450 (2017).
3. Hong, M., Clubb, J. D. & Chen, Y. Y. Engineering CAR-T Cells for Next-Generation Cancer Therapy. *Cancer Cell* **38**, 473–488 (2020).
4. Rafiq, S., Hackett, C. S. & Brentjens, R. J. Engineering strategies to overcome the current roadblocks in CAR T cell therapy. *Nat. Rev. Clin. Oncol.* **17**, 147–167 (2020).
5. Drent, E. *et al.* Combined CD28 and 4-1BB Costimulation Potentiates Affinity-tuned Chimeric Antigen Receptor–engineered T Cells. *Clin. Cancer Res.* **25**, 4014–4025 (2019).
6. Liu, X. *et al.* Affinity-Tuned ErbB2 or EGFR Chimeric Antigen Receptor T Cells Exhibit an Increased Therapeutic Index against Tumors in Mice. *Cancer Res.* **75**, 3596–3607 (2015).
7. Srivastava, S. & Riddell, S. R. Engineering CAR-T cells: Design concepts. *Trends Immunol.* **36**, 494–502 (2015).
8. Hudecek, M. *et al.* Receptor Affinity and Extracellular Domain Modifications Affect Tumor Recognition by ROR1-Specific Chimeric Antigen Receptor T Cells. *Clin. Cancer Res.* **19**, 3153–3164 (2013).
9. Watanabe, N. *et al.* Fine-tuning the CAR spacer improves T-cell potency. *OncoImmunology* **5**, e1253656 (2016).
10. Omer, B. *et al.* Chimeric Antigen Receptor Signaling Domains Differentially Regulate Proliferation and Native T Cell Receptor Function in Virus-Specific T Cells. *Front. Med.* **5**, (2018).
11. Wijewarnasuriya, D., Bebernitz, C., Lopez, A. V., Rafiq, S. & Brentjens, R. J. Excessive Costimulation Leads to Dysfunction of Adoptively Transferred T Cells. *Cancer Immunol. Res.* **8**, 732–742 (2020).

12. Zhao, Z. *et al.* Structural Design of Engineered Costimulation Determines Tumor Rejection Kinetics and Persistence of CAR T Cells. *Cancer Cell* **28**, 415–428 (2015).
13. Feucht, J. *et al.* Calibration of CAR activation potential directs alternative T cell fates and therapeutic potency. *Nat. Med.* **25**, 82–88 (2019).
14. Romero, P. A. & Arnold, F. H. Exploring protein fitness landscapes by directed evolution. *Nat. Rev. Mol. Cell Biol.* **10**, 866–876 (2009).
15. Goodman, D. B. *et al.* Pooled screening of CAR T cells identifies non-native signaling domains for next-generation immunotherapies. 2021.07.11.451980 (2021) doi:10.1101/2021.07.11.451980.
16. Kyung, T. *et al.* CARPOOL: A library-based platform to rapidly identify next generation chimeric antigen receptors. 2021.07.09.450900 (2021) doi:10.1101/2021.07.09.450900.
17. Long, A. H. *et al.* 4-1BB costimulation ameliorates T cell exhaustion induced by tonic signaling of chimeric antigen receptors. *Nat. Med.* **21**, 581–590 (2015).
18. Landoni, E. *et al.* Modifications to the Framework Regions Eliminate Chimeric Antigen Receptor Tonic Signaling. *Cancer Immunol. Res.* **9**, 441–453 (2021).
19. Gomes-Silva, D. *et al.* Tonic 4-1BB Costimulation in Chimeric Antigen Receptors Impedes T Cell Survival and Is Vector-Dependent. *Cell Rep.* **21**, 17–26 (2017).
20. Smith, E. L. *et al.* GPRC5D is a target for the immunotherapy of multiple myeloma with rationally designed CAR T cells. *Sci. Transl. Med.* **11**, eaau7746 (2019).
21. Frigault, M. J. *et al.* Identification of Chimeric Antigen Receptors That Mediate Constitutive or Inducible Proliferation of T Cells. *Cancer Immunol. Res.* **3**, 356–367 (2015).
22. Zettlitz, K. A. *et al.* ImmunoPET of Malignant and Normal B Cells with 89Zr- and 124I-Labeled Obinutuzumab Antibody Fragments Reveals Differential CD20 Internalization In Vivo. *Clin. Cancer Res. Off. J. Am. Assoc. Cancer Res.* **23**, 7242–7252 (2017).

23. Jensen, M., Tan, G., Forman, S., Wu, A. M. & Raubitschek, A. CD20 is a molecular target for scFvFc:zeta receptor redirected T cells: Implications for cellular immunotherapy of CD20+ malignancy. *Biol. Blood Marrow Transplant.* **4**, 75–83 (1998).
24. Hudecek, M. *et al.* The Nonsignaling Extracellular Spacer Domain of Chimeric Antigen Receptors Is Decisive for In Vivo Antitumor Activity. *Cancer Immunol. Res.* **3**, 125–135 (2015).
25. Kuleshov, M. V. *et al.* Enrichr: a comprehensive gene set enrichment analysis web server 2016 update. *Nucleic Acids Res.* **44**, W90–W97 (2016).
26. Marini, F. & Binder, H. pcaExplorer: an R/Bioconductor package for interacting with RNA-seq principal components. *BMC Bioinformatics* **20**, 331 (2019).
27. Margolin, A. A. *et al.* ARACNE: An Algorithm for the Reconstruction of Gene Regulatory Networks in a Mammalian Cellular Context. *BMC Bioinformatics* **7**, S7 (2006).
28. Alvarez, M. J. *et al.* Functional characterization of somatic mutations in cancer using network-based inference of protein activity. *Nat. Genet.* **48**, 838–847 (2016).
29. Clasquin, M. F., Melamud, E. & Rabinowitz, J. D. LC-MS data processing with MAVEN: a metabolomic analysis and visualization engine. *Curr. Protoc. Bioinforma.* **Chapter 14**, Unit14.11 (2012).
30. Plaks, V. *et al.* CD19 target evasion as a mechanism of relapse in large B-cell lymphoma treated with axicabtagene ciloleucel. *Blood* **138**, 1081–1085 (2021).
31. Johnson, N. A. *et al.* CD20 mutations involving the rituximab epitope are rare in diffuse large B-cell lymphomas and are not a significant cause of R-CHOP failure. *Haematologica* **94**, 423–427 (2009).
32. Schneider, D. *et al.* A tandem CD19/CD20 CAR lentiviral vector drives on-target and off-target antigen modulation in leukemia cell lines. *J. Immunother. Cancer* **5**, 42 (2017).
33. Salles, G. *et al.* Rituximab in B-Cell Hematologic Malignancies: A Review of 20 Years of Clinical Experience. *Adv. Ther.* **34**, 2232–2273 (2017).

34. Zah, E., Lin, M.-Y., Silva-Benedict, A., Jensen, M. C. & Chen, Y. Y. T Cells Expressing CD19/CD20 Bispecific Chimeric Antigen Receptors Prevent Antigen Escape by Malignant B Cells. *Cancer Immunol. Res.* **4**, 498–508 (2016).
35. Buatois, V. *et al.* Preclinical Development of a Bispecific Antibody that Safely and Effectively Targets CD19 and CD47 for the Treatment of B-Cell Lymphoma and Leukemia. *Mol. Cancer Ther.* **17**, 1739–1751 (2018).
36. Sommermeyer, D. *et al.* Fully human CD19-specific chimeric antigen receptors for T-cell therapy. *Leukemia* **31**, 2191–2199 (2017).
37. Reff, M. E. *et al.* Depletion of B Cells In Vivo by a Chimeric Mouse Human Monoclonal Antibody to CD20. *Blood* **83**, 435–445 (1994).
38. Zheng, W. *et al.* PI3K orchestration of the in vivo persistence of chimeric antigen receptor-modified T cells. *Leukemia* **32**, 1157–1167 (2018).
39. Constantinescu, S. N. *et al.* Ligand-independent oligomerization of cell-surface erythropoietin receptor is mediated by the transmembrane domain. *Proc. Natl. Acad. Sci.* **98**, 4379–4384 (2001).
40. Liu, W., Kawahara, M., Ueda, H. & Nagamune, T. Construction of a fluorescein-responsive chimeric receptor with strict ligand dependency. *Biotechnol. Bioeng.* **101**, 975–984 (2008).
41. Scheller, L., Strittmatter, T., Fuchs, D., Bojar, D. & Fussenegger, M. Generalized extracellular molecule sensor platform for programming cellular behavior. *Nat. Chem. Biol.* **14**, 723–729 (2018).
42. Arai, R., Wriggers, W., Nishikawa, Y., Nagamune, T. & Fujisawa, T. Conformations of variably linked chimeric proteins evaluated by synchrotron X-ray small-angle scattering. *Proteins Struct. Funct. Bioinforma.* **57**, 829–838 (2004).
43. Zah, E. *et al.* Systematically optimized BCMA/CS1 bispecific CAR-T cells robustly control heterogeneous multiple myeloma. *Nat. Commun.* **11**, 2283 (2020).

44. Simon, A. J., d'Oelsnitz, S. & Ellington, A. D. Synthetic evolution. *Nat. Biotechnol.* **37**, 730–743 (2019).
45. Safdari, Y., Farajnia, S., Asgharzadeh, M. & Khalili, M. Antibody humanization methods – a review and update. *Biotechnol. Genet. Eng. Rev.* **29**, 175–186 (2013).
46. Shah, N. N. *et al.* Bispecific anti-CD20, anti-CD19 CAR T cells for relapsed B cell malignancies: a phase 1 dose escalation and expansion trial. *Nat. Med.* **26**, 1569–1575 (2020).
47. Till, B. G. *et al.* Adoptive immunotherapy for indolent non-Hodgkin lymphoma and mantle cell lymphoma using genetically modified autologous CD20-specific T cells. *Blood* **112**, 2261–2271 (2008).
48. Till, B. G. *et al.* CD20-specific adoptive immunotherapy for lymphoma using a chimeric antigen receptor with both CD28 and 4-1BB domains: pilot clinical trial results. *Blood* **119**, 3940–3950 (2012).
49. Bhattacharyya, N. D. & Feng, C. G. Regulation of T Helper Cell Fate by TCR Signal Strength. *Front. Immunol.* **11**, (2020).
50. Brown, J. S. & Banerji, U. Maximising the potential of AKT inhibitors as anti-cancer treatments. *Pharmacol. Ther.* **172**, 101–115 (2017).
51. Fingar, D. C. & Blenis, J. Target of rapamycin (TOR): an integrator of nutrient and growth factor signals and coordinator of cell growth and cell cycle progression. *Oncogene* **23**, 3151–3171 (2004).
52. Lannutti, B. J. *et al.* CAL-101, a p110δ selective phosphatidylinositol-3-kinase inhibitor for the treatment of B-cell malignancies, inhibits PI3K signaling and cellular viability. *Blood* **117**, 591–594 (2011).
53. Scheffler, A. The Wound Healing Properties of Betulin from Birch Bark from Bench to Bedside. *Planta Med.* **85**, 524–527 (2019).

54. Truica, M. I., Burns, M. C., Han, H. & Abdulkadir, S. A. Turning Up the Heat on MYC: Progress in Small-Molecule Inhibitors. *Cancer Res.* **81**, 248–253 (2021).
55. Thirumoorthy, N., Manisenthil Kumar, K., Shyam Sundar, A., Panayappan, L. & Chatterjee, M. Metallothionein: An overview. *World J. Gastroenterol. WJG* **13**, 993–996 (2007).
56. Redza-Dutordoir, M. & Averill-Bates, D. A. Activation of apoptosis signalling pathways by reactive oxygen species. *Biochim. Biophys. Acta BBA - Mol. Cell Res.* **1863**, 2977–2992 (2016).
57. Diolaiti, D., McFerrin, L., Carroll, P. A. & Eisenman, R. N. Functional interactions among members of the MAX and MLX transcriptional network during oncogenesis. *Biochim. Biophys. Acta BBA - Gene Regul. Mech.* **1849**, 484–500 (2015).
58. Singh, N. *et al.* Antigen-independent activation enhances the efficacy of 4-1BB-costimulated CD22 CAR T cells. *Nat. Med.* **27**, 842–850 (2021).
59. Kim, J.-O., Kim, H. W., Baek, K.-M. & Kang, C.-Y. NF-κB and AP-1 regulate activation-dependent CD137 (4-1BB) expression in T cells. *FEBS Lett.* **541**, 163–170 (2003).
60. Ruttkay-Nedecky, B. *et al.* The Role of Metallothionein in Oxidative Stress. *Int. J. Mol. Sci.* **14**, 6044–6066 (2013).
61. Griffiths, B. *et al.* Sterol regulatory element binding protein-dependent regulation of lipid synthesis supports cell survival and tumor growth. *Cancer Metab.* **1**, 3 (2013).
62. Lewis, C. A. *et al.* SREBP maintains lipid biosynthesis and viability of cancer cells under lipid- and oxygen-deprived conditions and defines a gene signature associated with poor survival in glioblastoma multiforme. *Oncogene* **34**, 5128–5140 (2015).
63. Morgan, M. J. & Liu, Z. Crosstalk of reactive oxygen species and NF-κB signaling. *Cell Res.* **21**, 103–115 (2011).
64. Lingappan, K. NF-κB in oxidative stress. *Curr. Opin. Toxicol.* **7**, 81–86 (2018).

SUPPLEMENTARY INFORMATION

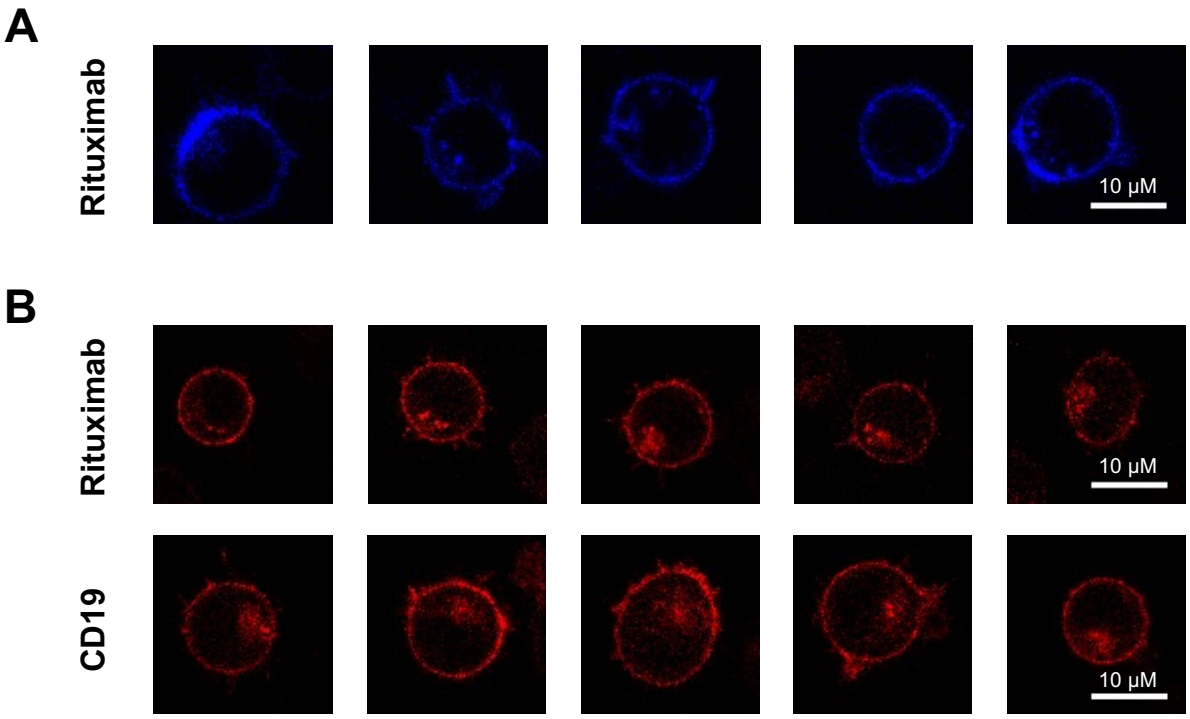

Supplementary Figure 4-1 . Rituximab CARs express evenly on T-cell surface. (**A**) CAR expressing Jurkat cells were stained with an anti-Fc antibody conjugated to DyLight 405 and imaged by confocal microscopy in the absence of antigen stimulation. By this method, only CARs on the cell surface or were internalized after having been stained by the anti-Fc antibody on the surface are labeled. (**B**) Jurkat cells transduced with CAR-HaloTag fusion proteins were stained with the red fluorescent dye tetramethylrhodamine (TMR) and imaged by confocal microscopy in the absence of antigen stimulation. TMR is a cell-permeable dye, thus it stains both intracellular and surface-anchored CAR molecules. **The reduction to practice and collection of experimental data shown in this figure were all executed by Ximin Chen.**

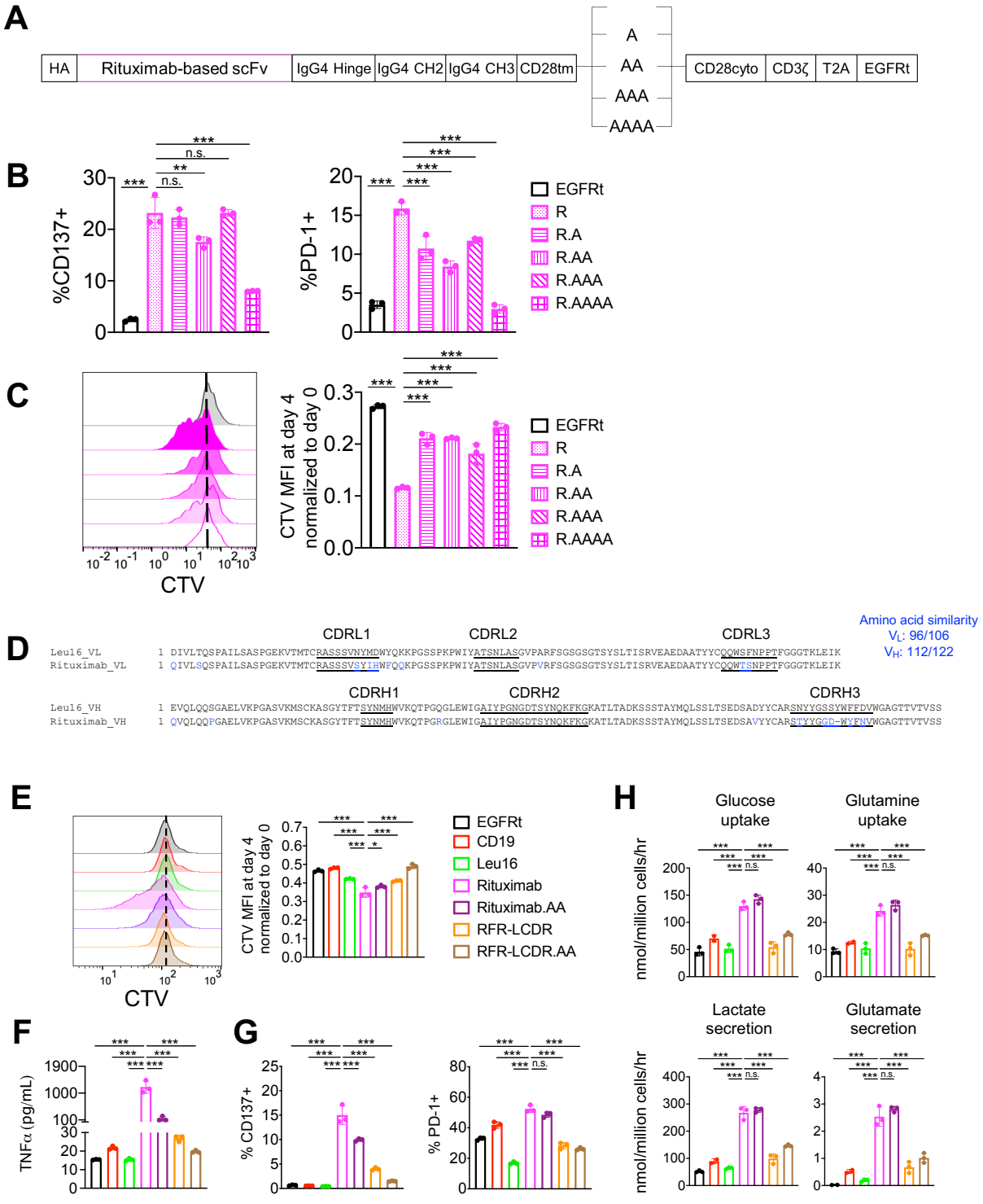

Supplementary Figure 4-2. Protein engineered CD20 CARs modulate antigen-independent activation and T-cell activity. (**A**) Schematic of alanine incorporation into the rituximab-based CAR. (**B**) Activation- and exhaustion-marker expression by CAR$^+$ T cells in the absence of antigen stimulation. Data bars indicate the means of technical triplicates ± 1 S.D. (**C**) Proliferation of CAR$^+$ T cells stained with CTV dye was assayed after a 4-day culture in the absence of target cells or

exogenous cytokines. CTV histogram on Day 4 (left) and fold-change of CTV MFI from Day 0 to Day 4 (right) are shown. (**D**) Alignment of Leu16 and rituximab scFv sequences using T-Coffee (*64*). (**E**) Proliferation of CAR^+ T cells stained with CellTrace Violet (CTV) dye was assayed after a 4-day culture in the absence of target cells or exogenous cytokines. CTV histogram on Day 4 (left) and fold-change of CTV MFI from Day 0 to Day 4 are shown (right). Data shown in the histogram correspond to one of technical triplicates shown in the bar graph. (**F**) TNF-α production by T cells in the absence of antigen stimulation. Cytokine concentration in the supernatant of cells cultured in the absence of exogenous cytokines for 48 hours was measured by ELISA. Data bars indicate the means of technical triplicates ± 1 S.D. (**G**) Activation and exhaustion marker expression by CAR^+ T cells in the absence of antigen stimulation. Data bars indicate the means of technical triplicates ± 1 S.D. (**H**) Metabolic analysis of CAR-T cells in culture in the absence of antigen stimulation. CAR-T cells were cultured for 72 hours in RPMI supplemented with 10% HI-dFBS, IL-2, and IL-15. Data bars indicate the means of technical triplicates ± 1 S.D. In (A)–(D), data are representative of two independent experiments using cells from two different healthy donors. Statistical significance in panels (A)–(D) was determined by two-tailed Student's *t* test with Sidak correction for multiple comparisons. *$p<0.05$, **$p<0.01$, ***$p<0.001$, n.s. not statistically significant. **The reduction to practice and collection of experimental data shown in this figure were executed by Ximin Chen with the help of co-authors listed in our manuscript.**

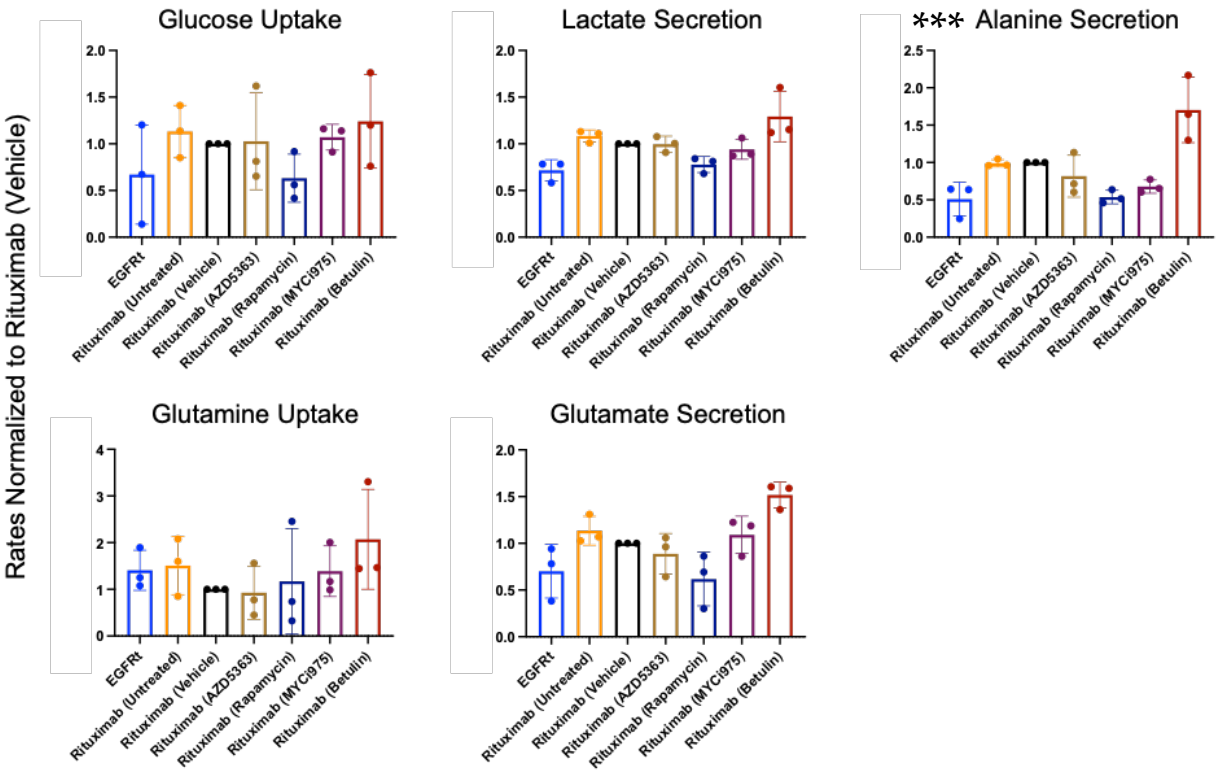

Supplementary Figure 4-3. Pharmacological inhibition of PI3K/AKT signaling modulates antigen-independent rituximab CAR-T cell metabolism. Metabolic analysis of CAR-T cells in culture in the absence of antigen stimulation. CAR-T cells were cultured for 46-49 hours in RPMI supplemented with 10% heat-inactivated, dialyzed fetal bovine serum (HI-dFBS), IL-2, and IL-15. Data bars indicate the means of biological triplicates from three healthy donors ± 1 S.D. Statistical significance was determined by one-way ANOVA test on pre-normalized metabolic rate data; alanine was the only statistically significant metabolite in stratifying metabolic differences between CAR-T cell lines, ***p<0.001.

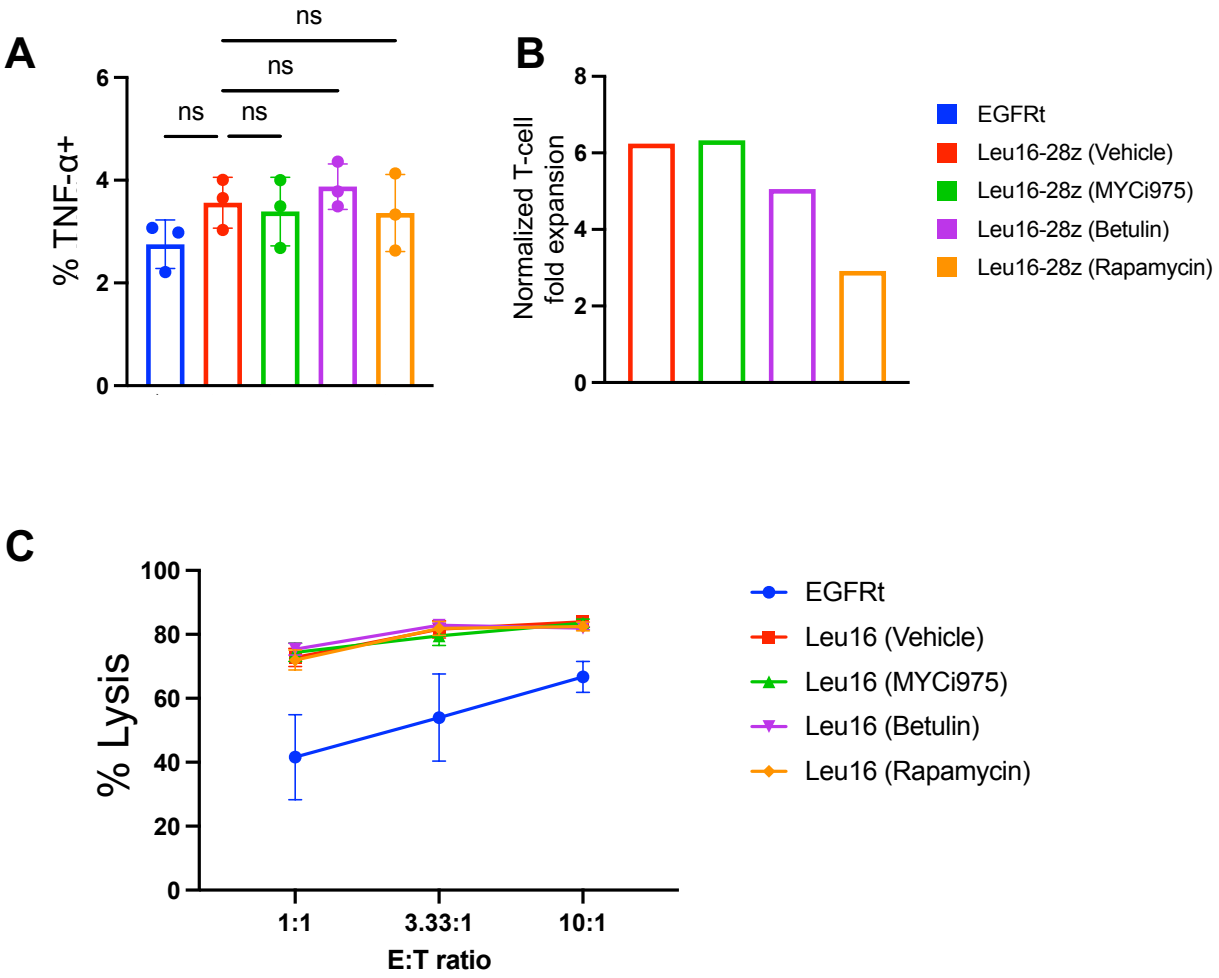

Supplementary Figure 4-4 . Characterization of pharmacologically treated Leu16 CAR-T cells *in vitro*. (**A**) TNF-α production CAR$^+$ T cells in the absence of antigen stimulation as quantified by intracellular flow cytometry. Data bars indicate the means of technical triplicates ± 1 S.D. ns not statistically significant. (**B**) Leu16 CAR-T cell fold expansion after 6 days of inhibitor culture was tracked. (**C**) A 24-hr lysis assay of CAR-T cells against Raji target cells at three effector-to-target (E:T) ratios. Data bars indicate the means of technical triplicates ± 1 S.D. Percent lysis was normalized to cell counts in target-only wells.

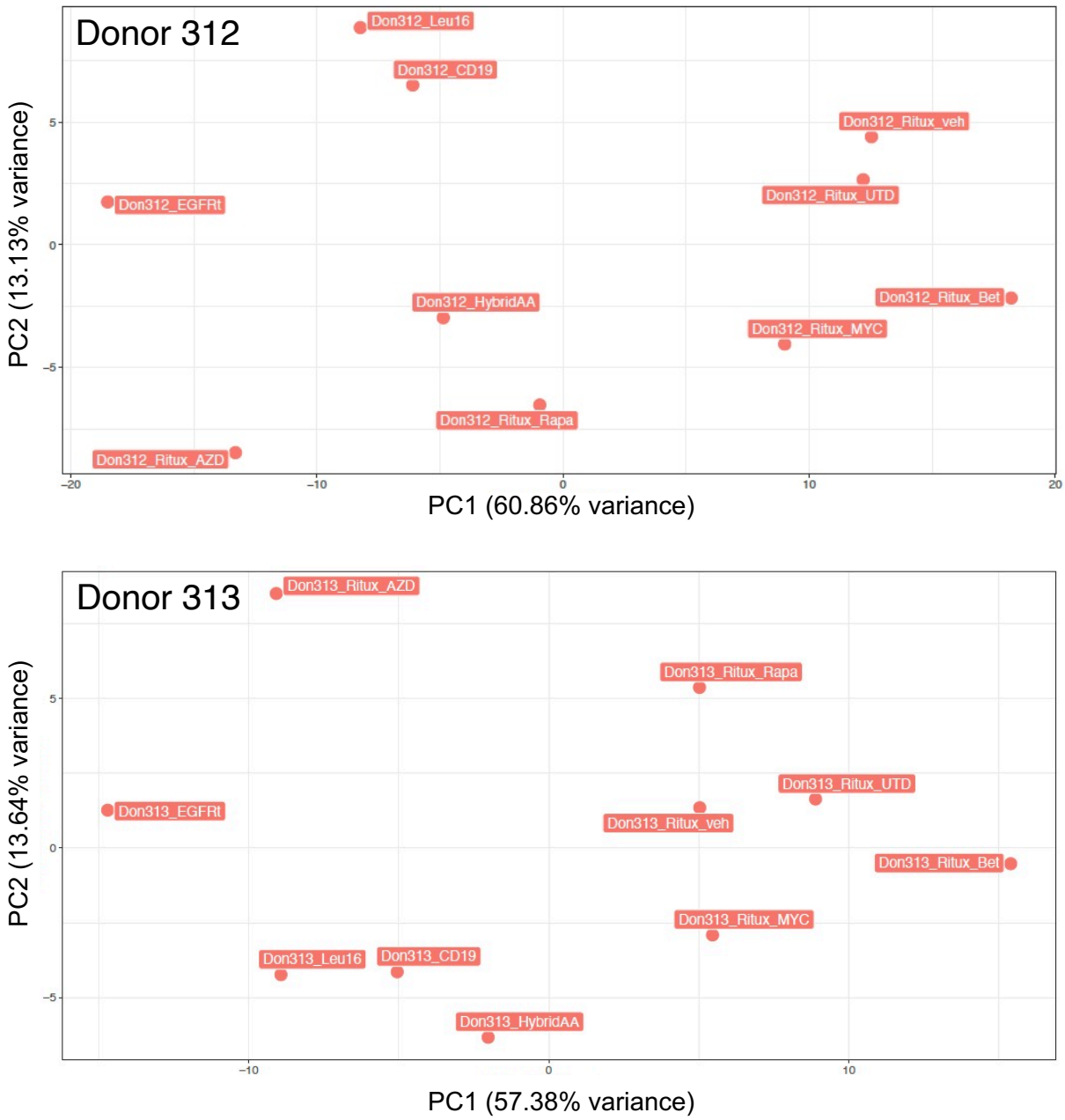

Supplementary Figure 4-5. Hybrid.AA CAR-T cells have a distinct transcriptome compared to PI3K/AKT inhibited rituximab CAR-T cells. CAR-T cells expressing the indicated CAR constructs, the transduction marker EGFRt, or rituximab CAR-T cells treated with the indicated inhibitors were cultured in the absence of CD20 antigen stimulation for 14 days prior to RNA extraction for bulk RNA-seq analysis. Principal component analysis (PCA) analysis conducted by the remaining two healthy donors. Abbreviations: Ritux_UTD – Rituximab (Untreated), Ritux_veh – Rituximab (Vehicle), Ritux_AZD – Rituximab (AZD5363), Ritux_Rapa – Rituximab (Rapamycin), Ritux_MYC – Rituximab (MYCi975), Ritux_Bet – Rituximab (Betulin).

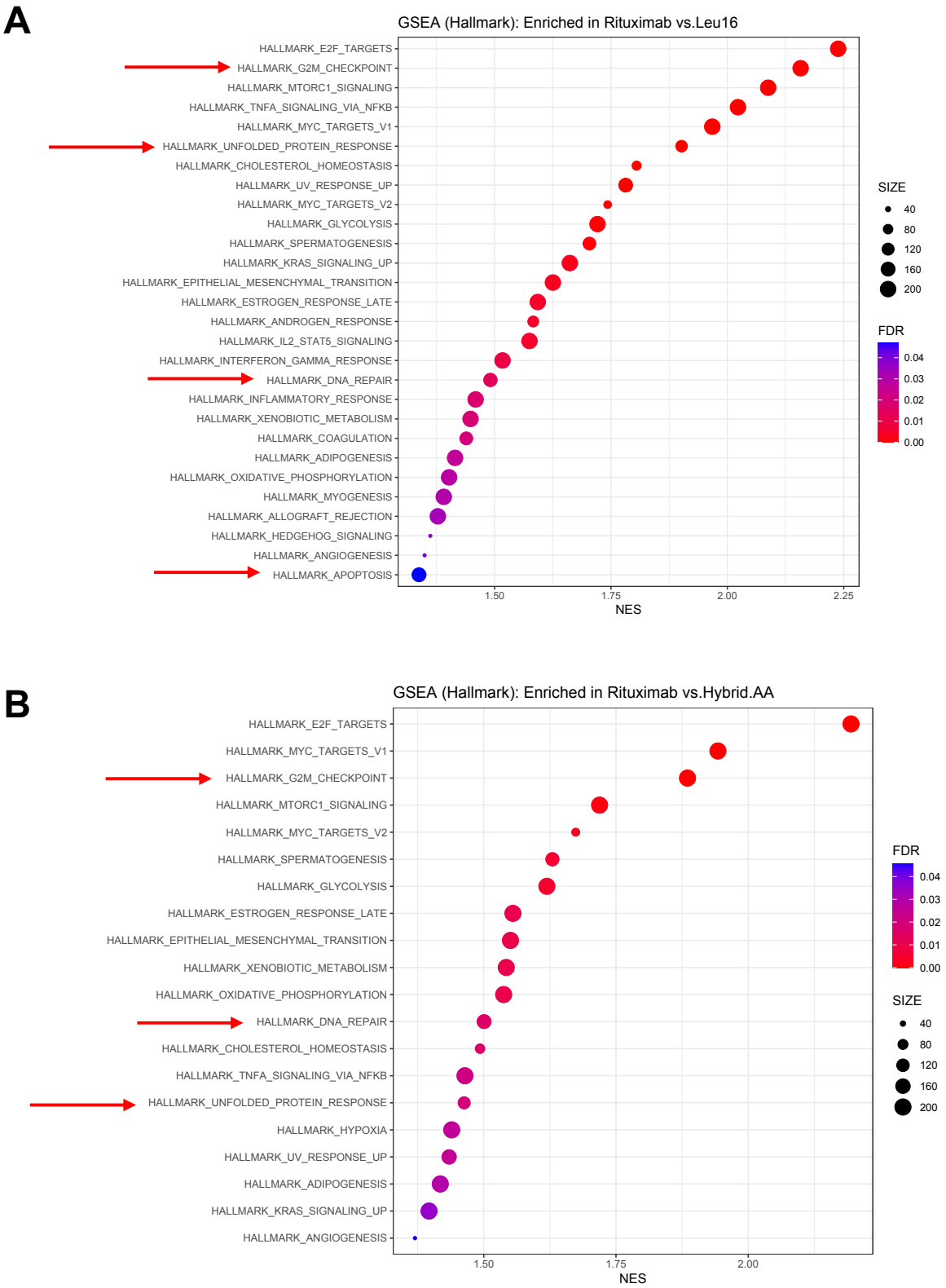

Supplementary Figure 4-6. Gene set enrichment analysis of protein engineered CD20 CAR-T cells highlight susceptibly of tonic signaling rituximab CAR-T cells to oxidative stress. T cells expressing the indicated CAR constructs or the transduction marker EGFRt were cultured in

the absence of CD20 antigen stimulation for 16–18 days prior to RNA extraction for bulk RNA-seq analysis. RNAseq data used for GSEA here were derived from the dataset shown in Fig. 4-3. (**A**) Statistically significant gene sets quantified by GSEA, comparing Rituximab vs. Leu16 CAR-T cells, in the Molecular Signatures Database (MSigDB) Hallmark set are plotted; positive NES value indicates enrichment in Rituximab CAR-T cells. (**B**) Statistically significant gene sets quantified by (**A**) Statistically significant gene sets quantified by GSEA, comparing Rituximab vs. Hybrid.AA CAR-T cells, in the Molecular Signatures Database (MSigDB) Hallmark set are plotted; positive NES value indicates enrichment in Rituximab CAR-T cells. Red arrow highlights gene set of interest.

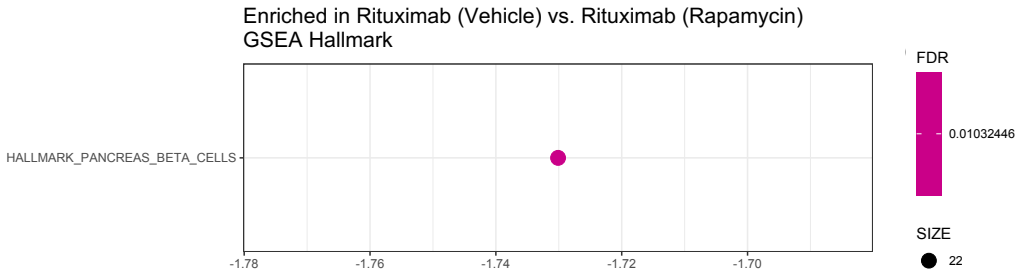

Supplementary Figure 4-7. Gene set enrichment analysis of vehicle-treated rituximab CAR-T cells highlight susceptibly to oxidative stress. CAR-T cells expressing the indicated CAR constructs, the transduction marker EGFRt, or rituximab CAR-T cells treated with the indicated inhibitors were cultured in the absence of CD20 antigen stimulation for 14 days prior to RNA extraction for bulk RNA-seq analysis. Statistically significant gene sets quantified by GSEA, comparing Rituximab (Vehicle) vs. Rituximab (Rapamycin) CAR-T cells, in the Molecular Signatures Database (MSigDB) Hallmark set are plotted; negative NES value indicates enrichment in Rituximab (Rapamycin).

Hybrid.AA Leu16

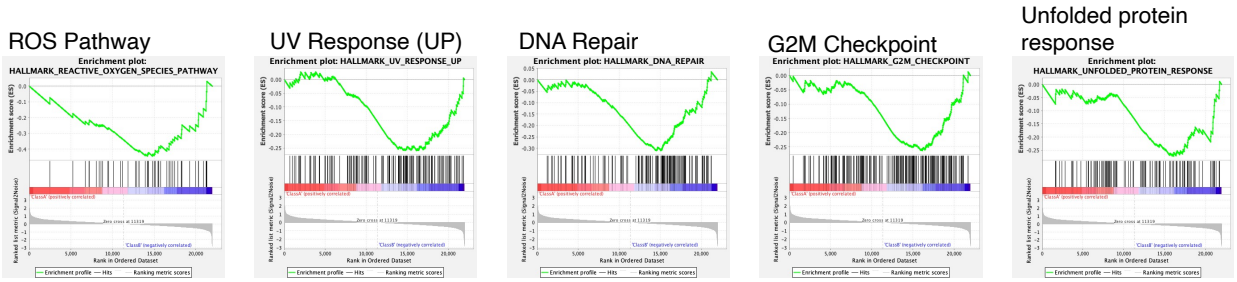

Supplementary Figure 4-8. Gene set enrichment analysis show elevation in oxidative stress in Leu16 CAR-T cells compared to Hybrid.AA CAR-T cells.

Supplementary Data 4-1: List of gene names for T-cell gene sets shown in custom heatmaps in Fig. 4-3 and Fig. 4-7.

Chapter 5. Summary and Future Work

Summary

Advances in adoptive T-cell immunotherapy have opened up the possibility of treating a broad spectrum of refractory cancers, spearheaded by the clinical success of CD19-targeting chimeric antigen receptor (CAR)-T cell therapies. However, major challenges must be overcome before adoptive T-cell immunotherapy can be effectively used to target the vast majority of tumors. Efforts in synthetic biology provides an expanding toolkit of engineered receptors and biomolecules that enable researcher-defined therapeutic programming of T cells to overcome the target antigen choice. Equally important, systems-level integration of multi-omics enables deep immune profiling of high-performing anti-tumor T cells while, generating hypotheses for how to potentiate enhanced anti-tumor CAR-T cell responses.

In Chapter 2, we continued to lay the groundwork necessary in reprogramming CAR-T cells to target intracellular antigens. We identified two key engineering components that need to coalesce to achieve the vision of enabling T cells to target the intracellular proteome. First, the endogenous T-cell killing capacity needs to be ablated in order for subsequent oncoprotein-responsive conditional killing to occur. Multiplexed CRISPR editing of T-cell cytolysis genes substantially reduces endogenous CAR-T cell killing. Second, an oncoprotein-responsive cytotoxic switch needs to be successfully engineered in order to execute conditional killing in the presence or absence of an intracellular oncoprotein of interest. We were unable to identify any oncoprotein switches by rational design, highlighting a need for high-throughput protein engineering approaches in achieving oncoprotein-responsive allostery. We further expanded our protein engineering capacity by developing a cell-based high-throughput screening procedure to assay for oncoprotein-responsive switches.

In Chapter 3 and Chapter 4, we identified clinically implementable strategies towards enhancing the robustness of CAR-T cell *in vivo* function. By analyzing the transcriptomes of

antigen stimulation-induced bifurcation of high- and low-performing CAR-T cells, we honed in on high histone deacetylation (HDAC) activity as a driver of CAR-T cell dysfunction in Chapter 3. In Chapter 4, we used tonic signaling as a guide in engineering superior CD20 CAR variants by rational protein design. We identified phosphoinositide 3-kinase/protein kinase B (PI3K/AKT) and nuclear factor kappa B (NF-κB) signaling as primary and secondary drivers of CD20 CAR tonic signaling, respectively. We demonstrated that pharmacological inhibition during *ex vivo* expansion of mechanistic target of rapamycin complex 1 (mTORC1) by rapamycin, an U.S. Food and Drug Administration (FDA)-approved drug, enhances CAR-T cell anti-tumor efficacy. Based on transcriptomic analyses, we propose a working hypothesis wherein CAR tonic signaling induces oxidative stress that decreases the anti-tumor efficacy of adoptively transferred CAR-T cells.

Future Work

Striking the balance between extensive CRISPR gene editing and T-cell fitness

We found in our *in vivo* experiments that multiplexed CRISPR editing of CAR-T cells comes at the cost of reduced T-cell efficacy. A tricky balance between the maximizing the amount of gene editing that can be achieved and CAR-T cell fitness needs to be identified. On the one hand, single knockout of Granzyme B (GrB) was insufficient to ablate endogenous T-cell killing. On the other hand, multiplex gene edited CAR-T cells were unable to effectively kill tumor cells. A gene-editing procedure that can maintain high editing efficacy without significant detriment to T-cell fitness could push us closer to finding this balance. Alternatively, a multiplex gene editing strategy that simultaneously targets cytolysis genes and genes known to enhance T-cell fitness when knocked out (for example, knocking out p38 kinase[1] or REGNASE-1[2]) could also help strike a better balance. Advances made in this space would substantially enhance the therapeutic efficacy of cytotoxic switched-equipped CAR-T cells.

Engineering intracellular oncoprotein-responsive cytotoxic switches through high-throughput screening

The inability to identify cytotoxic switches by rational design highlights the difficulty in predicting amino acid sequences that confers oncoprotein-dependent allostery, pointing to high-throughput screening as the more apt protein engineering strategy. A critical aspect to improve upon the current library screening format is the assay readout for cytotoxic switch. However, identifying the best screening readout for cytotoxicity can be tricky. The straightforward and relevant answer is to use cell death itself as the readout; the trickiness comes because there could be multiple reasons as to why a given cell died. Thus, using an assay that quantifies an apoptosis-specific readout, such as caspase activity, would further improve the chance of success in identifying cytotoxic switches through library screening.

Examining differences in antigen-dependent CAR-T cell responses among differentially performing CD20 CAR variants

Even though we observed a correlation between a non-zero but intermediate level of tonic signaling and superior *in vivo* tumor-killing efficacy, we disproved our hypothesis by demonstrating minimization of CAR tonic signaling as a way to augment anti-tumor. This works for both CARs that have strong and weak basal levels of tonic signaling. Therefore, the superiority of the best-performing CD20 CAR variant, hybrid.AA, likely stems from differences in the antigen-dependent CAR response. Further understanding of these antigen-dependent differences can deepen our understanding of how CAR protein sequence impacts CAR-T cell function.

Functionally testing the relationship between CAR tonic signaling, oxidative stress, and anti-tumor efficacy

Transcriptomic data was used as a source hypothesis-generation in proposing a working model wherein CAR tonic signaling causes oxidative stress, which in turn reduces CAR-T cell

efficacy. This hypothesis should be functionally tested through experiments to either prove or disprove interconnectivity of CAR tonic signaling, oxidative stress, and anti-tumor efficacy, and whether these connections are correlative or causal. Furthermore, we proposed a hypothesis that hybrid.AA CAR-T cells, despite having intermediate antigen-independent PI3K/AKT signaling, are better protected from oxidative stress by engaging in MXD4 activity. If this hypothesis were true, then one could overexpress MXD4 as a strategy towards enhancing CAR-T cell activity by protecting against detrimental c-Myc–induced oxidative stresses. If one can pinpoint the true biological problem due to CAR tonic signaling, then one could repurpose this knowledge towards developing a new guide for rational CAR protein design or developing new CAR-T cell manufacturing strategies that circumvent the defects associated with CAR tonic signaling.

References

1. Gurusamy, D. *et al.* Multi-phenotype CRISPR-Cas9 Screen Identifies p38 Kinase as a Target for Adoptive Immunotherapies. *Cancer Cell* **37**, 818-833.e9 (2020).
2. Wei, J. *et al.* Targeting REGNASE-1 programs long-lived effector T cells for cancer therapy. *Nature* **576**, 471–476 (2019).